AD_____

Award Number: W81XWH-05-1-0334

TITLE: New Advanced Technology for Muscular Dystrophy

PRINCIPAL INVESTIGATOR:
Johnny Huard, Ph.D.
Eric Hoffman, Ph.D.
John Day, Ph.D.
Kevin Campbell, Ph.D.
Xiao Xiao, Ph.D.
Paula Clemens, M.D.

CONTRACTING ORGANIZATION:

Children's Hospital of Pittsburgh
Pittsburgh, PA 15213

REPORT DATE: November 2009

TYPE OF REPORT: Final Addendum Report

PREPARED FOR: U.S. Army Medical Research and Materiel Command
Fort Detrick, Maryland 21702-5012

# REPORT DOCUMENTATION PAGE

*Form Approved*
*OMB No. 0704-0188*



| **1. REPORT DATE** *(DD-MM-YYYY)* | **2. REPORT TYPE** | **3. DATES COVERED** *(From - To)* |
|---|---|---|
| 01-11-2009 | Final Addendum | 1 MAR 2008 - 31 OCT 2009 |

**4. TITLE AND SUBTITLE**
New Advanced Technology for Muscular Dystrophy

**5a. CONTRACT NUMBER**

**5b. GRANT NUMBER**
W81XWH-05-1-0334

**5c. PROGRAM ELEMENT NUMBER**

**6. AUTHOR(S)**
Johnny Huard, Ph.D.

E-Mail:

**5d. PROJECT NUMBER**

**5e. TASK NUMBER**

**5f. WORK UNIT NUMBER**

**7. PERFORMING ORGANIZATION NAME(S) AND ADDRESS(ES)**
Children's Hospital of Pittsburgh
Pittsburgh, PA 15213

**8. PERFORMING ORGANIZATION REPORT NUMBER**

**9. SPONSORING / MONITORING AGENCY NAME(S) AND ADDRESS(ES)**
U.S. Army Medical Research and Materiel Command
Fort Detrick, Maryland 21702-5012

**10. SPONSOR/MONITOR'S ACRONYM(S)**

**11. SPONSOR/MONITOR'S REPORT NUMBER(S)**

**12. DISTRIBUTION / AVAILABILITY STATEMENT**
Approved for public release; distribution unlimited

**13. SUPPLEMENTARY NOTES**

**14. ABSTRACT**
Abstract on next page.

**15. SUBJECT TERMS**
Subject terms on next page.

| **16. SECURITY CLASSIFICATION OF:** | | | **17. LIMITATION OF ABSTRACT** | **18. NUMBER OF PAGES** | **19a. NAME OF RESPONSIBLE PERSON** |
|---|---|---|---|---|---|
| **a. REPORT** | **b. ABSTRACT** | **c. THIS PAGE** | | | USAMRMC |
| U | U | U | UU | 153 | **19b. TELEPHONE NUMBER** *(include area code)* |

**Standard Form 298 (Rev. 8-98)**
**Prescribed by ANSI Std. Z39.18**

**14. ABSTRACT**

Sub Project #1

Researchers continue to investigate whether gene transfer to skeletal muscle can enable both the production of proteins that might be therapeutic for muscle disorders and the systemic delivery of non-muscle proteins. Although the engineering of new mutant vectors has reduced the problems associated with viral cytotoxicity and immune rejection after gene transfer, the inability of most viral vectors to efficiently transduce mature muscle fibers continues to impede gene transfer to skeletal muscle. Results from our laboratory and others have shown that adenovirus (AV), retrovirus (RSV), and herpes simplex virus (HSV) vectors all can transduce neonatal mouse muscle efficiently; however, the muscle becomes largely resistant to viral transduction within a few days after birth. We have identified the primary barriers to viral gene transfer to mature skeletal muscle and have investigated methods by which to overcome these barriers. Among such approaches, the ex vivo technique constitutes the most efficient method for delivery of viral vectors (AV, RSV, and HSV) to mature skeletal muscle. In this project, we will investigate ex vivo gene transfer to the dystrophic skeletal muscle of mature mdx mice (which model Duchenne muscular dystrophy) by using isogenic muscle-derived cells (satellite cells or muscle-derived stem cells [MDSCs]) and retroviral vectors encoding for a functional human mini-dystrophin gene. We first will compare these 2 populations of muscle-derived cells—satellite cells and MDSCs—to identify which cell type serves as the more efficient gene delivery vehicle in mdx mice (Technical Objective #1). We then will evaluate whether restricting the transgene expression specifically to skeletal muscle fibers after ex vivo gene transfer influences the efficiency and long-term persistence of dystrophin expression in the mdx muscles (Technical Objective #2). Finally, we will evaluate the effects of fibrosis on ex vivo gene transfer to skeletal muscle via muscle-derived cells. We will investigate whether delivery of the antifibrosis agent decorin by gene therapy can prevent scar tissue development and improve the efficiency of ex vivo gene transfer to skeletal muscle in dystrophic mice (Technical Objective #3). In the Technical Objective # 1 Continuation, We plan to optimize dystrophin gene correction of murine dystrophin deficient MDSCs utilizing lenti-, adeno- associated-, and retro- viral vectors and investigate the utility of dystrophin corrected MDSCs to regenerate mdx dystrophic muscle. The overall goal of the proposed project is to ameliorate ex vivo gene transfer to skeletal muscle to facilitate the development of efficient, muscle-derived cell–based gene therapy for both inherited and acquired musculoskeletal diseases.

Sub-Project #2

Muscle responds to environmental and physiological cues quickly and effectively by adaptive remodeling. These cues can be hypertrophic stimuli (strength training), aerobic conditioning stimuli (endurance training), and responses to endogenous and pharmacological steroids (both cortisol-related corticosteroids, and anabolic steroids). There are also programmed atrophic (muscle wasting) stimuli that appear to be related to inactivity and starvation cues, and these appear to switch muscle to becoming a carbon source for the brain in times of stress. Recently, the molecular remodeling pathways responsible for both hypertrophy and atrophy have converged on the AKT1/Foxo/atrogin1 pathway (see Hoffman and Nader 2004 for review). The muscular dystrophies are due to single biochemical defects, and muscular dystrophy is increasingly viewed as a gradual failure to evoke appropriate environmental/physiological remodeling pathways. In other words, the finely tuned ability of normal muscle to quickly remodel in response to specific cues is compromised by the genetic failure of specific pathways. In the muscular dystrophies, the advent of genome-wide approaches is allowing us to define the parallel compensatory pathways that seem able to compensate for the biochemical defects for many years. However, these compensatory mechanisms gradually fail, leading to muscle wasting, weakness, and an early death. One of the more enigmatic and clinically pressing issues in both normal and dystrophic muscle is the action of glucocorticoids on muscle structure and function. In most normal muscle, glucocorticoids are catabolic, leading to muscle wasting. However, in many of the muscular dystrophies, glucocorticoids appear increased metabolic economy, and chronic treatment of Duchenne muscular dystrophy with prednisone is the only therapeutics demonstrated to lead to a rapid increase in strength, and slowing of disease progression. By combining our mRNA profiling data analysis of a bolus of glucocorticoids given to rats in an acute time series, normal muscle remodeling during aerobic training, and the changes in Duchenne muscle as a function of age, we have derived a novel model for the action of glucocorticoids on muscle. Specifically, we hypothesize that Duchenne muscle is able to alter metabolic gene transcription in response to glucocorticoid-mediated gene regulation, leading to substantially increased metabolic economy and improved muscle function. The proposed research includes a series of specific aims to test this hypothesis.

Sub-Project #3

Cord blood transplants engraft efficiently in patients with hematological disease, and have been proposed as a source for cell based therapies of muscular dystrophy. Since the University of Minnesota is a center for cord blood transplantation to treat blood disorders, with approximately 100 living cord blood transplant recipients in whom cord blood cells have successfully engrafted, we have undertaken studies to determine their engraftment in muscle. Furthermore, several hundred patients who had successful engraftment of cord blood donor cells, but subsequently died due to various causes provide autopsy specimens for investigation of donor cell engraftment and differentiation into skeletal muscle. While we are primarily interested in success of engraftment into skeletal muscle, cardiac muscle and central nervous system, we will also look at other tissues including spleen, lymph nodes, liver, bone marrow, gut and kidney in order to define the relative efficacy of donor engraftment and differentiation into each organ. Due to the fact that many forms of muscular dystrophy have multisystemic involvement (including the most common forms – Duchenne and myotonic dystrophy) the rate of successful engraftment in different tissues will be of clinical significance if cell based treatments are going to be effective for these disorders. Given the clinical evidence of successful hematapoietic recovery in these subjects, the rate of engraftment in bone marrow will provide a maximal value for successful chimerization against which results for other organs can be measured. The rate of engraftment and tissue-specific differentiation of donor cells in the various tissues studied will provide information useful in designing and assessing clinical trials of stem cell infusions in muscular dystrophy patients. We have made progress in developing methods for identifying the engrafted donor cells in recipient tissue, and demonstrating differentiation, so that study of engraftment efficacy and differentiation can now be undertaken.

Sub-Project #4

Dystroglycan is essential for maintaining muscle structural stability as it mediates the link between the muscle cell membrane and the surrounding protective extracellular matrix. Sugar structures added to dystroglycan are necessary for this interaction. In patients with mutations in fukutin-related protein (FKRP), dystroglycan sugars are abnormal and its link to the extracellular matrix is compromised. Improving our understanding of muscle structural stability is important to not only muscular dystrophy patients, but also to the effectiveness of military personnel. Thus, the goal of this study is to understand the role of FKRP in dystroglycan processing by: 1) study of dystroglycan processing and matrix binding with reduced or elevated FKRP expression; and 2) identification of regions of FKRP and binding proteins that are important for FKRP activity. Progress has been made in all aims of this study. RNA interference constructs and a viral vector have been created and screened for knockdown of FKRP expression and are now being optimized for use in muscle cell cultures. An FKRP expression virus has been generated and successfully achieves FKRP overexpression in muscle cells. We are currently analyzing dystroglycan processing and activity in this model. In addition, we have created tagged FKRP constructs for the study of FKRP binding interactions and functional domains. These early results indicate that we are well poised to meet the goals of this research study. Thus, these results will enhance our understanding of the role of FKRP in maintaining muscle stability in health and disease.

Sub-Project #5

In this proposal, we will use the DMD mouse (mdx) as the disease model, the non-pathogenic adeno-associated virus as the gene transfer vehicle and myostatin propeptide as the therapeutic gene. We will test the general hypothesis that gene therapy of DMD with myostatin inhibitors can improve muscle growth and ameliorate the pathologies of DMD. There are two specific aims in this two-year proposal. Specific Aim1: To examine if myostatin gene transfer into normal muscle can increase muscle mass and strength and also facilitate the repair of injured muscle. Specific aim 2: To study if myostatin gene delivery into dystrophic muscle can increase muscle mass and strength and also ameliorate muscular dystrophy pathologies.

Sub-Project #6

Dendritic cells are the only antigen presenting cell that can activate naïve T cells, and therefore, play a critical part in initiating a primary immune response. Because of this key role, dendritic cells may be an excellent target to mediate immunological therapy for gene transfer. We will, therefore, focus this project on testing the following hypothesis: Dendritic cells, known to be increased in dystrophic muscle, are professional APCs that initiate the adaptive immune response to HC-Ad vector-mediated dystrophin delivery. Dendritic cells can be engineered to effect antigen-specific immune suppression to enhance the effectiveness of dystrophin gene delivery to dystrophic muscle. The timing and trafficking of dendritic cells from muscle has a specific pattern that we are exploring. Progress has been made toward the generation of gene transfer vectors to prevent T cell activation.

**15. SUBJECT TERMS**

Sub-Project #1: Muscle-derived stem cells, minidystrophin, fibrosis, sex-related cell differences, muscle-specific promoters
Sub-Project #2: Muscular dystrophy, AKT1/Foxo/atrogin1 pathway, glucocorticoids
Sub-Project #3: Cord blood transplantation, muscle engraftment, muscular dystrophy
Sub-Project #4: Dystroglycan, FKRP, muscle stability
Sub-Project #5: Adeno-associated viral vector (AAV), muscular dystrophy, myostatin propeptide
Sub-Project #6: Dendritic cell suppression, T-cell activation, Adenovirus dystrophin delivery

## Table of Contents

# Sub-Project #1:
# Ex vivo gene transfer based on muscle-derived stem cells
# (Johnny Huard)
# Final Addendum Report

## INTRODUCTION

Researchers continue to investigate whether gene transfer to skeletal muscle can enable both the production of proteins that might be therapeutic for muscle disorders and the systemic delivery of non-muscle proteins. Although the engineering of new mutant vectors has reduced the problems associated with viral cytotoxicity and immune rejection after gene transfer, the inability of most viral vectors to efficiently transduce mature muscle fibers continues to impede gene transfer to skeletal muscle. Results from our laboratory and others have shown that adenovirus (AV), retrovirus (RSV), and herpes simplex virus (HSV) vectors all can transduce neonatal mouse muscle efficiently; however, the muscle becomes largely resistant to viral transduction within a few days after birth. We have identified the primary barriers of viral gene transfer to mature skeletal muscle and have investigated methods by which to overcome these barriers. Among such approaches, the *ex vivo* technique constitutes the most efficient method for delivery of viral vectors (AV, RSV, and HSV) to mature skeletal muscle. In this project, we will investigate *ex vivo* gene transfer to the dystrophic skeletal muscle of mature *mdx* mice (which model Duchenne muscular dystrophy) by using isogenic muscle-derived cells (satellite cells or muscle-derived stem cells [MDSCs]) and retroviral vectors encoding for a functional human mini-dystrophin gene. We first will compare these 2 populations of muscle-derived cells—satellite cells and MDSCs—to identify which cell type serves as the more efficient gene delivery vehicle in *mdx* mice (**Technical Objective 1**). We then will evaluate whether restricting the transgene expression specifically to skeletal muscle fibers after *ex vivo* gene transfer influences the efficiency and long-term persistence of dystrophin expression in *mdx* muscles (**Technical Objective 2**). Finally, we will evaluate the effects of fibrosis on *ex vivo* gene transfer to skeletal muscle via muscle-derived cells. We will investigate whether gene therapy to deliver decorin, an antifibrosis agent, can prevent scar tissue development and improve the efficiency of *ex vivo* gene transfer to skeletal muscle in dystrophic mice (**Technical Objective 3**). In the **Technical Objective # 1 Continuation**, We plan to optimize dystrophin gene correction of murine dystrophin deficient MDSCs utilizing lenti-, adeno- associated-, and retro- viral vectors and investigate the utility of dystrophin corrected MDSCs to regenerate mdx dystrophic muscle. The overall goal of the proposed project is to ameliorate ex vivo gene transfer to skeletal muscle to facilitate the development of efficient, muscle-derived cell–based gene therapy for both inherited and acquired musculoskeletal diseases.

## BODY

**Technical Objective 1: To perform *ex vivo* gene transfer to the skeletal muscle of mature *mdx* mice by using isogenic muscle-derived cells (satellite cells and MDSCs) and a retroviral vector encoding for a functional mini-dystrophin gene. We will conduct the following sets of experiments to achieve this objective:**

**Figure 1**

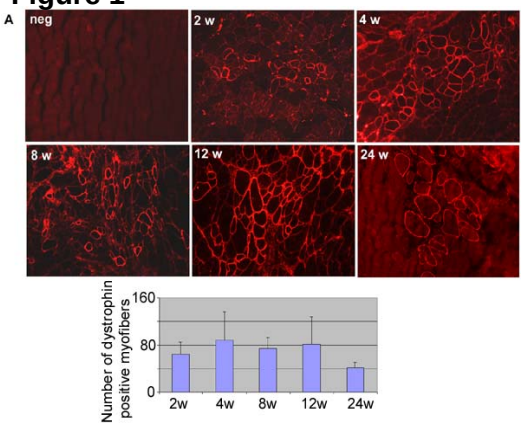


A. Isolation of satellite cells and muscle-derived stem cells.
B. In vitro transduction of satellite cells and MDSCs and subsequent injection of the transduced cells into the skeletal muscle of *mdx* mice.
C. Immunohistochemical and physiological evaluation of the outcome of the cell transplantation.

We have investigated *ex vivo* gene transfer approaches based on the use of MDSCs and a retroviral vector encoding for a functional human mini-dystrophin gene. This novel human mini-dystrophin gene, engineered by Dr. Xiao Xiao's laboratory (**Co-Investigator)**, has been demonstrated to effectively remedy dystrophic

deficiencies in the *mdx* mouse model. The MDSCs were obtained from *mdx* mice (*mdx* MDSCs) using the preplate technique. These *mdx* MDSCs were stably transduced with a retrovirus (RetroDys3999) that encodes for a human mini-dystrophin gene under the control of a CMV promoter (**Paper 1**). The dystrophin-expressing MDSCs continued to express stem cell markers, including CD34 and Sca-1 (**Paper 1**). After injection into the skeletal muscle of *mdx* mice, the genetically engineered *mdx* MDSCs were able to deliver dystrophin for up to 24 weeks (**Figure 1, and Paper 1**). As previously reported, staining with the human dystrophin-specific antibody (NCL-Dys3) revealed no human dystrophin in the muscles of the *mdx* mice that were not injected with MDSCs. In the second year of funding, we are proposing to test whether the dystrophin delivery resulting from MDSC-based *ex vivo* gene transfer can improve both the structure and function of *mdx* skeletal muscle more effectively than can satellite cells.

**Paper #1:** Ikezawa M, Cao B, Qu-Petersen Z, Peng H, Xiao X, Pruchnic R, Kimura S, Miike T, **Huard J**. Dystrophin delivery in mdx skeletal muscle by autologous muscle-derived stem cell transplantation**. Hum Gene Ther 2003 Nov 1; 14:1535-46.**

**Technical Objective 2: To evaluate whether restricting the transgene expression specifically to skeletal muscle fibers after *ex vivo* gene transfer influences the efficiency and long-term persistence of dystrophin expression in the skeletal muscle of *mdx* mice. We will conduct the following sets of experiments to achieve this objective:**

A. Genetic engineering of a retrovirus that encodes for a human mini-dystrophin gene under the control of the muscle creatine kinase (MCK) or desmin promoter.
B. *In vitro* transduction of satellite cells or MDSCs and subsequent injection of the transduced cells into the skeletal muscle of *mdx* mice.
C. Immunohistochemical and physiological evaluation of the outcome of the cell transplantation.

Immune response is one of the major problems facing adenoviral-mediated *ex vivo* gene transfer to skeletal muscle. Researchers recently have observed that the use of a muscle-specific promoter can improve long-term persistence of the transgene in skeletal muscle. Because the muscle creatine kinase (*MCK*) gene is highly active in all striated muscles and is expressed in all skeletal muscle fiber types, the transgene constructed under this promoter expresses in all types of muscle fibers. The *MCK* gene is not expressed in myoblasts, but becomes transcriptionally activated when myoblasts commit to terminal differentiation into myocytes. Therefore, researchers have speculated that a transgene driven by an *MCK* promoter would be expressed only in myotubes and myofibers; no transgene expression would occur in non-muscle cells, such as the antigen presenting cells (APCs). The lack of transgene expression in APCs could reduce the immune response against transduced cells post-transplantation. In contrast, viruses constructed with a transgene under the control of a viral promoter (e.g., CMV or RSV) do transduce non-muscle cells—including APCs, which can trigger an immune response and result in rejection of the transduced cells.

**Figure 2**

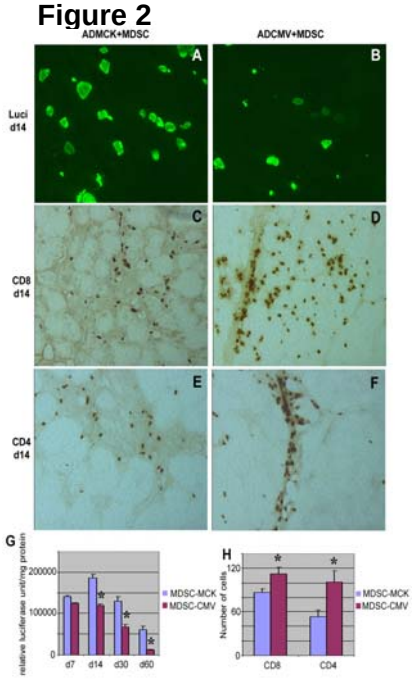


To characterize the role of muscle-specific promoters in the long-term persistence of a transgene, we injected an adenovirus (AD) carrying the luciferase reporter gene under the cytomegalovirus (CMV) promoter or the muscle creatine kinase (MCK) promoter into the skeletal muscle of *mdx* mice. As previously observed by others, our preliminary results reveal a significant difference in transgene persistence when using different promoters. We observed that the AD vector carrying the luciferase reporter gene under the MCK promoter (ADMCK) led to better persistence of transgene expression than did the AD vector carrying the luciferase reporter gene under the CMV promoter (ADCMV) (**Paper 2**). An examination of the immune response revealed that more CD8(+) lymphocytes were present in the muscle injected with ADCMV than in those injected with ADMCK at 7 days after injection (**Paper 2**). These

findings suggest that direct injection of an adenovirus carrying the transgene under a viral promoter results in transduction of, and the expression of the transgene by, the APCs—macrophages and dendritic cells—which induce a strong immune response in *mdx* mice. The use of muscle-specific promoters can significantly reduce immune response because the promoter is not active in the APCs, thus the transgene is not expressed by these cells (93).

Additionally, we have investigated whether a similar difference in the outcome of gene transfer occurs when using *ex vivo* gene transfer based on an adenovirus carrying the transgene under the MCK versus the CMV promoters. Other researchers have demonstrated that muscle cells could act as APCs and trigger immune rejection of genetically-transduced cells. To investigate this possibility, MDSCs were transduced with ADMCK or ADCMV *in vitro*, and then injected into mature skeletal muscle *in vivo*. Transgene expression within the injected muscle was monitored at different time-points and compared between the different groups. Despite the expression of luciferase in muscles injected with either the ADCMV-transduced cells (**Figure 2B, G**) or the ADMCK-transduced cells (**Figure 2A, G**) at 14 days post-transplantation, a massive infiltration of CD4/CD8–activated lymphocytes was observed in the muscles injected with ADCMV-transduced cells (**Figure 2C, E, H**), while significantly fewer infiltrates were observed within the muscles injected with ADMCK-transduced cells (**Figure 2D, F, H**). These results suggest that *ex vivo* gene transfer can prevent transduction of host APCs present within the injected muscle *in vivo* (e.g., macrophages and dendritic cells), but this method cannot prevent genetically engineered muscle-derived cells from becoming APCs after intramuscular injection. However, the use of a muscle-specific promoter can significantly reduce the immune response by eliminating the expression of the transgene in all non-muscle cells (**Paper 2**).

We also have observed that, relative to ADMCK-transduced MDSCs, ADCMV-transduced MDSCs act as more potent APCs by expressing the transgene and rapidly initiating the immune response against subsequent virus inoculation (**Figure 3**). In this experiment, MDSCs transduced with ADCMV or ADMCK were injected into the skeletal muscles of *mdx* mice; 1 week later, ADMCK was injected into the same muscles. Seven days after the second injection, we observed a significantly lower number of luciferase-expressing myofibers in the muscles that were originally injected with ADCMV-transduced MDSCs (**Figure 3A, G**) than in the muscles that were originally injected with ADMCK-transduced MDSCs (**Figure 3B, G**). At the same time-point, we noted the infiltration of a large number of CD4 and CD8 cells in the muscles that were originally injected with ADCMV-transduced MDSCs (**Figure 3C, E, H**), indicating a significantly higher immune response than in the muscles that were originally injected with ADMCK-transduced MDSCs (**Figure 3D, F, H**). More efficient gene transfer and a lower immune response were observed in the muscles injected with ADMCK-transduced MDSCs prior to ADMCK injection than in the muscles injected with ADCMV-transduced MDSCs prior to ADMCK injection (**Figure 3G, H**; note "*" indicates a significant difference). These new results (**Paper 2**) further validate our hypothesis that the use of a muscle-specific promoter to permit transgene expression only in muscle fibers could improve both the efficiency and persistence of transgene expression. **(Paper 2)**

**Figure 3**

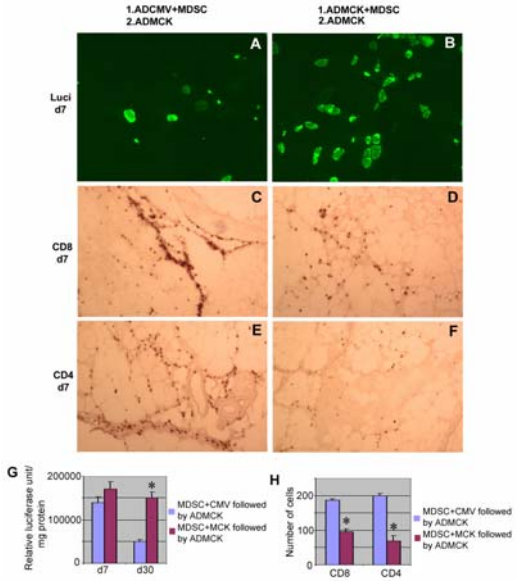


**Paper 2:** Cao B, Bruder J, Kovesdi I, **Huard J**. Muscle stem cells can act as antigen-presenting cells: implication for gene therapy. **Gene Ther 2004; 11(17);1321-30.**

Our prior studies have investigated the ability of MDSC-based *ex vivo* gene transfer to ameliorate the efficiency of non-viral transduction of myofibers. We hypothesized that the use of a plasmid vector that encodes for a given transgene under the control of a viral promoter may trigger an immune response because the transduced cells can act as antigen presenting cells (APCs) (**Paper 2**). We then used the *ex vivo* gene transfer approach based on MDSCs transduced with two plasmid vectors—mini-dystrophin gene under the muscle creatine kinase (MCK) promoter, and mini-dystrophin gene under the cytomegalovirus (CMV) promoter—to determine whether the promoter is a major determinant in the persistence of transgene expression (dystrophin) in *mdx* skeletal muscle

All animal experiments were performed in accordance with the guidelines established by the Institutional Animal Care and Use Committee (IACUC) at Children's Hospital of Pittsburgh (Protocol # 04/03). Plasmids carrying the mini-dystrophin reporter gene under the CMV or the MCK promoter were constructed in pcDNA 3.1(+) plasmid DNA backbone. Mini-dystrophin Δ3990 gene fragment was obtained by restriction enzyme digestion from plasmid DNA called PCR-dys-3990-X2. Primary MDSCs were isolated from C57BL/10JScSnDMD$^{mdx}$ mice (4 to 8 weeks of age) by using the preplate technique, as described previously. MDSCs were transduced with either CMV-dys or MCK-dys. After a 24 hour transduction, 1x10$^5$ cells were injected percutaneously into the gastrocnemius muscles of *mdx* mice (six mice per time-point). Mice were sacrificed 10, 60, or 120 days after injection. Muscle sections were fixed with cold acetone (-20ºC). To perform CD4/CD8 staining, cryosections were rinsed several times with TBS/Triton, and then blocked with 10% goat serum for 30 min. The sections were then incubated overnight at 4ºC with the following primary antibodies: purified rat anti-mouse CD4 (1:100; BD Biosciences), and purified rat anti-mouse CD8a (1:100; BD Biosciences). After three rinses in TBS/Triton, the secondary antibody, biotin-goat anti-rat (1:400; Vector), was applied for 30 minutes at room temperature, and then the tertiary antibody, Cy3–streptavidin (1:1000; Sigma) was added 30 min. To perform dystrophin staining, sections were blocked in the blocking buffer (MOM kit) for 30 minutes, followed by the addition of primary (monoclonal anti-dystrophin [1:20; Novacastra], secondary (biotin- anti-mouse [1:200; MOM kit]), and tertiary (Cy3–Streptavidin [1:1000; Sigma]) antibodies.

*Ex vivo gene transfer mediated by plasmid transduced MDSCs*

Examination of the muscle sections at early time points (10 days after injection) revealed similar levels of dystrophin expression by both populations of plasmid transfected cells (**Figure 4a, b**). However, 60 days after injection, the dystrophin expression decreased in the muscle injected with CMV-dys-transfected MDSCs (data not shown). Dystrophin expression was more persistent in the muscle injected with MCK-dys-transduced MDSCs (data not shown). We detected more dystrophin expression in the MDSC-MCK group 120 days after injection than in the MDSC-CMV group (**Figure 4c, d**).

We quantified the dystrophin expressing myofibers in the different groups at different time-points. Our results showed that MCK-dys-transfected–MDSCs displayed significantly more dystrophin positive myofibers at 60 and 120 days post-injection, but there was no significant difference evident at 10 days post-injection (**Figure 5**).

Immunostaining of muscles that were injected with plasmid-transfected cells at all time-points after injection revealed that the injection of the CMV-dys-transfected–MDSCs triggered greater CD4 lymphocyte infiltration than did the injection of MCK-dys-transduced–MDSCs (data not shown). Similar results were found for CD8-positive cell infiltration (data not shown).

**Figure 4**

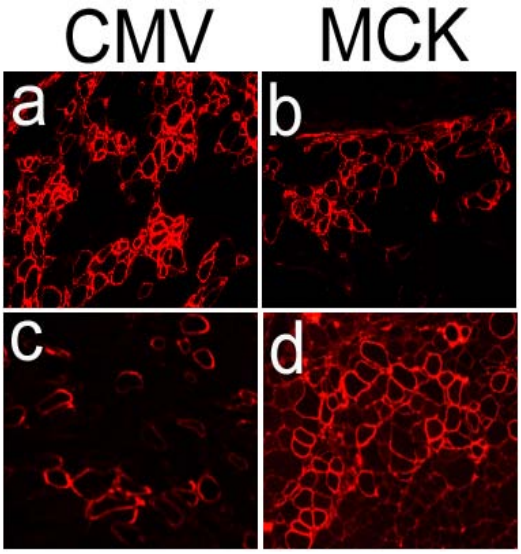


**Figure 5**

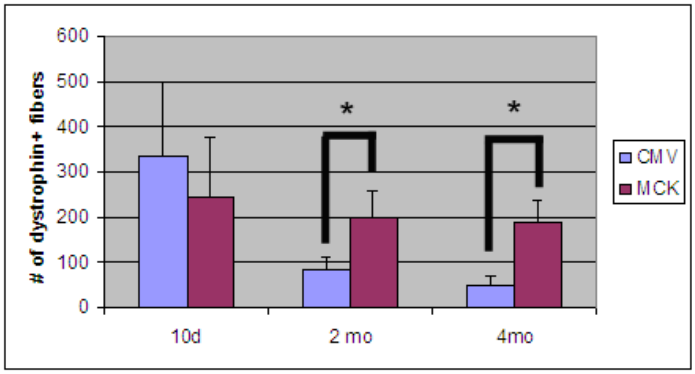


**Figure 4:** Dystrophin expression at 10 (a, b) and 120 (c, d) days post-transplantation. MCK-MDSC (d) persisted better than CMV-MDSC (c).

**Figure 5:** Quantification of dystrophin expression in transplanted *mdx* muscles. MCK-MDSC generated significantly more dystrophin-positive myofibers than CMV-MDSC at 2-month and 4-month time points. (* indicates $P<0.05$)

In this project, we demonstrated that the use of different promoters (CMV or MCK) within a given plasmid construct affects the efficiency and the persistence of dystrophin expression after plasmid-mediated gene transfer into the skeletal muscles of *mdx* mice. *Ex vivo* gene transfer of MCK-dys triggered a lower immune response that led to more efficient and more persistent dystrophin expression when compared to the *ex vivo* gene transfer of CMV-dys. We believe that MDSCs transfected with CMV-dys, and delivered via *ex vivo* gene transfer, acted as APCs after implantation into skeletal muscle as we have described previously (see **Paper 2** above). Our results suggest that the CMV-dys-transfected–MDSCs expressed dystrophin, and therefore rapidly initiated an immune response, while the MCK-dys transfected–MDSCs expressed dystrophin only after differentiation into myotubes and myofibers, ultimately leading to greater persistence of the transgene in the injected skeletal muscle. These results demonstrate that the use of a muscle-specific promoter to restrict the transgene expression to skeletal muscle can reduce the host immune response and prevent MDSCs from acting as APCs, thereby improving both the efficiency and long-term benefits of gene transfer in skeletal muscle.

**The results described above are included in a paper that will shortly be submitted for publication:**
**Paper 3:** Persistent dystrophin expression in the skeletal muscle of *mdx* mice by Cao, B; Wang, B, Xiao, X and **Huard, J**. Paper selected as the New Investigators Award (NIRA) at the Orthopaedic Research Society 2007.

The next set of experiments was designed to demonstrate the mechanism(s) by which MDSCs develop into APCs based on the results above (i.e., **Papers 1-3**).

**Figure 6**

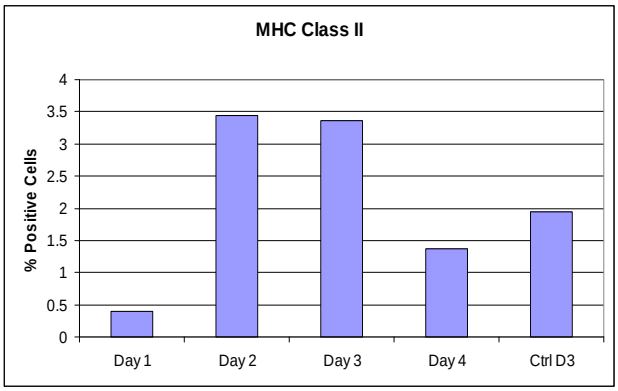


MDSCs were grown in proliferation medium (PM), which contained 20% serum, until sufficient quantities existed to induce differentiation. In order to optimize differentiation of MDSCs into APCs, these cells could be cultured in either RPMI (with 10% FBS, antibiotics, and HEPES), or DMEM (with 15% FBS). Since APCs are normally cultured in RPMI, we elected to use it for this experiment. We then tested whether MDSCs would display a different growth potential and change in marker profile when cultivated in RPMI in comparison to normal proliferation medium (PM). We found that MDSCs cultured with RPMI for 2 days displayed an increase in MHC CII markers, as seen in **Figure 6,** and a decrease (18%) in Sca-1 positive cells (data not shown). On Day 4, the cells were transferred back to PM and, within 24 hours, the number of MHC CII positive cells decreased by 2-fold, while the Sca-1 positive cell number increased (data not shown). These results indicate that MDSCs change their marker profile when cultivated in RPMI, a medium which favors the growth of APC cells.

**Figure 7**

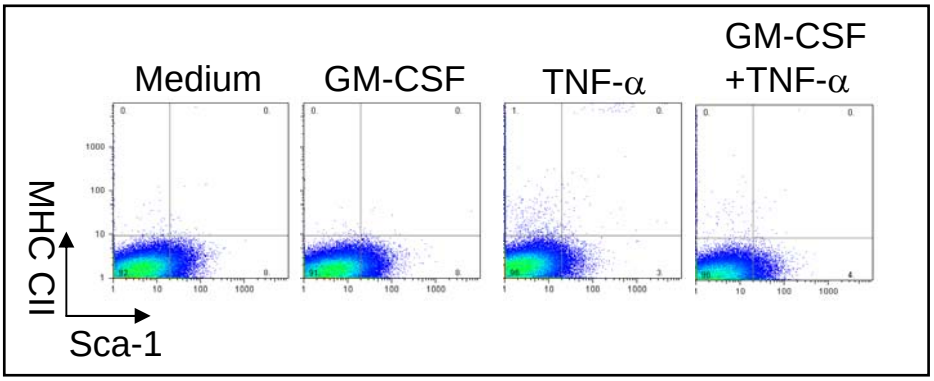


The MDSCs were then cultured in media with or without GM-CSF and TNF-α in order to see how their presence or absence affected the ability of MDSCs to differentiate into APCs. It has been previously shown that other types of stem cells can differentiate into dendritic cells when cultured in the presence of cytokines. Our preliminary results indicate that cytokines induce MHC CII expression by a population of MDSCs (**Fig. 7**). In the presence of

TNF-α alone, we detected more than a 1% increase in MHC CII positive cells and a 5% decrease in Sca-1 positive cells (**Fig.7**). These same MDSCs demonstrated an increase from 88 MHC CII positive cells in the control treatment to 1127 MHC CII positive cells in the TNF- α treated MDSCs. In addition, an increase of MHC CII positive cells (215) was observed when MDSCs were treated with both GM-CSF and TNF-α when compared to the control group. Therefore, by treating the MDSCs for two days with TNF-α we have seen an increase of about 13% in MHC CII positive cells and a 2.5% increase when the MDSCs were cultured in the presence of both GM-CSF and TNF-α. These results are preliminary, but, when taken together, indicate that MDSCs cultivated in conditions that favor the growth of APCs demonstrate an increase in the number of MHC C11-expressing cells, indicating a potential differentiation toward APC-like cells. These preliminary studies will need to be repeated and reproduced with other type of stem cells before publication of results.

**Technical Objective 3: To evaluate the effects of fibrosis on *ex vivo* gene transfer to the skeletal muscle of *mdx* mice by muscle-derived cells. We will conduct the following sets of experiments to achieve this objective:**

A. Analysis of muscle fibrosis at different time-points after *ex vivo* gene transfer to the skeletal muscle of old and young *mdx* mice.
B. Examination of whether the use of an adeno-associated virus (AAV) vector that encodes for decorin can prevent fibrosis.

Muscle-derived stem cells (MDSCs) are a potential cell source for many tissue engineering and cell therapy applications in orthopaedics. Members of our laboratory are working to identify the optimal cell phenotype for particular applications. While working with our model of muscle injury and fibrosis, we have identified 2 important variables—cell age and cell sex—that researchers should consider when developing cell therapies for fibrosis prevention. Fibrosis, or fibrous scar tissue formation, involves the deposition of extracellular matrix that disrupts the healing of muscle tissue and interferes with the restoration of its healthy architecture. As a result, we have recently come to the conclusion that the relationship between fibrosis and muscle regeneration appears to be mutually exclusive. Pursuing this relationship further, we have investigated the relationships of cell age and cell sex to fibrosis and muscle regeneration. MDSCs were isolated from normal 3-week-old mice by the preplate technique.

**Figure 8**

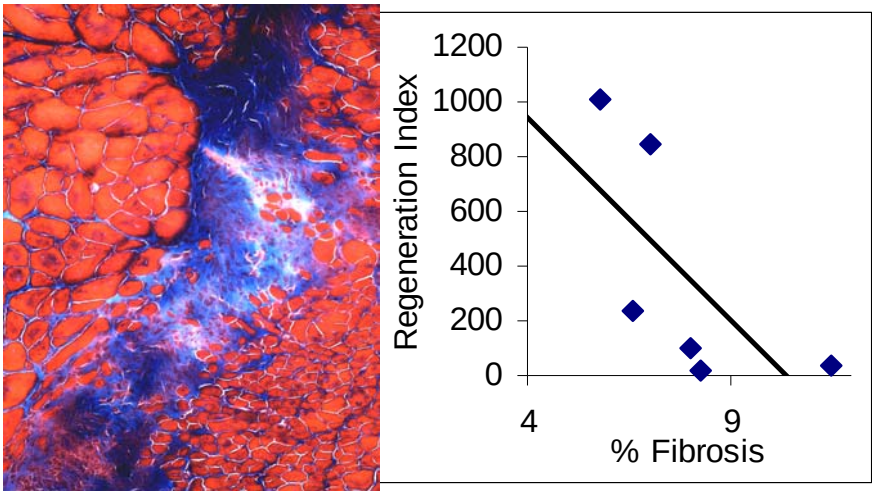


**Figure 8:** A) Fi brosis anal ysis by t richrome st aining. B) Pl ot of percent fibrosis vs. regeneration.

***Cell age:*** To obtain aged cells, MDSCs were expanded in culture as previously described; routine subculturing techniques were used to culture the cells continuously for 6 months. Quantification was performed to record the population doubling (PD) level as a measure of cell age. ***Cell sex:*** Both male MDSCs (M-MDSCs) and female MDSCs (F-MDSCs) were obtained; cell sex was confirmed by fluorescent in situ hybridization for the X and Y chromosomes. MDSCs were transplanted into the gastrocnemius of *mdx* mice, which lack the dystrophin protein. Mice were sacrificed 2 weeks after transplantation, and the muscles were isolated, frozen, and sectioned. Sections were immunostained to detect dystrophin expression. The degree of muscle regeneration was determined by calculating a regeneration index

(RI), which was equal to the number of dystrophin-positive fibers/$10^5$ donor cells. Trichrome staining of tissue sections was performed to assess the degree of muscle fibrosis. This staining revealed the collagen content of the muscle tissue by staining cell nuclei black, muscle fibers red, and collagen blue. Five non-consecutive sections from throughout the muscles were analyzed for fibrosis by a blinded investigator. Northern Eclipse imaging software was used to quantify the area of fibrosis. Statistical relationships between the degree of regeneration and fibrosis and between both of those variables and cell age and cell sex were determined by linear regression and correlation analyses. Statistically significant differences were identified by a Student's *t*-test and 2-way ANOVA (SigmaStat version 2.0). Our results indicated that the degrees of muscle regeneration and fibrosis were inversely proportional (**Fig. 8**).

**Figure 9**

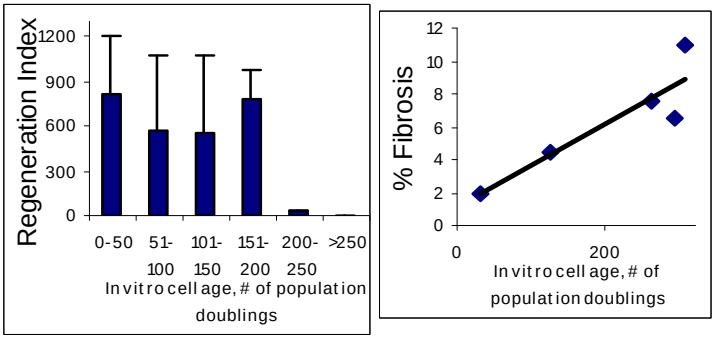


In muscles exhibiting increased fibrosis, there was a clear trend toward lower regeneration, regardless of donor cell sex or donor cell age. Our analysis of the effect of in vitro cell age on the RI revealed a large decrease as the cells aged in vitro (**Fig. 9**, and **Paper 4**). We also observed a large amount of skeletal muscle fibrosis in the muscles that received donor cells of higher in vitro ages (**Fig. 9**).

**Paper 4:** Deasy BM, Gharaibeh BM, Pollett JB, Jones MM, Lucas MA, Kanda Y, **Huard J**. Long-term self renewal of postnatal muscle-derived stem cells. **Mol Biol Cell 2005 Jul; 16(7):3323-33**.

Other members of our laboratory have observed that the transplantation of M-MDSCs results in less skeletal muscle regeneration than does the transplantation of F-MDSCs (**Paper 5**). Using 25 male and female populations displaying similar stem cell characteristics in vitro, we found that the F-MDSCs regenerated skeletal muscle more efficiently. Despite using additional isolation techniques, we could not obtain a male subfraction with a regeneration capacity similar to that of their female counterparts. Rather than being directly hormonal or due to host immune response, this difference in regeneration potential may arise from innate sex-related differences in the stress responses of MDSCs from both sexes. In comparison to F-MDSC, M-MDSC appear to differentiate more readily after stress, which leads to *in vivo* donor cell depletion. For convenience, male cells are utilized *in vivo* due to the ease of tracking the Y-chromosome. These findings should persuade researchers to report cell sex, a largely unexplored variable, and consider the implications of relying on cells of one sex.

**Paper 5:** Deasy B, Lu A, Tebbets J, Feduska J, Schugar R, Pollett J, Sun B, Urish K, Gharaibeh B, Cao B, Rubin R, **Huard J**. A role for cell sex in stem cell mediated skeletal muscle regeneration: female cells have higher muscle regeneration efficiency. **J. Cell Biology vol 177, #1, 73-86, 2007.**

**Figure10**

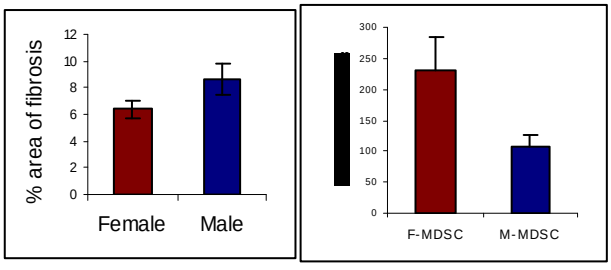


We recently found that muscle injected with M-MDSCs displayed more fibrosis than did muscle injected with F-MDSCs (**Fig. 10**). These results indicate that the formation of fibrosis is indirectly correlated to the amount of muscle regeneration (**Fig. 10**). These results may explain, at least in part, the more diminished regeneration observed with male MDSCs when compared to their female counterpart. These results were presented at the Orthopaedic Research Society (**Paper 6**), and are being further evaluated as we repeat our experiments with additional cell populations.

**Paper 6:** Liu, T; Deasy, B; Li, Y; **Huard, J.** Stem cell-mediated muscle healing: Effect of cell age and sex on fibrosis and regeneration. **Presented at the Orthopaedic Research Society, Chicago, 19-22, 2006.**

The results included in this section (**Technical Objective 3**) indicate that both age and sex are major determinants in the ability of MDSCs to promote tissue repair and regeneration. The preliminary results presented in **Figure 10** indicate that increased fibrosis might explain the reduced *in vivo* muscle regeneration capacity of M-MDSCs and MDSCs subjected to long-term expansion in culture (**Paper 6**). Our findings indicate that the prevention of fibrosis will increase the regeneration capacity of MDSC genetically engineered to

**Figure 11**

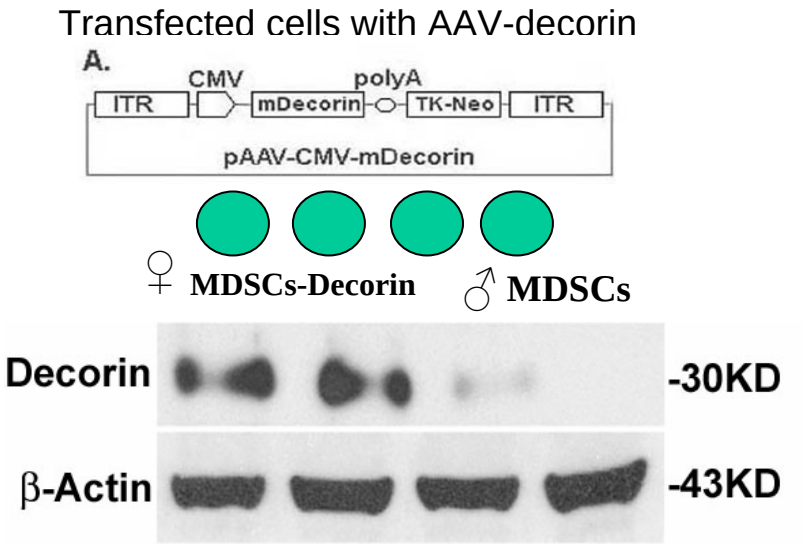


express dystrophin when injected into skeletal muscle of *mdx* mice. As outlined in **Figure 11**, we are in the process of creating genetically engineered MDSCs to express decorin, an anti-fibrotic agent that blocks TGF-β1 and decreases muscle fibrosis in skeletal muscle. We will examine the regeneration potential resulting from the implantation of these cells into skeletal muscle during the next funding period.

We have shown that decorin, a small leucine-rich proteoglycan, can inhibit TGF-β1 to prevent fibrous scar formation and improve muscle healing after injury. In the decorin-treated muscle, an enhancement of muscle regeneration is observed through histological examination. We have recently determined whether decorin has a direct effect on myogenic cells' differentiation. Our results indicate that myoblasts genetically engineered to express decorin (CD cells) differentiated into myotubes at a significantly higher rate than did control myoblasts (C2C12). This enhanced differentiation led to the up-regulation of myogenic genes (*Myf5, Myf6, MyoD*, and *myogenin*) in CD cells *in vitro*. We speculate that the higher rate of differentiation exhibited by the CD cells is due to the up-regulation of follistatin, PGC-1α, p21, and the myogenic genes, and the down-regulation of TGF-β1 and myostatin. Decorin gene transfer *in vivo* promoted skeletal muscle regeneration and accelerated muscle healing after injury. These results suggest that decorin not only prevents fibrosis, but also improves muscle regeneration and repair.

**Paper 7:** Li Y., Li J., Zhu J., Sun, B., Branca M., Tang Y., Foster W., Xiao X**., Huard, J.** Decorin gene transfer promotes muscle cell differentiation and muscle regeneration. **Mol. Therapy. Vol. 15 #9, 1616-1622, 2007.**

***Technical Objective 1 Continuation:***
***To optimize dystrophin gene correction of murine dystrophin deficient MDSCs utilizing lenti-, adeno-associated-, and retro- viral vectors and investigate the utility of dystrophin corrected MDSCs to regenerate* mdx *dystrophic muscle.***

The outcome of this continuation study was to attempt to determine the optimal viral vector for *ex vivo* dystrophin gene correction of MDSCs isolated from mdx mice (mice that are deficient for the dystrophin) via lentivirus, adeno-associated virus (AAV), or retrovirus transduction. The transduced *mdx* MDSCs would then be reintroduced into the gastrocnemius muscles of *mdx*/SCID mice and the regeneration indices of the 3 virally transduced cell populations would be evaluated histologically and physiologically as outlined in the original proposal.

During the first year funding we focused on the genetic modification of muscle derived stem cells (MDSCs) by the recombinant adeno-associated viral- and lenti-viral vectors carrying the reporter (eGFP) and therapeutic gene (mini-dystrophin). Based on the experimental design to fulfill **Technical Objectives #1** and **#2**, we constructed and produced both recombinant adeno-associated viral and lenti-viral vectors related to our project.

The MDSCs were isolated from 2-week-old *mdx* and wild-type male mice, and then were *in vitro* transduced by different gene delivery vectors. According to our previous studies, we chose AAV2-CMV-eGFP and lenti6-CMV-eGFP to test transduction efficiency before the MDSCs genetic modification by human-mini-dystrophin; however, the challenges, such as listed below were found to interfere with the successful outcome of the designed Technical Objective. Currently, we are continuing to further determine which kind of vector is optimal for mouse MDSC transduction.

1. <u>*Mdx* MDSCs differentiated myotubes showed positive dystrophin staining *in vitro*.</u>

As shown in **Fig. 1**, the results of the dystrophin immunofluorescent (IF) staining of myotubes were a surprise do to the fact that not only did the wild-type myotubes stain positive, but the dystrophin defective myotubes isolated from *mdx* mice also reacted to the dystrophin antibody. We therefore tested MDSCs isolated from different *mdx* mice and also tested several different primary dystrophin antibodies; however, we were unable to achieve specificity for the dystrophin antibody.

As an alternative approach to compensate for the false dystrophin positive IF staining of the myotubes *in vitro,* we directly tested muscle tissues after the MDSCs were genetically modified and implantated *in vivo*.

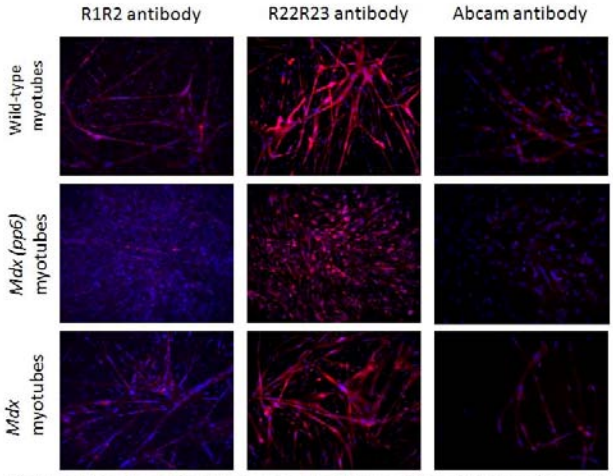


**Fig.1 IF staining for dystrophin in *mdx* and wild-type differentiated myotubes.** The dystrophin positive myotubes represented in red color and nuclei were in blue color. MDSCs are isolated from Gas muscles of 2-week-old male mice (wild-type and *mdx*). Primary antibodies were rabbit polyclonal antibodies from homemade (R1R2, and R22R23) and Abcam.

2. <u>Low transduction efficiencies in mouse MDSCs were revealed in both rAAV and lenti-vectors</u>

Unlike the high transfection efficiencies exhibited by the human-mini-dystrophin-GFP fusion protein revealed in a commercial mouse myoblast cell line (C2C12) and human embryonic kidney cell lines such as 293 and 293T (**Fig. 2**), both the rAAV-eGFP and lenti-eGFP viral vectors showed relatively low transduction efficiency after viral infection, even after the eGFP positive cells were continuously split over several generations (**Fig. 3**).

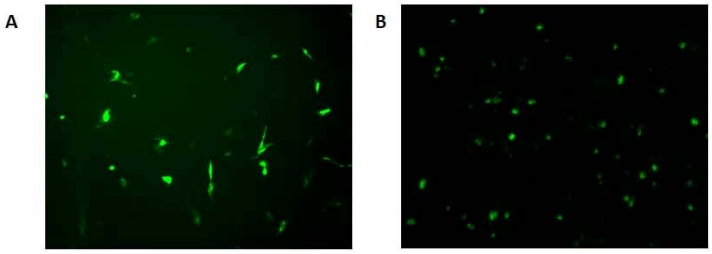


**Fig. 2 The expression of mini-dystrophin-GFP fusion protein after transfection.** (A) 24 hours post-transfection of Mini-dystrophin-GFP fusion in C2C12 by Biotex. (B) 4 days post-transfection of Lenti-Mini-dystrophin-GFP fusion in 293 cells,

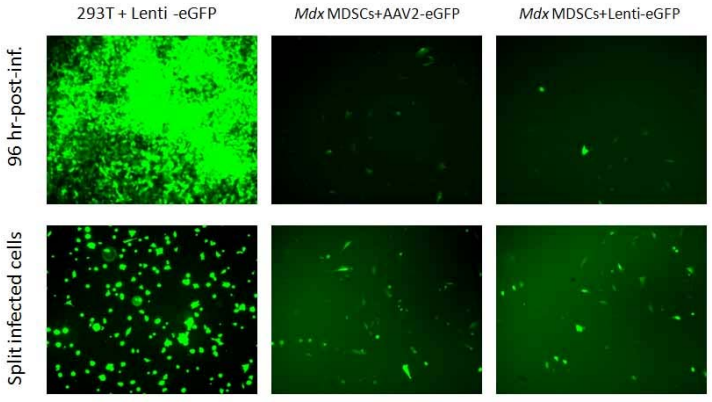


**Fig. 3 The expression of eGFP reporter in *mdx* MDSCs infected with rAAV and lenti-vectors.** High efficiency transduction were revealed in 293T infected by lenti-vector, but not in *mdx* MDSCs infected with either rAAV or lenti-vector.

These results indicate that both the rAAV and lenti-vectors, currently used in this project, are not suitable for the genetic modification of murine MDSCs probably due to the unique tropisms of the viruses, which can cause low infection efficiencies. In future studies, we will need to either optimize the virus backbone or use muscle-derived stem cells from an alternative source.

3. <u>High transduction efficiencies revealed in human myogenic endothelial (myo-endo) cells</u>

Myo-endo-cells, isolated from adult human skeletal muscle, have been shown to posses the capacity for self-renewal and the multilineage potential to regenerate different tissues of the musculoskeletal system in our previous studies (**Paper 8** below). In order to develop rAAV- and lenti-based myogenic-endothelial (myo-endo) progenitor cell *ex vivo* gene therapy regimes for the treatment musculoskeletal degenerative diseases (including DMD), we also investigated the efficiency of rAAV and lenti-vectors transduction of these myo-endo cells cultured over 10 passages. In this study, we infected myo-endo cells (Passage 3) with AAV2-GFP and continuously split the cells (1:3) to keep them at a cellular confluency of approximately 50%. The results demonstrated that over 50% of cells remained GFP positive through each passage examined by fluorescence microscopy and flow cytometry, which is similar to the transduction efficiency observed using the Lenti-GFP viral vector (**Fig. 4**). Unlike the results revealed above by the mouse muscle-derived stem cells, these results indicate that both rAAV and lenti-viral vector mediated transduction is not affected when the cell cultures are split.

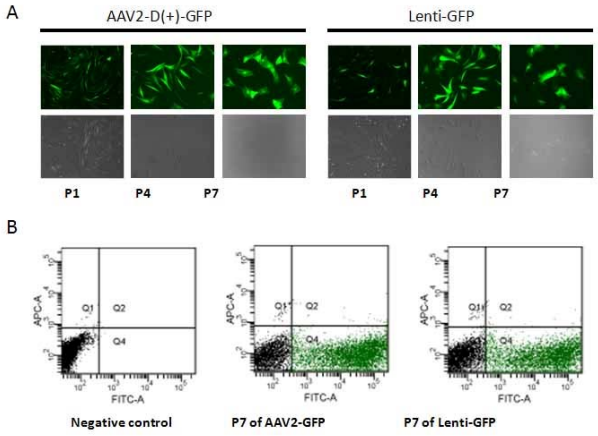


**Fig. 4 Stable transduction of rAAV-GFP in cultured dividing myo-endo cells.** The efficient transduction of both rAAV-GFP and Lenti-GFP has shown in the passage 1, 4 and 7 by fluorescent microscopy (A). The flow cytometry analysis showed that 51% of AAV2-GFP and 45% of Lenti-GFP in the passage 7 (B).

In summary, the viral vectors utilized in muscle derived stem cell (MDSC) *ex vivo* gene therapy will need to be further optimized due to the different tropisms of the viruses or the use of different stem cell sources could be tested. In the future, we plan to continue to develop new and more efficient viral vectors for multiple applications.

**Paper 8** Michael Y. Mi, Ying Tang, Bo Zheng, **Johnny Huard,** Bing Wang, Stable transduction of rAAV-GFP in cultured dividing myo-endo cells. Poster presentation at the **American Society of Gene Therapy meeting , 2009.**

**Human Muscle-derived Stem Cells:**

Although beyond the scope of the current proposal, we have been actively looking at the potential origin of the murine MDSCs and have isolated 2 populations of cells from human skeletal muscle biopsies that appear to originate from the walls of blood vessels which exhibit very similar characteristics to the murine MDSCs. We have documented anatomic, molecular and developmental relationships between endothelial and myogenic cells within human skeletal muscle. Cells co-expressing myogenic and endothelial cell markers (CD56, CD34, CD144) (Myo-endothelial [myo-endo] cells) (**Paper 9**) as well as cells expressing the pericyte marker CD146 (pericytes) (**Paper 10**) have been identified by immunohistochemistry and isolated by flow cytometry (**Figure 12**). Both of these cell populations have been shown to regenerate myofibers in the injured skeletal muscle of SCID mice in a more effective manner than CD56+ myogenic progenitors. Cultured myo-endo cells proliferate long-term, retain a normal karyotype, are not tumorigenic and better

**Figure 12**

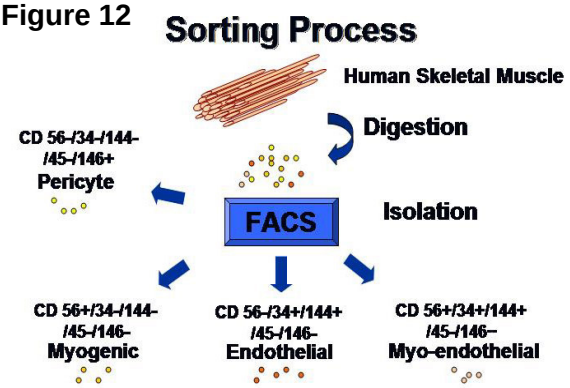

survive under oxidative stress than CD56+ myogenic cells. Clonally derived CD56+CD34+CD144+ cells were also found able to differentiate into myogenic, osteogenic and chondrogenic cells in culture and to regenerate skeletal muscle in vivo. The infarcted hearts of mice injected with pericytes have displayed significant improvement in cardiac contraction as well as a 38% reduction in scar area fraction and a significant reduction in infarction size when compared with controls These novel human myoendothelial and pericyte progenitor cells display similar characteristic to the murine MDSC and are amenable to biotechnological handling, including purification by flow cytometry and long term expansion *in vitro*, and therefore represent potential therapeutic cell types for skeletal and cardiac muscle repair.

**Paper 9.** Bo Zheng, Baohong Cao, Mihaela Crisan, Bin Sun, Guang-heng Li, Alison Logar, Solomon Yap, Jonathan B. Pollett, Lauren Drowley, Theresa Cassino, Burhan Gharaibeh, Bridget M. Deasy, **Johnny Huard*,** Bruno Péault, **A** LINEAGE OF MYOGENIC ENDOTHELIAL CELLS IN HUMAN SKELETAL MUSCLE. **Nature Biotechnology, vol. 25, #9, 1025-1034, 2007. * Cooresponding author**

**Paper 10** Crisan M, Park, TS Casteilla, L, Sun B, Zheng B, Yap S, Norotte C, Corselli M, Traas J, Deasy B, Andriolo G, Bühring HJ, Lazzari L, Giacobino JP, **Huard J**, Péault B. Perivascular origin of mesenchymal stem cells in multiple human tissues. **Cell Stem Cell, 2008 Sep 11;3(3):301-13.**

We hope that the results we have included in our progress report are a strong indicator that the valued financial support of the Department of Defense has been used to carry out the technical objectives outlined in our application. All papers that have been published as a result of this support acknowledge funding by the Department of Defense.

**KEY RESEARCH ACCOMPLISHMENTS**

- Stably transduced MDSC's with human mini-dystrophin gene. When transduced cells were in injected in dystrophic skeletal muscle of mdx mice, the muscle fibers could express human dystrophin for up to 24 weeks.
- Demonstrated that MDSCs transduced with transgenes promoted by MCK were more efficient at transgene expression then cells transduced with CMV when injected into skeletal muscle. The use of a muscle-specific promoter that restricts transgene expression to differentiated muscle cells reduces the immune response.
- Demonstrated that MDSC's could act as APC's and this could explain the latter difference in promoter efficiency. Preventing MDSCs from becoming APCs could thereby improve the efficiency of ex vivo gene transfer of dystrophin to mdx skeletal muscle
- Demonstrated how MDSCs could develop into APC's. Showed that MDSC expression of MHC Class II could be increased by culturing the cells with TNF-alpha and GM-CSF.
- Demonstrated that both sex and age are major determinants in the ability of MDSCs to promote muscle regeneration and promote fibrosis. Female cells regenerate more efficiently and younger cells regenerate better and form less fibrosis.
- Demonstrated that MDSC's genetically engineered to express decorin can reduce fibrosis formation upon MDSC skeletal muscle transplantation.
- Identified the origin of murine MDSCs and their human counterparts (myo-endo cells) within blood vessel walls.
- Demonstrated the inefficiency of our rAAV and lentiviral vectors at transducing murine MDSCs and the excellent transduction efficiency of the rAAV and lentiviral vectors at transducing myo-endothelial cells

## REPORTABLE OUTCOMES

**Paper 1:** Ikezawa M, Cao B, Qu-Petersen Z, Peng H, Xiao X, Pruchnic R, Kimura S, Miike T, **Huard J**. Dystrophin delivery in mdx skeletal muscle by autologous muscle-derived stem cell transplantation**. Hum Gene Ther 2003 Nov 1; 14:1535-46.**

**Paper 2:** Cao B, Bruder J, Kovesdi I, **Huard J**. Muscle stem cells can act as antigen-presenting cells: implication for gene therapy. **Gene Ther 2004; 11(17);1321-30.**

**Paper 3:** Persistent dystrophin expression in the skeletal muscle of *mdx* mice by Cao, B; Wang, B, Xiao, X and **Huard, J**. Paper selected as the New Investigators Award (NIRA) at the Orthopaedic Research Society 2007.

**Paper 4:** Deasy BM, Gharaibeh BM, Pollett JB, Jones MM, Lucas MA, Kanda Y, **Huard J**. Long- term self renewal of postnatal muscle-derived stem cells. **Mol Biol Cell 2005 Jul; 16(7):3323-33**..

**Paper 5:** Deasy B, Lu A, Tebbets J, Feduska J, Schugar R, Pollett J, Sun B, Urish K, Gharaibeh B, Cao B, Rubin R, **Huard J**. A role for cell sex in stem cell mediated skeletal muscle regeneration: female cells have higher muscle regeneration efficiency **J. Cell Biology vol 177, #1, 73-86, 2007.**

**Paper 6:** Liu, T; Deasy, B; Li, Y; **Huard, J.** Stem cell-mediated muscle healing: Effect of cell age and sex on fibrosis and regeneration. **Presented at the Orthopaedic Research Society, Chicago, 19-22, 2006.**

**Paper 7:** Li Y., Li J., Zhu J., Sun, B., Branca M., Tang Y., Foster W., Xiao X**., Huard, J.** Decorin gene transfer promotes muscle cell differentiation and muscle regeneration, **Mol. Therapy. Vol. 15 #9, 1616-1622, 2007.**

**Paper 8** Michael Y. Mi, Ying Tang, Bo Zheng, **Johnny Huard,** Bing Wang, Stable transduction of rAAV-GFP in cultured dividing myo-endo cells. Poster presentation at the **American Society of Gene Therapy meeting , 2009.**

**Paper 9.** Bo Zheng, Baohong Cao, Mihaela Crisan, Bin Sun, Guang-heng Li, Alison Logar, Solomon Yap, Jonathan B. Pollett, Lauren Drowley, Theresa Cassino, Burhan Gharaibeh, Bridget M. Deasy, Johnny Huard*, Bruno Péault, **A LINEAGE OF MYOGENIC ENDOTHELIAL CELLS IN HUMAN SKELETAL MUSCLE. Nature Biotechnology, vol. 25, #9, 1025-1034, 2007.**

**Paper 10** Crisan M, Park, TS Casteilla, L, Sun B, Zheng B, Yap S, Norotte C, Corselli M, Traas J, Deasy B, Andriolo G, Bühring HJ, Lazzari L, Giacobino JP, **Huard J**, Péault B. Perivascular origin of mesenchymal stem cells in multiple human tissues. **Cell Stem Cell, 2008 Sep 11;3(3):301-13.**

## CONCLUSIONS:

We have demonstrated the feasibility of restoring dystrophin in dystrophic muscle using an ex vivo approach with a retrovirus and mini-dystophin gene. We have also shown that the use of a muscle-specific promoter can reduce immune rejection of muscle cells upon transplantation. MDSC's can act as Antigen Presenting Cells by up regulating Major Histocompatibility Complex Class II antigen which was demonstrated by culturing the cells in the presence of TFN-alpha and GM-CSF Finally we have demonstrated the importance of donor cell doubling age and sex on the success of MDSC transplantation and their ability to regenerate muscle and reduce the formation of fibrosis. Earlier passages regenerate better and form less fibrosis and female MDSCs regenerate muscle and form less fibrosis then male MDSC cells. We also engineered MDSCs to express decorin in order to reduce the formation of fibrosis at the site of MDSC transplantation. We were also able to demonstrate that murine and human muscle-derived stem cells have a common site of origin in skeletal muscle – blood vessel walls. Over the past year we further examined the use of ex vivo gene therapy utilizing several additional viral vectors and demonstrated the inefficiency of our rAAV and lentiviral vectors at transducing murine MDSCs and the excellent transduction efficiency of the rAAV and lentiviral vectors at transducing myo-endothelial cells

**APPENDICES**

**Appendix 1 (Paper #1):** Ikezawa M, Cao B, Qu-Petersen Z, Peng H, Xiao X, Pruchnic R, Kimura S, Miike T, **Huard J**. Dystrophin delivery in mdx skeletal muscle by autologous muscle-derived stem cell transplantation**. Hum Gene Ther 2003 Nov 1; 14:1535-46.**

**Appendix 2 (Paper #2):** Cao B, Bruder J, Kovesdi I, **Huard J**. Muscle stem cells can act as antigen-presenting cells: implication for gene therapy. **Gene Ther 2004; 11(17);1321-30.**

**Appendix 3 (Paper 3):** Persistent dystrophin expression in the skeletal muscle of *mdx* mice by Cao, B; Wang, B, Xiao, X and **Huard, J**. Paper selected as the New Investigators Award (NIRA) at the Orthopaedic Research Society 2007.

**Appendix 4 (Paper 4):** Deasy BM, Gharaibeh BM, Pollett JB, Jones MM, Lucas MA, Kanda Y, **Huard J**. Long-term self renewal of postnatal muscle-derived stem cells. **Mol Biol Cell 2005 Jul; 16(7):3323-33**..

**Appendix 5 (Paper 5):** Deasy B, Lu A, Tebbets J, Feduska J, Schugar R, Pollett J, Sun B, Urish K, Gharaibeh B, Cao B, Rubin R, **Huard J**. A role for cell sex in stem cell mediated skeletal muscle regeneration: female cells have higher muscle regeneration efficiency. **J. Cell Biology vol 177, #1, 73-86, 2007.**

**Appendix 6 (Paper 6):** Liu, T; Deasy, B; Li, Y; **Huard, J.** Stem cell-mediated muscle healing: Effect of cell age and sex on fibrosis and regeneration. **Presented at the Orthopaedic Research Society, Chicago, 19-22, 2006.**

**Appendix 7 (Paper 7):** Li Y., Li J., Zhu J., Sun, B., Branca M., Tang Y., Foster W., Xiao X**., Huard, J.** Decorin gene transfer promotes muscle cell differentiation and muscle regeneration, **Mol. Therapy. Vol. 15 #9, 1616-1622, 2007.**

**Appendix 8 (Paper 8)** Michael Y. Mi, Ying Tang, Bo Zheng, **Johnny Huard,** Bing Wang, Stable transduction of rAAV-GFP in cultured dividing myo-endo cells. Poster presentation at the **American Society of Gene Therapy meeting , 2009.**

**Appendix 9 (Paper 9):** Bo Zheng, Baohong Cao, Mihaela Crisan, Bin Sun, Guang-heng Li, Alison Logar, Solomon Yap, Jonathan B. Pollett, Lauren Drowley, Theresa Cassino, Burhan Gharaibeh, Bridget M. Deasy, Johnny Huard*, Bruno Péault, **A LINEAGE OF MYOGENIC ENDOTHELIAL CELLS IN HUMAN SKELETAL MUSCLE. Nature Biotechnology, vol. 25, #9, 1025-1034, 2007.**

**Appendix 10 (Paper 10):** Crisan M, Park, TS Casteilla, L, Sun B, Zheng B, Yap S, Norotte C, Corselli M, Traas J, Deasy B, Andriolo G, Bühring HJ, Lazzari L, Giacobino JP, **Huard J**, Péault B. Perivascular origin of mesenchymal stem cells in multiple human tissues. **Cell Stem Cell, 2008 Sep 11;3(3):301-13.**

# Sub-Project #2**
# Molecular pathways in Duchenne dystrophy and compensatory pathway drug screening
# (Eric Hoffman)

** Note that this subproject was completed February 2007. The following is a reiteration of the final report. There are no additional updates.

## Introduction

## Muscle Transcriptional Response to Glucocorticoids: Final Report**

Synthetic glucocorticoids are drugs widely used for a variety of conditions such as respiratory diseases, autoimmune diseases, cancer, and transplantation. Their beneficial effects are accompanied by several side effects including muscle catabolism that results in weakness and atrophy (Kettelhut et al, 1988). Despite the strong catabolic effect on normal skeletal muscle, glucocorticoids show an overall anabolic effect on dystrophic muscle. Moreover, they are the only drugs shown to have a significant positive effect on both strength and function in patients with Duchenne muscular dystrophy (DMD). The paradoxical effect on dystrophic muscle has been attributed to their anti-inflammatory and immunosupresive action although the exact mechanism of action has not been described. Based on previous studies, we proposed that the muscle anabolic or catabolic response to glucocorticoids is in part determined by the training state of the muscle. Some of the muscular dystrophies show a pseudotrained state due to membrane instability mimicking training. This would then explain the enigmatic anabolic response of dystrophinopathies and sarcpglyconopathy patients and animals to glucocorticoids.

This research proposal is to understand both the signaling and transcriptional responses of muscle to glucocorticoids. A series of state-of-the-art techniques will be employed. ChIP-on-chip (chromatin immunoprecipitations on microarrays) will assess glucocorticoid receptor occupancy in myogenic cells. mRNA profiling and targeted phosphoprotein immunoblot assays in hypertrophied and non-hypertrophied muscle is planned, as well as phosphoproteome assessments to determine phosphorylation signaling in a genome-wide fashion.

## BODY

### Aim 1. Pathway validation for prednisone-induced metabolic remodeling of cells.

- Aim 1A. Validate glucocorticoid receptor binding to the GRE elements of key “gate-keepers” in energy metabolism pathways (LDHB, PDH, GOT1) using chromatin immunoprecipitation assays (ChIP).
- Aim 1B. Validate the relative lack of glucocorticoid transcriptional response machinery (P23, ERR3, EAR2, PKCtheta) as being responsible for the poor prednisone-induced muscle transcriptional response of GOT1/LDHB/PDH that we have observed in vivo.

This specific aim focuses on chromatin immunoprecipitation assays analyzed either via candidate gene approach (targeted promoter amplification), or microarray assays on promoter tiling arrays (ChIP-on-chip). We have focused on the latter technique, as we feel that a genome-wide assessment of promoter occupancy with glucocorticoids will serve to both validate our previous hypotheses, while extending this to a full assessment of promoter occupancy.

Over the last year of funding, we have successfully produced amplification material needed from C2C12 myotubes for ChIP-on-chip assays, and have produced a series of Affymetrix promoter tiling arrays for genes downstream of MyoD, Rb, and and Pax7.

For ChIP-on-chip we have processed a total of 27 genome-wide Affymetrix tiling arrays:

- MyoD antibodies, 6 arrays (3 MyoD MB, 3 MyoD MT)
- Pax7: two Pax7 antibodies (one monoclonal, one polyclonal), 2 arrays on C2C12 MB (1 monoclonal antibody, 1 polyclonal antibody)
- Rb antibodies: 5 arrays (3 Rb MB, 2 Rb MT)
- Glucocorticoid receptor: 3 arrays
- IgG control antibodies: 11 arrays (6 IgG MB, 5 IgG MT)

The MyoD ChIP-chip has proven most successful, with around 100 downstream targets identified. About 25% of these validated the findings of the other two published ChIPchip studies and our previous Slug candidate gene paper. To date, we have done ChIP validation of two of the novel downstream targets (Rapsn and Hes 6) using real time PCR.

For methylation studies, 6 tiling arrays have been done to date. The complex data is still under analysis.

Future goals: We anticipate writing 1-2 publications on the DoD-supported ChIP-on-chip data over the next few months.

**Aim 2. Show that training of muscle in vivo leads to induction of corticosteroid transcriptional machinery, and an increased metabolic cluster transcriptional response prednisone**.

- Aim 2A. Groups of normal rats will be treadmill-trained daily for 1 month, or reserved as untrained controls. Groups will then be split into corticosteroid treated (bolus 50 mg/kg methylprednisone), and untreated, and sacrificed at times 0, 1 hr, 2 hr, and 8 hr (16 groups, 5 rats/group, 80 rats total). Muscle and liver will be collected.
- Aim 2B. Use expression profiling and quantitative RT-PCR of muscle and liver to confirm our previous findings in untrained rats, and then show that training enables prednisone-mediated transcriptional induction of the metabolic cluster (GOT1, LDHB, PDH). Show that the same transcriptional response cluster (P23, ERR3, EAR2, PKCtheta) is induced by training. (3 animals/group x 16 groups x 2 tissues= 96 microarrays; RT-PCR will be done on all 5 animals/group).
- Aim 2C. Use nucleated temporal clustering of the expression profiles to conduct a “gene discovery” for prednisone-responsive genes in trained vs untrained muscle. This will extend the “increased metabolic economy cluster” beyond our current metabolic cluster. Validate these trained-specific, glucocorticoid responsive downstream candidate genes by RT-PCR or protein studies in muscle, identification of GRE elements in gene promoters, and ChIP studies.
- Aim 2D. Determine the relative activity of the AKT1/FOXO/atrogin1 pathway in trained vs. untrained, and prednisone-treated vs. un-treated muscle.
- Aim 2E. Conduct pilot proteomic studies of soluble fractions of muscle at time 0 vs 1 hr post-prednisone bolus in trained and untrained rats.

Changes in Specific Aim 2:

1. The original protocol proposed treadmill running as the method of training. We have switched to a much better experimental system, synergist ablation. As shown below, this creates a 50% increase in muscle mass within 2 wks, and provides a nicely staged and dramatic induction of the “hypertrophy” response proposed to be studied. Much of Aim 2 had been accomplished in Year 1 using this new model, and was previously reported to the DoD.

2. Aim 2E proposed pilot proteomic studies. Due to rapidly increasing expertise and instrumentation in our Center, we have been able to fast-track this sub-aim, and have made substantial progress in genome-wide

assessment of phoshoproteins in the proteome before and after glucocorticoids. For this newly expanded sub-aim, we have switched to C2C12 cells. Extensive new data obtained in the last year of the award is described below (Aim 2E).

Progress in Aims 2A-2D.

In order to test our hypothesis we implemented an animal model. Twelve Sprague Dawley adrenalectomized rats were randomly assigned to 4 groups: hypertrophied non treated, hypertrophied treated, non hypertrophied non treated and non hypertrophied treated. The hypertrophy was induced by surgical ablation of synergistic muscles. Functional overloading of skeletal muscle induces a compensatory hypertrophy as an adaptive response to increased functional demand. (Johnson TL et al. 1991). The model used for our study consists of a 2 week period of overload of the plantaris muscle (a slow twitch muscle) by removal of the gastrocnemius and soleus muscles. This procedure resulted in a in an average 57% weight increased in overloaded plantaris group vis-à-vis the control (sham) group. See table for detail.

| | SHAM | | | | | |
|---|---|---|---|---|---|---|
| | Untreated | | | Treated | | |
| | Rat 1 at R | 2 at R | 3 at R | 4 at R | 5 at R | 6 |
| Rat Weight (g) | 250 | 230 | 240 | 260 | 245 | 235 |
| Left Plantaris (g) | 0.271 | 0.154 | 0.220 | 0.195 | 0.185 | 0.210 |
| Right Plantaris (g) | 0.250 | 0.194 | 0.220 | 0.223 | 0.155 | 0.223 |
| **Plant./Rat Weight (g/kg)** | **1.042** | **0.757** | **0.917** | **0.804** | **0.694** | **0.921** |
| **Average Plant./Rat Weight (g/kg)** | | | | | | **0.856** |
| | SYNERGISTIC ABLATION | | | | | |
| | Untreated | | | Treated | | |
| | Rat 7 | Rat 8 | Rat 9 | Rat 10 | Rat 11 | Rat 12 |
| Rat Weight (g) | 230 | 265 | 240 | 235 | 290 | 235 |
| Left Plantaris (g) | 0.290 | 0.312 | 0.330 | 0.374 | 0.401 | 0.290 |
| Right Plantaris (g) | 0.337 | 0.305 | 0.350 | 0.331 | 0.363 | 0.340 |
| **Plant./Rat Weight (g/kg)** | **1.363** | **1.164** | **1.417** | **1.500** | **1.317** | **1.340** |
| **Increase in Weight vs. Average SHAM** | **59%** | **36%** | **66%** | **75%** | **54%** | **57%** |

Treatment of animals was done by the administration of 50 mg/kg dose of methylprednisolone sodium succinate via a right external jugular vein cannulation over 30 seconds. Plantaris muscles were collected after 2 hours of the glucocorticoid bolus administration and frozen in liquid nitrogen. Extraction of total RNA was carried out using trizol reagent. The purity and integrity of the total RNA was assessed by 2100 bioanalyzer. RNA was converted to double stranded cDNA using a One cycle cDNA synthesis kit (Affymetrix). The expression profiling was done using Affymetrix rat 230 0.2 arrays. We are currently in the process of data analysis. Raw data will be analyzed with the PLIER probe set algorithmn (Affymetrix), and significant differences based on expression values will be determined with a power-based analysis using Hierarchical Clustering Explorer (http://www.cs.umd.edu/hcil/hce) and GeneSpring (Agilent) software. Differentially expressed genes will then be grouped within annotated networks and canonical pathways using Ingenuity Software (Ingenuity Systems).

The molecular remodeling pathways responsible for both muscle hypertrophy and atrophy have converged on the AKT1/Foxo/atrogin1 pathway (Hoffman and Nader 2004). These pathways do not require

transcription, but are instead based upon protein phosphorylation states. The phosphorylation state of AKT1 in each group was tested by western blot. Muscle samples were homogenized in a buffer (cell lytic MT Sigma) for protein extraction. Halt protease and phosphatase inhibitor cocktails (Pierce) were added. An aliquot of the supernatant was used to measure total protein content using Biorad DC protein assay. Supernatant was then incubated with Laemmli buffer and subjected to SDS-PAGE for subsequent western blot. AKT1 phosphorylation was determined using a phosphospecific antibody against ser473 (rabbit anti-AKT1 phosphorylated at serine 473 Quemicon). Total AKT1 was determined using a rabbit anti AKT1 (Quemicon). Membranes were then incubated with anti-rabbit secondary antibodies conjugated to horseradish peroxidase (Upstate). Proteins inmunoblots were visualized by enhanced chemiluminescence and the bands will be quantified by scanning densitometry. The data to date validates our hypothesis, and we are currently in the process of finishing the statistics on all immunoblots.

Future goals: We have made substantial progress in this aim. The replacement of the treadmill with the synergist ablation has resulted in a much cleaner and staged experimental system, although we have had some trouble keeping the adrenalectomized animals viable after surgery. Thus, we may have to cut down on the time points and number of animals studied.

In the last year of the proposed research, we have attempted on four separate occasions to generate the 7 hr time point data with adequate numbers of rats, but had serious difficultly with viability of the adenalectomized and catheterized rats. At this point, the graduate student, Andreas Baudy, conducting this set of sub-aims, plans to travel to SUNY Buffalo to collaborator Richard Almon who has much more experience with this animal model and experimental methods. While initiation of this set of experiments went much faster than we originally anticipated, completion of the aims has taken much longer. We anticipate completing this aim, and publishing two manuscripts on this data, during the ensuing 12 months following the end of this award.

Aim 2E. Proteomics studies.

Our model of glucocorticoid action includes signaling pathways upstream and downstream of AKT1, and these signaling pathways are largely based upon phosphorylation/kinase activities. Phosphoproteomics is a newly emerging field where the phosphorylation status of most or all proteins can be studied using high throughput mass spectrometers. Here, we have coupled large-scale isolation of phosphoproteins using IMAC, with quantitative assessments of “change” in a time series using SILAC (stable isotope labeling). The use of SILAC is becoming a standard quantitative method but it has only once been done in combination with phosphoproteomics at a single 24 hr time point (Gruhler et al., 2005). As described below, we have accomplished a time series following prednisone application and done quantitative phosphoproteomics. This will not only allow me to capture more phosphoproteins but it might, depending on the sensitivity, allow us measure cause and effect in signaling cascades.

We used stable isotope labeling with amino acids (SILAC) to conduct quantitative proteomic profiling between treated and non-treated myotubes. Myoblasts were fully labeled with $^{13}C_6$-Arg and $^{13}C_6$, $^{15}N_2$-Lys by growing the cells in custom made medium. Concurrently, control cells were grown in normal medium. Cells were differentiated for 5 days prior to Prednisone treatment. Cyclohexamide was used to block downstream translational effects so the only changes seen should be due to translocation and not translation. Unlabeled myotubes were treated with 1µM and both labeled (untreated) and unlabeled (treated) were harvested at the acute time points of 0 minutes, 5 minutes, 15 minutes, and 30 minutes. The unlabeled treated cells were mixed at 1:1 ratio with fully labeled control cells, and then fractionated into their nuclear and cytosolic compartments using a differential detergent extraction method. Protein (100µg) from each fraction was ran on a 1D gel and cut into 35 sections. In-gel digestion and peptide extraction was performed and analyzed by LC-MS and MS-MS. Data was search against the IPI mouse database and rigorously filtered using Xcorr values of 1.9, 2.5, and 3.5 for singly, doubly, and triply charged peptides respectively. Other filters used include a ΔCN of 0.1 and peptide probability of at least 1x10-3. For quantitiation of proteins, the relative abundance of the monoisotopic peak for the labeled to unlabeled peptide was used. A minimum of three different peptide ratios for each

identified protein was required to be included in further analysis. For each protein identified, a mean of the ratios were determined as well as their standard deviation. Data was normalized to 1.0 to account for unequal mixing of labeled and unlabeled cells. To account for protein changes due to the act of labeling and handling, the control time point (0 minutes) was subtracted out from its corresponding values in the other time points. Z-scores and p-values were then calculated for each protein. Significantly altered proteins (greater than a z-score of +/- 10) were further investigated for protein signaling networks using Ingenuity Pathway Analysis.

A summary of the number of proteins included in statistical analysis are listed in Table 1. Not all proteins were recognized by Ingenuity and where therefore not included in pathway analysis. The number of proteins that were identified and used in analysis is found under “Unique” in the table.

**Table 1**:

| **No. Protein Quantitated** | **Cytosol** | **Unique** | **Nucleus** | **Unique** |
|---|---|---|---|---|
| **Control (time 0min)** | 334 | 322 | 318 | 308 |
| **5 minute** | 298 | 287 | 483 | 471 |
| **15 minute** | 404 | 392 | 331 | 321 |
| **30 minute** | 359 | 348 | 329 | 322 |
| **Total** | | 543 | | 642 |

Concurrency of protein identification between the different time points was relatively low. Table 2 summarizes concurrency between the time points for each fraction.

**Table 2:**

| **% Concurrency** | **Cytosol** | **%** | **Nucleus** | **%** |
|---|---|---|---|---|
| **4 of 4** | 196 | 36.1 | 149 | 23.2 |
| **3 of 4** | 88 | 16.2 | 128 | 19.9 |
| **2 of 4** | 102 | 18.8 | 147 | 22.9 |
| **1 of 4** | 157 | 28.9 | 218 | 40.0 |

Proteins with a z-score of +/-10 or greater (equivalent to about a 1.5- or greater fold change) were analyzed with Ingenuity to determine common networks and pathways that are changing. In total, 57 cytosolic and 52 nuclear proteins were included in the final analysis.

For significantly altered proteins in the cytosol, 5 networks with a good score were identified (the score is a numerical value used to rank networks according to how relevant they are to the genes in the input dataset). Table 3 lists what proteins belong to these networks and the top 3 functions associated with these networks. Proteins in bold green represent proteins that were found to significantly increase in the cytosol due to prednisone treatment. Proteins found in bold red were found to be significantly decreased in the cytosol upon treatment.

**Table 3.**

**Cytosol Networks**

| **id** | **genes** | **score** | **focus genes** | **top functions** |
|---|---|---|---|---|
| **1** | **ACTB, ACTN4**, AIP, AKT1, **ANXA4**, **ARCN1**, CDH1, **DNAJB4**, GAST, **HSP90AB1**, IL15, IQGAP1 (includes | **30** | **18** | **Protein Synthesis, Cancer, Tumor Morphology** |

| | | | | |
|---|---|---|---|---|
| | EG:8826), ITGA2B, MRCL3, MYC, MYCN, MYL1, MYL6B, PDCD5, PLS3, RANBP1, RCC1 (includes EG:1104), RPL7, RPL19, RPL22, RPL35, RPS5, RPS9, RPS13, RPS19, RPS4X, SYNPO, TLN1, TPM1, VCP | | | |
| 2 | ACTA2, ACTB, ANXA1, ANXA2, CCT5, CKB, CKM, CLIC4, DYSF, EEF1A1, GDNF, HTR2C, IGF1, IL3, MARCKS, MSN, MYH6, MYH9, MYO1C, MYOG, NCF1, PLA2G1B, PLEC1, PTD004, PYGM, RAN, RPL4, RPL7, RPL10, RPL29 (includes EG:6159), RPS14, RPS19, RPS4X, TCP1, TXNL2 | **28** | **17** | **Cellular Assembly and Organization, Protein Synthesis, Cellular Development** |
| 3 | ACTA2, ACTN1, ANXA3, ANXA5, ANXA6, ARPC2, CALD1, CLIC1, CSRP2, EPB41, F2, FLNA (includes EG:2316), GJA1, HRAS, ITGB6, KSR1, MYH9, MYH11, PACSIN1, PACSIN2, PDLIM1, PDLIM7, PLS3, PROC, PROS1, SMAD5, SOS1, SRF (includes EG:445445), SYN1, TGFB1, TPM1, TPM2, TPM3, TPM4, TRIO | **23** | **15** | **Tissue Morphology, Hematological System Development and Function, Cell Morphology** |
| 4 | AARS, ACTA1, ACTG1, CAP1, CAPG, CD9, CLEC11A, ESD, FGF1, FLNB, FOS, FSCN1, GNB2L1, GP1BA, GSTM5, HNRPC, IFNAR1, IFNAR2, IL4, ITGB1, LDHA, LOC112714, MAP3K5, MIF, NFE2L2, PGAM2, PRDX1, SPI1, THOP1, TLN1, TSC1, TUBB, TXN, TXNRD1, YWHAZ | **21** | **14** | **Cellular Movement, Cell Death, Cell Signaling** |
| 5 | ABCE1, ALDOA, ATBF1 (includes EG:463), BIN1, CDK4, CEBPA, CHI3L1, CLTC, CRYAB, CYP7A1, DNM1, EEF1A2, ENO3, FDPS, FGF19 (includes EG:9965), HSPA8, INSIG1, MYF6, MYH3, MYOD1, NES, PLD1, PLD2, PPARGC1B, RNASEL, SERPINB1, SH3GLB1, SIX1, SMARCA2, SNCA, SREBF1, TNNC1, TNNC2, TNNI1, TNNT2 | **21** | **14** | **Cellular Development, Cell Cycle, Connective Tissue Development and Function** |
| 6 | IFRD1, MYH8 | 2 | 1 | Cell-To-Cell Signaling and Interaction, Nervous System Development and Function, Skeletal and Muscular System Development and Function |

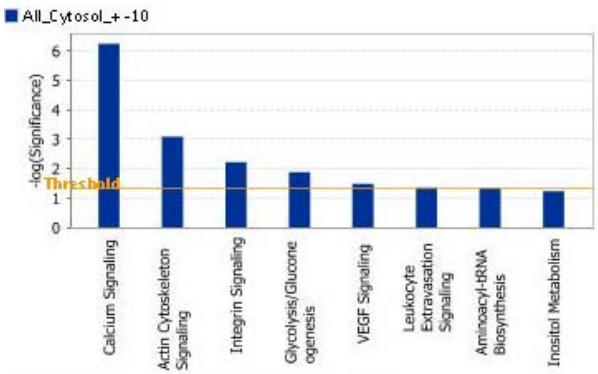


**Figure 1: Top Canonical Pathways for Significantly Changed Cytosolic Proteins.**

For significantly altered proteins in the nucleus, 4 networks with a good score were identified (the score is a numerical value used to rank networks according to how relevant they are to the genes in the input dataset). Table 4 lists what proteins belong to these networks and the top 3 functions associated with these networks. Proteins in bold green represent proteins that were found to significantly increase in the nucleus due to prednisone treatment. Proteins found in bold red were found to be significantly decreased in the nucleus upon treatment.

**Table 4**

**Nuclear Networks**

| id | genes | score | focus genes | top functions |
|---|---|---|---|---|
| 1 | **ACTN3**, **ANXA1**, **ANXA2**, **ANXA3**, ATBF1 (includes EG:463), **CRYAB**, **DES** (includes EG:13346), DYSF, EGFR, FGF10, FN1, GDF2, HNRPA1, HNRPC, HRAS, **HSPB1**, HSPB8, IGF1R, ITGB1BP1, **LRPPRC**, **MYH9**, MYOD1, **NES**, **NME2**, PRTN3, RPL27A, RPS19, S100A1, S100A4, SOS1, **SYNC1**, **TAGLN**, **TNNC2**, **TNNT3**, **TPM4** | **28** | **16** | **Skeletal and Muscular System Development and Function, Tissue Morphology, Cellular Growth and Proliferation** |
| 2 | **ACAA2**, **ACTN1**, ASGR2, **ATP2A1**, C5ORF13, CCL13, **CNN3**, CREB1, **DDOST** (includes EG:1650), ERBB2, **FLNA (includes EG:2316)**, FOXA1, GATA6, HNRPC, HOXC8, HOXD3, IGF1, ITGB6, JAG1, KLF4, **LDHA**, MKL1, **MYH11**, MYOCD, **NDUFA10 (includes EG:4705)**, OPRM1, PDLIM7, PTRF, RPN2, RRAD, SRF (includes EG:445445), **TAGLN**, TGFB1, **TNNT2**, TPM2 | **23** | **14** | **Cell Morphology Renal and Urological Disease, Cancer** |
| 3 | **AHNAK**, **ANPEP**, ATP5F1, **CALD1**, CEBPA, CHI3L1, **CKAP4**, DBN1, **EEF1A2**, IL3, IL6, KRAS, LEP, **MRCL3**, MYCN, **MYO1C**, ND1, ND4, **NDUFS1**, NDUFS5, NDUFS6, NDUFS2 (includes EG:4720), NDUFV2, NFKBIB, RPL4, RPL7, RPL10, | **21** | **13** | **Energy Production, Molecular Transport, Cell Cycle** |

| | | | | |
|---|---|---|---|---|
| | RPL29 (includes EG:6159), RPS19, RPS4X, **SLC25A5**, **SLC3A2, SLC7A5**, SLC7A7, **TPM1** | | | |
| **4** | A2M, ATP5A1, ATP5A2, ATP5B, **ATP5C1**, ATP5C2, ATP5D, ATP5E, ATP5J, ATP5O, CAMK2A, **CLTC**, CTGF, DAB2, **FER1L3**, FOS, HGS, HNRPC, HNRPK, **HNRPU**, HRAS, **HSP90B1**, **KBTBD10**, **LRP1**, MLF1, NUMB, PLAT, PLAUR, **RPLP2**, RPLP0 (includes EG:6175), SHC1, VWF, XRCC5, YAP1, YWHAZ | **11** | **8** | **Cell Death, Cellular Function and Maintenance, Cellular Development** |
| **5** | AOF2, **IMMT** | 2 | 1 | Gene Expression |
| **6** | **RAB14**, SMARCB1 | 2 | 1 | Cancer, Cell Cycle, Renal and Urological Disease |

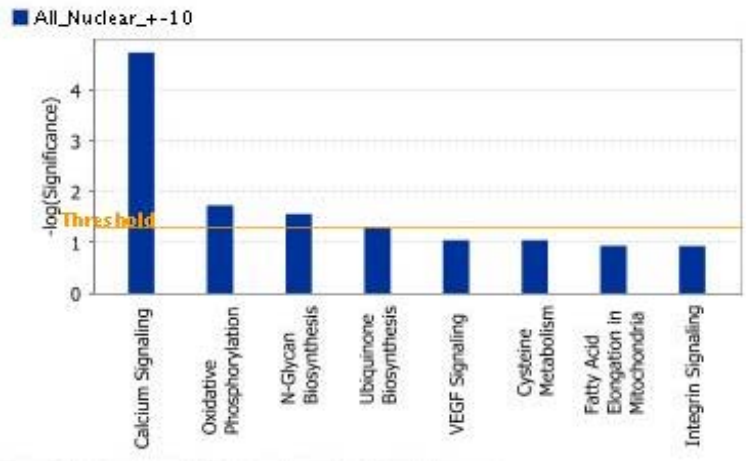


**Figure 2: Top Canonical Pathways for Significantly Changed Nuclear Proteins.**

A few proteins such as EEF1A1 and CRYAB appear to be translocating between the nucleus and the cytosol. However, majority of the proteins did not show a change in one subcellular fraction and a concurrent opposite change the other indicating that they are translocating to other subcellular compartments not quantitated (ie membrane organelles, cytoskeleton, etc). Other experiments will need to be carried out to determine where these proteins are translocating. Overall, it is not surprising based on previous literature that pathways such as calcium signaling and protein synthesis are affected. Novel pathways not previously described and will be of focud for follow-up studies include oxidative phosphorylation, actin cytoskeletal signaling, and integrin signaling.

**Future Goals**

Significant progress has been made in this sub-aim, quite above and beyond that originally proposed in the original grant application. Validation experiments using other techniques are required to confirm results discovered using this proteomic approach. Validation experiments using other techniques will be carried out in

primary muscle cells to determine biological relevance as well as confirm results found. We anticipate 3 publications emanating from this Aim 2E over the following few months.

**Aim 3. Demonstrate that the membrane dystrophies (dystrophinopathies, sarcoglycanopathies) are able to show prednisone-induced activation of the metabolic cluster in muscle without pre-training. Moreover, show that denervation of dystrophic muscle ablates this prednisone-induced metabolic cluster.**

- Aim 3A. Dystrophic mice (mdx [dystrophin deficient], and beta-sarcoglycan deficient [colony currently maintained at our Center]), and normal control strains will have one leg denervated at 3 months of age.
- Aim 3B. Use expression profiling and quantitative RT-PCR of all 72 mice, and show that innervated dystrophic muscle mimics the molecular response of "trained" normal muscle (Aim 1), while denervated dystrophic muscle mimics the response of "untrained" normal muscle.
- Aim 3C. Determine the relative activity of the AKT1/FOXO/atrogin1 pathway in all 24 groups (3 genotypes, denervated/innervated, and prednisone-treated vs. un-treated muscle). This will be done by measuring transcript levels of the "atrogenes" (atrogin1, MuRF1), and phosphorylation state of AKT1 using phosphorylation-specific antibodies (already in hand).

With the rapid expansion and extensive work on the high throughput proteomics in Aim 2E, we have de-prioritized the proposed work in this Aim. We felt that the results from Aim 2E were both more technically innovative and significant, compared to the more descriptive experiments proposed in Aim 3. Thus, we will not be able to carry out Aim 3 under the auspices of this concluded research.

**Key Research Accomplishments**

- ChIP-on-chip methods established for promoter occupancy screens
- Synergist ablation model for hypertrophy established.
- Initial group of 20 adrenalectomized rats completed.
- mRNA profiling of 15 minute time point synergist ablation/glucocorticoids completed, 45 minute underway.
- Phosphoproteome methods established, and initial pathways downstream of glucocorticoids have been defined.
- Scans for prednisone-induced phosphorylation completed

**Reportable Outcomes**

We anticipate that approximately 5 manuscripts will derive from the DoD-supported research over the next year. This project has involved new cutting-edge developments of methods that are considered state-of-the-art, both in molecular genetics (ChIP-on-chip, methylation assays), and proteomics (proteomic profiling, phosphoproteome). While the laboratory publishes quite frequently (about 20 publications/year), our publications on this particular DoD-supported project have been slower than usual due to the extensive technology development required.

**Conclusions**

Progress has been made in Aims 1 and 2, with new methods in proteomic profiling and phosphoproteomics significantly expanding the Aim 2E subaim. Aim 3 was not initiated due to the more descriptive nature of these experiments, and the great expansion of proteomics work in Aim 2E.

## References

1- Hoffman EP, and Nader G. Balancing muscle hypertrophy and atrophy; Nature Medicine 2004 June; Vol 10, No6: 584-5.
2- Johnson TL, and Klueber KM. Skeletal muscle following tonic overload: functional and structural analysis. Med Sci Sports Exerc. 1991 Jan;23(1):49-55.
3- Kettelhut, I.C., Wing, S.S., Goldberg, A.L. 1988. Endocrine regulation of protein breakdown in skeletal muscle. Diabetes Metab Rev. 4:751-772.

## Appendices

**n/a**

# Sub-Project #3**
# Efficacy of cord blood transplantation into muscle
# (John Day)

** Note that this subproject was completed February 2008. The following is a reiteration of the final report. There are no additional updates.

## Introduction

Several hundred Minnesota patients who had successful engraftment of cord blood donor cells subsequently died, providing autopsy specimens for our investigation of cord blood cell engraftment and differentiation into somatic tissues. Since Duchenne muscular dystrophy directly affects multiple organs and body systems (e.g., skeletal and cardiac muscle, eye, brain, gut), the rate of successful engraftment in different tissues is important to assess the utility of cell based treatments for this disease. Since these subjects had successful hematapoietic recovery, the degree of engraftment in bone marrow will provide a maximal value for successful chimerization against which results for other organs can be measured. The specific aims of this proposal include: 1) use of genetic markers to quantify the number of donor cord blood cells present in various tissues of recipients from biopsies or autopsies; 2) use of histological methods to identify donor cord blood cells in various tissues; 3) use of histological methods to determine whether donor cells differentiate into various tissues, including muscle, heart, central nervous system and bone marrow; 4) identification of engrafted multipotent adult progenitor cells (MAPCs) in recipients, using the same methods and investigating tissues available from biopsies of patients or in their tissues at autopsy should they die.

## Body

### Specific Aim 1: 1) use of genetic markers to quantify the number of donor cord blood cells present in various tissues of recipients from biopsies or autopsies.

PCR based assay of Y-chromosome content in recipient tissue

We have procured autopsy tissues of multiple organs from female recipients of male cord blood donors and have extracted DNA from formalin-fixed and paraffin-embedded material. We have optimized extraction of DNA from small amounts of fixed embedded tissue, and developed and refined methods to identification of Y-chromosomes by PCR amplification, and have begun to quantify the number of engrafted cord blood cells in each specimen. In some tissues the number of donor derived cells is apparently quite low, so that genetic validation of donor DNA is difficult, PCR being performed on DNA with extremely low concentration of template strands. We have initiated quantitative PCR, which will allow more precise determination of relative donor cell content in the various tissues.

PCR primers for SRY, present on the Y-chromosome and thus only from donor cells in these female patients, were amplified with a nested PCR combination that provided both specificity and sensitivity for this assay. The initial six specimens showed results as recorded in the table; PCR results are evident in figure 1 for SRY (left) and the housekeeping gene, HPRT (right), demonstrating the utility of DNA extracted from this fixed, paraffin-embedded tissue, and the qualitative presence of donor cells (the negative result for SRY in 02-083 liver may be due to inadequate DNA, given faint HPRT in that specimen).

| Donor Y Chromosome Presence in Female Recipients | | |
|---|---|---|
| **Patient Number** | **Tissue Source** | **SRY gene Present** |
| **02-083** | **Liver** | **-** |
| **02-116** | **Liver** | **+** |
| **02-083** | **Spleen** | **+** |
| **02-116** | **Spleen** | **+** |
| **02-083** | **Cardiac** | **+** |
| **02-116** | **Cardiac** | **-** |

**Figure 1**

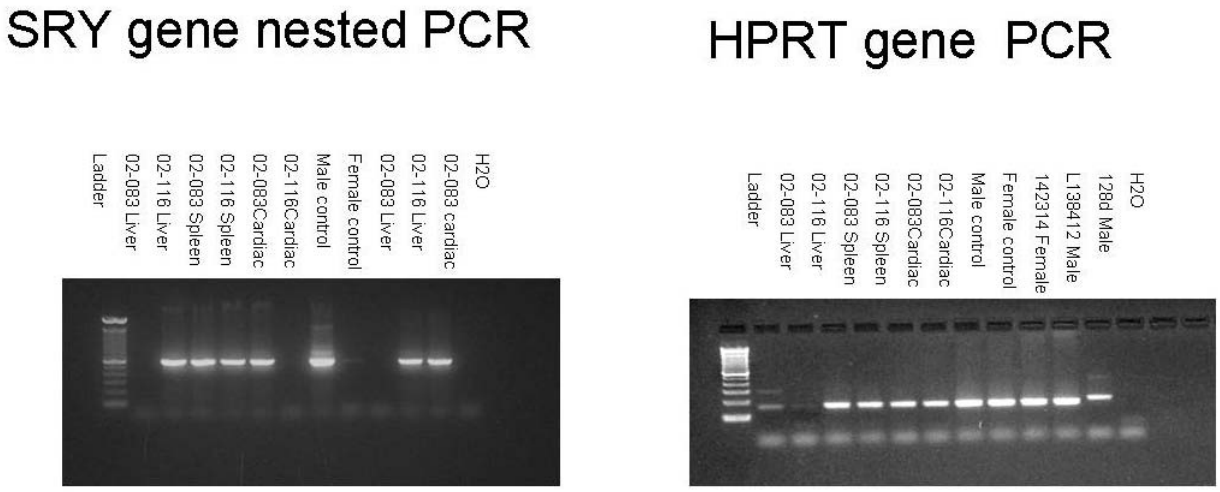


Future Goals for Specific Aim 1

As reported last year, we have developed small pool PCR techniques and have initiated studies that use small pool PCR to better define the extent of Y-chromosome donor cell engraftment in various tissues of recipients, providing a measure of donor engraftment efficacy in the various tissues. We will also continue working with the cord blood donor program to assure that all relevant material is being harvested and effectively preserved from autopsies of affected individuals. Now that we have demonstrated the qualitative presence of SRY gene in the above tissue, we will proceed to quantitate the relative amounts of that DNA in each tissue using Real Time quantitative PCR. Both SRY gene and DFFRY gene from the Y chromosome will be used as well as hTert and HPRT genes as controls.

Specimens have been procured from six additional patients and four control patients, and the above assays will be repeated on the new tissue, as will the new quantitative studies.

**Specific Aim 2: Use histological methods to identify donor cord blood cells in various tissues.**

We have now developed the specific FISH and IF methods necessary for characterization of Y-chromosome donor cells in recipient tissue. Figure 1 shows control muscle, with IF of desmin (green), and red fluorophore FISH of the Y-chromosome. Some cells had clear FISH labels, but non-specific orange artifacts obscured the finding. Consequently we have also used a green fluorophore label of the Y chromosome (Figure 2), which in some tissues is more specific; in the female cord blood cell recipient (Figure 3) Y-chromosome-positive donor cells are identified, some of which contain the cytoplasmic protein beta-actin. .

**Figure 2**

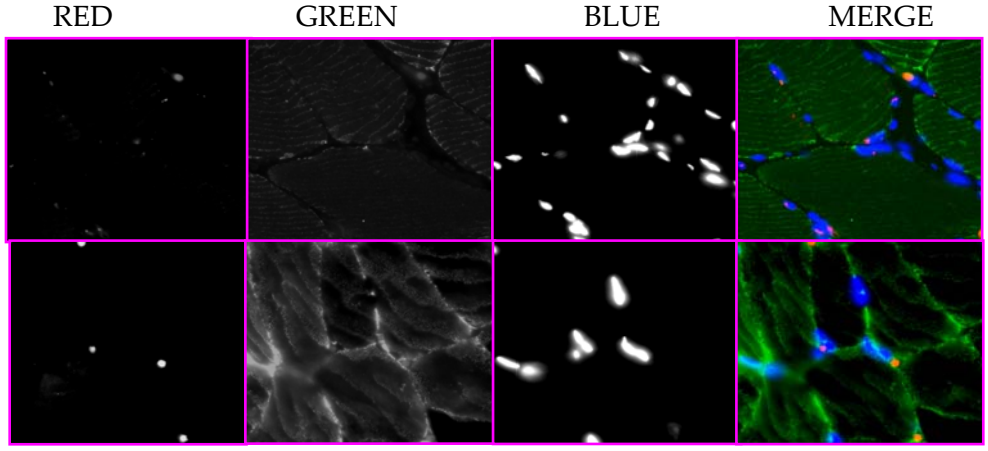


Red – Y chromosome probe
Green – Desmin
Blue - Nucleus

Future Goals of Specific Aim 2.

Our primary histotechnician left the laboratory shortly after onset of funding for this project, but was replaced 6 months ago, so that all work is moving forward well. We will continue to increase the sensitivity of the FISH assay, working to refine the histological preparation of tissue by thinner sectioning of the tissue and pretreatment to increase probe access to nuclei, as well as developing more sensitive DNA probes.

**Specific Aim 3: Use of histological methods to determine whether donor cells differentiate into various tissues, including muscle, heart, central nervous system and bone marrow.**

We have now demonstrated cytoplasmic markers of somatic differentiation in donor cells that are identified by Y-chromosome FISH (Figure 3). We have treated sections to increase FISH probe access to nuclei, but that has also interfered with some IF studies. Antibodies to cytoplasmic rather than cell surface markers have to date been easier to use for the IF studies in some tissues. We are continuing to improve the sensitivity of the FISH probe so that treatment of the sections can be milder, which will improve the characterization of cells possible by IF.

**Figure 3**

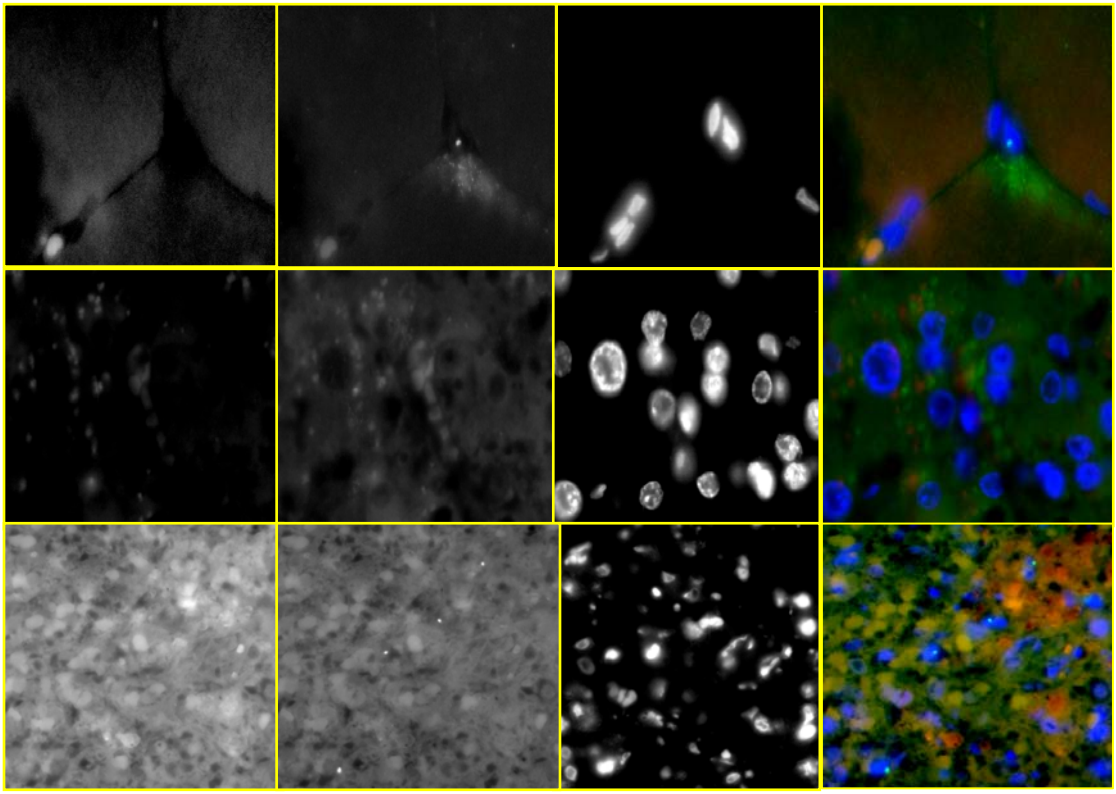


Red – Beta-actin
Green – Y chromosome probe
Blue - Nucleus

Future Goals of Specific Aim 3

Having now identified donor cells in recipient tissue, we will expand the characterization of the cells by immunofluorescence to cytoplasmic and cell surface markers.

**Specific Aim 4: Identification of engrafted multipotent adult progenitor cells (MAPCs) in recipients, using the same methods and investigating tissues available from biopsies of patients or in their tissues at autopsy should they die.**

To date no tissue from MAPC engrafted recipients has become available to study, but we are continuing to work with the Blood and Marrow Transplantation program at the University of Minnesota to assure that we receive appropriate tissues as they become available. Having now developed the methods for cord blood cells, we anticipate that studies with MAPCs will proceed with relatively minor adaptations..

Future Goals of Specific Aim 4
We are continuing to work with the BMT program to identify appropriate MAPC recipients and to procure all relevant tissues as they become available.

**Key Research Accomplishments**

- Procurement of additional autopsy material from 3 females successfully engrafted by male cord blood donor cells.
- Increasingly successful extraction of DNA from fixed tissue of these female cord blood cell recipients
- Successful PCR amplification of Y-chromosome DNA from donor cells in recipient tissues
- Successful development of Y-chromosome FISH and IF of recipient tissues verifying the presence of donor cells, some with evidence of differentiation.

**Reportable Outcomes**
None at this time

**Conclusions**
The tissue from recipients of cord blood cells shows at least low levels of engraftment in somatic tissues, with some evidence of donor cell differentiation. These studies will help determine the extent of donor cell engraftment and somatic cell differentiation of cord blood cells in various recipient tissues.

**Appendices**
None

# Sub-Project #4**
# Understanding the role of FKRP in dystoglycan processing: Relevance to muscular dystrophies with glysosylation defects
# (Kevin Campbell)

** Note that this subproject was completed February 2007. The following is a reiteration of the final report. There are no additional updates

## Introduction

A stable interaction between a muscle cell and its surrounding extracellular matrix is essential for normal muscle activity. When the muscle membrane to matrix interaction is weakened, as in a number of muscular dystrophies, muscle is more easily injured and accumulates muscle damage. A muscle cell is linked to the matrix primarily via the protein dystroglycan which spans the cell membrane and directly binds to laminin in the extracellular matrix. The post-translational addition of specific sugar moieties to the extracellular α-dystroglycan is necessary for laminin binding, and defects in proteins necessary for this modification lead to a group of diseases known as dystroglycanopathies (Barresi and Campbell, 2006). Patients with mutations in fukutin-related protein (FKRP), a putative sugar modifying enzyme, exhibit dystroglycanopathy muscle disease with disruption of the dystroglycan-laminin interaction. However, currently little is known about the role of FKRP in dystroglycan sugar processing. Our goal is to better understand how FKRP expression impacts α-dystroglycan modification and function by: i) assessing α-dystroglycan activity with functional depletion of FKRP; ii) determining the effect of increased FKRP activity on α-dystroglycan processing and function, and exploring the treatment potential of FKRP gene therapy; and 3) determining the functional domains involved in α-dystroglycan-FKRP processing and identifying FKRP-interacting proteins. During the period of DOD grant support, we have achieved significant progress. In particular, we have assessed the potential for shRNA knockdown as a means to model FKRP disease in cell culture, analyzed the effect of FKRP overexpression on dystroglycan glycosylation and laminin binding, and attempted to identify binding interactions between FKRP and other proteins that function in dystroglycan processing. We are confident that our research progress in this area will enhance and promote our current understanding of the cellular role of FKRP and its functional interaction with dystroglycan. With these advances, we will be better equipped to manage and treat specific forms of muscular dystrophy and to understand muscle strength and endurance in military recruits.

**BODY**

### Specific Aim 1: To assess α-dystroglycan activity with functional depletion of FKRP, and develop a cell-based model for FKRP-related muscular dystrophies.

The goals of aim 1 and our research findings are detailed below.

a) Obtain FKRP RNA oligonucleotides and short hairpin RNA plasmids to optimize FKRP knockdown

In order to facilitate screening of shRNA plasmids directed against various regions of the FKRP mRNA, we cloned a mouse FKRP expression construct into an ires GFP expression vector to allow FKRP and GFP coding sequences to be transcribed onto a single mRNA. This allows us to use shRNA against GFP as a positive control for successful knockdown and enables us to test FKRP knockdown in a recombinant system. Initially, three shRNA plasmids (simFKRP-A, simFKRP-B, and simFKRP-C) targeted to different regions of the FKRP mRNA were cloned into an Adenovirus 5 shuttle vector under control of the cytomegalovirus (CMV) promoter.

The FKRP shRNA plasmids were cotransfected with FKRPiresGFP in TSA cells at a ratio of 10:1. We assessed GFP fluorescence of live cells and prepared cell lysates for western blotting to measure FKRP knockdown (the anti-FKRP antibody is described in Aim 2). From this initial screen, we identified shRNA

construct simFKRP-A as the most promising, with knockdown efficiency comparable to that of the standard GFP knockdown shRNA (see Fig. 1A).

b) Analyze α-dystroglycan glycosylation with FKRP knockdown

After selection of simFKRP-A for further shRNA experiments, this plasmid was recombined into Adenovirus 5 (with GFP marker) and virus particles were generated by the University of Iowa Gene Transfer Vector Core facility (see Fig.1B). We then tried various infection protocols to achieve FKRP knockdown in C2C12 myotubes. In a preliminary experiment, application of 500 MOI Ad5simFKRP-A during the first 48hr of C2C12 differentiation led to extensive green fluorescence and decreased α-dystroglycan glycosylation (assessed by western blotting). Suggesting that viral FKRP shRNA delivery may be suitable to model FKRP deficient muscular dystrophy. However, in multiple repeat experiments, these results could not be reproduced. In fact, we were unable to achieve significant infection levels with the simFKRP-A shRNA virus in subsequent experiments even with increased viral particles and multiple infections as demonstrated by the minimal GFP fluorescence in Ad5simFKRP-A/eGFP infected cells (Fig. 3A). Western blotting for protein expression confirmed the poor infection as there was no change in endogenous FKRP expression or α-dystroglycan glycosylation in the Ad5simFKRP-A/eGFP treated cells (Fig. 3B, mock vs Adsim-A).

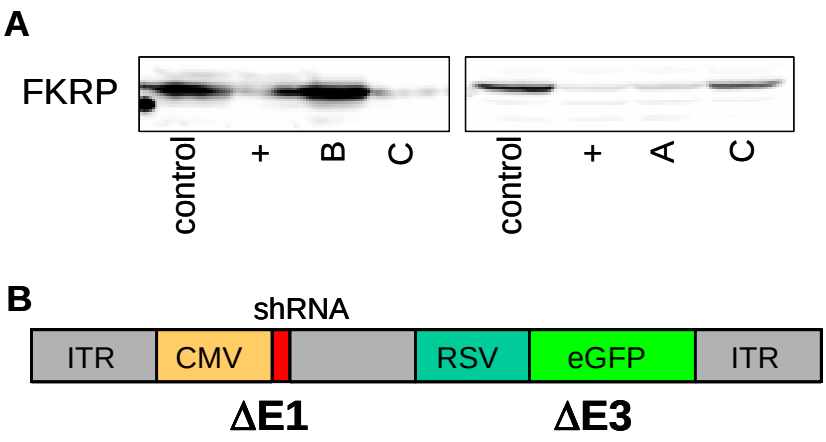


**Fig. 1**: Testing shRNA knockdown of recombinant FKRP expression. **A**, Immunoblot analyses of FKRP expression in TSA cell lysates transfected with mouse FKRPiresGFP and shRNA constructs A, B, and C against FKRP. + is a positive control for mRNA knockdown. SimFKRP-A showed the most effective knockdown of FKRP protein expression in our experiments. **B**, simFKRP-A shRNA in an adenoviral shuttle vector was used to generate Ad5simFKRP-A virus particles. Short hairpin loop FKRP RNA and eGFP expression are driven by the cytomegalovirus (CMV) and Rous sarcoma virus (RSV) promoters, respectively. ITR, inverted terminal repeat (viral sequence).

c) Assess laminin binding by α-dystroglycan in FKRP RNAi treated cells

As we have not yet achieved reliable FKRP knockdown, we are presently unable to assess α-dystroglycan laminin binding in an FKRP knockdown model. We intend to conduct these experiments when the technical difficulties have been resolved.

Significance and Future Goals

The failure of our FKRP shRNA knockdown experiments is a setback. However, the minimal GFP expression in treated cells suggests that the problem is due to poor viral delivery of the shRNA, not necessarily a problem with the shRNA itself. Thus, the shRNA simFKRP-A construct still has significant potential, we simply have to better deliver it into cells. We think that our current lot of Ad5simFKRP-A virus may have lost efficacy. Therefore, we will generate a new batch of virus for testing.

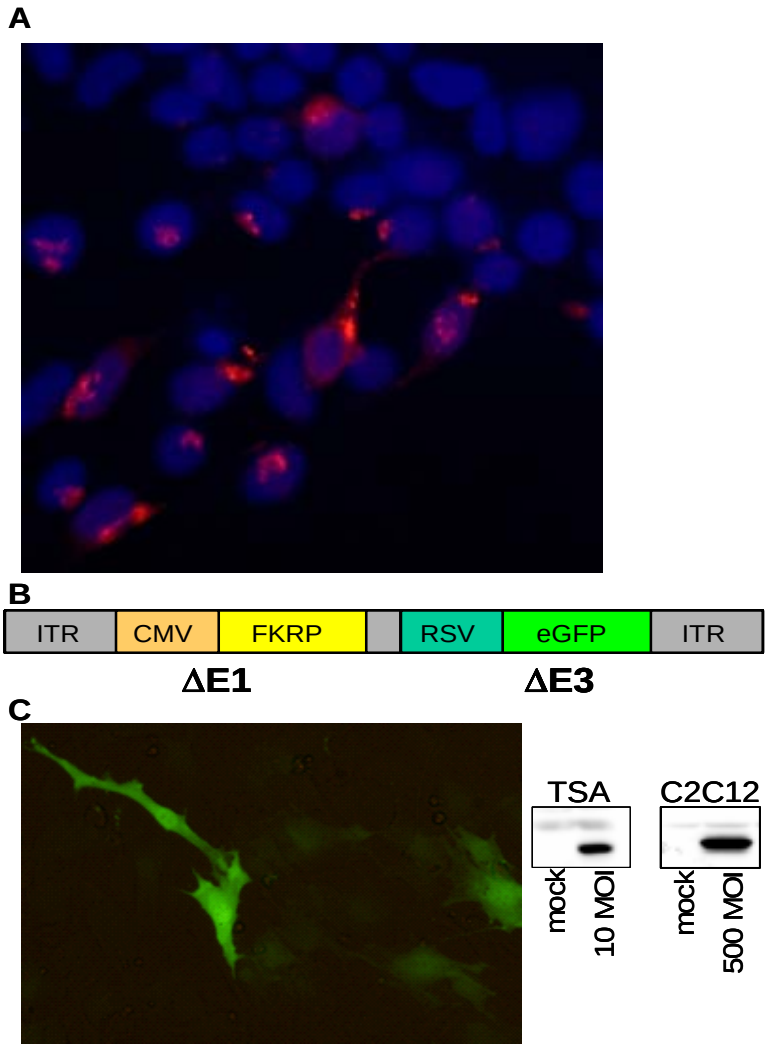


**Fig. 2**: Recombinant FKRP expression in cultured cells. **A**, Immunofluorescence with anti-FKRP (Rbt 341) detects mouse FKRP expression (red) in transfected TSA cells. FKRP staining is consistent with localization to the Golgi apparatus. Nuclei are stained with DAPI (blue). Rabbit secondary antibody control does not stain replicate cells (data not shown). **B**, Ad5-FKRP/eGFP adenoviral construct. FKRP and eGFP expression is driven by the cytomegalovirus (CMV) and Rous sarcoma virus (RSV) promoters respectively, ITR, inverted terminal repeat (viral sequence). **C** (left), Adenoviral infection of cultured cells was demonstrated by eGFP fluorescence in differentiated C2C12 myotubes. Right, recombinant FKRP was detected by anti-FKRP (Rbt 341) on western blots in Ad5CMV-FKRP-eGFP infected TSA cell and C2C12 myotube lysates.

**Specific Aim 2: To determine the effect of increased FKRP expression on α-dystroglycan processing and function, and explore the treatment potential of FKRP gene therapy.**

The goals of aim 2 and our research findings are detailed below.

a) Develop FKRP adenovirus and FKRP adeno-associated virus constructs for FKRP gene delivery

*FKRP antibody*

In order to detect FKRP endogenous and recombinant expression, and test the efficacy of various FKRP viral constructs, we first developed a rabbit polyclonal antibody against the C-terminus of mouse FKRP (Rbt 341). We have optimized affinity purification of this antisera to improve detection and specificity. This antibody detects FKRP protein by immunofluorescence (Fig. 2A) and immunoblot of cells expressing recombinant FKRP (as shown in Fig. 2C). anti-FKRP antibody also detects endogenous FKRP protein in enriched preparations (see below, Fig. 3B). With this antibody, we can now confirm FKRP overexpression in Aim 2 experiments.

*FKRP viruses*

We have generated an adenovirus expressing the human FKRP cDNA under control of the CMV virus (see Fig. 2B). We have subsequently tested FKRP expression by viral infection of TSA and muscle C2C12 cell cultures. We are able to detect virus infection of differentiating C2C12 myotubes in culture, as demonstrated by GFP fluorescence in Fig. 2C. By immunoblot, we are able to detect FKRP overexpression in lysate preparations in both cell types tested (see Fig. 2C).

We were also developing an adeno-associated virus (AAV) with the human FKRP cDNA under control of the rous sarcoma virus (RSV) promoter. However, in using the AAV system for muscle delivery of other proteins, we found that the protein expression efficacy of AAV was much weaker than similar adenoviral constructs. For this reason, we are not pursuing the AAV-FKRP virus at this time. However, we may resume this work in the future.

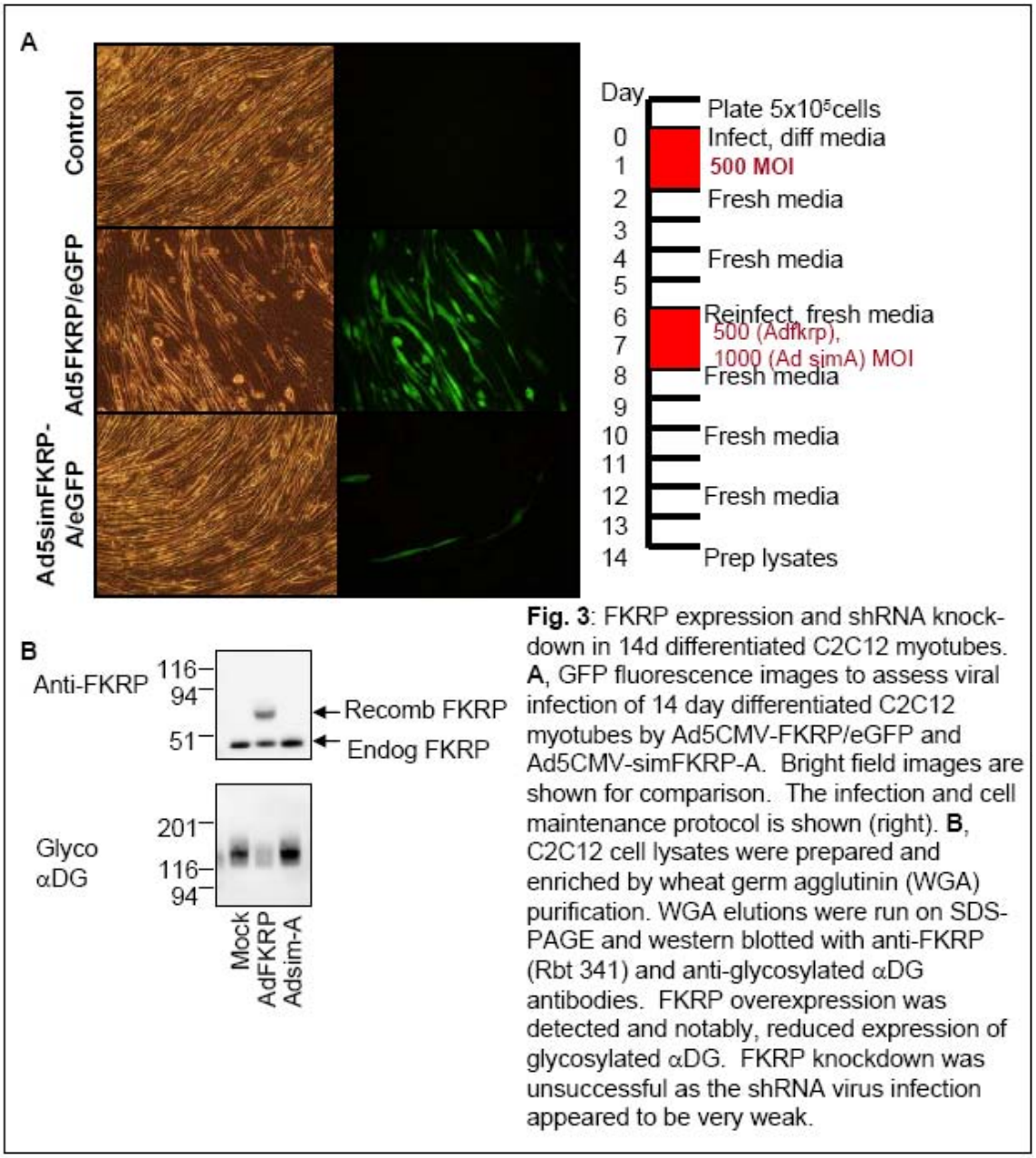


**Fig. 3**: FKRP expression and shRNA knock-down in 14d differentiated C2C12 myotubes. **A**, GFP fluorescence images to assess viral infection of 14 day differentiated C2C12 myotubes by Ad5CMV-FKRP/eGFP and Ad5CMV-simFKRP-A. Bright field images are shown for comparison. The infection and cell maintenance protocol is shown (right). **B**, C2C12 cell lysates were prepared and enriched by wheat germ agglutinin (WGA) purification. WGA elutions were run on SDS-PAGE and western blotted with anti-FKRP (Rbt 341) and anti-glycosylated αDG antibodies. FKRP overexpression was detected and notably, reduced expression of glycosylated αDG. FKRP knockdown was unsuccessful as the shRNA virus infection appeared to be very weak.

b) Optimize FKRP expression by viral delivery in tsA-201 and differentiated C2C12 myotube cultures

We tested various conditions for viral delivery to differentiating C2C12 cells. Single or dual 48 hour infection protocols with 14 day differentiation and single infection with 6 or 7 day differentiation were tried. We successfully detected recombinant wild-type FKRP in C2C12 samples with all of these protocols as demonstrated by GFP fluorescence (Fig. 3A, Ad5FKRP/eGFP) and western blotting of WGA enriched proteins (Fig. 3B). In addition, a smaller molecular weight band, believed to be endogenous muscle FKRP was detected in uninfected and infected samples (Fig. 3B, endog FKRP).

We also developed a virus for expression of an FKRP construct with a C-terminal 2x FLAG tag. This virus recapitulated our findings with the wild-type FKRP virus: it produced abundant infection and successfully overexpressed the recombinant FKRP (data not shown). Both viruses were used for analysis of α-dystroglycan glycosylation and laminin binding.

c) Analyze endogenous and expressed α-dystroglycan glycosylation and laminin binding with FKRP overexpression

Mock and Ad5FKRP/eGFP infected C2C12 14 day differentiated myotube lysates were enriched by WGA purification and separated by SDS-PAGE (note, Ad5simFKRP-A shRNA results are described above). We used an antibody against a glycosylated epitope of α-dystroglycan (antibody IIH6) to determine effects of FKRP on dystroglycan sugar structures. Contrary to our hypothesis, FKRP overexpression decreased detection of glycosylated α-dystroglycan and slightly reduced α-dystroglycan molecular weight (Fig. 3B). These results were reliably replicated across a number of experiments. To exclude the possibility that viral protein expression alone affects α-dystroglycan processing, we also tested C2C12 cells infected with a GFP expression virus (Ad5eGFP) versus the Flag-tagged FKRP virus (Ad5C-FKRP/eGFP), differentiated for 6 days and enriched with WGA purification. As shown in Fig. 4, α-dystroglycan glycan antibody IIH6 and another glycan-recognizing antibody VIA4-1 both showed reduced staining of FKRP infected samples.

To measure α-dystroglycan functional activity, we also tested α-dystroglycan laminin binding in Ad5eGFP and Ad5C-FKRP/eGFP C2C12 samples using the laminin overlay assay. In agreement with the glycosylated antibody results, we found that α-dystroglycan laminin binding was also reduced with FKRP overexpression (Fig. 4, bottom). These laminin binding data are still preliminary and further experiments will be done to confirm these findings.

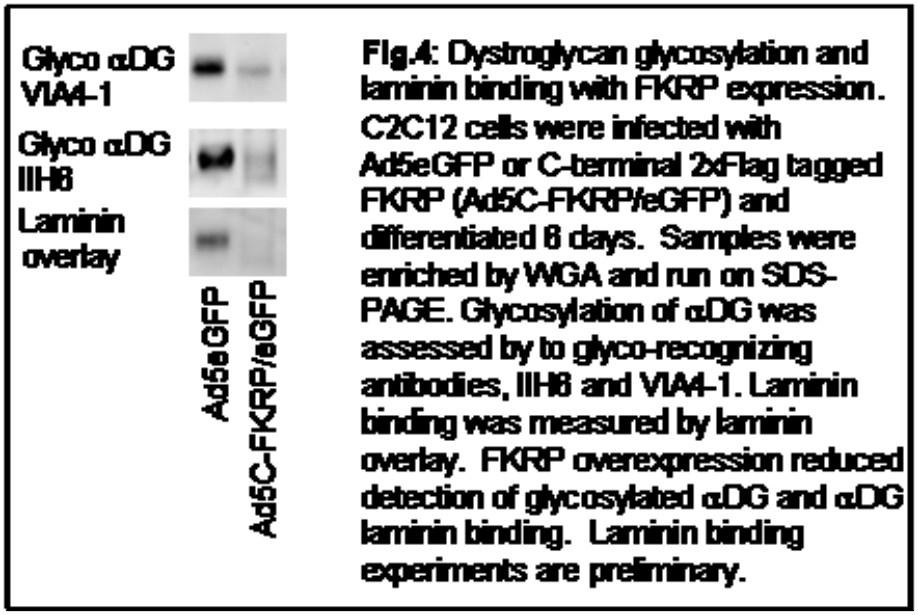


**Fig.4: Dystroglycan glycosylation and laminin binding with FKRP expression. C2C12 cells were infected with Ad5eGFP or C-terminal 2xFlag tagged FKRP (Ad5C-FKRP/eGFP) and differentiated 6 days. Samples were enriched by WGA and run on SDS-PAGE. Glycosylation of αDG was assessed by to glyco-recognizing antibodies, IIH6 and VIA4-1. Laminin binding was measured by laminin overlay. FKRP overexpression reduced detection of glycosylated αDG and αDG laminin binding. Laminin binding experiments are preliminary.**

Significance and Future Goals

Patients with moderate to severe FKRP mutations demonstrate reduced α-dystroglycan glycosylation and laminin binding. Therefore, consistent with other dystroglycanopathy diseases, loss of glycosyltransferase or putative glycosyltransferase activity is believed to reduce the addition, branching or modification of α-dystroglycan sugar structures; and all identified mutations are believed to be loss of function mutations. Alternately, protein expression has been demonstrated to enhance α-dystroglycan glycosylation or directly add sugars to α-dystroglycan for dystroglycanopathy-linked genes POMT1, POMGnT1, LARGE and LARGE 2 (Manya et al., 2004; Barresi et al., 2004; Brockington et al., 2005; and Grewal et al., 2005), indicating that these proteins are directly or indirectly involved in sugar additions to dystroglycan. Our findings that FKRP overexpression also reduces α-dystroglycan glycosylation and laminin binding are very interesting. First, they suggest that FKRP activity may be mechanistically distinct from other dystroglycanopathy related proteins. Second, they suggest that FKRP is not directly involved in the addition of sugars to α-dystroglycan OR that FKRP adds or modifies sugars in such a way as to minimize or limit the addition of IIH6 or VIA4-1 glycoepitopes. Notably, the shift in α-dystroglycan molecular weight with FKRP overexpression is much smaller than the shift typically observed in patients indicating that α-dystroglycan posttranslational modification still occurs, albeit differently. Regardless, these data indicate that it may be possible to have gain of function or dominant negative FKRP effects and future studies will be enlightening as to the mechanisms of FKRP action. In the future, we will confirm our findings of FKRP overexpression effects on α-dystroglycan laminin binding, and will examine the consequences of FKRP overexpression on α-dystroglycan binding to other extracellular matrix partners.

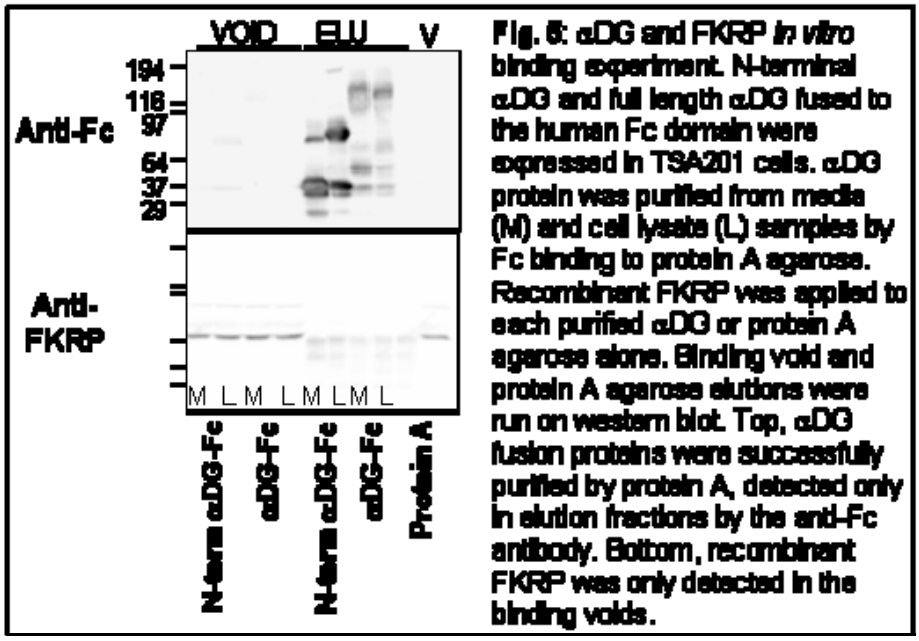


**Fig. 6: αDG and FKRP *in vitro* binding experiment. N-terminal αDG and full length αDG fused to the human Fc domain were expressed in TSA201 cells. αDG protein was purified from media (M) and cell lysate (L) samples by Fc binding to protein A agarose. Recombinant FKRP was applied to each purified αDG or protein A agarose alone. Binding void and protein A agarose elutions were run on western blot. Top, αDG fusion proteins were successfully purified by protein A, detected only in elution fractions by the anti-Fc antibody. Bottom, recombinant FKRP was only detected in the binding voids.**

**Specific Aim 3: To determine the functional domains involved in α-dystroglycan-FKRP processing and identify FKRP-interacting proteins.**

The goals of aim 3 and our research findings are detailed below.

a) Develop a series of FKRP deletion constructs

We created a cDNA construct of mouse FKRP lacking the N-terminus and transmembrane domain for bacterial expression. A GST cDNA was attached to the 5' of FKRP to enable purification. Inducible expression of the GST-FKRP (-TM) construct in bacteria produced a strong band. However, the expressed GST-FKRP fusion protein has poor solubility as it is found predominately in insoluble fractions, and appears to undergo proteolysis (data not shown). Consequently, we redirected our strategy to use FKRP constructs tagged with the FLAG epitope.

We first designed a wild-type mouse FKRP construct in pcDNA for mammalian expression. The construct was transfected into TSA 201 cells and efficiently produced recombinant FKRP protein (see Fig. 2A and Fig. 5, lower blot). Next, this mouse FKRP was used as a template to develop tagged FKRP constructs. Two FLAG

epitopes in tandem were added to the N- or the C-terminus of mouse FKRP using two cycles of PCR engineering (see Figure 6, top). The FLAG-tagged FKRP cDNAs were then inserted into pcDNA3 vector for mammalian expression. The FLAG-tagged FKRP expression constructs were transfected into TSA cells to test for protein expression. Both the N-terminal and C-terminal tagged FKRP proteins are overexpressed in cell lysates and can be detected by the FLAG M2 monoclonal antibody (Sigma) or the polyclonal FKRP antibody (see Figure 6, right). We have also purified the FLAG-tagged FKRP protein from cell lysates using FLAG M2 coupled affinity gel (Sigma).

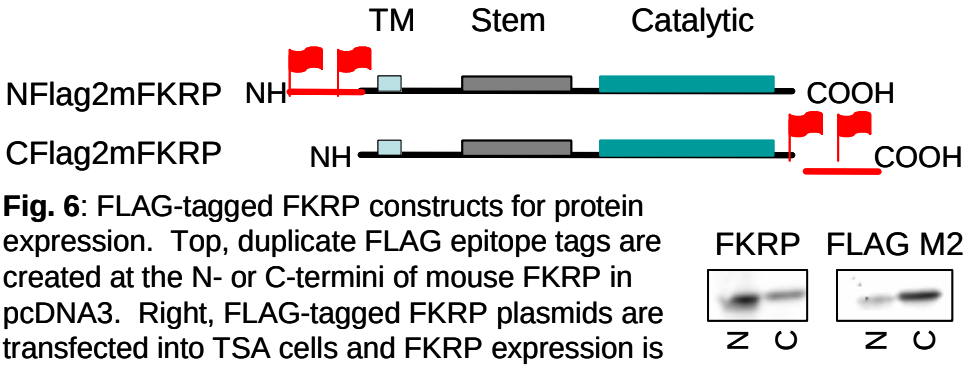


**Fig. 6**: FLAG-tagged FKRP constructs for protein expression. Top, duplicate FLAG epitope tags are created at the N- or C-termini of mouse FKRP in pcDNA3. Right, FLAG-tagged FKRP plasmids are transfected into TSA cells and FKRP expression is detected by FKRP and FLAG antibodies. N indicates NFlag2mFKRP; C indicates CFlag2mFKRP.

Given the insolubility of the GST-FKRP protein, we planned to develop FKRP mutants and deletion constructs using the N-terminal FLAG tagged mouse FKRP cDNA. In fact, with great difficulty, we created a virus particles for expression of FKRP with the common LGMD2I patient mutation, L276I, in the NFLAG2FKRP backbone. However, the University of Iowa Gene Transfer Vector Core was unable to produce viral recombination for the control NFLAG2FKRP construct. It is believed to form secondary structures that inhibit recombination and thus is not efficient for generation of virus particles. Therefore, NFLAG2FKRP is not a suitable background for developing FKRP mutants or deletions, and no further NFLAG2 based constructs were attempted. We are currently exploring options for other N-terminal tags to develop such deletion constructs.

<u>b) Analyze glycosylation status of α-dystroglycan fusion proteins with FKRP wild type and deletion virus treatments to functionally map α-dystroglycan-FKRP interactions</u>

We tested C2C12 myotube α-dystroglycan glycosylation in the presence of virally expressed N-terminal 2x FLAG tagged FKRP with common LGMD2I patient mutation, L276I. The virus successfully expressed mutant FKRP protein. However, we were unable to obtain the control N-terminal tagged FKRP virus (see above). Therefore, we cannot interpret results of the L276I experiment in the absence of the appropriate positive control.

<u>c) Perform in vitro binding assay experiments with GST-FKRP fusion proteins and α-dystroglycan, POMT1, POMGnT1, fukutin, and LARGE</u>

We tested whether FKRP could directly bind to α-dystroglycan or the N-terminal fragment of α-dystroglycan by *in vitro* binding assay. As shown in Fig. 5, recombinant wild-type FKRP was only found in the binding void, indicating that FKRP and α-dystroglycan do not directly interact in our experimental conditions. These data suggest that FKRP may influence α-dystroglycan processing indirectly, perhaps through intermediate protein adaptors or via regulation of proteins that involved in α-dystroglycan glycosylation.

We also examined protein-protein interactions between FKRP and other dystroglycanopathy proteins, fukutin and LARGE. We used M2 FLAG agarose to purify FLAG tagged FKRP from transfected cells. FLAG-FKRP could not pull down recombinant LARGE (Fig. 7) nor fukutin (data not shown) in binding studies under our experimental conditions.

d) Develop a solid phase FKRP binding assay with GST-FKRP fusion proteins to identify FKRP binding partners

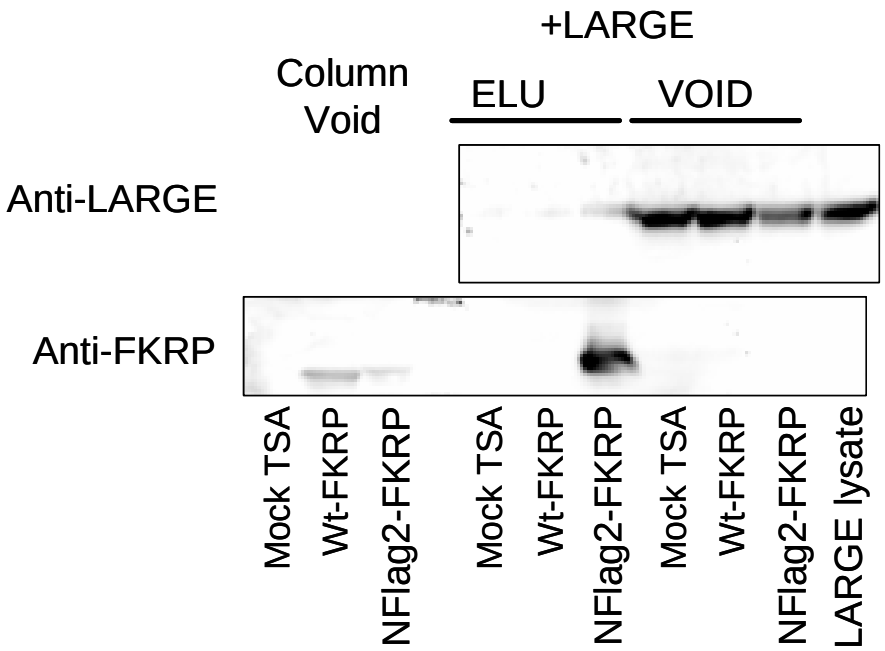


**Fig. 7**: FKRP and LARGE *in vitro* binding experiment. FKRP (wild type or N-terminal Flag tagged) or LARGE protein was expressed in TSA201 cells. Untransfecte, wt-FKRP or NFlag2FKRP lysates were applied to M2 FLAG agarose. Column voids were collected and agarose was washed. Large infected TSA lysates were then applied to the columns, LARGE binding void and elutions were collected and run on SDS-PAGE. Western bloting shows that NFlag2FKRP but not wild-type FKRP binds to the M2 FLAG column. No appreciable levels of LARGE were detected in the column elutions. These data indicate that LARGE and FKRP are unlikely to form direct protein-protein interactions.

Large scale purification of recombinant protein is most efficiently obtained via purification of GST fusion proteins from bacterial cell lysates. However, we found that GST-FKRP fusion protein was insoluble (see "a" above) when expressed in bacteria. As it is technically difficult to prepare large scale recombinant protein from mammalian expression systems, we do not currently have FKRP constructs available to promote the development of a solid phase FKRP binding assay. We are currently considering other options for high throughput FKRP binding assays.

Significance and Future Goals

Protein insolubility and poor recombination for generation of specific FKRP constructs hampered our ability to complete all intended studies. Despite these problems, we were able to establish that FKRP does not appear to directly bind α-dystroglycan, fukutin or LARGE. Importantly, the lack of FKRP to α-dystroglycan binding further suggests that FKRP's role in α-dystroglycan processing is not to directly add or modify α-dystroglycan sugars. We will continue to test recombinant FKRP interactions to other dystroglycanopathy proteins and develop additional constructs to map FKRP activity.

**Key Research Accomplishments**

- We developed a polyclonal antibody for fukutin-related protein (FKRP) detection.
- We identified short hairpin RNA (shRNA) constructs for knock down of recombinant FKRP expression.
- We produced a virus to express the shRNA for FKRP knock down.
- We produced viruses for expression of FKRP and FKRP fusion proteins.
- We analyzed of dystroglycan glycosylation with FKRP overexpression in C2C12 mouse muscle cells: FKRP overexpression reduces detection of α-dystroglycan glyco-epitopes

- We analyzed of dystroglycan laminin binding with FKRP overexpression in C2C12 mouse muscle cells: FKRP overexpression reduces α-dystroglycan laminin binding
- We examined FKRP binding interactions with α-dystroglycan and other putative glycosyltransferases fukutin and LARGE; FKRP does not bind to any of these proteins in our experiments.

**Reportable Outcomes**

- REAGENTS:
  - i) Rbt341 - anti-FKRP antibody (for detection of endogenous FKRP)
  - ii) Ad5CMV-hFKRP virus (for exogenous FKRP expression in mice and cultured cells)
  - iii) Ad5CMV-CFLAG2FKRP virus (for exogenous FKRP fusion protein expression in mice and cultured cells)
  - iv) Ad5CMVsimFKRP-A virus (for knockdown of recombinant FKRP expression)
  - v) Plasmids for FKRP expression: pcDNA CMV-CFLAG2FKRP, pcDNA CMV-NFLAG2FKRP, pcDNA CMV-L276I-NFLAG2FKRP
- MANUSCRIPTS:
  - i) None at this time. Expect to begin preparation of 1st manuscript in 2 to 3 months
- FUNDING:
  - i) FKRP antibody developed in this DOD-funded work was used to collect preliminary data for future MDA and NIH grants.

**Conclusions**

Significant progress has been accomplished and important findings have been made in all three aims of our study. Viral vector reagents, cDNA constructs, and antibodies have been developed for the in depth study of FKRP activity. Notably, our experiments show that FKRP overexpression in muscle cell cultures actually reduces α-dystroglycan glyco-epitopes and laminin binding properties. This and other findings implicate FKRP for a distinctly different role in α-dystroglycan processing compared to other dystroglycanopathy-related genes. Combined, this research promotes a better understand of the role FKRP plays in the glycosylation of α-dystroglycan and its functional interaction with the extracellular matrix.

**References**

Barresi, R., Michele, D.E., Kanagawa, M., Harper, H.A., Dovico, S.A., Satz, J.S., Moore, S.A., Zhang, W., Schachter, H., Dunamski, J.P., Cohn, R.D., Nishino, I. and Campbell, K.P. LARGE can functionally bypass alpha-dystroglycan glycosylation defects in distinct congenital muscular dystrophies. *Nat Med.* 10:696-703, 2004.

Barresi, R. and Campbell, K.P. Dystroglycan: from biosynthesis to pathogenesis of human disease. *J Cell Sci. 119*:199-207, 2006.

Brockington, M., Yuva, Y., Prandini, P., Brown, S.C., Torelli, S., Benson, M.A., Herrmann, R., Anderson L.V.B., Bashir, R., Burgunder, J.M., Fallet, S., Romero, N., Fardeau, M., Straub, V., Storey, G., Pollitt, C., Richard, I., Sewry, C.A., Bushby, K., Voit, T., Blake, D.J. and Muntoni, F. Mutations in the fukutin-related protein gene (FKRP) identify limb girdle muscular dystrophy 2I as a milder allelic variant of congenital muscular dystrophy MDC1C. *Human Molec Genet. 10*: 2851-2859, 2001.

Brockington, M., Torelli, S., Prandini, C., Boito, N.F., Dolatshad, N.F., Longman, C., Brown, S.C. and Muntoni, F. Localization and functional analysis of the LARGE family of glycosyltransferases: significance for muscular dystrophy. *Human Molec Genet.* 14:657-665, 2005.

Frosk, P., Greenberg, C.R., Tennese, A.A.P., Lamont, R., Nylen, E., Hirst, C., Frappier, D., Roslin, N.M., Zaik, M., Bushby, K., Straub, V., Zatz, M., de Paula, F., Morgan, K., Fujiwara, T.M. and Wrogemann, K. The most common mutation in FKRP causing limb girdle muscular dystrophy type 2I (LGMD2I) may have occurred only once and is present in Hutterites and other populations. *Human Mut. 25*:38-44, 2005.

Grewal., P.K., McLaughlan, J.M., Moore, C.J., Browning., C.A. and Hewitt, J.E. Characterization of the LARGE family of putative glycosyltransferases associated with dystroglycanopathies. *Glycobiology*. 15:912-923, 2005.

Manya, H., Chiba, A., Yoshida, A., Wang, X., Chiba, Y., Jigami, Y., Margolis, R.U. and Endo, T. Demonstration of mammalian protein O-mannosyltranferase activity: Coexpression of POMT1 and POMT2 required for enzymatic activity. *PNAS*. 101:500-505, 2004.

Walter, M.C., Petersen, J.A., Stucka, R., Fischer, D., Schroder, R., Vorgerd, M., Schroers, A., Schreiber, H., Hanemann, C.O., Knirsch, U., Rosenbohm, A., Huebner, A., Barisic, N., Horvath, R., Komoly, S., Reilich, P., Muller-Felber, W., Pongratz, D., Muller, J.S., Auerswald, E.A. and Lochmuller, H. FKRP (826C>A) frequently causes limb-girdle muscular dystrophy in German patients. *J Med Genet. 41*:e50, 2004.

**Appendices**

n/a

# Sub-Project #5**

# Enhancing dystrophic muscle growth by gene transfer of myostatin inhibitor (Xiao Xiao)

** Note that this subproject was completed February 2008. The following is a reiteration of the final report. There are no additional updates.

## Introduction

Congenital muscular dystrophy (CMD) is a group of severe forms of muscular dystrophy leading to early death in human patients(1-3, 7).. The majority of cases are caused by genetic mutations in the major laminin, laminin containing the $\alpha$2 chain (formerly named merosin), in the muscle basement membrane(4, 6, 8, 10). The early morbidity/fatality and the lack of effective treatment require urgent search for novel therapeutics. Previously, we utilized mini-agrin, which has been proven to have a therapeutic effect in transgenic MCMD mice, to treat MCMD mice by AAV vector(9). Our preliminary studies showed that over-expression of mini-agrin protein greatly improved general health and muscle morphology in MCMD mice. However, the treated disease mice still developed gradual paralysis and displayed shorter life span than wild type mice. To further improve the current gene therapy paradigm, we have developed complementary gene therapy strategy for laminin alpha2-deficient CMD.

## BODY

**1. Specific Aim 1 (Year 1): To examine if myostatin gene transfer into normal muscle can increase muscle mass and strength and also facilitate the repair of injured muscle.** With respect to the approved statement of specific aim 1, we have studied the muscle enhancing effect of delivering the myostatin propeptide into normal wild type mice. Myostatin was discovered in 1997 and has been extensively documented as a negative regulator of muscle growth. Myostatin blockades therefore offers an effective strategy for treating a number of muscle degenerative diseases, including sarcopenia and muscular dystrophy. In this study, we described a different strategy of myostatin blockade by AAV mediated gene delivery of myostatin propeptide

### 1.1. Construction of AAV-MPRO and AAV-MPRO76AFc Plasmids

Our original purpose was to clone the myostatin propeptide (MPRO) gene into AAV vector, therefore, the pAAV-MPRO vector was constructed. The myostatin propeptide gene was driven by cytomegalovirus (CMV) promoter which has a strong transcriptional activity in muscle cells(2). Later on, Dr. Se-Jin Lee's group reported that the mutated propeptide (amino acid 76-aspartate was changed to alanine), resistant to metalloproteinases cleavage, were more stable in vivo (4). Therefore, pAAV-MPRO76AFc plasmid was established in which the mutation was made and the mouse IgG Fc domain was fused with the propeptide C-terminus to further increase its half life in vivo. It is noteworthy that the pAAV-MPRO76AFc plasmid was driven by the chicken beta-actin promoter (CAG) promoter, which is a robust transcription promoter in liver cells(1). We intended to use this promoter because we planned to deliver AAV vector carrying myostatin propeptide gene into the liver cell. Then the hepatocytes will severe as factory, the propeptide will be consistently produced from the liver, circulate into the blood circulation, and act on whole-body muscle cells.

### 1.2. MPRO Gene Delivery into Neonate of Normal Mice

Previously we have shown that widespread gene delivery of AAV8 vectors can be easily achieved in neonate mice, therefore, we treated normal neonate mice with AAV-MPRO and evaluated its affect (3). The AAV-MPRO vector was injected into 3-day-old neonate mice by i.p. injection. As shown in Fig.1a, the AAV-MPRO treated mouse significantly gained weight compared with the untreated littermates. The skinned treated

mice appeared more muscular than the control one (Fig1b). The weight of the skeletal muscles (TA, Gas, Quads and Diaphragm) were significantly heavier than muscles of the control mice ($p<0.05$) (Figure 1c). Even the quadriceps muscle, which showed the lowest increase among the skeletal muscles examined, displayed a 37% increase in muscle mass over the controls. It is also noteworthy that a significant weight increase was not observed in the treated cardiac muscle, which indicates that heart hypertrophy will not be a concern for future propeptide gene delivery based therapies.

The observed increases in skeletal mass could be due to either the enlargement of the individual muscle fibers (hypertrophy), or because of an increase in the overall number of muscle fibers (hyperplasia). To answer this question, and also to examine
muscle histology, cryo-thin-sections of the quadriceps and diaphragm muscles were taken from treated and

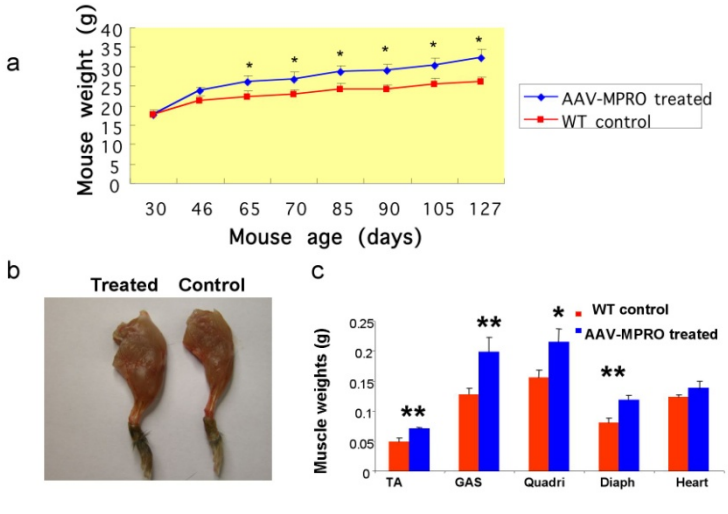


**Figure 1. The muscle growth enhancing Effects in normal mice by delivery of AAV-MPRO vectors at neonatal age.** The AAV-MPRO vector was delivered into 3 -day-old neonatal mice (3 males and 3 females for each group), and the mice were sacrificed 4 months after gene delivery. **a.** AAV-MPRO treated mice gained more weight than controls. (*, $p<0.05$) (25 % increase over untreated). **b.** The treated skinned mice appeared more muscular than controls... **c.** There are increases in skeletal muscle weight but not cardiac muscle weight following AAV-MPRO delivery into neonatal mice. (**, $p<0.01$ and *, $p<0.05$).

wild type control mice. These tissue sections were H& E stained for histology examinations and subjected to immunofluorescent staining against dystrophin for the purpose of muscle radius analysis. As shown in Fig.2, the AAV-MPRO treated muscles displayed normal histology, with the exception that the muscle fibers were noticeably larger in size compared to their control counterparts. For the AAV-MPRO treated quadriceps muscle, the average fiber radius was 28.4±6.96 m, which was significantly larger than the average control fiber radius of 22.29±7.85 m ($p< 0.00001$) (Fig.2.b). All combined, these results strongly suggest that treatment with the AAV-MPRO vector does not compromise normal morphology, but it does result in increased muscle mass as a result of muscle hypertrophy.

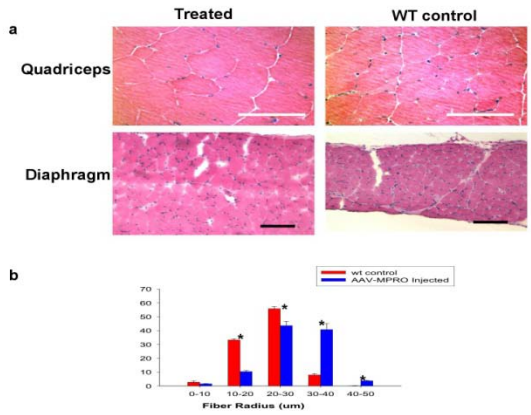


**Figure 2. Muscle Hypertrophy Occurred in AAV-MPRO Treated Mice. a.** The diameters of treated skeletal myofibers were larger than the untreated controls as shown by H&E staining. **b.** Semiquantitative morphometric analysis of the skeletal myofibers (from quadriceps muscle) showed that the majority of the untreated control myofibers had their radii measured 10-30 um, while the majority of the treated myofibers measured 20-40um. (*, $p<0.05$) .

### 1.3 MPRO76AFc Gene Delivery into Adult Mice

We next examined delivering AAV vector carrying the MPRO gene into adult mice to see whether the skeletal muscle mass can be increased. In this section, in order to have a systemic effect, we utilized pAAV-MPRO76AFc construct which would produce the stable propeptide. We utilized intrasplenic injection method to purposely deliver AAV vector into the liver cells. We hypothesized that the propeptide gene would be produced by transduced hepatocytes and secreted into the blood stream.
Four-month-old C57/BL10 mice (5 females) were treated with the AAV8-MPRO76AFc vector by intrasplenic injection, and the age matched control mice (5 females) were injected with AAV8-CMV-GFP vector. Similar to the results obtained in neonatal group, we observed

significant skeletal muscle mass increase for all the skeletal muscle examined (Fig.3b) though only marginal increase of body weight was noticed over four months of treatment (Fig3a). The AAV-MPRO76AFc treated muscle fiber size was bigger, and the muscle morphology appeared normal (Fig 3c). As expected, RT-PCR analysis indicated that the treated liver and heart were the major organs to produce propeptide (Data not

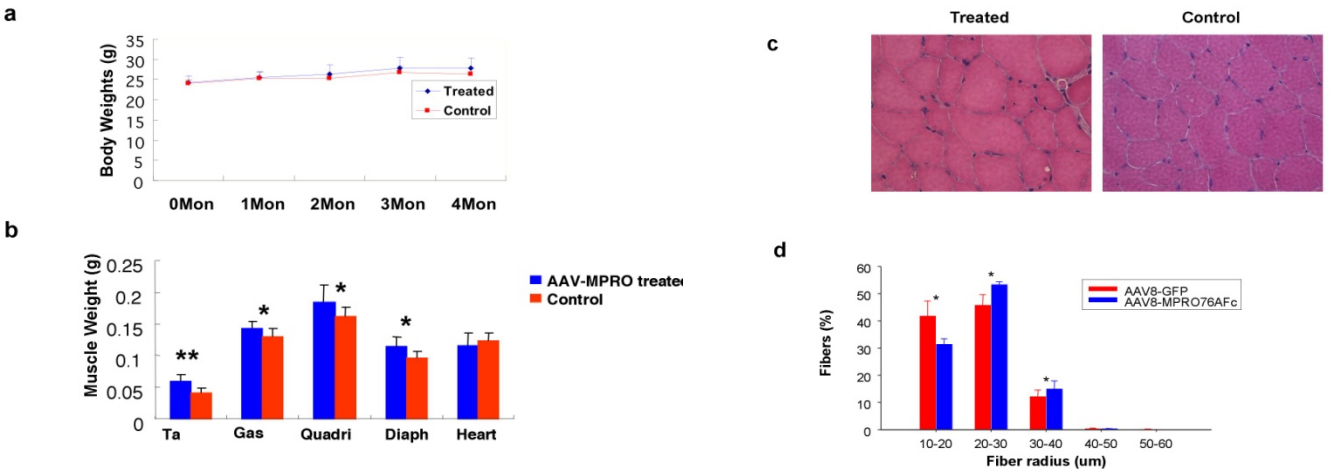


**Figure 3. The Effects Of Myostatin Propeptide Delivery Into Adult Mice.** The AAV-MPRO76AFc vector was delivered into 4-month-old adult mice (5 females in each group) by intrasplenic injection. **a.** There was no significant total weight gain in the treated mice compared to the controls 4 months after gene delivery. **b.** There was an increase in skeletal, but not cardiac muscle weight in AAV-MPRO76AFc treated mice. (Student's t test was used; **, p<0.01; *, P<0.05). **c.** H&E staining displayed muscle hypertrophy in AAV-MPRO76AFc treated skeletal muscles. **d.** Morphometric analysis indicated that the AAV8-CAG-MPRO myofiber was larger. when compared to their control counterparts. Standard error is labeled as a bar. Student's t test was used; *, p<0.05.

shown). The absence of specific band in skeletal muscle further proved our hypothesis that the propeptide will be produced from the liver or heart cells, secreted and circulated through the blood to ultimately act on the skeletal muscles of the body.

**2. Specific Aim 2 (Year 2)**: **To examine if myostatin gene transfer into dystrophic muscle can increase muscle mass and strength and also ameliorate muscular dystrophy pathologies.** According to the approved statement of specific aim 2, we have investigated the therapeutic effect of delivering myostatin propeptide into Duchenne Muscular Dystrophy (DMD) mouse model. DMD affects 1 in 3500 males. The progressive muscle wasting and degeneration usually confine patients to a wheelchair in their early teens, and leads to death by their twenties due to respiratory or cardiac failure. The disease is caused by mutations in the dystrophin gene, which encodes a large cytoskeletal protein in both skeletal and cardiac muscle cells. Since

DMD is caused by the recessive and monogenic mutations, gene therapy has been actively investigated as a potential remedy. Instead of using dystrophin gene, we proposed to deliver myostatin propeptide gene to amend dystrophic pathology by promoting muscle growth.

**MPRO76AFc Gene Delivery into *mdx* mice**

The serotype 8 AAV-MPRO76AFc vector was delivered into 3-month-old mdx mice by simple tail vein injection, and there were five mice for each group. We were very excited to notice that the injected mice started to gain weight even two weeks after vector injection ($p<0.01$) (Fig 4a), and the difference became very significant after one and half months of treatment ($p<0.001$).

Since the increase of serum Creatine Kinase (CK) level, which indicates muscle damage, is an important manifestation for DMD, we next examined whether AAV mediated the propeptide gene deliver have effect on it in *mdx* mice. As shown in Fig4b, although the average serum CK level of treated mice (610 ± 261 IU/L) was still far above the wild type mouse (6.7 ± 2.3 IU/L), it was indeed slightly lower than *mdx* mice (906 ± 289) (n=5 for each group, p=0.06).

The mice were sacrificed and the skeletal muscles were carefully dissected. As expected, except the heart, the weight of tibialis anterior (TA), Quadricepts muscle, and the diaphragm muscle from treated mice are all heavier than the control *mdx* mice (Fig4c). Surprisingly, we did not observe the significant weight increase of the gastrocnemius (Gas) muscle from treated mice (Fig 4c). This result was different from our previous one obtained from normal mice, in which all examined skeletal muscle including gastrocnemius displayed larger

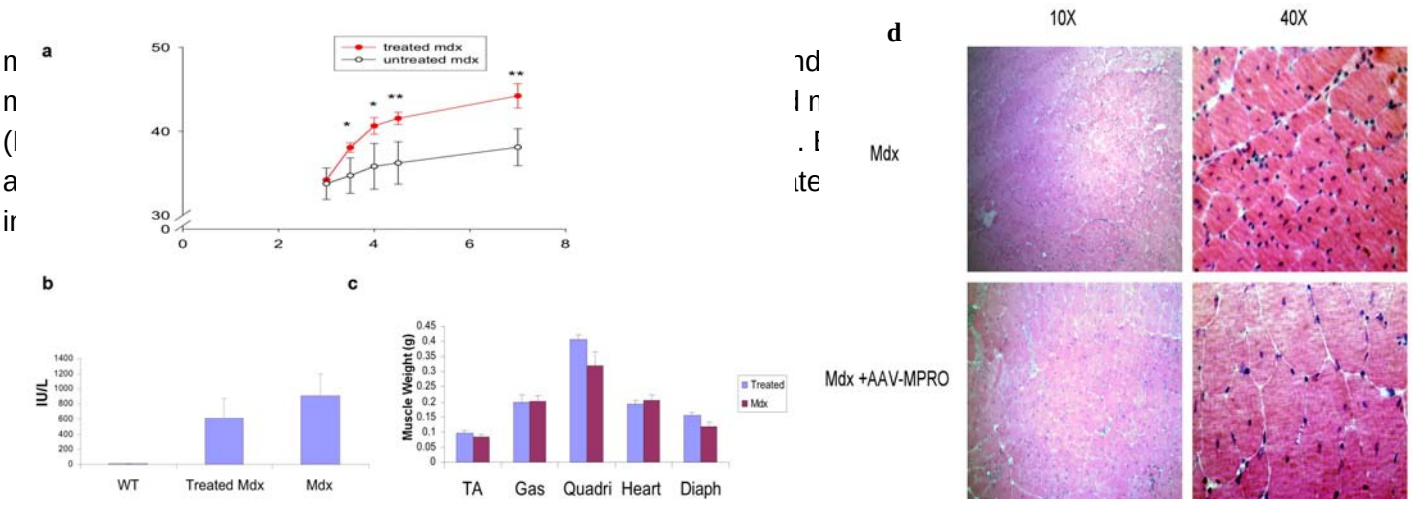


**Figure 4.** The Therapeutic Effect of Myostatin Propeptide gene delivery in mdx mice. The serotype 8 AAV-MPRO76AFc vector was delivered into 3-months old mdx mice by tail vein injection. Four months after treatment, the mice were sacrificed. **a. The growth curve of treated mdx mice versus untreated controls**. The treated mdx mice had a higher bodyweight (16% increase) when compared to the untreated mdx . **b**. **The serum creatine kinase level of treated *mdx* mice was lower than the untreated controls**. **c. The weight of the majority skeletal muscles of treated mdx mice was greater than the controls, especially the quadriceps and diaphragm muscles.**. **d.** The histology of treated mdx was improved. The treated muscle displayed more uniform muscle fiber sizes and less mononuclear cell infiltration.

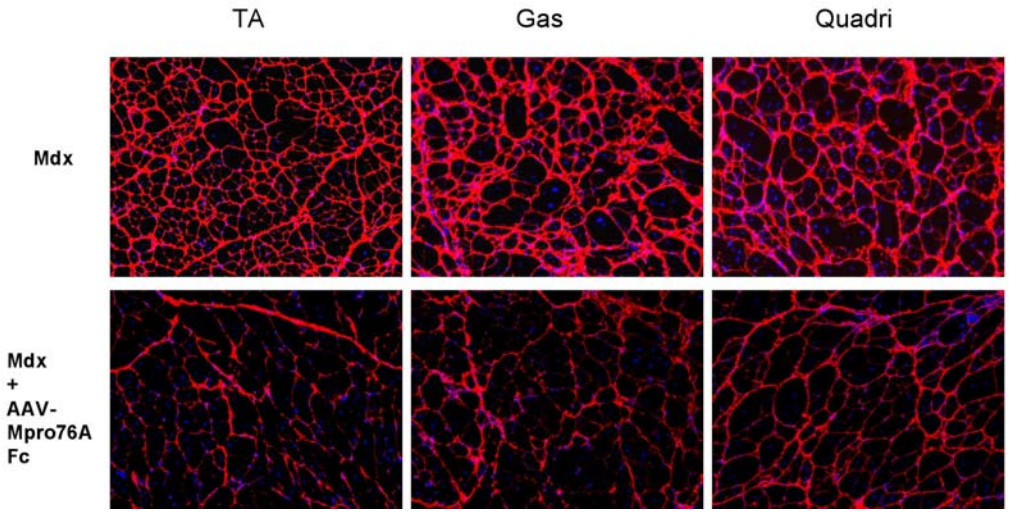


**Figure 5. Reduction of fibrosis in limb muscle of mdx mice injected with AAV-MPRO76A-Fc vector**. The cryo-thin-section of muscles from *mdx* mice and treated mice were subjected to collagenIII immunofluoscent staining. Noticeably, the intensity of collagen III decreased in examined muscles.

**Key Research Accomplishments**:

1. We have delivered myostatin propeptide gene into laminin alpha2-deficient CMD mice and the therapeutic effect was evaluated. Unlike mdx mice for which myostatin propeptide delivery can ameliorate its muscle pathology, the delivery of propeptide had a severe side effect on laminin alpha2-deficient CMD mice. The injected mice died even early than untreated controls. This phenomenon is consistent with previous discovery(5).
2. We have delivered AAV-IGF1 vector into laminin alpha2-deficient CMD mice and did not observe significant therapeutic effect.
3. We have delivered AAV-BCL-XL into laminin alpha2-deficient CMD mice and did not observe significant therapeutic effect.

**Reportable Outcomes**:

Our manuscript entitled “Myostatin propeptide gene delivery by AAV8 vectors enhances muscle growth and ameliorates dystrophic phenotypes in *mdx* mice” has been accepted by the journal Human Gene Therapy (see attachment). This project is related with DOD grant.

**Conclusions**: Single AAV-IGF1, AAV-Bcl-XL, or AAV-MPRO gene delivery can not offer therapeutic benefit for laminin alpha 2 deficient $dy^{w}/dy^{w}$ mice.

**Recommend changes**: No.

**References**

1. **Allamand, V., and P. Guicheney.** 2002. Merosin-deficient congenital muscular dystrophy, autosomal recessive (MDC1A, MIM#156225, LAMA2 gene coding for alpha2 chain of laminin). Eur J Hum Genet **10:**91-4.
2. **D'Alessandro, M., I. Naom, A. Ferlini, C. Sewry, V. Dubowitz, and F. Muntoni.** 1999. Is there selection in favour of heterozygotes in families with merosin-deficient congenital muscular dystrophy? Hum Genet **105:**308-13.
3. **Emery, A. E.** 2002. The muscular dystrophies. Lancet **359:**687-95.

4. **Kuang, W., H. Xu, P. H. Vachon, L. Liu, F. Loechel, U. M. Wewer, and E. Engvall.** 1998. Merosin-deficient congenital muscular dystrophy. Partial genetic correction in two mouse models. J Clin Invest **102:**844-52.
5. **Li, Z. F., G. D. Shelton, and E. Engvall.** 2005. Elimination of myostatin does not combat muscular dystrophy in dy mice but increases postnatal lethality. Am J Pathol **166:**491-7.
6. **O'Brien, D. P., G. C. Johnson, L. A. Liu, L. T. Guo, E. Engvall, H. C. Powell, and G. D. Shelton.** 2001. Laminin alpha 2 (merosin)-deficient muscular dystrophy and demyelinating neuropathy in two cats. J Neurol Sci **189:**37-43.
7. **Pegoraro, E., M. Fanin, C. P. Trevisan, C. Angelini, and E. P. Hoffman.** 2000. A novel laminin alpha2 isoform in severe laminin alpha2 deficient congenital muscular dystrophy. Neurology **55:**1128-34.
8. **Pegoraro, E., H. Marks, C. A. Garcia, T. Crawford, P. Mancias, A. M. Connolly, M. Fanin, F. Martinello, C. P. Trevisan, C. Angelini, A. Stella, M. Scavina, R. L. Munk, S. Servidei, C. C. Bonnemann, T. Bertorini, G. Acsadi, C. E. Thompson, D. Gagnon, G. Hoganson, V. Carver, R. A. Zimmerman, and E. P. Hoffman.** 1998. Laminin alpha2 muscular dystrophy: genotype/phenotype studies of 22 patients. Neurology **51:**101-10.
9. **Qiao, C., J. Li, T. Zhu, R. Draviam, S. Watkins, X. Ye, C. Chen, and X. Xiao.** 2005. Amelioration of laminin-{alpha}2-deficient congenital muscular dystrophy by somatic gene transfer of miniagrin. Proc Natl Acad Sci U S A.
10. **Tome, F. M., T. Evangelista, A. Leclerc, Y. Sunada, E. Manole, B. Estournet, A. Barois, K. P. Campbell, and M. Fardeau.** 1994. Congenital muscular dystrophy with merosin deficiency. C R Acad Sci III **317:**351-7.

**Appendices:**

**Appendix 11:** “Myostatin propeptide gene delivery by AAV8 vectors enhances muscle growth and ameliorates dystrophic phenotypes in *mdx* mice”, Human Gene Therapy, 2008.

# Sub-Project #6**
# Dendritic cells and muscle gene transfer
# (Paula Clemens)

** Note that this subproject was completed last February 2008. The following is a reiteration of the final report. There are no additional updates.

**Introduction:**

Dendritic cells are the only antigen presenting cell (APC) that can activate naïve T cells, and therefore, play a critical part in initiating a primary immune response. Because of this key role, dendritic cells may be an excellent target to mediate immunological therapy for gene transfer. We have previously demonstrated success in suppressing immunity and enhancing the effectiveness of muscle gene transfer by co-administering gene vectors expressing cytokines CTLA4Ig and CD40Ig that block costimulation of T and B cells, respectively. Based on this previous data, we predict that interference with antigen presentation to T cells will beneficially suppress immunity to adenoviral (Ad) vector gene transfer.

The number of dendritic cells are significantly increased in dystrophic muscle, which points toward increased importance of addressing the immunity induced by manipulation of dystrophic muscle. In the mouse model of Duchenne muscular dystrophy (DMD), the *mdx* mouse, dendritic cells are increased 7-fold over levels observed in normal muscle. Since dendritic cells may be the principal mediator of the deleterious immune response to muscle gene transfer in their antigen presentation role, they may be an excellent target to mediate immunological therapy.

In our previous experiments of high-capacity Ad (HC-Ad) vector-mediated gene delivery to dystrophic skeletal muscle without immune suppression, an immune response developed to both Ad and dystrophin antigens. Importantly, the anti-dystrophin immune response was observed months after gene delivery to either neonatal or adult mice. The anti-Ad immune response was observed after gene transfer to adult animals and resulted in loss of vector over time and precluded successful vector re-administration.

We will, therefore, focus this project on testing the following hypothesis: Dendritic cells, known to be increased in dystrophic muscle, are professional APCs that initiate the adaptive immune response to HC-Ad vector-mediated dystrophin delivery. Dendritic cells can be engineered to effect antigen-specific immune suppression to enhance the effectiveness of dystrophin gene delivery to dystrophic muscle.

**Body:**

**Adenoviral (Ad) vector-induced dendritic cell (DC) activation in TA muscle:**

*EGFP expression and Ad vector-induced DC activation in TA muscle after intramuscular administration of AdEGFP*

In a series of experiments, we followed the migration of muscle DCs that was induced by muscle gene delivery. A first-generation Ad vector, carrying the marker gene enhanced green fluorescent protein, (AdEGFP) was injected intramuscularly in the TA. EGFP expression increased with time and reached its highest level 7 days after injection, comprising approximately 70-80% positive fibers (Fig 1D), as compared to 3 days (Fig 1B) and 5 days (Fig 1C) after AdEGFP injection, which resulted in 30% and 50% of fibers expressing EGFP, respectively. No EGFP-expressing fibers were observed in muscle injected with PBS (data not shown) or at one day after AdEGFP administration (Fig 1A).

Immunohistochemistry was used to demonstrate the distribution of DCs in TA muscle, draining LNs and spleen. Seven days after vector injection in the TA muscle, the majority of activated DCs ($CD11c^+$ $CD86^+$) and inactivated DCs ($CD11c^+$ $CD86^-$) were observed in treated muscle (Fig 1J), which temporally correlated with the time point of highest EGFP expression and was significantly greater than at 1 day after vector injection (Fig 1I). The number of activated DCs increased over time at the margin of white and red pulp in spleen (data not shown) and in the paracortical area of draining LNs as demonstrated by comparing the numbers of activated DCs at 1 d (Fig 1G) and at 7d (Fig 1H) after AdEGFP injection into the TA muscle. Fewer activated DCs were found in spleen (Fig 1E) and draining LNs (Fig 1F) of mice that received an IM PBS injection. No activated DCs were found in PBS injected TA muscle (data not shown).

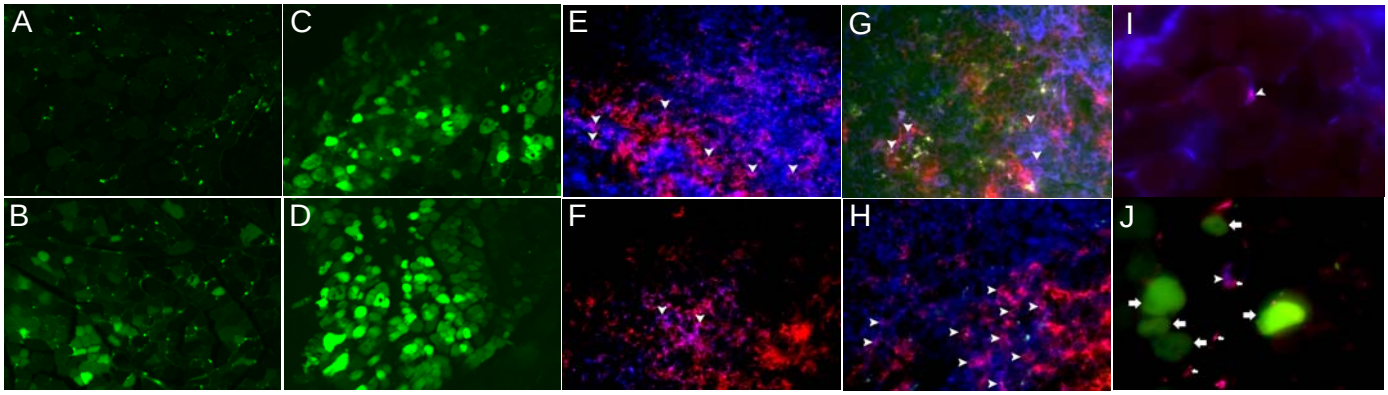


**Figure 1.**
**EGFP expression in TA muscle after AdEGFP injection and Ad vector-induced DC activation.**
EGFP expression in left TA muscle from mice day 1 (A), 3 (B), 5 (C), 7 (D) after AdEGFP injection. Muscles were removed from euthanized mice and fixed in 4% paraformaldehyde in PBS overnight at 4ºC, then cryoprotected with 30% sucrose at 4ºC overnight. Cryosections of muscle tissues were mounted in fluorescence medium, and the EGFP expression was observed using a fluorescence microscope, original magnification, ×200. Immunohistochemical demonstration of the distribution of DCs in TA muscle, draining lymph nodes and spleen (E-J, original magnification, ×600). Red cells are CD11c positive reflecting total inactive and active DCs. Cells that immunostain for CD11c and CD86 (blue) are activated DCs. Spleen (E) and lymph node (F) collected from a PBS-injected mouse is a positive control for both CD11c-expressing and CD86-expressing cells. The number of activated DCs increased over time at the margin of white and red pulp in spleen (data not shown), in the paracortical area of draining lymph nodes at day 1 (G) and day 7 (H), and in AdEGFP injected muscle at day 1 (I) and day 7 (J). Arrowheads indicate $CD11c^{+}CD86^{+}$ cells. Small arrows indicate $CD11c^{+}CD86^{-}$ cells and large arrows indicate EGFP-expressing muscle fibers.

Conclusions: In this study, we found that $CD11c^{+}$ $CD86^{+}$ DCs appeared in Ad vector-injected TA muscle. Both $CD11c^{+}$ $CD86^{+}$ and $CD11c^{+}$ $CD86^{-}$ DCs increased with time in Ad vector-injected TA muscle as compared with PBS-injected TA muscle. Moreover, these cells increased in T cell-dependent areas of draining LNs and spleen. The maximum level of accumulated activated DCs in secondary lymphoid organs is seen 7 days after Ad vector injection when EGFP expression reached its highest level. Our results demonstrate activation of resident and recruited DCs in muscle in response to AdEGFP-mediated gene transfer. These activated APCs migrate to lymphoid organs where they induce adaptive immunity.

**DC migration from skeletal muscle:**
Although migration of antigen-presenting DCs through lymphatics to draining LNs is an important step in the initiation of an adaptive immune response, very little is known about how muscle DCs migrate from muscle treated with gene transfer. In DC migration studies, some groups tag endogenous DCs to follow their movement in time; while others rely on *ex vivo* labeling of DCs, followed by adoptive transfer to recipient animals. It has been shown that the *ex vivo* labeling and adoptive transfer approach has a higher reliability and sensitivity than endogenous labeling. Therefore, we used the second technique for tracking DCs *in vivo* from muscle.

*Characterization of BMDCs*
DCs were isolated from BM of C57BL/10 or CD45.2 donor mice, cultured with IL-4 and GM-CSF for 7 days, and purified by passage over anti-CD11c antibody-coated magnetic beads. After purification, approximately 90% of cells expressed CD11c and CD86, which indicated maturation of DCs. After labeling of C57BL/10 DCs with CFSE, there was no change in the phenotypic expression of CD11c and CD86. Our finding of a high proportion of mature DCs after *ex vivo* purification is consistent with many other studies, which also showed that *ex vivo* stimulation promotes DC dissemination from a tissue of interest to lymphoid organs in subsequent *in vivo* studies.

*In vivo migration pathways of CFSE-labeled DCs after foot pad (FP) injection*
Numerous studies have investigated DC migration after FP injection, but their trafficking at early time points has not been documented. Furthermore, our interest was to compare DC migration from muscle with DC migration from the FP. We performed parallel experiments with either adoptive transfer of CFSE-labeled

C57BL/10 DCs to C57BL/10 mice or C57BL/6 (CD45.2) DCs to C57BL/6 (CD45.1) mice. Similar results were obtained in the parallel experiments. We show the data with CFSE-labeled C57BL/10 DCs.

Following FP injection of CFSE-labeled DCs, the transferred $CFSE^+$DCs were found in popliteal and inguinal LNs and spleen. The number of these cells increased in a time-dependent manner (Fig 2a). On day 2 after adoptive transfer, most recovered $CFSE^+$DCs were found in popliteal LNs, with fewer $CFSE^+$DCs found in inguinal LNs (Fig 2b). There were very few recovered DCs from spleen on day 1 or 2 (Fig 2b). This study confirmed the results of others showing that CFSE-labeled DCs adoptively transferred to FP migrated to draining LNs, then traveled to the spleen from the blood stream through the efferent lymphatics.

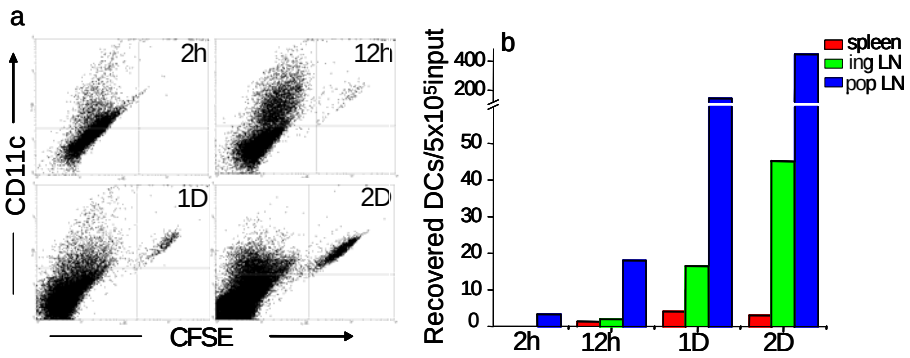


**Figure 2. In vivo migration of CFSE-DCs after FP injection.** Purified, CFSE-labeled mature DCs were injected subcutaneously into the FP of both hind limbs of syngeneic C57BL/10 mice (*n* = 2 mice/group for each time point). The absolute number of DCs recovered from each tissue was calculated by multiplication of the frequency of $CD11c^+$ transferred cells by the total number of resident leukocytes. Data are presented as the number of recovered DCs per $1\times10^5$ injected cells. (a) FACS data demonstrates increasing numbers of CFSE-labeled DCs recovered from popliteal LNs at each time point. The experiment shown is representative of 6 independent experiments. (b) Quantification of FACS data from spleen and inguinal and popliteal lymph nodes.

*In vivo migration pathways of CFSE-DCs after TA muscle injection*

In contrast, after adoptive transfer of $CFSE^+$DCs to the TA, a few DCs appeared in the spleen within 12 h (Fig 3a). Over the next 36 hours, the number of $CFSE^+$DCs in the spleen decreased, and was undetectable after 2 days (Fig 3b).

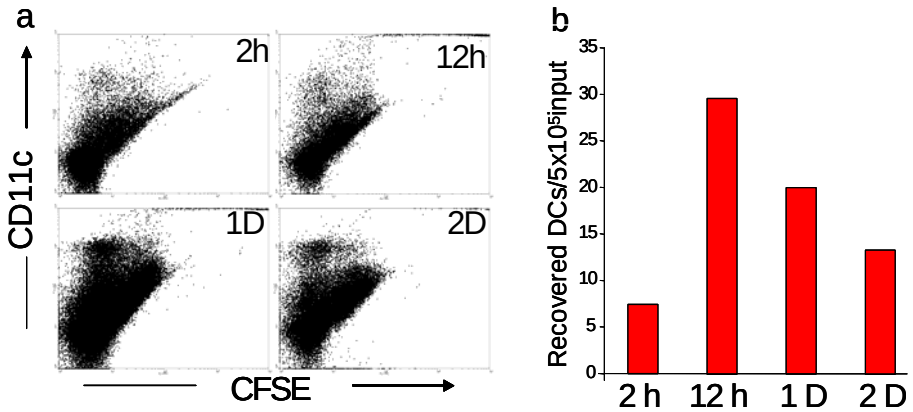


**Figure 3. Trafficking of $CFSE^+$DCs to the spleen from TA muscle.** (a) FACS plots of $CFSE^+$ splenocytes immunostained for CD11c. The panels are labeled for the time of splenocyte collection after TA muscle injection of CFSE-stained DCs. (b) Quantification of FACS data shown in (a).

On day 1 after adoptive transfer to the TA, we recovered the largest number of $CFSE^+$DCs from popliteal LNs, a smaller number of such cells from inquinal LNs and very few from BM (Fig 4a). After 2 days, these cells were reduced in both inguinal and popliteal LNs (Fig 4b), and were undetectable thereafter.

Quantification of FACS data (Fig 4c) showed that by 12 hours after adoptive transfer of CFSE-labeled DCs to the TA, large numbers of DCs migrated to the popliteal LNs, and this population increased considerably at 1

day, and decreased thereafter. In contrast, the peak number of CFSE$^+$DCs recovered in spleen occurred at 12h.

Conclusions: To compare DC mobilization from skeletal muscle, which has not been studied to any degree in the past, to known mobilization pathways, we performed parallel studies of DC mobilization from muscle and from the FP. We confirmed the results of others showing that CFSE-labeled DCs adoptively transferred to the FP migrated to popliteal LNs and subsequently reached inguinal LNs. The majority of these cells stayed in draining LNs, while a very small fraction migrated from draining LNs to spleen.

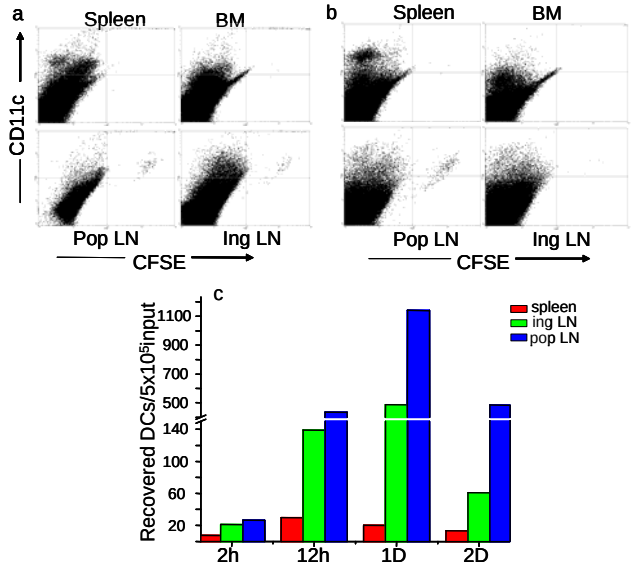


**Figure 4. *In vivo* migration pathways of CFSE-DCs after TA muscle injection.** Freshly prepared, CFSE-labeled DCs were injected into both TA muscles of syngeneic C57BL/10 mice (*n* = 2 mice/group for each time point). The experiment shown is representative of 6 independent experiments. After 1D (a) or 2D (b), popliteal lymph node, inguinal lymph node, spleen and bone marrow were collected and the number of CFSE$^+$ DCs was determined. Data are presented as number of recovered DCs per $1\times10^5$ injected cells. (c) Quantification of FACS data.

In our novel studies of DC migration from skeletal muscle, we observed that adoptively transferred CFSE-labeled DCs trafficked to the popliteal and inguinal LNs. Interestingly, our study found that after adoptive transfer of labeled DCs into TA muscle, the peak number of CFSE$^+$DCs recovered in spleen occurred at 12h, not 24h after injection when the largest number of these cells appeared in the popliteal LNs. This finding suggests that a subfraction of the transferred DCs from the muscle injection site could travel through the bloodstream directly to spleen. Although there is ample experimental evidence that draining LNs are the terminal targets for most DCs that leave peripheral tissues, recent investigations suggest that tissue-resident DCs can somehow return to the blood and carry antigen to organs other than LNs. One interpretation of our results is that muscle resident DCs could reach the spleen by dissemination through the bloodstream, perhaps gaining access through the well-developed capillary network of skeletal muscle, without going through lymphatics. Another possibility is that DCs migrating from skeletal muscle could take on specific homing factors that confer tropism to the spleen. The existence of a direct route of antigen transport to the spleen could have interesting implications for the immune mechanisms of many inflammatory, autoimmune muscle disorders and genetic treatment of DMD/BMD. For example, after gene transfer, DCs migrating to the spleen are likely to stimulate a T cell-independent B cell response and induce humoral immunity, whereas, DC migration to draining LNs through lymphatic vessels is required to stimulate naïve T cells and initiate a primary immune response.

**Key Research Accomplishments:**

- Isolation of dendritic cells from bone marrow and muscle
- FACS analysis of derived dendritic cells
- Fluorescent labeling of dendritic cells and demonstration that this does not change the activation phenotype
- Trafficking studies of labeled dendritic cells
- Demonstration of the dendritic cell trafficking pattern from skeletal muscle with implications for immunity induced by gene transfer

- PCR mutagenesis of T-cell mimic peptide transgene and a control peptide transgene
- Cloning of plasmids from which high-capacity adenoviral vectors can be rescued

**Reportable Outcomes:**
American Society of Gene Therapy, Seattle, WA, 6/07
Wang L, Clemens PR. Study of Adenovirus Vector-induced Activation of Muscle Dendritic Cells and Analysis of Mouse Dendritic Cell Migration from the Tibialis Anterior Muscle.

Manuscript in preparation: Wang L, Clemens PR. Activation of Muscle Dendritic Cells Induced by Adenoviral Vector and Migration of Dendritic Cells from Murine Skeletal Muscle

**Conclusions:**
In conclusion, our study of DC activation and trafficking from skeletal muscle yielded important evidence implicating DCs in the deleterious immunological consequences induced by Ad vector-mediated gene transfer to skeletal muscle. Therefore, these cells may be an excellent target to mediate immune suppression to facilitate successful gene transfer. Because other studies have suggested that DCs act coordinately to mediate the acute and chronic inflammatory aspects of dystrophic changes in DMD muscle, then it will also be important to study DC trafficking from dystrophic muscle in the future.

**List of Personnel that provided effort for the completion of contract W81XWH-05-1-0334 and received salary compensation**

**Project 1**

- Johnny Huard
- Burhan Gharaibeh
- Baohong Cao
- Aiping Lu
- Joe Vella
- Allison Bean
- Mitra Lavasani
- Jon Watchko
- Terry O'Day

**Project 2**

- Eric Hoffman
- Rashmi Rawat
- Olumee- Shabon
- Po Zhao
- Zuyi Wang
- Erica Reeves
- Ken Soong
- Julieta Uthurralt
- Josephine Chen

**Project 3**

- John Day
- Laura Ranum
- Joline Dalton
- Danielle Jim
- Marcy Weatherspoon

**Project 4**

- Kevin P. Campbell
- Aaron Beedle
- Tobias Willer
- Lindy Mc Donough

Investigator: Johnny Huard

**Project 5**

- Xiao Xiao
- Chun-ping Qiao
- Jianbin Lin

**Project 6**

- Paula Clemens
- Lei Wang
- Chau-ching Liu

HUMAN GENE THERAPY 14:1535–1546 (November 1, 2003)


# Dystrophin Delivery in Dystrophin-Deficient DMD$^{mdx}$ Skeletal Muscle by Isogenic Muscle-Derived Stem Cell Transplantation

MAKOTO IKEZAWA,[1,3] BAOHONG CAO,[1] ZHUQING QU,[1] HAIRONG PENG,[1] XIAO XIAO,[2] RYAN PRUCHNIC,[1] SHIGEMI KIMURA,[3] TERUHISA MIIKE,[3] and JOHNNY HUARD[1,2]

## ABSTRACT

**Duchenne's muscular dystrophy (DMD) is a lethal muscle disease caused by a lack of dystrophin expression at the sarcolemma of muscle fibers. We investigated retroviral vector delivery of dystrophin in dystrophin-deficient DMD$^{mdx}$ (hereafter referred to as mdx) mice via an *ex vivo* approach using mdx muscle-derived stem cells (MDSCs). We generated a retrovirus carrying a functional human mini-dystrophin (RetroDys3999) and used it to stably transduce mdx MDSCs obtained by the preplate technique (MD3999). These MD3999 cells expressed dystrophin and continued to express stem cell markers, including CD34 and Sca-1. MD3999 cells injected into mdx mouse skeletal muscle were able to deliver dystrophin. Though a relatively low number of dystrophin-positive myofibers was generated within the gastrocnemius muscle, these fibers persisted for up to 24 weeks postinjection. The injection of cells from additional MDSC/Dys3999 clones into mdx skeletal muscle resulted in varying numbers of dystrophin-positive myofibers, suggesting a differential regenerating capacity among the clones. At 2 and 4 weeks postinjection, the infiltration of CD4- and CD8-positive lymphocytes and a variety of cytokines was detected within the injected site. These data suggest that the transplantation of retrovirally transduced mdx MDSCs can enable persistent dystrophin restoration in mdx skeletal muscle; however, the differential regenerating capacity observed among the MDSC/Dys3999 clones and the postinjection immune response are potential challenges facing this technology.**

## OVERVIEW SUMMARY

**This study investigated the feasibility of dystrophin delivery in dystrophin-deficient DMD$^{mdx}$ (mdx) skeletal muscle via the transplantation of isogenic muscle-derived stem cells (MDSCs). The expression of stem cell antigens was preserved in mdx MDSCs retrovirally transduced to express a functional mini-dystrophin gene (MD3999). Although a limited number of dystrophin-expressing muscle fibers was detected within the muscle injected with MD3999 cells, these regenerated muscle fibers persisted for up to 24 weeks postimplantation. The presence of CD4- and CD8-positive lymphocytes and various cytokines within the injected muscle and the differential regenerative capacity displayed by MDSC/Dys3999 clones could affect the outcome of stem cell–mediated *ex vivo* gene transfer for treatment of muscular dystrophies.**

## INTRODUCTION

DUCHENNE'S MUSCULAR DYSTROPHY (DMD) is characterized by a lack of dystrophin protein in the sarcolemma of muscle fibers (Hoffman *et al.*, 1987; Arahata *et al.*, 1988; Watkins *et al.*, 1988; Engel *et al.*, 1994), a condition that results in the clinical manifestation of progressive muscle weakness accompanied by ongoing degeneration and regeneration of skeletal myofibers. Dystrophin cDNA is 14-kb long and comprises 79 exons scattered over nearly 3 million base pair (bp) lengths on the X-chromosome. The dystrophin-deficient DMD$^{mdx}$ (mdx) mouse, an animal model of DMD, carries a nonsense mutation in exon 23 of the dystrophin gene; this mutation causes a lack of dystrophin expression and results in muscle pathology similar to human DMD (Bulfield *et al.*, 1984; Hoffman *et al.*, 1987; Sicinski *et al.*, 1989). Becker muscular dystrophy (BMD), which is also caused by a dystrophin gene mutation, is a milder

[1]Growth and Development Laboratory, Children's Hospital of Pittsburgh; Department of Orthopaedic Surgery and [2]Molecular Genetics and Biochemistry, University of Pittsburgh, Pittsburgh, PA 15213.
[3]Department of Child Development, Kumamoto University, Kumamoto 860, Japan.

dystrophic disease for which the age of onset can sometimes be as late as the third or fourth decade of life (Engel *et al.*, 1994). Observation of a number of mildly affected patients with BMD bearing large in-frame deletions—including one patient displaying an absence of over 40% of the central rod domain of the dystrophin gene—suggests that a functional mini-dystrophin gene could alleviate the DMD phenotype (England *et al.*, 1990). Gene therapy studies based on viral and nonviral vectors have been performed to evaluate delivery of both the full-length dystrophin and many versions of mini-dystrophin genes extensively to assuage the muscle weakness commonly observed in mdx mice (Acsadi *et al.*, 1996; Hauser *et al.*, 1997; Akkaraju *et al.*, 1999; Chapdelaine *et al.*, 2000; Hartigan-O'Connor and Chamberlain, 2000; Wang *et al.*, 2000; Campeau *et al.*, 2001; Gilbert *et al.*, 2001; Fabb *et al.*, 2002; Gilchrist *et al.*, 2002; Harper *et al.*, 2002; Larochelle *et al.*, 2002; Scott *et al.*, 2002; Watchko *et al.*, 2002).

Retroviral vectors also have been widely used to deliver genes in skeletal muscle; these vectors represent some of the most frequently used viral vectors in many fields of gene therapy because retroviral transduction is relatively safe (low immunogenicity) and the transgene expression is stable (integrated into genomic DNA) (Mulligan, 1993). Researchers have demonstrated that a truncated (6.3 kb) human dystrophin cDNA can be retrovirally transduced and expressed in mdx mouse myoblasts *in vitro* (Dunckley *et al.*, 1992), and that retroviral transduction of activated satellite cells in regenerating skeletal muscle can facilitate direct and stable dystrophin gene transfer into muscle tissues *in vivo* (Dunckley *et al.*, 1993). Because the retrovirus requires dividing cells for its integration, the ongoing process of muscle degeneration and regeneration that occurs in mdx mouse skeletal muscle is thought to promote the efficient retroviral transduction observed in skeletal muscle *in vivo*.

Alternatively, the transplantation of normal myoblasts into dystrophin-deficient muscle (both mdx and DMD patient muscle) can create a reservoir of normal myoblasts capable of delivering genes, including dystrophin, within the regenerated skeletal muscle fibers (Morgan *et al.*, 1988, 1990, 1993; Dunckley *et al.*, 1992; Huard *et al.*, 1992, 1994a,b,c; Karpati *et al.*, 1992; Salvatori *et al.*, 1993; Tremblay *et al.*, 1993; Beauchamp *et al.*, 1994, 1999; Kinoshita *et al.*, 1994; Mendell *et al.*, 1995; Vilquin *et al.*, 1995; Fan *et al.*, 1996; Guerette *et al.*, 1997; Gussoni *et al.*, 1997, 1999; Partridge *et al.*, 1997; Qu and Huard, 2000; Smythe *et al.*, 2000, 2001; Camirand *et al.*, 2001). The transplantation of myoblasts can enable transient delivery of dystrophin and improve the strength of injected dystrophic muscle, but this approach has various limitations, including immune rejection, poor cellular survival rates, and limited dissemination of the injected cells (Morgan *et al.*, 1988, 1990, 1993; Dunckley *et al.*, 1992; Huard *et al.*, 1992, 1994a,b,c; Karpati *et al.*, 1992; Salvatori *et al.*, 1993; Tremblay *et al.*, 1993; Beauchamp *et al.*, 1994; Kinoshita *et al.*, 1994; Mendell *et al.*, 1995; Vilquin *et al.*, 1995; Fan *et al.*, 1996; Guerette *et al.*, 1997; Gussoni *et al.*, 1997, 1999; Partridge *et al.*, 1997; Beauchamp *et al.*, 1999; Qu and Huard, 2000; Smythe *et al.*, 2000, 2001; Camirand *et al.*, 2001). To improve the efficiency of cell transplantation, we and others have been studying various subpopulations of muscle-derived cells that may display stem cell characteristics (Gussoni *et al.*, 1999; Lee *et al.*, 2000; Blau *et al.*, 2001; Goodell *et al.*, 2001; Seale *et al.*, 2001; Deasy *et al.*, 2002; Goldring *et al.*, 2002; Jackson *et al.*, 2002; Qu-Petersen *et al.*, 2002). Our research group has used a modified preplate technique to isolate a unique population of myogenic cells that display stem cell characteristics and an improved transplantation capacity in skeletal muscle (Qu *et al.*, 1998; Lee *et al.*, 2000; Qu-Petersen *et al.*, 2002). Although the reason for this improved transplantation capacity is not fully understood, the unique ability of this cell population to display immune-privileged behavior—in combination with high self-renewal and multipotent differentiation abilities—suggests a possible mechanism for this improved cell transplantation behavior (Qu-Petersen *et al.*, 2002).

In this paper we investigate the combination of cell therapy using mdx muscle-derived stem cells (MDSCs) and gene therapy based on retroviral gene transfer to deliver a functional mini-dystrophin (3.9 kb) (Wang *et al.*, 2000; Watchko *et al.*, 2002) in mdx skeletal muscle. The injected mdx muscles were monitored for dystrophin restoration and the presence of immune response at various time points (up to 24 weeks post-transplantation). Our findings demonstrate the feasibility of dystrophin delivery in mdx skeletal muscle based on *ex vivo* gene transfer using genetically engineered mdx MDSCs, and highlight potential limitations of this gene transfer technology.

## MATERIALS AND METHODS

### *Animals*

All animals used in this study were mdx mice (C57BL/10 ScSn-DMD$^{mdx}$/J) purchased from the Jackson Laboratory (Bar Harbor, ME) and housed in the Rangos Research Center Animal Facility of Children's Hospital of Pittsburgh.

### *Retrovirus construction*

SnaBI/*Sal*I DNA fragment of pAAV-Mini-becker1 (pA3999) (Wang *et al.*, 2000) carrying human mini-dystrophin was cloned into the *Sna*BI/*Sal*I site of retrovirus plasmid pLNCX2 (CLONTECH Laboratories, Palo Alto, CA) to generate pLNCDys3999 (Fig. 1A). Two micrograms of retrovirus plasmid pLNCDys3999 was transfected to pantropic retrovirus-producing cell line $GP_2293$ (CLONTECH Laboratories) with 5 $\mu$l of LipofectAMINE 2000 (GIBCO BRL, Rockville, MD) following the manufacturer's protocol. After 2 weeks of selection (G418, 500 $\mu$g/ml), stably transduced $GP_2293$/pLNCDys3999 cells were transfected with plasmid from the vesicular stomatitis virus, which encodes the envelope glycoprotein (pVSV-G) (CLONTECH Laboratories), using LipofectAMINE 2000. The second day after transfection, medium containing the virus was collected and filtered using a 0.45-$\mu$m cellulose acetate membrane (Nalge Company, Rochester, NY). Collected retrovirus solutions (RetroDys3999) were frozen at −80°C until use.

### *Cell culture*

mdx MDSCs and mouse myoblast cell line (C2C12) cells were cultured in proliferation medium using collagenated flasks or 6- or 12-well plates. Proliferation medium contains Dul-

becco's modified Eagle's medium (DMEM) supplemented with 10% fetal bovine serum, 10% horse serum (HS), 0.5% chick embryo extract, and 1% penicillin and streptomycin (all of which were purchased from GIBCO BRL). In order to induce differentiation, proliferation medium was replaced by differentiation medium consisting of DMEM supplemented with 1% fetal bovine serum and 1% HS. Pantropic retrovirus-producing cell line $GP_2293$ (CLONTECH Laboratories) and human fibrosarcoma cell line HT1080 were cultured in DMEM supplemented with 10% fetal bovine serum and 1% penicillin and streptomycin. For selection of neomycin-resistant cells, 500 to 1000 $\mu$g/ml of Geneticin (G418 sulfate, GIBCO BRL) was added to the medium described above.

### *Examination of RetroDys3999 and the existence of replication-competent retrovirus*

Cells from the mouse myoblast cell line C2C12 were transduced with RetroDys3999 and grown to less than 50% confluence. Total RNA was isolated and subjected to reverse transcriptase-polymerase chain reaction (RT-PCR) to detect human mini-dystrophin expression. RetroDys3999-transduced C2C12 cells (C2C12/RetroDys3999) were used to assess the existence of replication-competent retrovirus. Human fibrosarcoma cell line HT1080 and a retrovirus carrying LacZ (RVlacZ (Cosset *et al.*, 1995)) were used for this experiment. Medium was collected from the C2C12/RetroDys3999-confluent T25 flask and filtered (conditioned medium). The HT1080 cells were transduced with RVlacZ (HT1080/LacZ). Conditioned medium and polybrene (final concentration 8 $\mu$g/ml) were added to HT1080/LacZ cells. After 2 weeks of culture, medium was collected, filtered, and added, together with polybrene, to the HT1080 cell line. Two days later, the cells were fixed with 1% glutaraldehyde (Sigma, St. Louis, MO) for 1 min, rinsed twice in phosphate-buffered saline (PBS), and incubated in X-gal substrate (0.4 mg/ml 5-bromo-4-chloro-3-indolyl $\beta$-D-galactoside [Boehringer-Mannheim, Indianapolis, IN], 1 m*M* $MgCl_2$, 5 m*M* $K_4Fe(CN)_6$/5 m*M* $K_3Fe(CN)_6$ in PBS) for 3 hr at 37°C to evaluate LacZ expression.

### *MDSC isolation and retroviral transduction*

MDSCs were isolated from neonatal mdx mice and highly purified as described in previous publications (Qu *et al.*, 1998; Qu-Petersen *et al.*, 2002). MDSCs were grown to less than 30% confluence, and $2.5 \times 10^3$ cells were plated in 1 well of a 12-well plate. The next day, 400 $\mu$l of retrovirus solution (RetroDys3999) and 8 $\mu$g of polybrene were diluted to a total volume of 1.2 ml in proliferation medium (PM) and added to the cells for transduction. Transduced cells were selected by G418 (1 mg/ml) for 2 weeks until colonies appeared. Colonies then were picked up and expanded. Clones were termed MD39xx.

### *Immunocytochemistry for cells in culture*

Cells were fixed with cold methanol for 2 min, and then rinsed twice with PBS and blocked by 5% HS for 1 hr. Next, the cells were incubated overnight at room temperature (RT) with the primary antibodies NCL-DYS3 (Novocastra Laboratories, Newcastle upon Tyne, UK), biotin anti-mouse-Sca-1 (1:200, BD Pharmingen, San Diego, CA, USA), biotin anti-mouse-CD34 (1:200, BD Pharmingen), and mouse anti-desmin (1:200, D-1033, Sigma). After several rinses with PBS, biotinylated anti-mouse IgG (1:250, Vector Laboratories, Burlingame, CA) was added as a secondary antibody, and the cells were incubated for 1 hr at RT. Finally all cells were rinsed three times with PBS, and Cy3-conjugated streptavidin (1:300, Sigma) was applied for 1 hr at RT. Stainings without the primary antibodies were performed as negative controls.

### *RT-PCR*

Cells were grown in 6-well plates. When the cells had grown to semiconfluence (i.e., very few myotubes were found), total RNA was isolated using 1 ml of TRIzol reagent (GIBCO BRL) per well following the manufacturer's instructions. Reverse transcription reactions were performed using the First Strand Synthesis Kit and random primer purchased from GIBCO BRL following the manufacturer's protocol. One microliter of first-strand cDNA was used for PCR analysis for dystrophin and $\beta$-actin. Primer sequences for human dystrophin were sense: ATG CTT TGG TGG GAA GAA GTA G, and antisense: CCC TGT CAG GCC TTC GAG G; and for mouse $\beta$-actin sense: GTG GGC CGC TCT AGG CAC CAA, and antisense: CTC TTT GAT GTC ACG CAC GAT TTC. Reaction conditions included a 94°C denaturing step (5 min), 30 ($\beta$-actin) or 35 (dystrophin) cycles of 94°C (15 sec), 65°C ($\beta$-actin) or 67°C (dystrophin) (15 sec), 72°C (30 sec), and a final extension step of 72°C (7 min).

### *Cell transplantation*

Adult mdx mice (2–3 months old) were used as recipients for cell transplantation. Transduced cells were trypsinized by

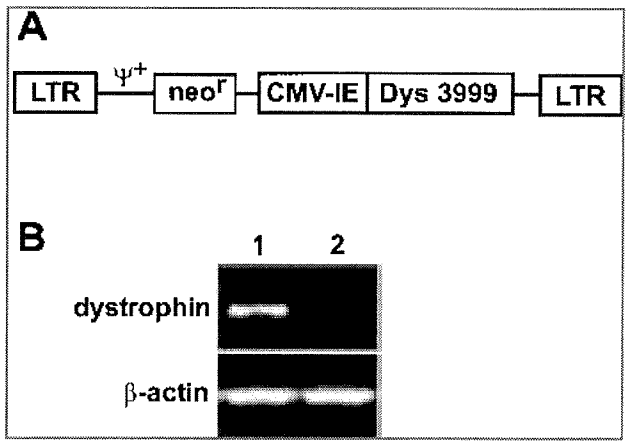


**FIG. 1.** **A**: Construction of RetroDys3999, which carries the viral long terminal repeat (LTR), virus packaging signal ($\psi^+$), neomycin resistance gene (neo$^r$), and human mini-dystrophin gene (Dys3999) driven by the CMV-IE promoter (CMV-IE). **B**: Reverse transcriptase-polymerase chain reaction (RT-PCR) for dystrophin (top) and $\beta$-actin (bottom). Lane 1: C2C12 cells transduced with RetroDys3999; lane 2: nontransduced C2C12 cells (negative control).

0.25% trypsin (Invitrogen, Carlsbad, CA) and resuspended in Hanks' balanced salt solution (HBSS). A Drummond syringe was used to inject $3 \times 10^5$ MD39xx cells into the gastrocnemius muscles of mdx mice. Control injections were performed using (1) nontransduced mdx MDSCs and (2) HBSS alone. In order to investigate the persistence of transgene expression, injected mdx mice were sacrificed at different time points postinjection. For the repeated injection experiment, 3 mdx mice received injections into the right gastrocnemius muscle and, 2 weeks later, the same number of cells was injected into the left gastrocnemius muscle of the same mice. The animals were sacrificed 2 weeks after the second injection. The same number of cells ($3 \times 10^5$ cells per muscle) from 8 mdx MDSC/Dys3999 clones also was injected into the gastrocnemius muscles of mdx mice (2–3 mice per clone). Two weeks after injection, the mice were sacrificed. Injected gastrocnemius muscles were frozen in liquid nitrogen-chilled 2-methylbutane and kept at −80°C. Muscles were cryosectioned at 8-$\mu$m thickness and were eval-

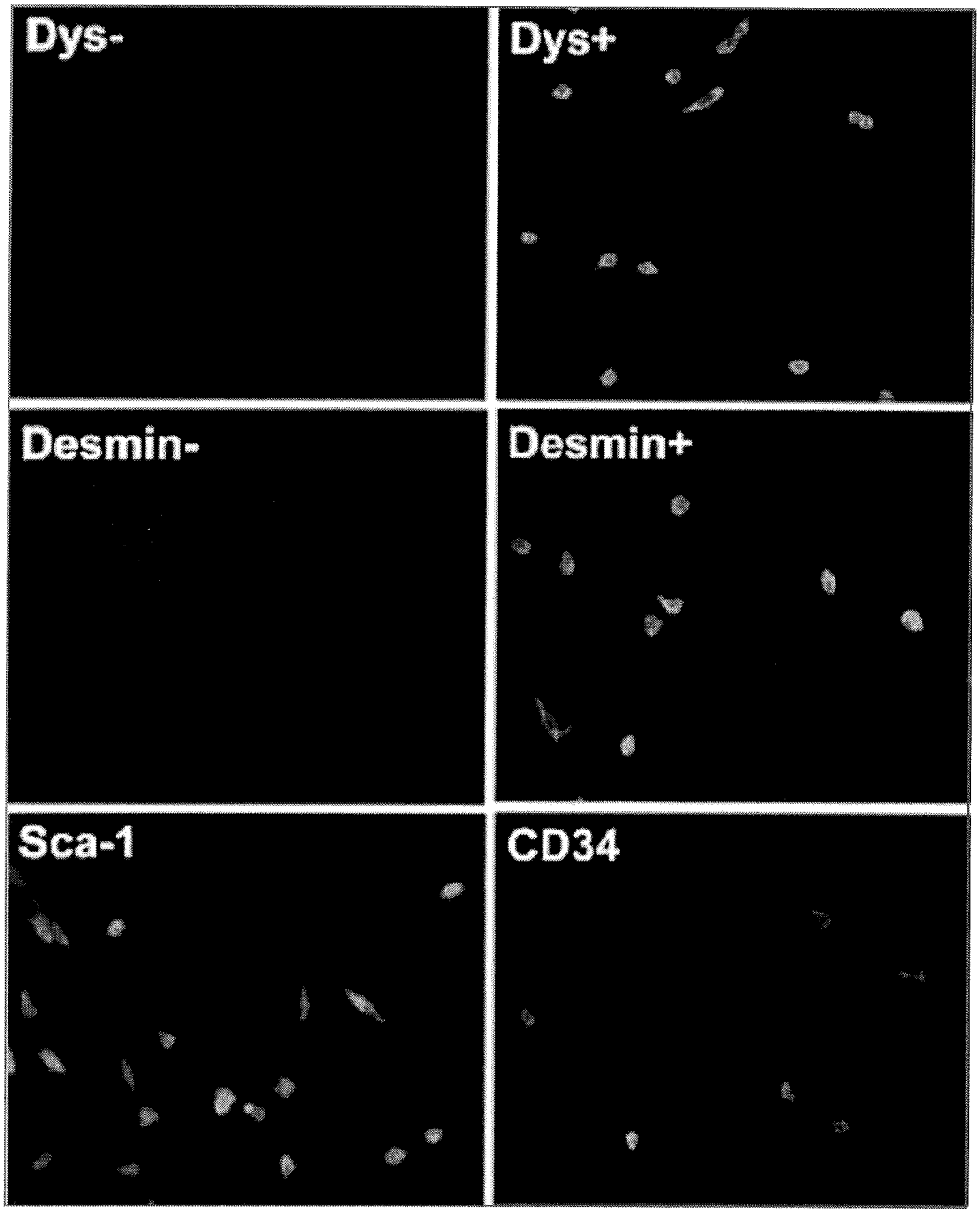


**FIG. 2.** Characterization of dystrophin-deficient $DMD^{mdx}$ (mdx) muscle-derived stem cells (MDSCs) transduced with RetroDys3999 (MD3999). Immunocytochemistry revealed that MD3999 cells expressed dystrophin (Dys) while continuing to express CD34, Sca-1, and desmin. Negative controls for dystrophin (Dys-) and desmin (Desmin-) are also shown. Original magnification ×100.

uated by hematoxylin and eosin (H&E) staining and immunohistochemistry (see below).

### *Immunohistochemistry for dystrophin expression in muscle*

The Mouse on Mouse (M.O.M.) Immunodetection Kit Fluorescein (Vector Laboratories) and NCL-DYS3 (Novocastra Laboratories) were used in accordance with the manufacturers' protocols, except for two steps: (1) cryosections were immediately treated with blocking buffer without the fixation step and (2) Cy3-conjugated streptavidin (1:1000 at RT for 1 hr; Sigma) was used instead of fluorescein avidin. Dystrophin-positive myofibers were counted in the section from each muscle that showed the highest number of dystrophin-positive myofibers. The average number was obtained by counting the dystrophin-positive myofibers in all the muscle sections in a given group. Staining without the primary antibody was used as a negative control.

### *Detection of CD4- and CD8-positive activated lymphocytes and cytokines*

Muscle sections were fixed with cold acetone for 5 min, and the endogenous peroxidase activity was quenched with hydrogen peroxide ($H_2O_2$, 0.3%) for 30 min. After several rinses and 40 min of blocking by 10% HS, sections were incubated for 1 hr at RT using the following antibodies: rat anti-mouse CD4 and rat anti-mouse CD8a (1:100, BD Biosciences); rabbit anti-mouse interleukin (IL)-1$\alpha$ (1:100, Chemicon, Temecula, CA); biotinylated rabbit anti-mouse IL-1$\beta$ (2 $\mu$g/ml; Chemicon); mouse anti-transforming growth factor (TGF)-$\beta_1$ (1:200, Novocastra Laboratories); rabbit anti-TGF-$\alpha_2$ (1:200, Santa Cruz Biotechnology, Santa Cruz, CA); biotinylated anti-mouse CD54 (1:100; BD Biosciences); and goat anti-mouse tumor necrosis factor (TNF)-$\alpha$ (5 $\mu$g/ml, Leinco Technologies, St. Louis, MO). Secondary antibodies included the following: biotinylated goat anti-rat IgG (1:400; Vector Laboratories); fluorescein isothiocyanate (FITC) goat anti-rabbit (1:100, Chemicon), Cy3-conjugated anti-mouse IgG (1:100; Sigma), and Cy3-conjugated anti-goat IgG (1:100, Sigma). For biotinylated antibodies, Cy3-conjugated streptavidin (1:1000; Sigma) was applied. For CD4/CD8 staining, a third antibody (streptavidin/horseradish peroxidase [HRP], 1:800; DAKO, Carpinteria, CA) was used for 40 min at RT. After several rinses, the peroxidase activity was revealed using 3′,3′-diaminobenzidine (1 mg/ml; Sigma) and hydrogen peroxide (0.03%). Stainings without primary antibodies were used as negative controls.

## RESULTS

### *Retroviral transduction of muscle cells* in vitro

RetroDys3999 (Fig. 1A) was used to transduce C2C12 cells, and human dystrophin expression was monitored by RT-PCR. Human dystrophin mRNA was detected in the retrovirally-transduced C2C12 myoblasts (Fig. 1B, lane 1), but not in control nontransduced C2C12 cells (Fig. 1B, lane 2).

RetroDys3999-transduced C2C12 cells (C2C12/RetroDys 3999) also were used to assess the existence of replication-competent retrovirus. Human fibrosarcoma cell line HT1080 and a retrovirus carrying LacZ (RVlacZ (Cosset *et al.*, 1995)) were used for this experiment. No LacZ-positive cells were found in the HT1080 cells, indicating that no replication-competent retrovirus was generated from the RetroDys3999-transduced C2C12 cells (data not shown).

### *mdx MDSCs transduced by RetroDys3999*

mdx MDSCs were isolated from the tibialis anterior muscle of mdx mice. The cells were transduced with the RetroDys3999 and selected by G418 (Lee *et al.*, 2000). The characteristics of the stably transduced cells (MD3999) were examined by immunocytochemistry. More than 95% of the MD3999 cells expressed dystrophin, stem cell markers CD34 and Sca-1, and the myogenic marker desmin (Fig. 2). These results suggest that MD3999 cells at least partially retained their stem cell characteristics after retroviral transduction *in vitro*. Negative controls in which the dystrophin or desmin antibodies were omitted revealed no staining.

### *Isogenic cell transplantation*

mdx MD3999 cells were injected intramuscularly into mdx mice, and the injected animals were sacrificed at different time points (2, 4, 8, 12, or 24 weeks postinjection; see Fig. 3 for schematic representation of the experimental design). Human dystrophin expression was detected at each postinjection time point by immunohistochemistry using anti-human dystrophin mouse monoclonal antibody NCL-DYS3. No human dystrophin-positive myofibers were found in the noninjected areas indicating, as previously reported (Huard *et al.*, 1993), that the antibody NCL-DYS3 reacts specifically with human dystrophin and not with mouse dystrophin expressed in revertant myofibers (Fig. 4A). The number of dystrophin-positivemyofibers observed at all time points remained constant, though a nonsignificant decrease was noted at 24 weeks postinjection (Fig. 4B).

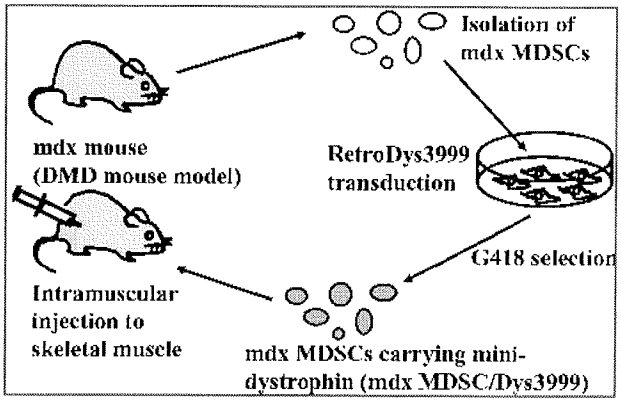


**FIG. 3.** Schematic representation of the different steps involved in autologous muscle-derived stem cell (MDSC) transfer in dystrophin-deficient $DMD^{mdx}$ (mdx) skeletal muscle, including MDSC isolation, retroviral transduction, and cell transplantation.

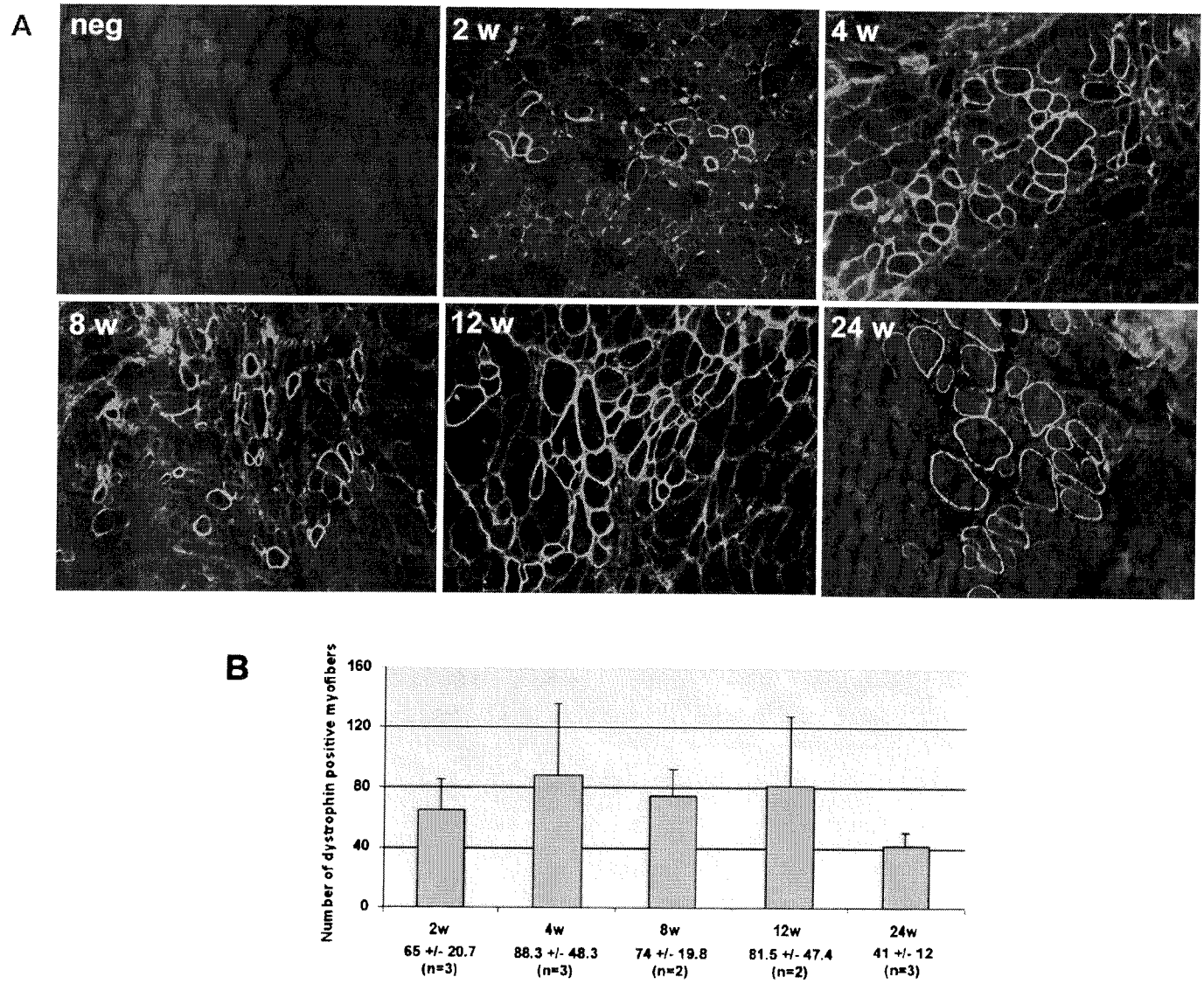


**FIG. 4.** Human dystrophin expression in dystrophin-deficient $DMD^{mdx}$ (mdx) mouse muscle implanted with mdx MD3999 cells at different time points (2, 4, 8, 12, and 24 weeks [w] postinjection [**A**]). neg: negative control for dystrophin staining. The injections were made with one trajectory in all cases. The numbers of dystrophin-positive myofibers in mdx muscle injected with mdx MD3999 cells remained constant, although we noted a nonsignificant decrease at 24 weeks postinjection. The number of dystrophin-positive myofibers (average ± the standard error) and the number of samples used for each time point posttransplantation are shown (**B**). Original magnification of (A) × 200.

### *Transplanted, transduced MDSCs triggered an immune response*

We detected the presence of activated lymphocytes at the site of the implanted MDSCs. CD4- and CD8-positive activated lymphocytes were detected in the injected area at 2 weeks (Fig. 5C and 5D) and 4 weeks postinjection (data not shown), but not in the noninjected muscles (Fig. 5A and 5B). We also detected various levels of cytokine expression in the injection site (Fig. 5E and 5J). No increase in cell infiltration occurred in the muscles injected with nongenetically engineered mdx MDSCs or HBSS alone when compared to noninjected mdx muscle (data not shown). To determine whether the immune response observed 2 and 4 weeks postimplantation limited the regenerating capacity of the injected cells, we performed a second transplantation 2 weeks after the first MDSC injections (Fig. 6). Initially, $3 \times 10^5$ mdx MD3999 cells were injected into the right gastrocnemius muscles of mdx mice and, 2 weeks later, an equivalent number of mdx MD3999 cells were injected into the left gastrocnemius muscles of the same mice. Two weeks after the second injection (4 weeks after the first injection), both injected gastrocnemius muscles were harvested and the number of regenerated dystrophin-expressing myofibers was quantified and compared. Fewer dystrophin-positivemyofibers were present in the left gas-

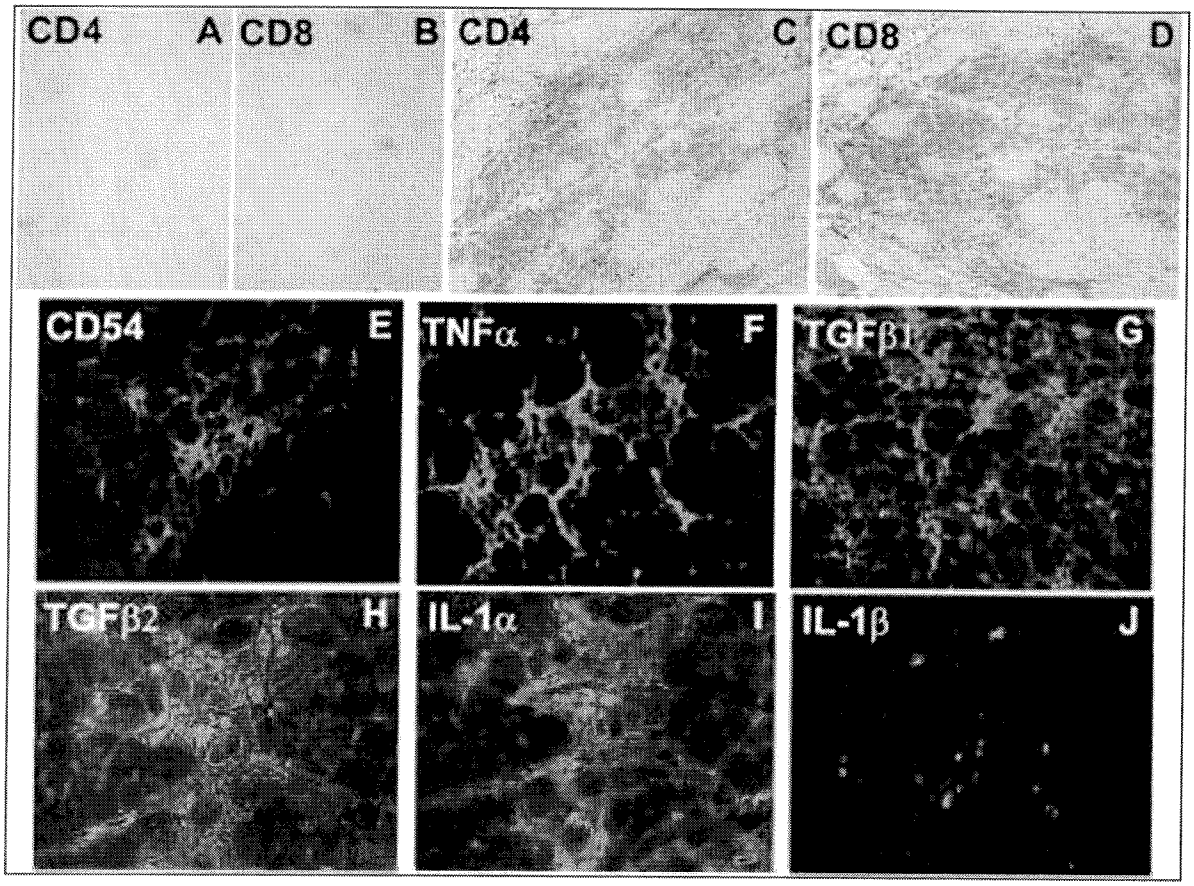


**FIG. 5.** Immunohistochemical detection of CD4 and CD8 cells in dystrophin-deficient $DMD^{mdx}$ (mdx) muscle injected with MD3999 cells at 2 weeks postinjection. **A** and **B**: CD4 and CD8 immunostaining in noninjected mdx mouse muscle (control). **C** and **D**: CD4 and CD8 cell infiltration in the injected mdx muscle. A variety of cytokines, including CD54 (**E**), tumor necrosis factor (TNF)-$\alpha$ (**F**), transforming growth factor (TGF)-$\beta_1$ (**G**), TGF-$\beta_2$ (**H**), interleukin (IL)-1$\alpha$ (**I**), and IL-1$\beta$ (**J**), also were detected in the injection site. Original magnification × 200.

trocnemius muscle (second injection) than in the right gastrocnemius muscle (first injection; Fig. 6). In light of the immune response previously observed 2 weeks after MD3999 injection, it is feasible that the first injection of MD3999 cells in this experiment triggered an immune response that rapidly eliminated the cells injected in the second transplantation. However, we cannot rule out the possibility that the smaller number of dystrophin-positive myofibers observed in the muscles injected at the later time point is attributable to the high variation in the number of dystrophin-positive myofibers generated in the transplanted animals. Given the persistent dystrophin expression observed 24 weeks posttransplantation, it also is possible that myofibers are more resistant than mononucleated cells to immune rejection.

### *Differential regenerative capacity among retrovirally-transduced MDSC clones*

Based on the low number of dystrophin-positive myofibers found within the injected mdx skeletal muscle following implantation of mdx MD3999 cells, we elected to test whether a differential regenerative capacity exists among clones of retrovirally transduced MDSCs. Eight clones were picked up from mdx MDSCs after RetroDys3999 transduction and were grown as described above. These clones (MD3903, MD3904, MD3905, MD3907, MD3918, MD3919, MD3926, and MD3927) were injected into the muscles of mdx mice, and the mice were sacrificed 2 weeks postinjection. The number of dystrophin-positive myofibers in the injected muscles ranged from 343 ± 32.3 (MD3903) to 0 (MD3927) (Fig. 7A). We paid special attention to the MD3927 clone, because no dystrophin-positive myofibers were found within the mdx muscle injected with these cells. Dystrophin expression of MD3927 clone cells *in vitro* was confirmed by RT-PCR (Fig. 7B), and these cells were able to fuse into myotubes when cultured in differentiation medium (Fig. 7C). Although at 2 weeks postinjection we observed many mononucleated cells of unknown origin in the areas injected with MD3927 cells, immunohistochemistry revealed an absence of dystrophin-positive myofibers (Fig. 7D). These results suggest that a differential regenerative capacity exists among various MD39xx clones and, consequently, that the level of dystrophin restoration within the injected mdx muscle is highly dependent on which MD39xx clone is used.

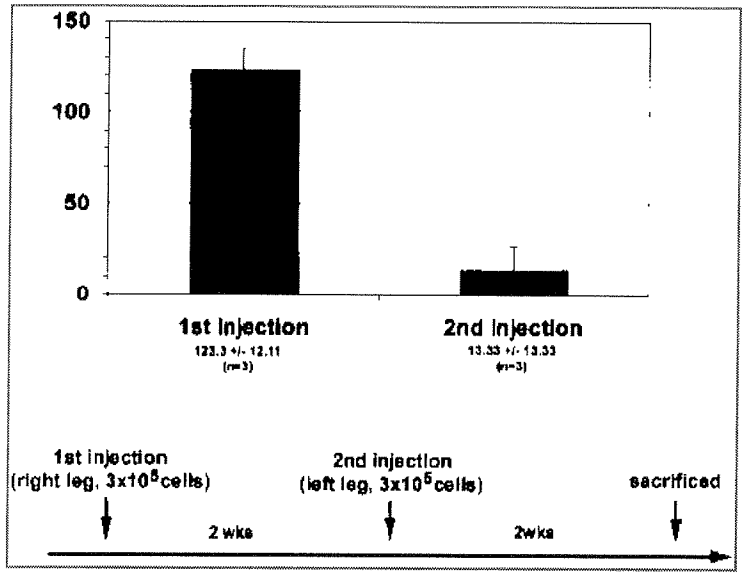


**FIG. 6.** The different numbers of dystrophin-positive myofibers generated by the first and second transplantation of genetically engineered muscle-derived stem cells (MDSCs). The second injection of dystrophin-deficient $DMD^{mdx}$ (mdx) MD3999 cells was performed 2 weeks after the first injection. The mean ± standard error of the number of dystrophin-positive muscle fibers and the numbers of samples (*n*) also are shown.

## DISCUSSION

In this study, we investigated the efficacy of *ex vivo* gene transfer based on a retrovirus vector carrying a functional human mini-dystrophin and isogenic MDSCs obtained from dystrophin-deficient mdx mice. Characterization of the dystrophin-expressing transduced cells (MD3999 cells) indicated that the cells preserved their stem cell marker profile (CD34-positive, Sca-1–positive) despite retroviral transduction (Fig. 2). Transplantation of these retrovirally transduced MDSCs resulted in dystrophin delivery in mdx mouse skeletal muscle. Although the number of dystrophin-positive myofibers observed in the mdx muscle was relatively low, it remained stable for up to 6 months postinjection. This low number of regenerating dystrophin-expressing muscle fibers within the injected mdx muscle is likely attributable to the low regenerative capacity of selected MDSC/Dys3999 clones. Indeed, further research revealed that some MDSC/Dys3999 clones display a high regenerative capacity when injected into skeletal muscle while others display very low regenerative efficiency. We hypothesize that some of the injected cells do not fuse with myofibers following injection but become quiescent like satellite cells, as previously described (Qu-Petersen *et al.*, 2002). The persistence of dystrophin-positive myofibers may be related to the ongoing regeneration mediated by the activation and subsequent proliferation of these quiescent satellite cells. Alternatively, because the mini-dystrophin gene used in this study is functional (Wang *et al.*, 2000; Watchko *et al.*, 2002), dystrophin generated by the fusion of injected cells also may protect the muscle fibers against further cycles of degeneration and regeneration.

Despite the fact that RetroDys3999 does not encode for any viral proteins, CD4- and CD8-positive lymphocytes were detected in the injected area at 2 and 4 weeks postinjection. These data suggest an immune reaction against the injected, retrovirally transduced mdx MDSCs as previously reported with adenovirally transduced mdx myoblasts expressing full-length dystrophin (Floyd *et al.*, 1998). Although the cells used in this experiment were derived from mdx mice and should not generate an immune response when injected into mdx mice, the retroviral transduction of the cells to express human dystrophin may have triggered the immune response. Notably, despite the presence of revertant, dystrophin-positive myofibers in the skeletal muscle of DMD patients (Nicholson *et al.*, 1990), DMD patients and mdx mice who undergo myoblast transplantation using cells obtained from HLA-compatible donors develop antibodies specific for the dystrophin protein (Roy *et al.*, 1993; Vilquin *et al.*, 1995).

To determine whether these infiltrated lymphocytes limit the ability of this technology to deliver dystrophin within the injected mdx muscle, we performed a second injection of MD3999 cells (same quantity) and compared the number of dystrophin-positive myofibers generated by the first injection to that generated by the second. Indeed, we observed that the second injection failed to generate as many dystrophin-positive myofibers as the first injection. We hypothesize that the second MD3999 injection occurred at a time of massive CD4- and CD8-positive cell activation triggered by the first injection, resulting in quicker rejection of the injected cells. However, the difference could be related to the high variability in the number of dystrophin-positive myofibers observed in the injected animals. We also cannot exclude the possibility that the dystrophin-expressing MDSCs injected in the second transplantation did not readily fuse into myofibers and thus were rapidly

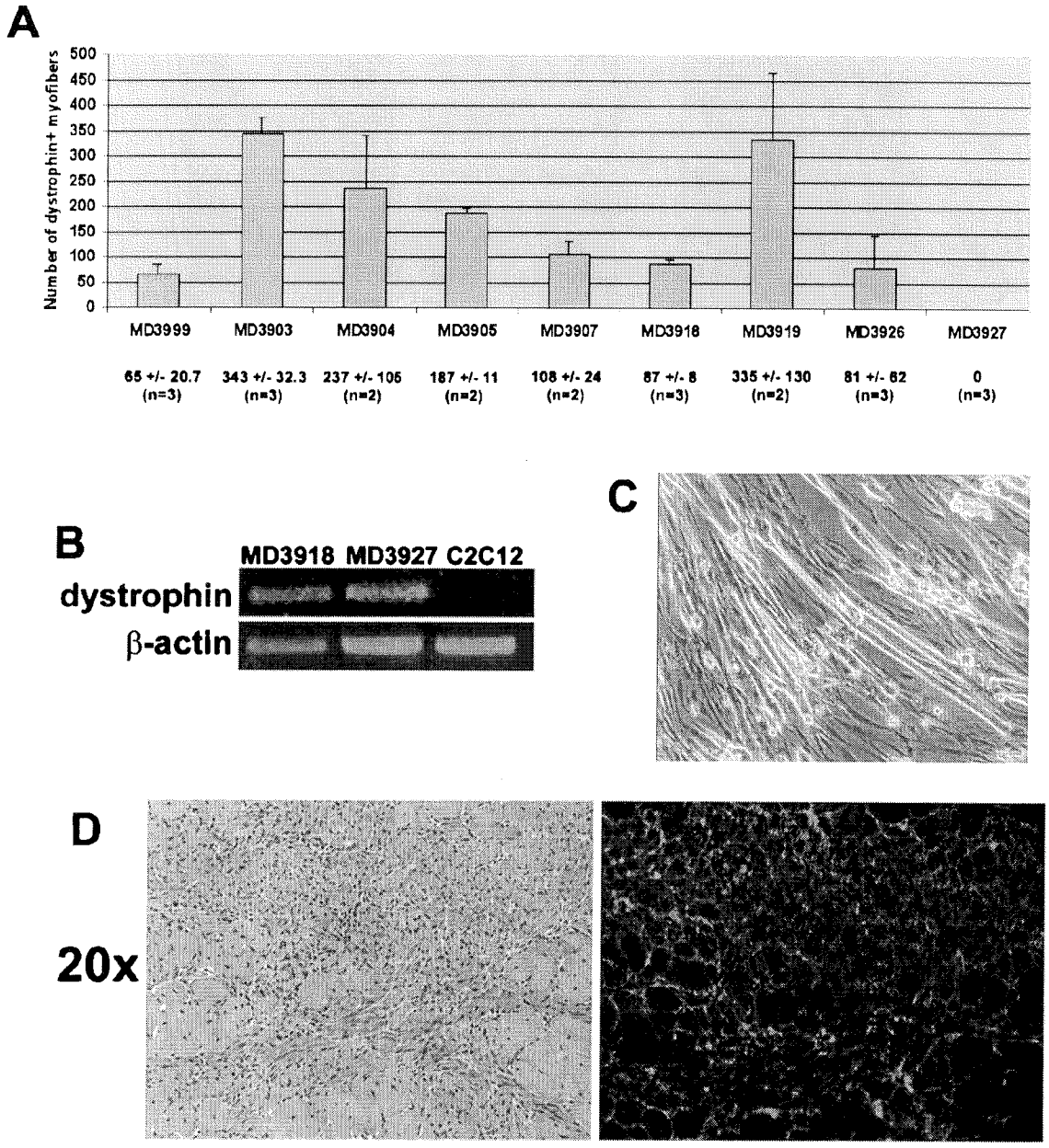


**FIG. 7.** The number of dystrophin-positive myofibers in dystrophin-deficient $DMD^{mdx}$ (mdx) muscle injected with different mdx MDSC/Dys3999 clones at 2 weeks postinjection (**A**). The average of the numbers of human dystrophin-positive myofibers (± standard error) and the numbers of samples (*n*) are shown. Reverse transcriptase-polymerase chain reaction (RT-PCR) analysis of MD3918, MD3927, and C2C12 cells for dystrophin and β-actin showed that both MD3918 and MD3927 express the human mini-dystrophin gene (**B**). MD3927 cells are capable of differentiating into myotubes after 10 days of culturing in differentiation medium (**C**). However, immunohistochemistry (**D**) revealed no dystrophin-positive myofibers in the MD3927 clone cell-injected muscle 2 weeks postinjection. Original magnification × 200 (C, D).

rejected. In contrast, the vast majority of cells injected in the first transplantation had differentiated into myotubes and myofibers by 2 weeks postinjection. We therefore believe that the use of a muscle-specific promoter such as muscle creatine kinase (MCK), which would drive the transgene expression only in differentiated muscle cells like muscle fibers, may be an alternative approach by which to prevent the rejection of genetically engineered MDSCs prior to their fusion into myotubes and myofibers (Hauser *et al.*, 2000; Hartigan-O'Connor *et al.*, 2001).

Clearly, the *ex vivo* technique based on genetically engineered mdx MDSCs cannot, in its current form, enable delivery of an amount of dystrophin sufficient to alleviate the muscle weakness that characterizes DMD. In an attempt to identify cells with the capacity for more efficient dystrophin delivery, we tried to pick up additional mdx MDSC/Dys3999 clones. Analysis of these mdx MDSC clones (MD39xx) indicated that their ability to deliver dystrophin was variable. One clone, MD3927, exhibited particularly interesting behavior. Although MD3927 cells demonstrated the capacity to fuse into myotubes and express dystrophin *in vitro*, no dystrophin-expressing myofibers were observed 2 weeks after injection of these cells into mdx muscle. Numerous mononucleated cells were found in the injected area, but no dystrophin expression was observed at the injection site. The exact mechanism behind this occurrence is unclear. The selection of MDSC clones that display a good regenerative capacity in skeletal muscle likely would help to improve the delivery of dystrophin via this technology. Some clones, such as MD3903, were able to deliver dystrophin much more efficiently than were the original, MD3999 clone cells (343 ± 32.3 vs. 65 ± 20.7). It is paramount to utilize MDSC clones that display an improved regenerative capacity to achieve efficient retroviral *ex vivo* dystrophin delivery in mdx skeletal muscle.

In summary, this report demonstrates the feasibility of isogenic mdx MDSC-mediated *ex vivo* dystrophin gene transfer in mdx skeletal muscle. This transfer method enabled stable delivery of the dystrophin gene into dystrophin-deficient mdx mouse muscle for up to 24 weeks posttransplantation. However, we observed an infiltration of CD4 and CD8 activated lymphocytes and the secretion of a variety of cytokines in the injection site. This immune response may have been triggered by the human mini-dystrophin gene engineered into the mdx MDSCs, although we cannot exclude the potential contribution of the retrovirus or the neomycin resistance gene product to this immune response. We believe this immune response was related to the observed decrease in the number of dystrophin-positive myofibers at later time points. Although we have not yet determined why different MD39xx clones display disparate survival or differentiation behaviors, this finding should attract the attention of researchers in the field. Screening for and utilizing transduced MDSC clones that display an improved transplantation capacity may lead to efficient dystrophin delivery via this technology.

## ACKNOWLEDGMENTS

The authors wish to thank Marcelle Pellerin, James Cummins, and Brian Gearhart (Children's Hospital of Pittsburgh, Pittsburgh, PA) as well as Bing Wang (University of Pittsburgh, Pittsburgh, PA) for technical support and advice, and Ryan Sauder (University of Pittsburgh, Pittsburgh, PA) for editorial assistance with the manuscript. This work was supported by grants to Dr. Johnny Huard from the Muscular Dystrophy Association (USA), the National Institutes of Health (NIH PO1 AR 45925-01), the Orris C. Hirtzel and Beatrice Dewey Hirtzel Memorial Foundation, the William F. and Jean W. Donaldson Chair at Children's Hospital of Pittsburgh, and the Henry J. Mankin Endowed Chair at the University of Pittsburgh.

## REFERENCES

ACSADI, G., LOCHMULLER, H., JANI, A., HUARD, J., MASSIE, B., PRESCOTT, S., SIMONEAU, M., PETROF, B.J., and KARPATI, G. (1996). Dystrophin expression in muscles of mdx mice after adenovirus-mediated in vivo gene transfer. Hum. Gene Ther. **7,** 129–140.

AKKARAJU, G.R., HUARD, J., HOFFMAN, E.P., GOINS, W.F., PRUCHNIC, R., WATKINS, S.C., COHEN, J.B., and GLORIOSO, J.C. (1999). Herpes simplex virus vector-mediated dystrophin gene transfer and expression in MDX mouse skeletal muscle. J. Gene Med. **1,** 280–289.

ARAHATA, K., ISHIURA, S., ISHIGURO, T., TSUKAHARA, T., SUHARA, Y., EGUCHI, C., ISHIHARA, T., NONAKA, I., OZAWA, E., and SUGITA, H. (1988). Immunostaining of skeletal and cardiac muscle surface membrane with antibody against Duchenne muscular dystrophy peptide. Nature **333,** 861–863.

BEAUCHAMP, J.R., MORGAN, J.E., PAGEL, C.N., and PARTRIDGE, T.A. (1994). Quantitative studies of efficacy of myoblast transplantation. Muscle Nerve **18**(Suppl), 261.

BEAUCHAMP, J.R., MORGAN, J.E., PAGEL, C.N., and PARTRIDGE, T.A. (1999). Dynamics of myoblast transplantation reveal a discrete minority of precursors with stem cell-like properties as the myogenic source. J. Cell Biol. **144,** 1113–1122.

BLAU, H.M., BRAZELTON, T.R., and WEIMANN, J.M. (2001). The evolving concept of a stem cell: Entity or function? Cell **105,** 829–841.

BULFIELD, G., SILLER, W.G., WIGHT, P.A., and MOORE, K.J. (1984). X chromosome-linked muscular dystrophy (mdx) in the mouse. Proc. Natl. Acad. Sci. U.S.A. **81,** 1189–1192.

CAMIRAND, G., CARON, N.J., ASSELIN, I., and TREMBLAY, J.P. (2001). Combined immunosuppression of mycophenolate mofetil and FK506 for myoblast transplantation in mdx mice. Transplantation **72,** 38–44.

CAMPEAU, P., CHAPDELAINE, P., SEIGNEURIN-VENIN, S., MASSIE, B., and TREMBLAY, J.P. (2001). Transfection of large plasmids in primary human myoblasts. Gene Ther. **8,** 1387–1394.

CHAPDELAINE, P., MOISSET, P.A., CAMPEAU, P., ASSELIN, I., VILQUIN, J.T., and TREMBLAY, J.P. (2000). Functional EGFP-dystrophin fusion proteins for gene therapy vector development. Protein Eng. **13,** 611–615.

COSSET, F.L., TAKEUCHI, Y., BATTINI, J.L., WEISS, R.A., and COLLINS, M.K. (1995). High-titer packaging cells producing recombinant retroviruses resistant to human serum. J. Virol. **69,** 7430–7436.

DEASY, B.M., QU-PETERSON, Z., GREENBERGER, J.S., and HUARD, J. (2002). Mechanisms of muscle stem cell expansion with cytokines. Stem Cells **20,** 50–60.

DUNCKLEY, M.G., LOVE, D.R., DAVIES, K.E., WALSH, F.S., MORRIS, G.E., and DICKSON, G. (1992). Retroviral-mediated transfer of a dystrophin minigene into mdx mouse myoblasts in vitro. FEBS Lett. **296,** 128–134.

DUNCKLEY, M.G., WELLS, D.J., WALSH, F.S., and DICKSON, G. (1993). Direct retroviral-mediated transfer of a dystrophin minigene into mdx mouse muscle in vivo. Hum. Mol. Genet. **2,** 717–723.

ENGEL, A.G., YAMAMOTO, M., and FISCHBECK, K.H. (1994). Muscular dystrophies: Dystrophinopathies. In *Myology.* Engel AG, Franzini-Armstrong C, ed. (McGraw Hill Inc., New York) pp. 1133–1187.

ENGLAND, S.B., NICHOLSON, L.V., JOHNSON, M.A., FORREST, S.M., LOVE, D.R., ZUBRZYCKA-GAARN, E.E., BULMAN, D.E., HARRIS, J.B., and DAVIES, K.E. (1990). Very mild muscular dystrophy associated with the deletion of 46% of dystrophin. Nature **343,** 180–182.

FABB, S.A., WELLS, D.J., SERPENTE, P., and DICKSON, G. (2002). Adeno-associated virus vector gene transfer and sarcolemmal ex-

pression of a 144 kDa micro-dystrophin effectively restores the dystrophin-associated protein complex and inhibits myofibre degeneration in nude/mdx mice. Hum. Mol. Genet. **11,** 733–741.

FAN, Y., MALEY, M., BEILHARZ, M., and GROUNDS, M. (1996). Rapid death of injected myoblasts in myoblast transfer therapy. Muscle Nerve **19,** 853–860.

FLOYD, S.S., JR., CLEMENS, P.R., ONTELL, M.R., KOCHANEK, S., DAY, C.S., YANG, J., HAUSCHKA, S.D., BALKIR, L., MORGAN, J., MORELAND, M.S., FEERO, G.W., EPPERLY, M., and HUARD, J. (1998). Ex vivo gene transfer using adenovirus-mediated full-length dystrophin delivery to dystrophic muscles. Gene Ther. **5,** 19–30.

GILBERT, R., NALBANTOGLU, J., HOWELL, J.M., DAVIES, L., FLETCHER, S., AMALFITANO, A., PETROF, B.J., KAMEN, A., MASSIE, B., and KARPATI, G. (2001). Dystrophin expression in muscle following gene transfer with a fully deleted ("gutted") adenovirus is markedly improved by trans-acting adenoviral gene products. Hum. Gene Ther. **12,** 1741–1755.

GILCHRIST, S., ONTELL, M., KOCHANEK, S., and CLEMENS, P. (2002). Immune response to full-length dystrophin delivered to Dmd muscle by a high-capacity adenoviral vector. Mol. Ther. **6,** 359–368.

GOLDRING, K., PARTRIDGE, T., and WATT, D. (2002). Muscle stem cells. J. Pathol. **197,** 457–467.

GOODELL, M.A., JACKSON, K.A., MAJKA, S.M., MI, T., WANG, H., POCIUS, J., HARTLEY, C.J., MAJESKY, M.W., ENTMAN, M.L., MICHAEL, L.H., and HIRSCHI, K.K. (2001). Stem cell plasticity in muscle and bone marrow. Ann. N.Y. Acad. Sci. **938,** 208–218; discussion 218–220.

GUERETTE, B., ASSELIN, I., SKUK, D., ENTMAN, M., and TREMBLAY, J.P. (1997). Control of inflammatory damage by anti-LFA-1: Increase success of myoblast transplantation. Cell Transplant. **6,** 101–107.

GUSSONI, E., BLAU, H.M., and KUNKEL, L.M. (1997). The fate of individual myoblasts after transplantation into muscles of DMD patients. Nat. Med. **3,** 970–977.

GUSSONI, E., SONEOKA, Y., STRICKLAND, C.D., BUZNEY, E.A., KHAN, M.K., FLINT, A.F., KUNKEL, L.M., and MULLIGAN, R.C. (1999). Dystrophin expression in the mdx mouse restored by stem cell transplantation. Nature **401,** 390–394.

HARPER, S.Q., HAUSER, M.A., DELLORUSSO, C., DUAN, D., CRAWFORD, R.W., PHELPS, S.F., HARPER, H.A., ROBINSON, A.S., ENGELHARDT, J.F., BROOKS, S.V., and CHAMBERLAIN, J.S. (2002). Modular flexibility of dystrophin: Implications for gene therapy of Duchenne muscular dystrophy. Nat. Med. **8,** 253–261.

HARTIGAN-O'CONNOR, D., and CHAMBERLAIN, J.S. (2000). Developments in gene therapy for muscular dystrophy. Microsc. Res. Tech. **48,** 223–238.

HARTIGAN-O'CONNOR, D., KIRK, C.J., CRAWFORD, R., MULE, J.J., and CHAMBERLAIN, J.S. (2001). Immune evasion by muscle-specific gene expression in dystrophic muscle. Mol. Ther. **4,** 525–533.

HAUSER, M.A., AMALFITANO, A., KUMAR-SINGH, R., HAUSCHKA, S.D., and CHAMBERLAIN, J.S. (1997). Improved adenoviral vectors for gene therapy of Duchenne muscular dystrophy. Neuromuscul. Disord. **7,** 277–283.

HAUSER, M.A., ROBINSON, A., HARTIGAN-O'CONNOR, D., WILLIAMS-GREGORY, D.A., BUSKIN, J.N., APONE, S., KIRK, C.J., HARDY, S., HAUSCHKA, S.D., and CHAMBERLAIN, J.S. (2000). Analysis of muscle creatine kinase regulatory elements in recombinant adenoviral vectors. Mol. Ther. **2,** 16–25.

HOFFMAN, E.P., BROWN, R.H., JR., and KUNKEL, L.M. (1987). Dystrophin: The protein product of the Duchenne muscular dystrophy locus. Cell **51,** 919–928.

HUARD, J., BOUCHARD, J.P., ROY, R., MALOUIN, F., DANSEREAU, G., LABRECQUE, C., ALBERT, N., RICHARDS, C.L., LEMIEUX, B., and TREMBLAY, J.P. (1992). Human myoblast transplantation: Preliminary results of 4 cases. Muscle Nerve **15,** 550–560.

HUARD, J., TREMBLAY, G., VERREAULT, S., LABRECQUE, C., and TREMBLAY, J.P. (1993). Utilization of an antibody specific for human dystrophin to follow myoblast transplantation in nude mice. Cell Transplant. **2,** 113–118.

HUARD, J., ACSADI, G., JANI, A., MASSIE, B., and KARPATI, G. (1994a). Gene transfer into skeletal muscles by isogenic myoblasts. Hum. Gene Ther. **5,** 949–958.

HUARD, J., ROY, R., GUERETTE, B., VERREAULT, S., TREMBLAY, G., and TREMBLAY, J.P. (1994b). Human myoblast transplantation in immunodeficient and immunosuppressed mice: Evidence of rejection. Muscle Nerve **17,** 224–234.

HUARD, J., VERREAULT, S., ROY, R., TREMBLAY, M., and TREMBLAY, J.P. (1994c). High efficiency of muscle regeneration after human myoblast clone transplantation in SCID mice. J. Clin. Invest. **93,** 586–599.

JACKSON, K.A., MAJKA, S.M., WULF, G.G., and GOODELL, M.A. (2002). Stem cells: A minireview. J. Cell. Biochem. Suppl. **38,** 1–6.

KARPATI, G., HOLLAND, P., and WORTON, R.G. (1992). Myoblast transfer in DMD: Problems in the interpretation of efficiency. Muscle Nerve **15,** 1209–1210.

KINOSHITA, I., VILQUIN, J.T., GUERETTE, B., ASSELIN, I., ROY, R., and TREMBLAY, J.P. (1994). Very efficient myoblast allotransplantation in mice under FK506 immunosuppression. Muscle Nerve **17,** 1407–1415.

LAROCHELLE, N., OUALIKENE, W., DUNANT, P., MASSIE, B., KARPATI, G., NALBANTOGLU, J., and LOCHMULLER, H. (2002). The short MCK1350 promoter/enhancer allows for sufficient dystrophin expression in skeletal muscles of mdx mice. Biochem. Biophys. Res. Commun. **292,** 626–631.

LEE, J.Y., QU-PETERSEN, Z., CAO, B., KIMURA, S., JANKOWSKI, R., CUMMINS, J., USAS, A., GATES, C., ROBBINS, P., WERNIG, A., and HUARD, J. (2000). Clonal isolation of muscle-derived cells capable of enhancing muscle regeneration and bone healing. J. Cell Biol. **150,** 1085–1100.

MENDELL, J.R., KISSEL, J.T., AMATO, A.A., KING, W., SIGNORE, L., PRIOR, T.W., SAHENK, Z., BENSON, S., MCANDREW, P.E., RICE, R., NAGARAJA, H., STEPHENS, R., LANTRY, L., MORRIS, G., and BURGHES, A.H.M. (1995). Myoblast transfer in the treatment of Duchenne's muscular dystrophy. N. Engl. J. Med. **333,** 832–838.

MORGAN, J.E., WATT, D.J., SLOPER, J.C., and PARTRIDGE, T.A. (1988). Partial correction of an inherited biochemical defect of skeletal muscle by grafts of normal muscle precursor cells. J. Neurol. Sci. **86,** 137–147.

MORGAN, J.E., HOFFMAN, E.P., and PARTRIDGE, T.A. (1990). Normal myogenic cells from newborn mice restore normal histology to degenerating muscles of the mdx mouse. J. Cell Biol. **111,** 2437–2449.

MORGAN, J.E., PAGEL, C.N., SHERRATT, T., and PARTRIDGE, T.A. (1993). Long-term persistence and migration of myogenic cells injected into pre-irradiated muscles of mdx mice. J. Neurol. Sci. **115,** 191–200.

MULLIGAN, R.C. (1993). The basic science of gene therapy. Science **260,** 926–932.

NICHOLSON, L.V., JOHNSON, M.A., GARDNER-MEDWIN, D., BHATTACHARYA, S., and HARRIS, J.B. (1990). Heterogeneity of dystrophin expression in patients with Duchenne and Becker muscular dystrophy. Acta Neuropathol. (Berl) **80,** 239–250.

PARTRIDGE, T., BEAUCHAMP, J., MORGAN, J., TREMBLAY, J.P., HUARD, J., WATT, D., WERNIG, A., IRINTCHEV, A., GROUNDS, M., SPRINGER, M.L., BARTLETT, R.J., MENDELL, J., VILQUIN, J.T., and BOWER, J.J. (1997). Meeting of the Cell Transplantation Society in Miami. Cell Transplant. **6,** 195–198.

QU, Z., and HUARD, J. (2000). Matching host muscle and donor myoblasts for myosin heavy chain improves myoblast transfer therapy. Gene Ther. **7,** 428–437.

QU, Z., BALKIR, L., VAN DEUTEKOM, J.C., ROBBINS, P.D., PRUCHNIC, R., and HUARD, J. (1998). Development of approaches to improve cell survival in myoblast transfer therapy. J. Cell Biol. **142,** 1257–1267.

QU-PETERSEN, Z., DEASY, B., JANKOWSKI, R., IKEZAWA, M., CUMMINS, J., PRUCHNIC, R., MYTINGER, J., CAO, B., GATES, C., WERNIG, A., and HUARD, J. (2002). Identification of a novel population of muscle stem cells in mice: Potential for muscle regeneration. J. Cell Biol. **157,** 851–864.

ROY, R., TREMBLAY, J.P., HUARD, J., RICHARDS, C., MALOUIN, F., and BOUCHARD, J.P. (1993). Antibody formation after myoblast transplantation in Duchenne-dystrophic patients, donor HLA compatible. Transplant Proc. **25,** 995–997.

SALVATORI, G., FERRARI, G., MEZZOGIORNO, A., SERVIDEI, S., COLETTA, M., TONALI, P., GIAVAZZI, R., COSSU, G., and MAVILIO, F. (1993). Retroviral vector-mediated gene transfer into human primary myogenic cells leads to expression in muscle fibers *in vivo*. Hum. Gene Ther. **4,** 713–723.

SCOTT, J., LI, S., HARPER, S., WELIKSON, R., BOURQUE, D., DELLORUSSO, C., HAUSCHKA, S., and CHAMBERLAIN, J. (2002). Viral vectors for gene transfer of micro-, mini-, or full-length dystrophin. Neuromuscul. Disord. **12**(Suppl), S23.

SEALE, P., ASAKURA, A., and RUDNICKI, M.A. (2001). The potential of muscle stem cells. Dev. Cell **1,** 333–342.

SICINSKI, P., GENG, Y., RYDER-COOK, A.S., BARNARD, E.A., DARLISON, M.G., and BARNARD, P.J. (1989). The molecular basis of muscular dystrophy in the mdx mouse: A point mutation. Science **244,** 1578–1580.

SMYTHE, G.M., HODGETTS, S.I., and GROUNDS, M.D. (2000). Immunobiology and the future of myoblast transfer therapy. Mol. Ther. **1,** 304–313.

SMYTHE, G.M., HODGETTS, S.I., and GROUNDS, M.D. (2001). Problems and solutions in myoblast transfer therapy. J. Cell. Mol. Med. **5,** 33–47.

TREMBLAY, J.P., MALOUIN, F., ROY, R., HUARD, J., BOUCHARD, J.P., SATOH, A., and RICHARDS, C.L. (1993). Results of a triple blind clinical study of myoblast transplantations without immunosuppressive treatment in young boys with Duchenne muscular dystrophy. Cell Transplant. **2,** 99–112.

VILQUIN, J.T., WAGNER, E., KINOSHITA, I., ROY, R., and TREMBLAY, J.P. (1995). Successful histocompatible myoblast transplantation in dystrophin-deficient mdx mouse despite the production of antibodies against dystrophin. J. Cell Biol. **131,** 975–988.

WANG, B., LI, J., and XIAO, X. (2000). Adeno-associated virus vector carrying human minidystrophin genes effectively ameliorates muscular dystrophy in mdx mouse model. Proc. Natl. Acad. Sci. U.S.A. **97,** 13714–13719.

WATCHKO, J., O'DAY, T., WANG, B., ZHOU, L., TANG, Y., LI, J., and XIAO, X. (2002). Adeno-associated virus vector-mediated minidystrophin gene therapy improves dystrophic muscle contractile function in mdx mice. Hum. Gene Ther. **13,** 1451–1460.

WATKINS, S.C., HOFFMAN, E.P., SLAYTER, H.S., and KUNKEL, L.M. (1988). Immunoelectron microscopic localization of dystrophin in myofibres. Nature **333,** 863–866.

Address reprint requests to:
*Johnny Huard, Ph.D.*
*Growth and Development Laboratory*
*Children's Hospital of Pittsburgh*
*4100 Rangos Research Center*
*3460 Fifth Avenue*
*Pittsburgh, PA 15213*

*E-mail:* jhuard@pitt.edu

Received for publication October 23, 2002; accepted after revision September 8, 2003.

Published online: September 23, 2003.

**This article has been cited by:**

1. Ashley C. Wozniak, Jiming Kong, Erika Bock, Orest Pilipowicz, Judy E. Anderson. 2005. Signaling satellite-cell activation in skeletal muscle: Markers, models, stretch, and potential alternate pathways. *Muscle & Nerve* **31**:3, 283. [CrossRef]

Gene Therapy (2004) 11, 1321–1330

www.nature.com/gt

***RESEARCH ARTICLE***

# *Muscle stem cells can act as antigen-presenting cells: implication for gene therapy*

B Cao[1], J Bruder[2], I Kovesdi[3] and J Huard[1,4]

[1]*Growth and Development Laboratory, Children's Hospital of Pittsburgh and Department of Orthopaedic Surgery, University of Pittsburgh, Pittsburgh, PA, USA;* [2]*GenVec, Inc., Gaithersburg, MD, USA;* [3]*KILA Consultants, LLC, Rockville, MD, USA; and* [4]*Department of Molecular Genetics and Biochemistry, University of Pittsburgh, Pittsburgh, PA, USA*

*Research has shown that the use of a muscle-specific promoter can reduce immune response and improve gene transfer to muscle fibers. We investigated the efficiency of direct and ex vivo gene transfer to the skeletal muscles of 6- to 8-week-old mdx mice by using two adenoviral vectors: adenovirus (AD) encoding the luciferase gene under the cytomegalovirus (CMV) promoter (ADCMV) and AD encoding the same gene under the muscle creatine kinase (MCK) promoter (ADMCK). Direct intramuscular injection of ADMCK triggered a lower immune response that enabled more efficient delivery and more persistent expression of the transgene than did ADCMV injection. Similarly, ex vivo gene transfer using ADCMV-transduced muscle-derived stem cells (MDSCs) induced a stronger immune response and led to shorter transgene expression than did ex vivo gene transfer using ADMCK-transduced MDSCs. This immune response was due to the release of the antigen after MDSC death or to the ADCMV-transduced MDSCs acting as antigen-presenting cells (APCs) by expressing the transgene and rapidly initiating an immune response against subsequent viral inoculation. The use of a muscle-specific promoter that restricts transgene expression to differentiated muscle cells could prevent MDSCs from becoming APCs, and thereby could improve the efficiency of ex vivo gene transfer to skeletal muscle.*
Gene Therapy (2004) **11,** 1321–1330. doi:10.1038/sj.gt.3302293; Published online 3 June 2004

**Keywords:** *muscle-derived stem cells; antigen-presenting cells; adenovirus; direct/ex vivo gene transfer; skeletal muscle; MCK and CMV promoters*

## *Introduction*

Gene therapy based on the transfer of a functional gene into a particular tissue to alleviate a genetic deficiency has emerged as an exciting form of molecular medicine. Several limitations hinder the efficiency of gene delivery in skeletal muscle. The low transfection efficiency continues to be the main obstacle confronting gene transfer based on nonviral vectors, although progress is being made on this front.[1–3] The efficiency of gene transfer mediated by viral vectors (adenovirus (AD), retrovirus (RSV), and herpes simplex virus (HSV) vectors) is limited due to immune rejection problems, cellular cytotoxicity related to viral transduction, and a poor level of viral transduction in adult muscle compared to that observed in newborn muscle.[4–8] Researchers have focused extensive effort on increasing the efficiency of gene transfer while decreasing the immunogenicity and the cellular cytotoxicity associated with viral infection.[4–8] In addition, other viral vectors, including the adeno-associated virus, have been used to deliver genes in skeletal muscle and have remedied some of the difficulties facing viral gene transfer to skeletal muscle.[9–12] In light of these findings, the cellular cytotoxicity barriers associated with viral-mediated gene transfer have been fully characterized and can be partially circumvented; however, immune rejection continues to pose challenges that impede efficient gene transfer to skeletal muscle.

The selection of appropriate promoters that restrict transgene expression to specific tissues, such as skeletal muscle fibers, may also play an important role in improving the efficiency and persistence of transgene expression.[13–22] Ishii A *et al* found that injection of an AD in which the β-galactosidase reporter gene is under the β-actin promoter with cytomegalovirus (CMV) enhancer (CAG) resulted in the transduction of up to 60% of the myofibers in the skeletal muscles of 5- to 6-week-old normal mice.[16] This finding implies that viral promoters may influence the level of adenoviral-mediated gene transfer in skeletal muscle. The use of viral promoters likely causes ubiquitous transgene expression in various cell types and tissues, and thus may lead to cytotoxicity and a systemic immune response directed against the viral vector or the transgene itself.[23] Researchers could prevent these side effects by developing methods to ensure tissue-specific transgene expression, perhaps by using transcriptional regulatory elements that are active only in the target tissue.

Several ADs that contain muscle-specific transcriptional regulatory elements have been reported. The muscle-specific expression of the transgene mediated by these vectors has resulted in improved persistence of transgene expression.[14,15,24] Recently, some researchers

*Correspondence: Dr J Huard, Director: Growth and Development Laboratory, 4100 Rangos Research Center, Children's Hospital of Pittsburgh, Pittsburgh, PA 15213, USA*
Received 1 October 2003; accepted 21 March 2004; published online 3 June 2004

have used the muscle creatine kinase (MCK) promoter for muscle-specific gene transfer.[14,15,21] MCK, the most abundant nonmitochondrial mRNA, is expressed in all types of skeletal muscle fibers.[25] The MCK gene is not expressed in myoblasts, but becomes transcriptionally activated when myoblasts commit to terminal differentiation.[24,26] Thus, using the MCK promoter to drive a transgene could restrict the transgene expression to differentiated myotubes and myofibers and prevent its expression in nondifferentiated myogenic cells and nonmuscle cells such as antigen-presenting cells (APCs). Such muscle-specific expression may help to limit the immune response associated with gene transfer to skeletal muscle.

Researchers have proposed *ex vivo* gene transfer based on genetically engineered myoblasts as an alternative approach for the treatment of muscle diseases,[4,27–31] but limitations similar to those associated with myoblast transplantation[32–38] also hinder the success of this technology. Recently, researchers have focused increasingly on the use of muscle-derived stem cells (MDSCs) in cell transplantation and *ex vivo* gene therapy applications aimed at gene transfer to skeletal muscle.[39–43] We have generated data that provide several lines of evidence supporting the existence of MDSCs that, in comparison to myoblasts, improve the outcome of transplantation in skeletal muscle.[27,43,44] We hypothesized that the use of a population of MDSCs would enhance the efficiency of *ex vivo* gene transfer to skeletal muscle.

Our study, presented here, investigated the ability of MDSC-based *ex vivo* gene transfer to ameliorate the efficiency of viral transduction of myofibers. This *ex vivo* gene transfer approach may also prevent the transduction of host APCs in the injected muscle. An *ex vivo* approach is advantageous because the viral transduction is carried out *in vitro*, allowing the transgene to be expressed specifically in the transduced cells, and thus avoiding viral transduction of nontargeted cells (eg APCs). Although this technique has been used to deliver genes in skeletal muscle, the long-term persistence of the transgene has been limited by the presence of an immune response.[31] We therefore hypothesized that the use of a viral vector that encodes for a given transgene under the control of a viral promoter may trigger an immune response because the transduced cells can act as APCs.

We first evaluated and compared the efficiency of gene transfer to mature skeletal muscle and the presence of an immune response after direct intramuscular injection of an AD encoding the luciferase gene under the CMV promoter (ADCMV) or an AD encoding the luciferase gene under the MCK promoter (ADMCK). We then used the *ex vivo* gene transfer approach based on MDSCs transduced with the adenoviral vectors (ADMCK and ADCMV) to determine whether the promoter is a major determinant in the persistence of transgene expression in skeletal muscle and to investigate whether adenovirally transduced MDSCs act as APCs when used as vehicles for *ex vivo* gene transfer to skeletal muscle.

## Results

### ADCMV and ADMCK transduction of mdx muscle

We injected the same titer of ADCMV and ADMCK into the hind limb muscles of 6- to 8-week-old mdx mice. Examination for luciferase expression 7, 14, 30, and 60 days after injection indicated that both viruses were able to transduce muscle fibers within the injected mdx skeletal muscle (Figure 1a–g). The transgene expression mediated by direct injection of ADCMV decreased dramatically within 30 days after injection (Figure 1g). However, we observed better persistence of the transgene expression and significantly higher levels of transgene expression 30 and 60 days after injection in the muscles injected with ADMCK (Figure 1f and g) than in those injected with ADCMV (Figure 1e and g).

### Immune response after viral injection

To elucidate the mechanism by which ADMCK injection resulted in better persistence of the transgene within the mdx skeletal muscle, we investigated the infiltration of lymphocytes within the injected muscle. Immunostaining for CD4 and CD8 cells revealed that ADCMV injection triggered a massive infiltration of CD4- and CD8-positive lymphocytes in the muscle at 7 days after injection; we detected fewer CD4- and CD8-positive lymphocytes in the muscle injected with ADMCK (data not shown). Even 60 days after injection, lymphocytes were present within the muscle injected with ADCMV, while very few lymphocytes were visible in the muscle injected with ADMCK (data not shown). By using an antibody against MHC class I and II, we observed massive expression of H-2K$^b$, H-2D$^b$ (MHC class I), and MHC class II in the muscle injected with ADCMV at 7 days after injection (Figure 2a–c). We also examined a costimulatory molecule at the same time point and observed CD28 expression in the injection sites (Figure 2d). The existence of these molecules demonstrates that ADCMV injection triggered the immune response. In contrast, ADMCK injection led to significantly weaker expression of these molecules (Figure 2e–h).

### Ex vivo gene transfer mediated by adenovirally transduced MDSCs

We transduced MDSCs *in vitro* with ADCMV or ADMCK, and then performed immunostaining for luciferase by using a polyclonal rabbit anti-luciferase antibody. We detected luciferase expression in the nondifferentiated MDSCs transduced by ADCMV, but not in the MDSCs transduced with ADMCK (Figure 3a and c). However, we observed luciferase expression in myotubes in both groups (Figure 3b and d). We then injected the same number of ADCMV-transduced MDSCs or ADMCK-transduced MDSCs into the gastrocnemius muscles of mdx mice.

Examination of the muscle sections at early time points (7 days after injection) revealed similar levels of transgene expression by both populations of virally transduced cells. However, at time points beyond 14 days after injection, the transgene expression decreased in the muscle injected with ADCMV-transduced MDSCs (Figures 4a and 5a). Transgene expression was more persistent in the muscle injected with ADMCK-transduced MDSCs (Figures 4b and 5a). Immunostaining of these muscle sections 14 days after injection revealed that the injection of the ADCMV-transduced MDSCs triggered significantly greater CD8- (Figures 4c and 5c) and CD4-positive (Figures 4e and 5b) lymphocyte infiltration than did the injection of ADMCK-transduced MDSCs

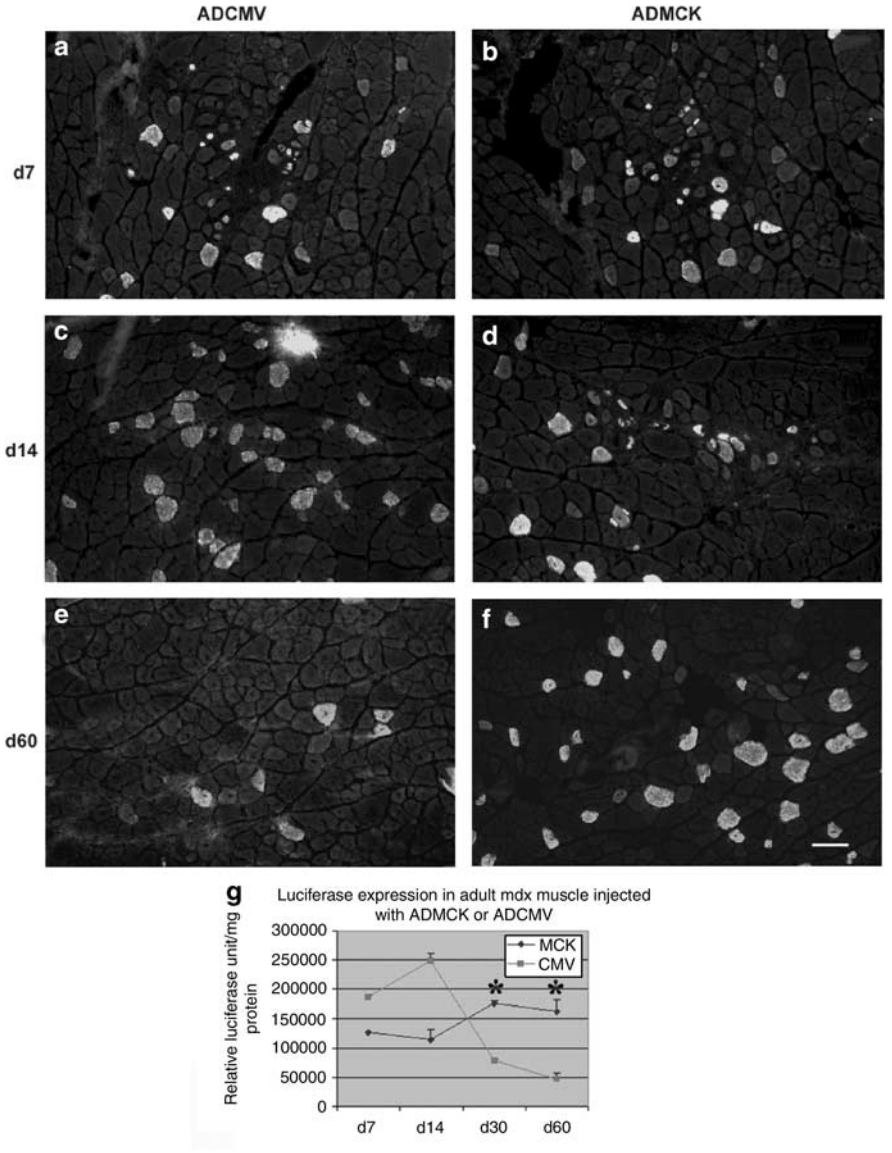


***Figure 1*** *Luciferase expression in the skeletal muscles of 6- to 8-week-old mdx mice, as determined by immunocytochemistry and luciferase assay. Immunocytochemical staining showed different numbers of myofibers expressing the luciferase transgene in ADCMV-injected muscle (a, c, e) and in ADMCK-injected muscle (b, d, f) at 7 (a, b), 14 (c, d), and 60 (e, f) days after injection. Luciferase assay revealed that ADMCK injection produced transgene expression that persisted 60 days after injection (g). In contrast, ADCMV injection resulted in high levels of transgene expression at days 7 and 14, but decreased levels thereafter (g). *Significant difference. Bar, 50 μm.*

(Figures 4d, f and 5b, c). We detected more luciferase expression in the MDSC-MCK group 60 days after injection than in the MDSC-CMV group (Figure 5a); however, the groups exhibited no difference in terms of the number of infiltrating CD4- and CD8-positive lymphocytes (Figures 5b and c).

Luciferase released from the dead ADCMV-transduced MDSCs and subsequently picked up by APCs may also have triggered an immune response. To investigate this possibility, we performed double staining of CD11b and luciferase. CD11b is a marker for macrophages, which likely are responsible for the removal of dead ADCMV-transduced MDSCs via phagocytosis. Our observations 7 days after injection revealed double-positive cells in the muscle injected with ADCMV-transduced MDSCs (Figure 6a, c and e), a finding that suggests potential phagocytosis of the transduced cells by macrophages. We observed a major reduction of double-positive cells in the muscle injected with ADMCK-transduced MDSCs (Figure 6b, d and f), which indicates that even if the macrophages picked up the dead ADMCK-transduced MDSCs, the macrophages did not express luciferase. These findings suggest another potential advantage associated with the use of the MCK promoter rather than the CMV promoter in *ex vivo* gene transfer applications.

### *Preinjection of ADCMV-transduced MDSCs significantly reduced the persistence of transgene expression after subsequent ADMCK injection*

We first transduced MDSCs with either ADCMV or ADMCK, and then injected the transduced cells into mdx mouse skeletal muscles. We injected ADMCK into both groups of mice 1 week later. At 7 days after the second injection, the muscles first injected with ADCMV-

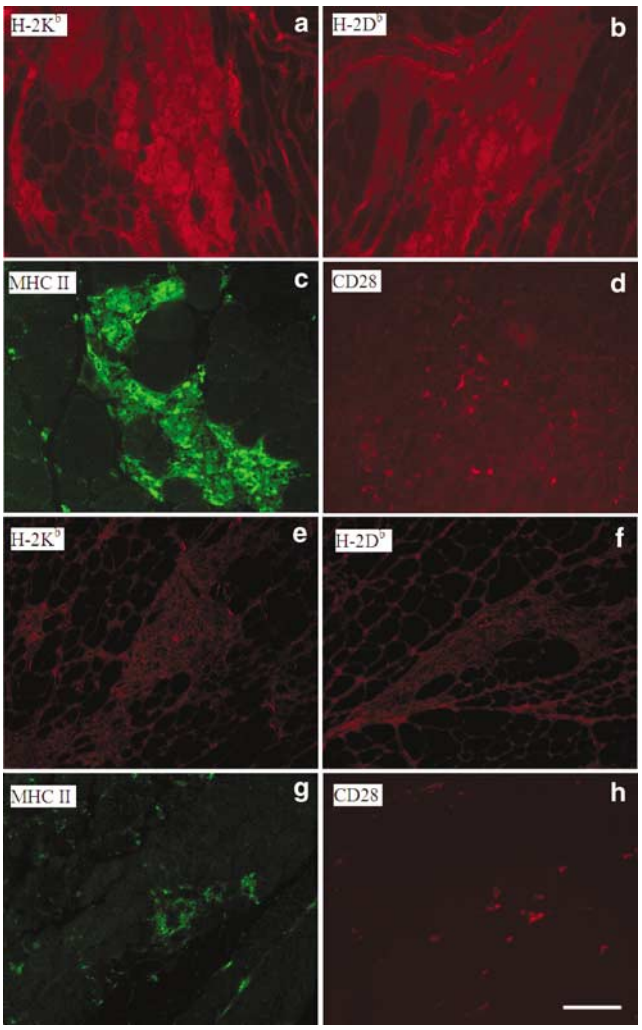


***Figure 2*** *MHC class I and II expression and costimulatory molecule expression in AD-injected skeletal muscles of 6- to 8-week-old mdx mice. We examined muscles for MHC class I, MHC class II, and CD28 expression 7 days after AD injection, and detected massive expression of MHC class I (H-2K$^b$ (a), H-2D$^b$ (b)), class II (c), and CD28 (d) at the ADCMV injection site. We observed no significant expression in the muscle injected with ADMCK (e–h). Bar, 50 μm.*

transduced MDSCs exhibited lower transgene expression than did the muscles first injected with ADMCK-transduced MDSCs (Figures 7a and b). The muscles first injected with ADMCK-transduced cells continued to exhibit higher transgene expression 30 days after subsequent injection with ADMCK when compared with the other experimental group (Figure 8a). Immunostaining for CD4- and CD8-positive lymphocytes 7 and 30 days after the second injection indicated that the muscles preinjected with ADCMV-transduced cells (Figures 7c, e and 8b, c) displayed significantly greater lymphocyte infiltration than did the muscles preinjected with ADMCK-transduced cells (Figures 7d, f and 8b, c). These results suggest that MDSCs can act as APCs when transduced with an AD that encodes for a reporter gene under the CMV promoter, but that the use of an AD that encodes the transgene under a muscle-specific promoter significantly reduces the immune response after subsequent injection of ADMCK.

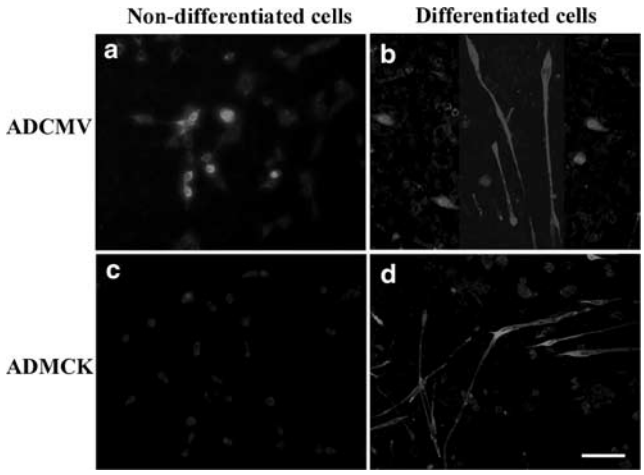


***Figure 3*** *Luciferase expression after AD transduction of MDSCs. Luciferase expression was detected 48 h after the transduction of MDSCs with ADCMV (a), and was detected in myotubes after incubation of the transduced cells in 2% serum medium (differentiation medium) for 5 days (b). Although luciferase was not expressed in the MDSCs transduced with ADMCK (c), luciferase expression was detected after these cells differentiated into myotubes (d). Bar, 50 μm.*

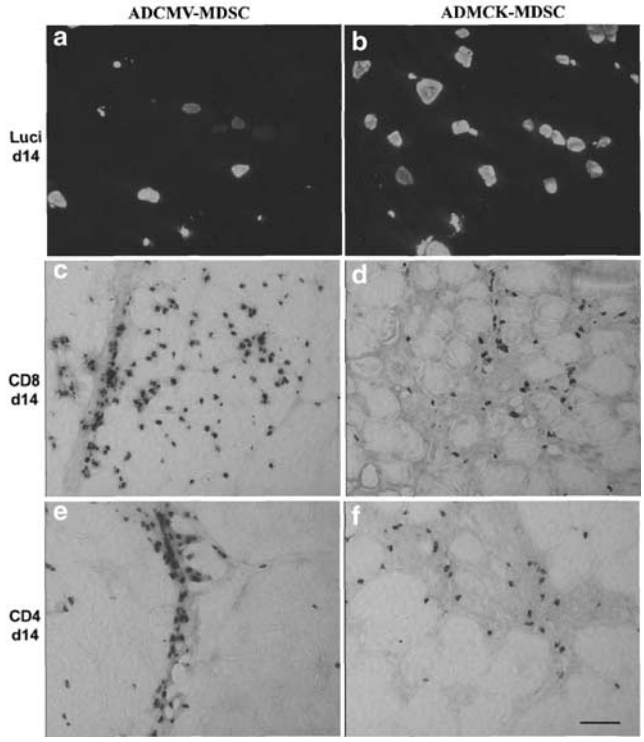


***Figure 4*** *Results of ex vivo gene transfer using ADMCK- or ADCMV-transduced MDSCs in the skeletal muscles of 6- to 8-week-old mdx mice. A decrease in luciferase expression was observed in the ADCMV-MDSC group at 14 days after injection (a) when compared to the ADMCK-MDSC group (b). CD4/CD8 staining indicated a greater infiltration of CD4- and CD8-positive cells in the muscles injected with ADCMV–MDSC (c, e) than in the muscles injected with ADMCK-MDSC (d, f). Bar, 50 μm.*

### *MDSCs acquired the APC function after adenoviral transduction*

We confirmed that nondifferentiated MDSCs transduced by ADCMV express luciferase *in vitro*, but MDSCs transduced by ADMCK do not. More importantly, a

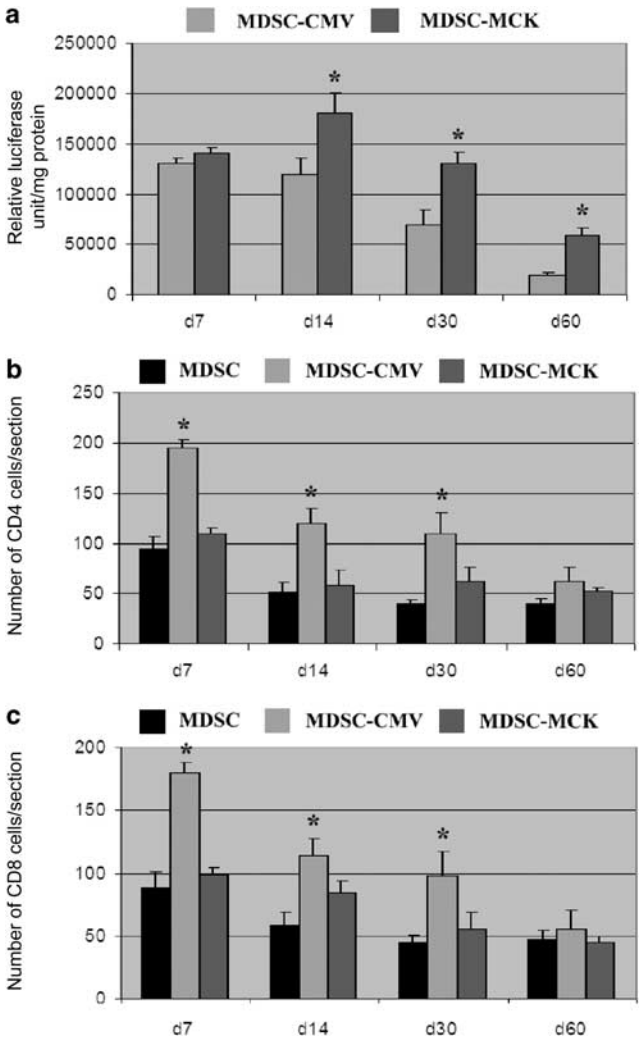


***Figure 5*** *Measurement of luciferase expression and CD4- and CD8-positive cells in the skeletal muscles of 6- to 8-week-old mdx mice injected with ADCMV- or ADMCK-transduced MDSCs. The luciferase expression level was similar at 7 days after injection in both the MDSC-MCK and the MDSC-CMV groups, but a decrease in luciferase expression was observed in the MDSC-CMV group at 14 days after injection. The ADMCK-transduced MDSCs displayed better persistence of transgene expression for up to 60 days after injection when compared to the ADCMV-transduced MDSCs (a). CD4- and CD8-positive cells were counted in the injected muscle. CD4- and CD8-positive cells from muscles injected with MDSCs alone (nontransduced) were counted and served as a control (black bar). From 7 to 30 days after injection, CD4/CD8 staining indicated a greater infiltration of CD4- and CD8-positive cells in the muscles injected with ADCMV-transduced MDSCs than in the muscles injected with ADMCK-transduced MDSCs (b, c). At 60 days after injection, no significant difference in the number of CD4- and CD8-positive cells was observed between the MDSC-MCK and the MDSC-CMV groups (b, c). *Significant difference.*

functional DQ-Ovalbumin assay[45] revealed that ADCMV-transduced MDSCs acquired the antigen-processing function, but ADMCK-transduced MDSCs did not (Figure 9). We did not detect dendritic cell antigen expression in the ADCMV-transduced MDSCs used for this study. Although this finding further supports the hypothesis that MDSCs transduced by ADCMV can act as APCs, we did not observe differentiation of the MDSCs into APCs.

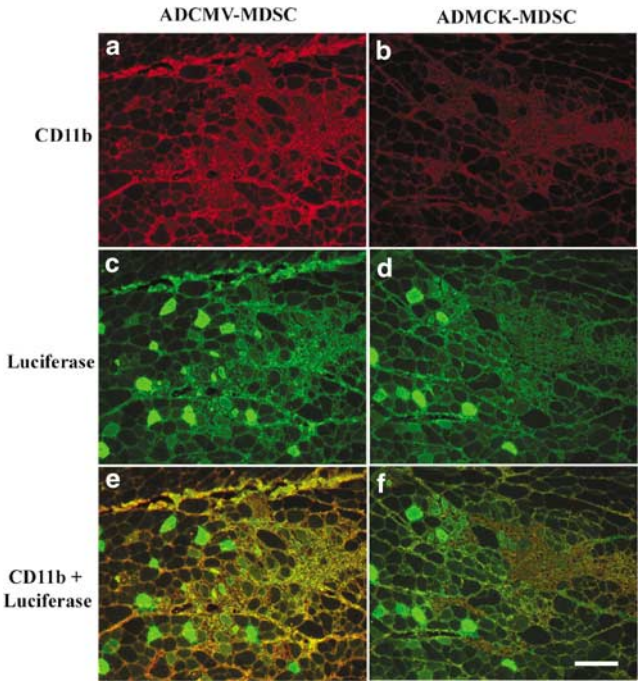


***Figure 6*** *Double staining for CD11b and luciferase in the skeletal muscles of 6- to 8-week-old mdx mice. Numerous CD11b-positive cells were detected at 7 days after injection in the muscle injected with ADCMV-transduced MDSCs (a). Luciferase was also expressed in both myofibers and mononucleated cells (c). No significant number of CD11b-positive cells was detected in the muscle injected with ADMCK-transduced MDSCs (b). Luciferase expression was mainly observed in the myofibers, however (d). Double exposure for both groups is shown in (e) and (f). Bar, 50 μm.*

## Discussion

In this project, we demonstrated that the use of different promoters (CMV or MCK) within a given adenoviral construct affects the efficiency and the persistence of transgene expression after adenoviral-mediated gene transfer into the skeletal muscles of mdx mice. Both direct and *ex vivo* gene transfer of ADMCK triggered a lower immune response that led to more efficient and more persistent transgene expression when compared to the direct or *ex vivo* gene transfer of ADCMV. ADCMV injected directly into the skeletal muscle transduced resident APCs, which consequently expressed the transgene and rapidly induced an immune response. MDSCs transduced with ADCMV and delivered via *ex vivo* gene transfer acted as APCs after implantation in skeletal muscle. Our results suggest that the ADCMV-transduced MDSCs expressed the transgene, and therefore rapidly initiated an immune response, while the ADMCK-transduced MDSCs expressed the transgene only after differentiation into myotubes and myofibers, ultimately leading to longer persistence of the transgene in the injected skeletal muscle. These results taken together demonstrate that the use of a muscle-specific promoter to restrict the transgene expression to skeletal muscle can prevent MDSCs from acting as APCs, and thereby can improve both the efficiency and long-term benefits of gene transfer in skeletal muscle.

Host immune response constitutes a major problem for gene therapy applications, particularly in techniques that involve the use of first-generation adenoviral

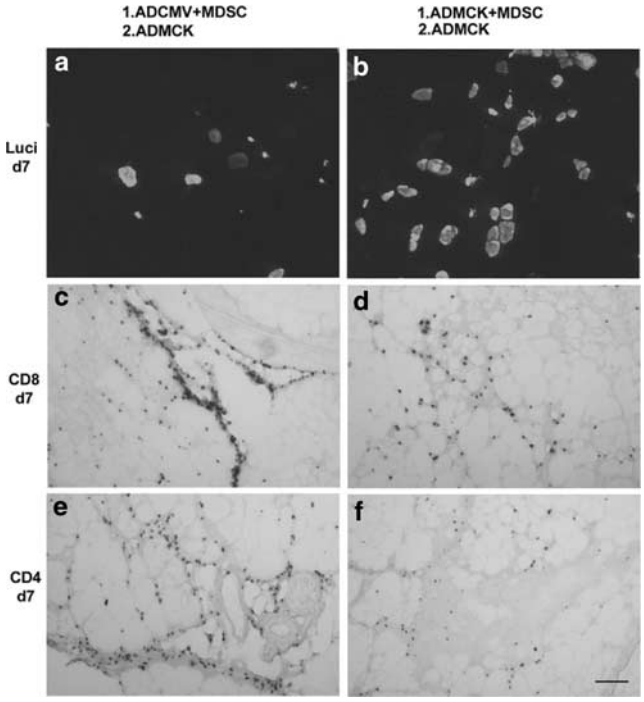


***Figure 7*** *Preinjection of ADCMV-transduced MDSCs in the skeletal muscles of 6- to 8-week-old mdx mice significantly reduces the persistence of transgene expression after subsequent ADMCK injection. ADMCK was injected into mdx skeletal muscles that had been injected with ADCMV- or ADMCK-transduced MDSCs 1 week earlier. At 7 days after the second injection, a lower number of luciferase-expressing myofibers was observed in the muscle that had first been injected with ADCMV-transduced MDSCs (a) than in the muscle that had first been injected with ADMCK-transduced MDSCs (b). The infiltration of a large number of CD4- and CD8-positive cells was observed 7 days after the second adenoviral injection (ADMCK) in the muscle that had first been injected with ADCMV-transduced MDSCs (c, e). Reduced lymphocyte infiltration was observed in the muscle that was preinjected with ADMCK-transduced MDSCs (d, f). Bar, 50 μm.*

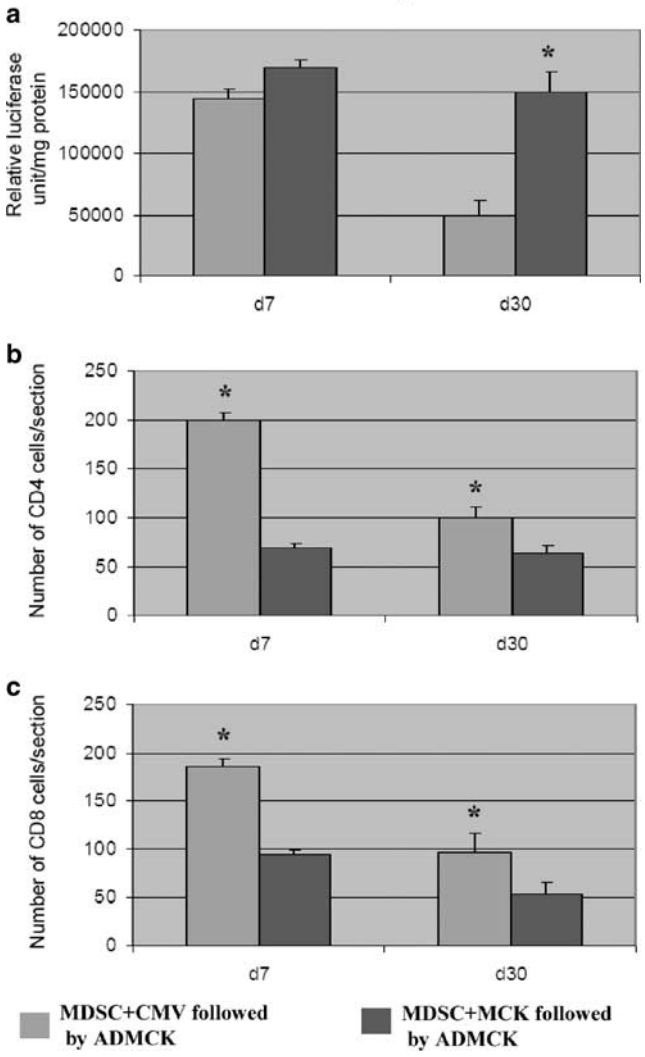


***Figure 8*** *Measurement of luciferase expression and CD4- and CD8-positive cells in the injected skeletal muscles of 6- to 8-week-old mdx mice. At 7 and 30 days after ADMCK injection, better gene transfer and transgene persistence were observed in the muscle first injected with ADMCK-transduced MDSCs than in the muscle first injected with ADCMV-transduced MDSCs (a). Greater CD4- and CD8-positive cell infiltration was also observed in the muscles first injected with ADCMV-transduced MDSCs in comparison with those first injected with ADMCK-transduced MDSCs (b, c). *Significant difference.*

vectors. These immune reactions generally occur in response to the direct presentation of the viral protein or the transgene by a group of cells called professional APCs. The expressed proteins are processed within the cytoplasm of the APCs, peptides are bound to MHC class I molecules, and the APCs migrate to lymph nodes for interaction with naive T cells. Macrophages and dendritic cells reportedly can function as professional APCs in skeletal muscle.[46]

It thus makes sense that after direct injection into the muscle, ADCMV transduced both macrophages and dendritic cells (professional APCs), which consequently expressed the luciferase gene delivered under the control of the CMV promoter. Presentation of the transgene by the APCs then induced the immune response indicated by the large infiltration of CD4- and CD8-positive lymphocytes and the expression of MHC class I and II and a costimulatory molecule (CD28) within the injected muscle. Although the direct injection of ADMCK also likely led to the transduction of APCs, the transduced cells did not express the luciferase reporter gene because the MCK promoter restricts transgene expression to differentiated muscle cells. Therefore, the immune response was significantly reduced, leading to longer persistence of the transgene (Figure 10a).

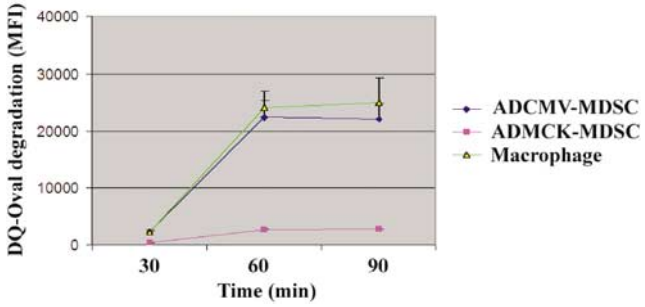


***Figure 9*** *ADCMV-transduced MDSCs acquired APC function. MDSCs were incubated with DQ-Ovalbumin (DQ-Oval) after being transduced with either ADCMV or ADMCK. Macrophages were used as a positive control for the assay. At 60 min after DQ-Oval exposure, ADCMV-transduced cells exhibited a high antigen-processing ability, as indicated by high fluorescence intensity (MFI) comparable to that observed in macrophages. In contrast, ADMCK-transduced cells exhibited low MFI.*

Our second set of experiments involved the use of *ex vivo* gene transfer to investigate whether MDSCs can also act as APCs in skeletal muscle. The *ex vivo* approach enabled us to restrict the viral transduction to MDSCs *in vitro* and prevented the transduction of resident APCs within skeletal muscle *in vivo*. However, we still observed severe immune responses after injection of the ADCMV-transduced MDSCs into skeletal muscle. In light of these findings, we hypothesized that adenovirally transduced MDSCs may act as APCs after injection into mouse skeletal muscle. We already had determined (in a previous set of experiments) that MDSCs transplanted into lethally irradiated mice can differentiate into macrophages and toward other hematopoietic lineages,[47] a finding that suggests that MDSCs can differentiate into APCs. However, we did not detect dendritic cell antigen expression in the ADCMV-transduced MDSCs used in the current study. Although this finding suggests a lack of differentiation of MDSCs toward APCs, the *in vitro* DQ-Ovalbumin assay indicated that the MDSCs did act as APCs. Furthermore, other researchers have reported that human muscle cells can act as APCs.[48–50] In the present study, MDSCs transduced with ADCMV expressed the transgene and triggered lymphocyte infiltration. However, ADMCK-transduced MDSCs expressed the transgene only after differentiation, resulting in a significant reduction in the immune response (Figure 10b). Our data indicate, as previously observed with the direct gene transfer approach, that the use of a muscle differentiation-specific promoter is critical to minimize immune rejection of the transgene after *ex vivo* gene transfer to skeletal muscle. Our results also indicate that the luciferase released from dying ADCMV-transduced MDSCs was taken up by APCs, which presented it in the context of MHC I via the crosspresentation pathway. In contrast, dying ADMCK-transduced MDSCs did not release the antigen because these cells only expressed luciferase after differentiation into myotubes. Although

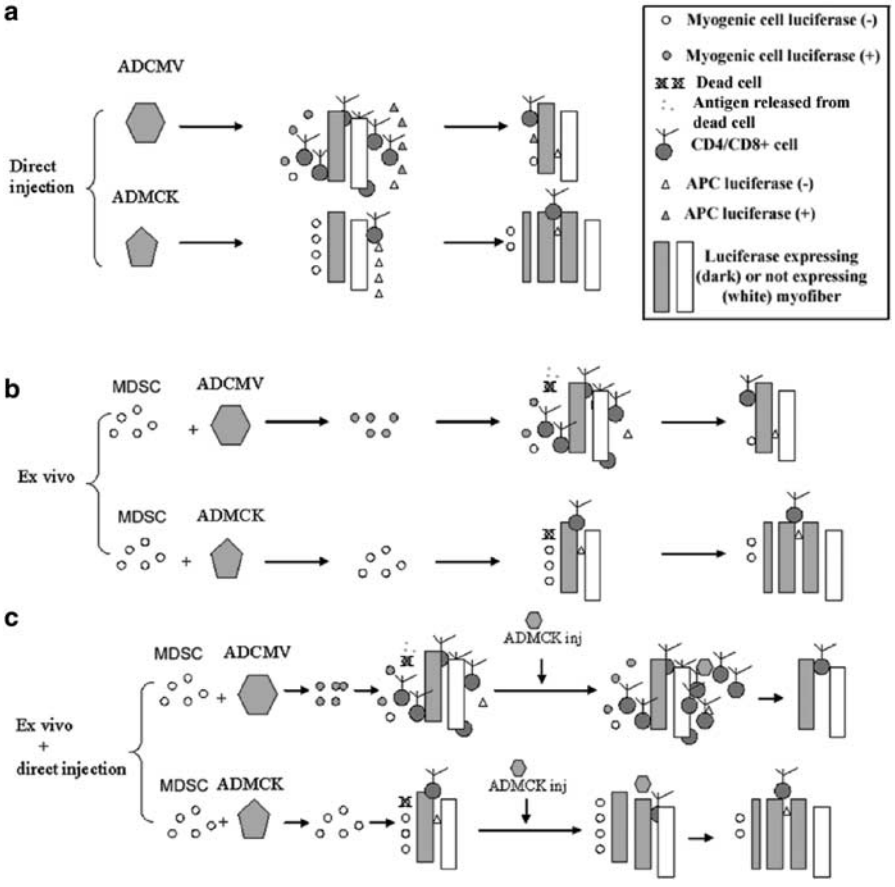


***Figure 10*** *Schematic representation of the different effects of ADCMV and ADMCK transduction. The upper panel (a) depicts the mechanism involved in direct viral injection. Both viruses transduce myogenic cells and APCs. After intramuscular injection, ADCMV-transduced host cells begin to express the transgene, and therefore trigger an immune response that eventually eliminates the transduced cells and myofibers. ADMCK-transduced cells express the transgene only after differentiation into myotubes and myofibers, and hence do not trigger a severe immune response. For the ex vivo approach (middle panel, b), injection of the ADCMV-transduced MDSCs triggered CD4- and CD8-positive cell infiltration (due to the expression of the transgene). This immune response significantly reduces the transduction efficiency and the persistence of the transgene expression. However, when ADMCK-transduced MDSCs are injected, the transgene is expressed only after the cells differentiate into myotubes. Hence, a decreased infiltration of CD4- and CD8-positive cells is observed and the transduced myofibers survive longer. Dead ADCMV-transduced cells may also release the antigen, which can help to elicit the immune response. Dead ADMCK-transduced cells, due to their lack of transgene expression, do not trigger an immune response via this mechanism. The ex vivo plus direct injection experiments further support the hypothesis that myogenic cells can act as APCs (lower panel, c). When ADCMV-transduced cells were injected into muscle, an immune response was observed. After the subsequent injection of ADMCK, the virus was rapidly rejected. However, when ADMCK-transduced cells were injected first, the transgene was not expressed in the cells until they differentiated into myotubes and myofibers; thus, a reduction in the immune response was observed. This behavior led to better persistence of transgene expression in the transduced muscle fibers after the second injection of ADMCK.*

by this mechanism ADCMV-transduced MDSCs are more likely to initiate an immune response than are ADMCK-transduced MDSCs, we still observed decreased transgene expression even when using ADMCK for the *ex vivo* gene transfer. We hypothesize that this decline in transgene expression may be attributable to necrosis of the dystrophin-deficient muscle fibers over time, although the decline could also be due to an immune response. The occurrence of an immune response would correlate with the results observed previously, which indicated that transgene expression driven by the MCK promoter can still cause an immune response, although it generally occurs at a later time point.[22] Such an immune response indicates that differentiated muscle fibers might also present antigens that trigger an immune response.[51]

Our final set of results supports the hypothesis that ADCMV-transduced MDSCs can act as APCs and contribute to an immune reaction after adenoviral injection into skeletal muscle. The ADCMV-transduced MDSCs injected into mdx skeletal muscle functioned as APCs and triggered immunorejection, as indicated by an infiltration of CD4- and CD8-positive lymphocytes. The injection of ADMCK into the muscles that had been injected earlier with ADCMV-transduced MDSCs resulted in transient expression of the transgene and a severe immune response. In contrast, ADMCK-transduced MDSCs injected intramuscularly did not act as APCs. We observed a weaker immune response after subsequent direct injection of ADMCK into the same muscles (Figure 10c).

In summary, our findings suggest that the use of a muscle-specific promoter can improve the outcome of both direct and *ex vivo* adenoviral gene transfer to skeletal muscle. In comparison with the use of a viral promoter, such as CMV, the use of a muscle-specific promoter in a direct gene transfer approach prevents transgene expression by host APCs and consequently leads to more persistent transgene expression. The use of a muscle-specific promoter can also reduce or delay the immune response elicited by *ex vivo* gene transfer based on MDSCs, since MDSCs transduced with a viral promoter *in vitro* can also act as APCs *in vivo*. These results may have important implications for the design of gene therapy approaches using MDSCs.

## Materials and methods

### Animals and viruses

*Animals.* C57BL/10J and C57BL/10JScSnDMD$^{mdx}$ mice (6–8 weeks of age) were obtained from the Jackson Laboratory (Bar Harbor, ME, USA). All animal experiments were performed in accordance with the guidelines established by the Institutional Animal Research and Care Committee (ARCC) at Children's Hospital of Pittsburgh (animal protocol 19/2000, 04/2003).

*Viruses.* ADs carrying the luciferase reporter gene under the CMV or the MCK promoter were used in these experiments. Both the 655bp human CMV promoter upstream of an artificial intron and the 3300 bp MCK promoter (p3300MCKCAT, a gift from Dr Steve Hauschka to Dr Bruder; Johnson *et al*[52]) were cloned into the deleted E1 region of an AD shuttle vector, upstream of the luciferase gene and simian virus (SV)40 poly-A sequences. The expression cassettes are oriented such that the luciferase is transcribed from right to left relative to the AD genome. The virus backbones contain the dl324 E3 deletion.

AdNull contains the CMV promoter and SV40 poly-A sequences in place of the E1 region and does not express any transgenes. All AD vectors were generated by using shuttle vectors as described previously.[53,54] The viruses generated by recombination between the shuttle vector and the AD DNA were plaque purified and propagated on 293 cells. At 2 days after vector administration, the viruses were purified from infected cells by using three freeze–thaw cycles followed by three successive bandings on CsCl gradients. The purified viruses were dialyzed against a buffer containing 10 mM Tris, pH 7.8, 150 mM NaCl, 10 mM $MgCl_2$, and 3% sucrose and were stored at $-80^{\circ}C$ until use. All viruses were tested and were found to have replication-competent AD levels of less than 1 in $1 \times 10^7$ plaque-forming units (PFU).

### Virus injection

Six mice per viral vector were analyzed at every time point. The mice were anesthetized using Metafane (Mallinckrodt Veterinary, Mundelein, IL, USA), and the viral suspension ($1 \times 10^7$ PFU in 30 µl of Hanks' balanced salt solution (HBSS)) was subsequently injected percutaneously into both gastrocnemius muscles by using a Hamilton syringe with a 30-gauge needle. Mice receiving ADCMV or ADMCK injections were euthanized at 7, 14, 30, or 60 days after viral injection. The injected muscles were isolated, and half of the samples were used for luciferase assay, while the remaining samples were frozen in isopentane precooled in liquid nitrogen. Serial cryostat sections (10 µm) were subsequently analyzed by immunocytochemistry for luciferase expression.

### Immunocytochemistry

*In vitro.* After being rinsed briefly with PBS, cells were fixed with cold methanol for 1 min. Cells then were blocked in 10% goat serum for 30 min. The primary antibodies used were polyclonal rabbit anti-luciferase (1:100; Abcam, Cambridge, UK) and anti-mouse dendritic cells–biotin conjugate (1:100; Leinco Technologies, Inc., St Louis, MO, USA). The subsequent antibodies were biotin-goat anti-rabbit (1:200; Chemicon, Temecula, CA, USA) followed by Cy3–streptavidin (1:1000; Sigma, St Louis, MO), for polyclonal rabbit anti-luciferase, and Cy3–streptavidin for anti-mouse dendritic cells–biotin conjugate.

*In vivo.* Muscle sections were fixed with cold acetone ($-20^{\circ}C$) for 2 min. After several rinses in TBS/Triton X-100, pH 7.4 (0.05 M Tris, 0.15 M NaCl, 1% Triton X-100), the cryosections were blocked with 10% goat serum for 30 min. In cases involving a secondary anti-mouse antibody, the mouse on mouse (MOM) kit (Vector Laboratories, Burlingame, CA, USA) was used. The sections then were incubated overnight at $4^{\circ}C$ in a humid chamber with the following primary antibodies: polyclonal rabbit anti-luciferase (1:100; Abcam), purified rat anti-mouse CD4 (1:100), purified rat anti-mouse CD8a (1:100), hamster anti-CD28 (1:100), mouse anti-H-2K$^b$ (1:100), mouse anti-H-2D$^b$ (1:100; all from BD Biosciences,

San Diego, CA, USA), and FITC-conjugated rat anti-MHC II (1:200; Chemicon).

After three rinses in TBS/Triton X-100, pH 7.4, the secondary antibodies biotin-goat anti-rabbit (1:200; Chemicon), biotin-goat anti-rat (1:400; Vector), biotin-goat anti-hamster (1:400; Vector), or anti-mouse-Cy3 (1:200; Sigma) were applied for 30 min at room temperature. The tertiary antibodies were FITC–streptavidin (1:200; Boehringer Mannheim, Indianapolis, IN, USA), peroxidase-conjugated streptavidin (1:800; DAKO, Glostrup, Denmark), or Cy3–streptavidin (1:1000; Sigma). The peroxidase activity (for CD4/CD8a) was revealed using 3,3′-diaminobenzidine (Sigma).

*Double staining for CD11b and luciferase.* After the initial block step, cryosections were stained with a primary antibody mix of rat anti-mouse CD11b (Chemicon) and rabbit anti-luciferase (Abcam), followed by biotin-goat anti-rat, Cy3–streptavidin, biotin-goat anti-rabbit, and FITC–streptavidin. To reveal any potential background generated by the primary and secondary antibodies, immunostaining controls were performed by using only primary or secondary antibodies followed by the tertiary antibodies. The conditions were also optimized to minimize the background staining. The number of CD4- and CD8-positive cells was quantified by using Northern Eclipse software (Empix Imaging, Inc., North Tonawanda, NY, USA). The section that had the highest number of positive cells was chosen for analysis. Counts were expressed as number of cells per section. Six muscles from six mice were counted.

### Luciferase assay

The luciferase assay was conducted with the Luciferase Assay System (Promega, Madison, WI, USA) according to the instructions of the manufacturer. In brief, to establish a standard curve of light units *versus* relative enzyme concentrations, serial dilutions of luciferase (Promega) were made with 1× Reporter Lysis Buffer. Muscles were weighed, homogenized, and centrifuged. The supernatant was mixed with the Luciferase Assay Reagent, and the light produced was read in a luminometer (Monolight 2010, Analytical Luminescence Laboratory, San Diego, CA, USA).

### Ex vivo approach using MDSCs

Primary muscle cells were isolated from normal newborn C57BL/10J mice by using the preplate technique, as described previously.[27,43] MDSCs were transduced with either ADCMV or ADMCK at a multiplicity of infection of 50 (MOI = 50). After 24 h transduction, $1 \times 10^5$ cells were injected percutaneously into the gastrocnemius muscles of mdx mice (six mice per time point). Mice were killed 7, 14, 30, or 60 days after injection.

### Serial injection of adenovirally transduced cells and ADs

MDSCs were transduced with ADCMV or ADMCK, as described above. A total of $1 \times 10^5$ transduced cells were injected into the gastrocnemius muscles (six mice per time point). After 1 week, ADMCK ($1 \times 10^7$ PFU in 30 μl HBSS) was injected into the same muscles that previously had been injected with the transduced MDSCs. Mice were killed 7, 14, and 30 days after the second injection.

### Antigen-processing assay

A total of $1.5 \times 10^2$ MDSCs were seeded in a 96-well plate. After 24 h, cells were transduced with ADCMV or ADMCK in HBSS for 3 h, and then were incubated with the proliferation medium overnight. A measure of 1 μl of DQ-Ovalbumin (Molecular Probes, Eugene, OR, USA) was added to each well and the transduced cells were incubated for 15 min at 37°C. CD11b-positive cells were also incubated with 1 μl of DQ-Ovalbumin for 15 min at 37°C as positive controls. After the incubation, the cells were washed with PBS and the same quantity of control cells was distributed into another 96-well plate. Mean fluorescence intensity (MFI) was determined at 30, 60, and 90 min by using a Wallac Victor² 1420 Multilabel Counter (PerkinElmer Life Sciences, Wallac Oy, Turku, Finland).

### Statistical analysis

Results are expressed as mean ± standard deviations. Student's *t*-test was used to compare data between the two groups. $P < 0.05$ was considered significant.

## Acknowledgements

This work was supported by the Muscular Dystrophy Association (USA) and the National Institutes of Health (NIH P01 AR 45925-01). The Growth and Development Laboratory is also supported by the Henry J Mankin Endowed Chair at the University of Pittsburgh and the William F and Jean W Donaldson Chair at Children's Hospital of Pittsburgh. We thank James Cummins, Marcelle Pellerin, Jessica Tebbets, and Arvydas Usas for their technical contributions. We also thank Dr Nick Giannoukakis (Division of Immunogenetics, Children's Hospital of Pittsburgh) for technical help and Ryan Sauder for excellent editorial assistance with the manuscript.

## References

1 Liu F, Huang L. Development of non-viral vectors for systemic gene delivery. *J Control Rel* 2002; **78**: 259–266.
2 Espinos E, Liu JH, Bader CR, Bernheim L. Efficient non-viral DNA-mediated gene transfer to human primary myoblasts using electroporation. *Neuromuscul Disord* 2001; **11**: 341–349.
3 Chapdelaine P *et al*. Functional EGFP–dystrophin fusion proteins for gene therapy vector development. *Protein Eng* 2000; **13**: 611–615.
4 Cao B, Mytinger JR, Huard J. Adenovirus mediated gene transfer to skeletal muscle. *Microsc Res Technol* 2002; **58**: 45–51.
5 Cao B *et al*. The role of receptors in the maturation-dependent adenoviral transduction of myofibers. *Gene Therapy* 2001; **8**: 627–637.
6 Bouri K *et al*. Polylysine modification of adenoviral fiber protein enhances muscle cell transduction. *Hum Gene Ther* 1999; **10**: 1633–1640.
7 Acsadi G *et al*. Dystrophin expression in muscles of mdx mice after adenovirus-mediated *in vivo* gene transfer. *Hum Gene Ther* 1996; **7**: 129–140.

8 Takeda S, Miyagoe-Suzuki Y. Gene therapy for muscular dystrophies: current status and future prospects. *Bio Drugs* 2001; **15**: 635–644.
9 Kessler PD *et al*. Gene delivery to skeletal muscle results in sustained expression and systemic delivery of a therapeutic protein. *Proc Natl Acad Sci USA* 1996; **93**: 14082–14087.
10 Wang B, Li J, Xiao X. Adeno-associated virus vector carrying human minidystrophin genes effectively ameliorates muscular dystrophy in mdx mouse model. *Proc Natl Acad Sci USA* 2000; **97**: 13714–13719.
11 Watchko J *et al*. Adeno-associated virus vector-mediated minidystrophin gene therapy improves dystrophic muscle contractile function in mdx mice. *Hum Gene Ther* 2002; **13**: 1451–1460.
12 Fisher KJ *et al*. Recombinant adeno-associated virus for muscle directed gene therapy. *Nat Med* 1997; **3**: 306–312.
13 Larochelle N *et al*. Efficient muscle-specific transgene expression after adenovirus-mediated gene transfer in mice using a 1.35 kb muscle creatine kinase promoter/enhancer. *Gene Therapy* 1997; **4**: 465–472.
14 Hartigan-O'Connor D *et al*. Immune evasion by muscle-specific gene expression in dystrophic muscle. *Mol Ther* 2001; **4**: 525–533.
15 Hauser MA *et al*. Analysis of muscle creatine kinase regulatory elements in recombinant adenoviral vectors. *Mol Ther* 2000; **2**: 16–25.
16 Ishii A *et al*. Effective adenovirus-mediated gene expression in adult murine skeletal muscle. *Muscle Nerve* 1999; **22**: 592–599.
17 Spitz F *et al*. Fiber-type specific and position-dependent expression of a transgene in limb muscles. *Differentiation* 2002; **70**: 457–467.
18 Roscilli G *et al*. Long-term and tight control of gene expression in mouse skeletal muscle by a new hybrid human transcription factor. *Mol Ther* 2002; **6**: 653–663.
19 Frauli M *et al*. Adenoviral-mediated skeletal muscle transcriptional targeting using chimeric tissue-specific promoters. *Med Sci Monit* 2003; **9**: BR78–84.
20 Grill MA *et al*. Tetracycline-inducible system for regulation of skeletal muscle-specific gene expression in transgenic mice. *Transgenic Res* 2003; **12**: 33–43.
21 Weeratna RD *et al*. Designing gene therapy vectors: avoiding immune responses by using tissue-specific promoters. *Gene Therapy* 2001; **8**: 1872–1878.
22 Larochelle N *et al*. The short MCK1350 promoter/enhancer allows for sufficient dystrophin expression in skeletal muscles of mdx mice. *Biochem Biophys Res Commun* 2002; **292**: 626–631.
23 Jooss K, Yang Y, Fisher KJ, Wilson JM. Transduction of dendritic cells by DNA viral vectors directs the immune response to transgene products in muscle fibers. *J Virol* 1998; **72**: 4212–4223.
24 Jaynes JB *et al*. Transcriptional regulation of the muscle creatine kinase gene and regulated expression in transfected mouse myoblasts. *Mol Cell Biol* 1986; **6**: 2855–2864.
25 Welle S, Bhatt K, Thornton CA. Inventory of high-abundance mRNAs in skeletal muscle of normal men. *Genome Res* 1999; **9**: 506–513.
26 Chamberlain JS, Jaynes JB, Hauschka SD. Regulation of creatine kinase induction in differentiating mouse myoblasts. *Mol Cell Biol* 1985; **5**: 484–492.
27 Qu Z *et al*. Development of approaches to improve cell survival in myoblast transfer therapy. *J Cell Biol* 1998; **142**: 1257–1267.
28 Campeau P *et al*. Transfection of large plasmids in primary human myoblasts. *Gene Therapy* 2001; **8**: 1387–1394.
29 Ozawa CR, Springer ML, Blau HM. A novel means of drug delivery: myoblast-mediated gene therapy and regulatable retroviral vectors. *Annu Rev Pharmacol Toxicol* 2000; **40**: 295–317.
30 Moisset PA *et al*. Successful transplantation of genetically corrected DMD myoblasts following *ex vivo* transduction with the dystrophin minigene. *Biochem Biophys Res Commun* 1998; **247**: 94–99.
31 Floyd Jr SS *et al*. *Ex vivo* gene transfer using adenovirus-mediated full-length dystrophin delivery to dystrophic muscles. *Gene Therapy* 1998; **5**: 19–30.
32 Rando TA, Blau HM. Methods for myoblast transplantation. *Methods Cell Biol* 1997; **52**: 261–272.
33 Skuk D *et al*. Dynamics of the early immune cellular reactions after myogenic cell transplantation. *Cell Transplant* 2002; **11**: 671–681.
34 Skuk D, Goulet M, Roy B, Tremblay JP. Myoblast transplantation in whole muscle of nonhuman primates. *J Neuropathol Exp Neurol* 2000; **59**: 197–206.
35 Skuk D, Goulet M, Roy B, Tremblay JP. Efficacy of myoblast transplantation in nonhuman primates following simple intramuscular cell injections: toward defining strategies applicable to humans. *Exp Neurol* 2002; **175**: 112–126.
36 Beauchamp JR, Morgan JE, Pagel CN, Partridge TA. Dynamics of myoblast transplantation reveal a discrete minority of precursors with stem cell-like properties as the myogenic source. *J Cell Biol* 1999; **144**: 1113–1122.
37 Qu Z, Huard J. Matching host muscle and donor myoblasts for myosin heavy chain improves myoblast transfer therapy. *Gene Therapy* 2000; **7**: 428–437.
38 Gussoni E, Blau HM, Kunkel LM. The fate of individual myoblasts after transplantation into muscles of DMD patients. *Nat Med* 1997; **3**: 970–977.
39 Miller JB, Schaefer L, Dominov JA. Seeking muscle stem cells. *Curr Top Dev Biol* 1999; **43**: 191–219.
40 Gussoni E *et al*. Dystrophin expression in the mdx mouse restored by stem cell transplantation. *Nature* 1999; **401**: 390–394.
41 Partridge TA. Stem cell route to neuromuscular therapies. *Muscle Nerve* 2003; **27**: 133–141.
42 Jankowski RJ, Deasy BM, Huard J. Muscle-derived stem cells. *Gene Therapy* 2002; **9**: 642–647.
43 Qu-Petersen Z *et al*. Identification of a novel population of muscle stem cells in mice: potential for muscle regeneration. *J Cell Biol* 2002; **157**: 851–864.
44 Lee JY *et al*. Clonal isolation of muscle-derived cells capable of enhancing muscle regeneration and bone healing. *J Cell Biol* 2000; **150**: 1085–1100.
45 Daro E *et al*. Polyethylene glycol-modified GM-CSF expands CD11b(high)CD11c(high) but notCD11b(low)CD11c(high) murine dendritic cells *in vivo*: a comparative analysis with Flt3 ligand. *J Immunol* 2000; **165**: 49–58.
46 Pimorady-Esfahani A, Grounds MD, McMenamin PG. Macrophages and dendritic cells in normal and regenerating murine skeletal muscle. *Muscle Nerve* 1997; **20**: 158–166.
47 Cao B *et al*. Muscle stem cells differentiate into haematopoietic lineages but retain myogenic potential. *Nat Cell Biol* 2003; **5**: 640–646.
48 Goebels N, Michaelis D, Wekerle H, Hohlfeld R. Human myoblasts as antigen-presenting cells. *J Immunol* 1992; **149**: 661–667.
49 Garlepp MJ *et al*. Antigen processing and presentation by a murine myoblast cell line. *Clin Exp Immunol* 1995; **102**: 614–619.
50 Curnow J, Corlett L, Willcox N, Vincent A. Presentation by myoblasts of an epitope from endogenous acetylcholine receptor indicates a potential role in the spreading of the immune response. *J Neuroimmunol* 2001; **115**: 127–134.
51 Dalakas MC, Hohlfeld R. Polymyositis and dermatomyositis. *Lancet* 2003; **362**: 971–982.
52 Johnson JE, Wold BJ, Hauschka SD. Muscle creatine kinase sequence elements regulating skeletal and cardiac muscle expression in transgenic mice. *Mol Cell Biol* 1989; **9**: 3393–3399.
53 Chinnadurai G, Chinnadurai S, Brusca J. Physical mapping of a large-plaque mutation of adenovirus type 2. *J Virol* 1979; **32**: 623–628.
54 Bruder JT, Jie T, McVey DL, Kovesdi I. Expression of gp19K increases the persistence of transgene expression from an adenovirus vector in the mouse lung and liver. *J Virol* 1997; **71**: 7623–7628.

# PERSISTENT DYSTROPHIN EXPRESSION IN THE SKELETAL MUSCLE OF mdx MICE BY USING A TISSUE SPECIFIC PROMOTER

*Cao, B; **Wang, B, ** Xiao, X; +*Huard, J
*Stem Cell Research Center, Children's Hospital of Pittsburgh and Department of Orthopaedic Surgery, University of Pittsburgh, Pittsburgh, PA
+jhuard@pitt.edu

## INTRODUCTION

Our study investigated the ability of muscle-derived stem cells (MDSCs)-based ex vivo gene transfer to ameliorate the efficiency of non-viral transduction of myofibers. We hypothesized that the use of a plasmid vector that encodes for a given transgene under the control of a viral promoter may trigger an immune response because the transduced cells can act as antigen presenting cells (APCs)[1]. We used the ex vivo gene transfer approach based on MDSCs transduced with two plasmid vectors: mini-dystrophin gene under the muscle creatine kinase (MCK) promoter; and mini-dystrophin gene under the cytomegalovirus (CMV) promoter to determine whether the promoter is a major determinant in the persistence of transgene expression in skeletal muscle

## MATERIALS AND METHODS

*Animals and plasmids:* All animal experiments were performed in accordance with the guidelines established by the Institutional Animal Research and Care Committee (ARCC) at Children's Hospital of Pittsburgh (Protocol # 04/03). Plasmids carrying the mini-dystrophin reporter gene under the CMV or the MCK promoter were constructed in pcDNA 3.1(+) plasmid DNA backbone. Mini-dystrophin Δ3990 gene fragment [2] was obtained by restriction enzyme digestion from plasmid DNA called PCR-dys-3990-X2 [2].

*Ex vivo approach using MDSCs:* Primary MDSCs were isolated from C57BL/10JScSnDMD$^{mdx}$ mice (4–8 weeks of age) by using the preplate technique, as described previously [3, 4]. MDSCs were transduced with either CMV-dys or MCK –dys. After 24 h transduction, 1x10^5 cells were injected percutaneously into the gastrocnemius muscles of mdx mice (six mice per time point). Mice were sacrificed 10, 60, or 120 days after injection.

*Immunocytochemistry:* In cases involving a secondary anti-mouse antibody, the mouse on mouse (MOM) kit (Vector Laboratories) was used. Muscle sections were fixed with cold acetone (-20ºC). CD4, CD8 staining: After several rinses in TBS/Triton, the cryosections were blocked with 10% goat serum for 30 min. The sections then were incubated overnight at 4ºC with the following primary antibodies: purified rat anti-mouse CD4 (1:100), purified rat anti-mouse CD8a (1:100, all from BD Biosciences). After three rinses in TBS/Triton, the secondary antibodies biotin-goat anti-rat (1:400; Vector) were applied for 30 min at room temperature. The tertiary antibodies were Cy3–streptavidin (1:1000; Sigma). Dystrophin staining: sections were blocked in the blocking buffer (MOM kit) for 30 min. The primary antibodies used were monoclonal anti-dystrophin (1:20; Novacastra). The subsequent antibodies were biotin- anti-mouse (1:200; MOM kit) followed by Cy3–streptavidin (1:1000; Sigma).

## RESULTS

*Ex vivo gene transfer mediated by plasmid transduced MDSCs*

Examination of the muscle sections at early time points (10 days after injection) revealed similar levels of dystrophin expression by both populations of plasmid transfected cells (Figure 1a, b). However, at time points of 60 days after injection, the dystrophin expression decreased in the muscle injected with CMV-dys-transfected MDSCs (data not shown). Dystrophin expression was more persistent in the muscle injected with MCK-dys-transduced MDSCs (data not shown). We detected more dystrophin expression in the MDSC-MCK group 120 days after injection than in the MDSC-CMV group (Figure 1c, d). We quantified the dystrophin expressing myofibers in the different groups at different time points. Result showed that MCK-dys-transfected MDSCs displayed significant higher number of dystrophin positive myofibers at 60 and 120 days post-injection although there is no significant difference at the early time point (10 days post-injection) (Figure 2).

*Determination of Immune response after cell transplantation*

Immunostaining of muscles that were injected with plasmid transfected cells at all time points after injection revealed that the injection of the CMV-dys-transfected MDSCs triggered greater CD4 lymphocyte infiltration than did the injection of MCK-dys-transduced MDSCs (data not shown). Similar results were found for CD8-positive cell infiltration (data not shown).

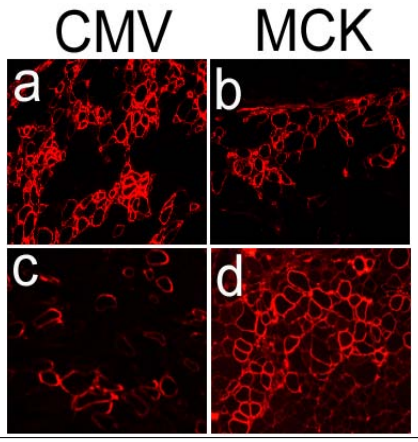


**Figure 1:** Dystrophin expression at 10 (a, b) and 120 (c, d) days post transplantation. MCK-MDSC (d) persisted better than CMV-MDSC (c).

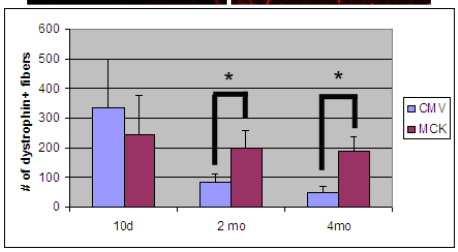


**Figure 2:** Quantitation of dystrophin expression in transplanted mdx muscles. MCK-MDSC generated significantly high number of dystrophin positive myofibers than CMV-MDSC at 2 months and 4 months time points. (* indicates $p<0.05$)

## DISCUSSION

In this project, we demonstrated that the use of different promoters (CMV or MCK) within a given plasmid construct affects the efficiency and the persistence of dystrophin expression after plasmid-mediated gene transfer into the skeletal muscles of mdx mice. Ex vivo gene transfer of MCK-dys triggered a lower immune response that led to more efficient and more persistent dystrophin expression when compared to the ex vivo gene transfer of CMV-dys. We believe that MDSCs transfected with CMV-dys and delivered via ex vivo gene transfer acted as APCs after implantation in skeletal muscle as we have described previously[1]. Our results suggest that the CMV-dys-transfected MDSCs expressed dystrophin, and therefore rapidly initiated an immune response, while the MCK-dys transfected MDSCs expressed the dystrophin only after differentiation into myotubes and myofibers, ultimately leading to longer persistence of the transgene in the injected skeletal muscle. These results demonstrate that the use of a muscle-specific promoter to restrict the transgene expression to skeletal muscle can reduce the host immune response and prevent MDSCs from acting as APCs, and thereby improve both the efficiency and long-term benefits of gene transfer in skeletal muscle.

## ACKNOWLEDGMENTS

The authors are grateful for technical assistance from Maria Branca, Jessica Tebbets and editorial assistance from Jim Cummins. This work was supported by funding from the Henry J. Mankin Endowed Chair for Orthopaedic Research at the University of Pittsburgh, the William F. and Jean W. Donaldson Chair at Children's Hospital of Pittsburgh, the Hirtzel Foundation, and a grant from the Department of Defense.

## REFERENCES

1.Cao, B., et al. Gene Ther, 2004. **11**(17): p. 1321-30. 2.Wang, B., et al. Proc Natl Acad Sci U S A, 2000. **97**(25): p. 13714-9. 3. Qu, Z., et al. J Cell Biol, 1998. **142**(5): p. 1257-67. 4. Qu-Petersen, Z., et al. J Cell Biol, 2002. **157**(5): p. 851-64.

** Department of Orthopaedic Surgery, University of Pittsburgh

Molecular Biology of the Cell
Vol. 16, 3323–3333, July 2005

# Long-Term Self-Renewal of Postnatal Muscle-derived Stem Cells

**B. M. Deasy,*†‡ B. M. Gharaibeh,† J. B. Pollett,† M. M. Jones,† M. A. Lucas,*† Y. Kanda,† and J. Huard*†‡§**

*Department of Bioengineering and †Growth and Development Laboratory, Children's Hospital of Pittsburgh, Pittsburgh, PA 15213; and Departments of ‡Orthopaedic Surgery and §Molecular Genetics and Biochemistry, University of Pittsburgh, Pittsburgh, PA 15260

Submitted February 28, 2005; 2000; Accepted April 22, 2005
Monitoring Editor: Marianne Bronner-Fraser

**The ability to undergo self-renewal is a defining characteristic of stem cells. Self-replenishing activity sustains tissue homeostasis and regeneration. In addition, stem cell therapy strategies require a heightened understanding of the basis of the self-renewal process to enable researchers and clinicians to obtain sufficient numbers of undifferentiated stem cells for cell and gene therapy. Here, we used postnatal muscle-derived stem cells to test the basic biological assumption of unlimited stem cell replication. Muscle-derived stem cells (MDSCs) expanded for 300 population doublings (PDs) showed no indication of replicative senescence. MDSCs preserved their phenotype (*Sca*I+/CD34+/desmin$^{low}$) for 200 PDs and were capable of serial transplantation into the skeletal muscle of mdx mice, which model Duchenne muscular dystrophy. MDSCs expanded to this level exhibited high skeletal muscle regeneration comparable with that exhibited by minimally expanded cells. Expansion beyond 200 PDs resulted in lower muscle regeneration, loss of CD34 expression, loss of myogenic activity, and increased growth on soft agar, suggestive of inevitable cell aging attributable to expansion and possible transformation of the MDSCs. Although these results raise questions as to whether cellular transformations derive from cell culturing or provide evidence of cancer stem cells, they establish the remarkable long-term self-renewal and regeneration capacity of postnatal MDSCs.**

## INTRODUCTION

The majority of stem cell research efforts are focused on the promising applications of multilineage plasticity of putative stem cells. The equally important characteristic of self-renewal capacity is often overlooked but is increasingly becoming a focus of stem cell biology (Molofsky *et al*., 2004; Zipori, 2004) from both basic science and clinical perspectives. The potential use of stem cells for gene therapy and functional tissue engineering will require the expansion of undifferentiated stem cell populations to achieve sufficient numbers for use in clinical applications. It will be necessary to develop cellular expansion techniques that regulate the extrinsic and intrinsic biostimuli that lead to self-renewal and differentiation, or symmetric and asymmetric divisions. In addition, practical scalable culture systems with corresponding models for prediction of output numbers will be required. Finally, the need to pay careful attention to any changes in cell quality attributable to extensive expansion or, more generally, to cellular aging adds another layer of complexity to the development of efficient expansion techniques.

Hayflick first reported in 1961 that normal human fibroblasts undergo a limited number of divisions in vitro (Hayflick and Moorhead, 1961); he estimated the maximum number of population doublings (PDs) to be ~50. After that initial report, many other investigators have verified that euploid cells in culture undergo a finite number of PDs. In contrast, the current consensus is that stem cells possess a unique proliferation capacity that is either several times greater than that displayed by euploid cells, or possibly unlimited (Potten and Morris, 1988; Rubin, 1997; Reyes *et al*., 2001; Rubin, 2002).

The capacity for long-term proliferation is regarded as an identifying characteristic of stem cells. Reports of stem cell replicative potentials show variability related to the developmental stage of the cell source, the species, and the culturing conditions. Human embryonic stem (ES) cells expanded for 250 PDs (Amit *et al*., 2000) or 130 PDs (Xu *et al*., 2001) have maintained their pluripotency and normal karyotype. However, due both to ethical issues surrounding the use of embryonic cells and to reports that the cells form teratomas in vivo, research investigating stem cells derived postnatally has grown. Nonembryonic stem cells, such as human hematopoietic stem cells (HSCs), seem to exhibit a slower doubling rate than ES cells, although researchers have expanded some of these cell populations $2 \times 10^6$-fold (20 PDs) over a 6-mo period (Piacibello *et al*., 1997) and ~1400-fold (10 PDs) over a 3-mo period (Gilmore *et al*., 2000). Varying degrees of expansion are reported for mesenchymal stem cells (MSCs), bone marrow stromal cells, and multipotent adult progenitor cells—all originating from the bone marrow—$10^9$-fold (30 PDs) (Colter *et al*., 2000), 50–70 PDs (Bianchi *et al*., 2003), and 120 PDs (Schwartz *et al*., 2002; Jiang *et al*., 2003), respectively.

In light of these findings, the generation of large numbers of cells via the expansion of stem cells seems feasible. However, numerous studies performed in the area of cellular

This article was published online ahead of print in *MBC in Press* (http://www.molbiolcell.org/cgi/doi/10.1091/mbc.E05–02–0169) on May 4, 2005.

Address correspondence to: Johnny Huard (jhuard@pitt.edu).

aging have shown that cells with a high replicative age often exhibit chromosomal abnormalities. Incomplete DNA replication at the telomeres (i.e., the G-rich repeat units at the ends of chromosomes) leads to telomere shortening with each cell cycle; cellular senescence occurs after the telomeres reach a critical length. The serial propagation or aging of cells in culture also leads to other degenerative cellular changes, including abnormal structures in the cytoplasm, changes in metabolism, loss of methyl groups, and reiterated sequences from DNA, and reduction in replicative efficiency and growth rate (Rubin, 1997). In addition to the concern that such expanded and aged populations might have a reduced regeneration capacity, the accumulation of damage over the cells' lifetimes increases the probability of genetic instability that can culminate in apoptosis or tumorigenic behavior.

Although extensively expanded stem cells may become targets of transformation due to accumulated damage, there may be a preexisting relationship to cancer. The self-renewal pathway may share some signals with pathways implicated in oncogenesis. Recent research has shown that the PTEN, notch, sonic hedgehog, and wnt signaling pathways may play a role in the self-renewal of HSCs (Karanu *et al*., 2000; Varnum-Finney *et al*., 2000; Bhardwaj *et al*., 2001; Reya *et al*., 2001; van Noort and Clevers, 2002; Stiles *et al*., 2004); these same pathways have been linked to oncogenicity. Furthermore, HSCs are thought to be more likely than committed progenitors to undergo transformation (Reya *et al*., 2001). Together, these findings clearly indicate the need to carefully examine the quality of expanded stem cell populations before using them as the basis for cell therapy and tissue engineering applications.

To test the long-term self-renewal potential of muscle-derived stem cells (MDSCs) and to identify any limits to the expansion of an MDSC population, we extensively expanded muscle stem cells for >300 PDs under normal culture conditions (225 d of expansion) and examined the cells to identify any in vitro phenotypic alterations, signs indicative of cellular aging and transformation, changes in the cells' capacity to differentiate, and changes in their capacity to regenerate skeletal muscle in vivo.

## MATERIALS AND METHODS

### *Proliferation Kinetics and Expansion of MDSCs in Culture*

MDSCs were obtained, as described previously, from normal (C57BL/6J) 3-wk-old mice (Qu-Petersen *et al*., 2002). Cells were cultured in DME medium supplemented with 10% fetal bovine serum, 10% horse serum (HS), 1% penicillin/streptomycin, and 0.5% chick embryo extract (Invitrogen, Carlsbad, CA) at an initial seeding density of 225 cells/cm$^2$. After a sufficient number of cells was obtained (~3–4 wk after isolation), 5600 cells (225 cells/cm$^2$) were plated in 25-cm$^2$ collagen-coated flasks, and routine cell passaging was performed every 2 or 3 d. After 2 or 3 d of growth, the cells were trypsinized, counted, and replated at a density of 225 cells/cm$^2$. This process was repeated for a 6-mo period.

The cell counts and cellular dilution factor were recorded at each passage and used to calculate the expansion potential or theoretical yield, number of population doublings, and doubling time. The number of population doublings was calculated by solving the exponential equation $N_i = N_0 2^{(t_i/PDT)}$ for $t_i$ /PDT, which is the number of population doublings at time $t_i$ or no. of PDs = $\log_2(N_i / N_o)$. Daily population doubling times were calculated using the following equation:

$$PDT = \frac{t_i}{\#\text{ of population doublings}} = t_i \Big/ \log_2 \frac{N_i}{N_0}$$

Local moving average PDT was calculated by fitting an exponential trend line to several measurements of N over a 1-wk period. The regression method provides a fitted curve of the form $N_i = N_0 e^{kt_i}$. Because PDT is defined as the time, $t_i$, such that $N_i = 2N_o$, k = ln2/PDT and PDT = ln2/k.

Cellular division time (DT) was measured directly by visual observation of time-lapsed images acquired at 10-min intervals over a 4-d period (Deasy *et al*., 2003). The mitotic fraction, or the fraction of daughter cells that are dividing ($\alpha$ or $F_D$), was calculated by using the measured PDT and DT at the given doubling level and solving the rearranged Sherley model for $\alpha$ (using Mathematica 4.2; Wolfram Research, Champaign, IL) as described previously (Sherley *et al*., 1995; Deasy *et al*., 2003):

$$PDT = DT\left[\frac{\ln(6a-2)}{\ln(2a)} - 1\right]$$

### *Morphological Analysis*

Phase contrast light microscopy images were acquired every 2 wk in three random fields. Northern Eclipse software package was used to collect morphometric data by outlining or tracing 20–30 cells per image or time point, with five to eight time points per doubling grouping. Quantitative measurements for cell area (number of pixels calibrated to microns squared), diameter (maximal cell length in micrometers), cell elongation (ratio of major axis to minor axis), and roundness (perimeter$^2$/4 * $\pi$ * area) were compared using nonparametric one-way analysis of variance (ANOVA) and Dunn's method for multiple comparisons.

### *Sca-1 and CD34 Expression by Flow Cytometry*

MDSCs were labeled with rat anti-mouse Sca-1 (phycoerythrin; BD Biosciences PharMingen, San Diego, CA) and CD34 (biotin; BD Biosciences PharMingen) monoclonal antibodies at 2-wk intervals. A separate portion of cells was treated with equivalent amounts of isotype control antibodies. Both fractions then were washed and labeled with streptavidin-allophycocyanin. 7-Amino-actinomycin D was added to exclude nonviable cells from the analysis. Appropriate gating was performed to determine Sca-1 and CD34 expression via flow cytometry with a FACStar Plus (BD Biosciences, San Jose, CA). One-way ANOVA was used to test for differences at various doubling levels; pairwise multiple comparisons to identify differences in expression were performed using the Tukey test with $\alpha = 0.05$ and power = 0.997.

### *Myogenic Marker Expression by Immunocytochemistry*

Expression of the myogenic marker desmin was examined at 2-wk intervals via immunocytochemistry. In brief, after cold methanol fixation the cells were blocked in 5% HS, and then they were incubated with antibodies for desmin (mouse monoclonal desmin, 1:250; Sigma-Aldrich, St. Louis, MO), secondary biotinylated IgG (1:250; Vector Laboratories, Burlingame, CA), and streptavidin-Cy3 (1:500; Sigma-Aldrich) to fluorescently label the antigenic binding and to determine the percentage of myogenic cells within the population. After ANOVA, pairwise multiple comparisons to identify differences in desmin expression were performed using the Tukey test with $\alpha = 0.05$ and power = 0.87.

### *In Vitro Myogenic Differentiation*

MDSCs were plated at 1000 cells/cm$^2$ in normal 20% serum DME medium for 3 d, and then they were placed in 2% serum DME medium for an additional 4 d to induce myogenic differentiation. On day 7, methanol-fixed cultures were blocked with 5% HS and were incubated with monoclonal mouse fast myosin heavy chain (anti-MyHC, 1:250; Sigma-Aldrich), biotinylated IgG (1:250; Vector Laboratories), and streptavidin-Cy3 (1:500). Differentiation efficiency was calculated as the ratio of myogenic nuclei to total nuclei. ANOVA and pairwise multiple comparisons to identify differences in differentiation were performed using the Tukey test with $\alpha = 0.05$ and power = 0.848.

### *In Vivo Self-Renewal*

MDSCs were retrovirally transduced to express green fluorescent protein (GFP) and neomycin resistance genes. The labeled cells (30–40 PDs) were transplanted into the gastrocnemius muscles of dystrophic primary recipient mice (n = 2). Each transplantation involved 0.2–1.0 $\times$ 10$^6$ donor cells. After 2 wk in vivo in the primary recipient, the cells were reharvested, selected in medium containing G418 (3 mg of active compound per milliliter of Geneticin, an analogue of neomycin; Invitrogen), and expanded for <3 wk. The MDSCs were subsequently transplanted into skeletal muscles of secondary recipients (n = 2). Reisolation of the serially transplanted MDSCs from secondary recipients was performed as described above. Although these experiments were semiquantitative in nature, we estimated that the percentage of GFP-positive cells in the primary muscle biopsy was 0.5–1% of the skeletal muscle biopsy (gastrocnemius) and isolated as obtained through the preplate technique. The GFP cells were recovered from preplates 1, 2, and 3. These cells were tested for GFP expression and the ability to differentiate into myotubes in vitro. The contralateral muscles of both the primary and secondary recipients were harvested, sectioned, and examined for GFP expression.

### *In Vivo Muscle Regeneration*

Regeneration efficiency was examined as a function of cell age by transplantation of 1–3 $\times$ 10$^5$ cells into the gastrocnemius muscles of 5- to 8-wk-old

mdx/SCID mice as described previously (Jankowski et al., 2002). Two weeks after transplantation, the mice were killed and the muscles were sectioned by cryostat (10 $\mu$m). Immunohistochemistry was performed to identify dystrophin-positive myofibers. Tissues sections were fixed with cold methanol, and immunostaining was performed using the mouse-on-mouse (M.O.M.) kit (Vector Laboratories) with DYS2 antibody (1:50; Novocastra, New Castle, United Kingdom). Populations of various doubling levels were grouped into six categories (0–50 PDs, 51–100 PDs, 101–150 PDs, 151–200 PDs, 201–300 PDs, and >300 PDs) and were compared with ANOVA. Pairwise multiple comparisons were performed using the Tukey test with $\alpha = 0.05$ and power = 1.0.

### *Transformation Analysis*

Soft agar growth in populations from six doubling levels was examined by plating 2000 cells per 9.6-cm$^2$ well in 0.35% low melting point agar as a top layer, with a bottom layer of 0.7% agar in 20% serum medium. Colonies were allowed to grow for 21 d at 37°C, at which time Northern Eclipse imaging software was used to score the colonies for both number and size. After ANOVA, pairwise multiple comparisons of the number of colonies were performed using the Tukey test with $\alpha = 0.05$ and power = 1.0.

DNA content was examined in the same populations via flow cytometry. Cells were fixed in ethanol for 2 h and then resuspended in 0.1% (vol/vol) Triton X-100 (Sigma-Aldrich) in phosphate-buffered saline with 0.2 mg/ml DNase-free RNase A (Sigma-Aldrich) and 20 ng/ml propidium iodide (Sigma-Aldrich) solution. Experiments were performed three times, and results were averaged. One-way ANOVA was used to identify differences among the doubling levels for the 2N, 4N, and >4N peaks. Numerical chromosomal analysis was performed through the use of standard Geimsa staining and banding techniques as described previously (Lee *et al.*, 2000). To test for the transformation of the highly expanded cells, subcutaneous injections into both SCID and syngeneic mice were performed. MDSCs that had been expanded to 15 PDs and MDSCs that had been expanded to 300 PDs were transplanted subcutaneously into the lower abdomen of both C57BL/6J-Prkdc SCID mice ($0.3–0.4 \times 10^6$ cells per site; n = 4) and C57/BL6J ($0.75–1.0 \times 10^6$ cells per site; n = 4). Tumor growth was followed by palpation and radiography, and mice were killed 130 d (SCID) and 150 d (syngeneic) after injection. Killed animals were dissected and were evaluated for growths at the site of injection and gross enlargement of spleen and lymph tissues. Hematoxylin and eosin staining was performed on 8-$\mu$m–thick sections of snap-frozen tissue.

## RESULTS

To examine the effects of long-term expansion, we isolated highly purified populations of MDSCs from 3-wk-old normal mice (C57BL/6J), as described previously (Qu-Petersen *et al.*, 2002) and maintained the cells in continuous culture for 6 mo. We cultured MDSCs at <30% visual confluence or a density of $2 \times 10^3–10^4$ (Figure 1A), and periodically analyzed the stem cell characteristics of MDSCs at different doubling levels.

### *Expansion Potential of MDSCs*

We were able to expand the MDSCs for >300 PDs (n = 3; Figure 1B) over a 6-mo period and obtained a theoretical yield of $>10^{100}$ cells (>1 googol cells). We expanded a total of four different populations to a high doubling number: mdsc1 (300 PDs; n = 3), mdsc2 (300 PDs; n = 2), mdsc3 (200 PDs; n = 1), and mdsc4 (200 PDs; n = 2). We focused our study on the population that displayed the best engraftment efficiency in skeletal muscle: the mdsc1 population (hereafter referred to simply as "MDSCs").

It is typical to observe very long doubling times early in the isolation process. Because cell death is common in cell populations obtained immediately after isolation, the population size actually tends to decrease during this initial period. For this reason, obtaining workable quantities of MDSCs can require several weeks, often leaving freshly isolated MDSCs in the same isolation flask for up to 2 wk. Measurements of doubling rate during the early isolation period are based on visual counts rather than hematocytometer counts.

We observed this expected lag in population growth during the first 4–6 wk after cell isolation (Figure 1C). Initially, the PDT was infinitely long, but by the 4-wk time point (28 d, as shown in the figure) the PDT had dropped sharply to ~52 h, whereas the number of PDs increased concurrently (Figure 1C). After the lag phase, we observed no significant differences ($p = 0.11$) between the growth rates of cells in culture for 2 d and those in culture for 3 d (schematic shown in Figure 1A). Two-day growth periods resulted in an average of 3 PDs (1.5 ± 0.35 PDs/d), whereas 3-d growth periods resulted in an average of ~5 PDs (1.6 ± 0.39 PDs/d). The population kinetics of the MDSCs cultured continuously for 6 mo indicate that the cells had an extended replicative lifetime (Figure 1, B and D). The PDT after the lag phase dropped sharply to ~14–16 h, and then it remained relatively constant for the remainder of the expansion in culture.

We observed no indication of replicative senescence (Figure 1D) or significant changes in cellular DT during expansion of the MDSCs. We used a unique combinatorial cell culture system (Deasy *et al.*, 2003) to obtain time-lapsed images to directly observe and measure median division time, which was similar for cells at 15 PDs (12 h), 25 PDs (12 h), 75 PDs (12 h), 125 PDs (14 h), 170 PDs (13 h), and 300 PDs (12.5 h; Figure 1E). We used the Sherley model (Sherley *et al.*, 1995) to calculate the mitotic fraction (i.e., the fraction of actively dividing daughter cells), which increased from 0.37—shortly after cell isolation (15 PDs) and essentially during the isolation process—to 0.75–0.98 after 75 PDs (Figure 1E).

### *Morphological Analysis*

Qualitative examination of cell morphology showed that the MDSC populations from early passages seemed to be similar to those from late passages. Figure 2 illustrates the cell density at which these cells were grown and the heterogeneous morphology of the cell populations. Most of the cells maintained a small round shape, although we did observe some well defined subpopulations, including a group of cells with a more spindle-shaped appearance (Figure 2A).

Morphological cellular features (cell area, diameter, and cell elongation and roundness) of MDSC populations were measured from phase contrast images. Figure 2B illustrates distribution of the measurements through the use of box plots with the median, 10th, 25th, 75th, and 90th percentiles as vertical boxes with error bars. The median cross-sectional area and diameter of cells expanded beyond 200 PDs were significantly larger than the area and diameter of cells in the other groups ($p < 0.05$; ANOVA). The roundness parameter is a measure of the shape of the cell, with values closest to 1 indicating the roundest cells. The elongation parameter is the ratio of the length of the major axis of the cell to that of its minor axis. The roundness and elongation measurements of MDSCs expanded beyond 300 PDs differed significantly from those obtained for all MDSCs expanded to a lesser degree; MDSCs expanded beyond 300 PDs were less round and more elongated. Cell populations expanded for 100–150 PDs were significantly rounder than the MDSCs in the other groups, although this difference was not qualitatively recognizable.

### *Stem Cell Marker Analysis*

The use of flow cytometry to analyze expression of the putative muscle-derived stem cell markers CD34 and Sca-1 revealed that the MDSCs maintained the same general profile for the first 200 PDs. In MDSC populations between 0 and 50 PDs, 90 ± 13% of cells were positive for CD34 expression and 78 ± 15% were positive for Sca-1 expression. We observed no significant difference in the total expression of Sca-1 by MDSC populations expanded for various PDs up

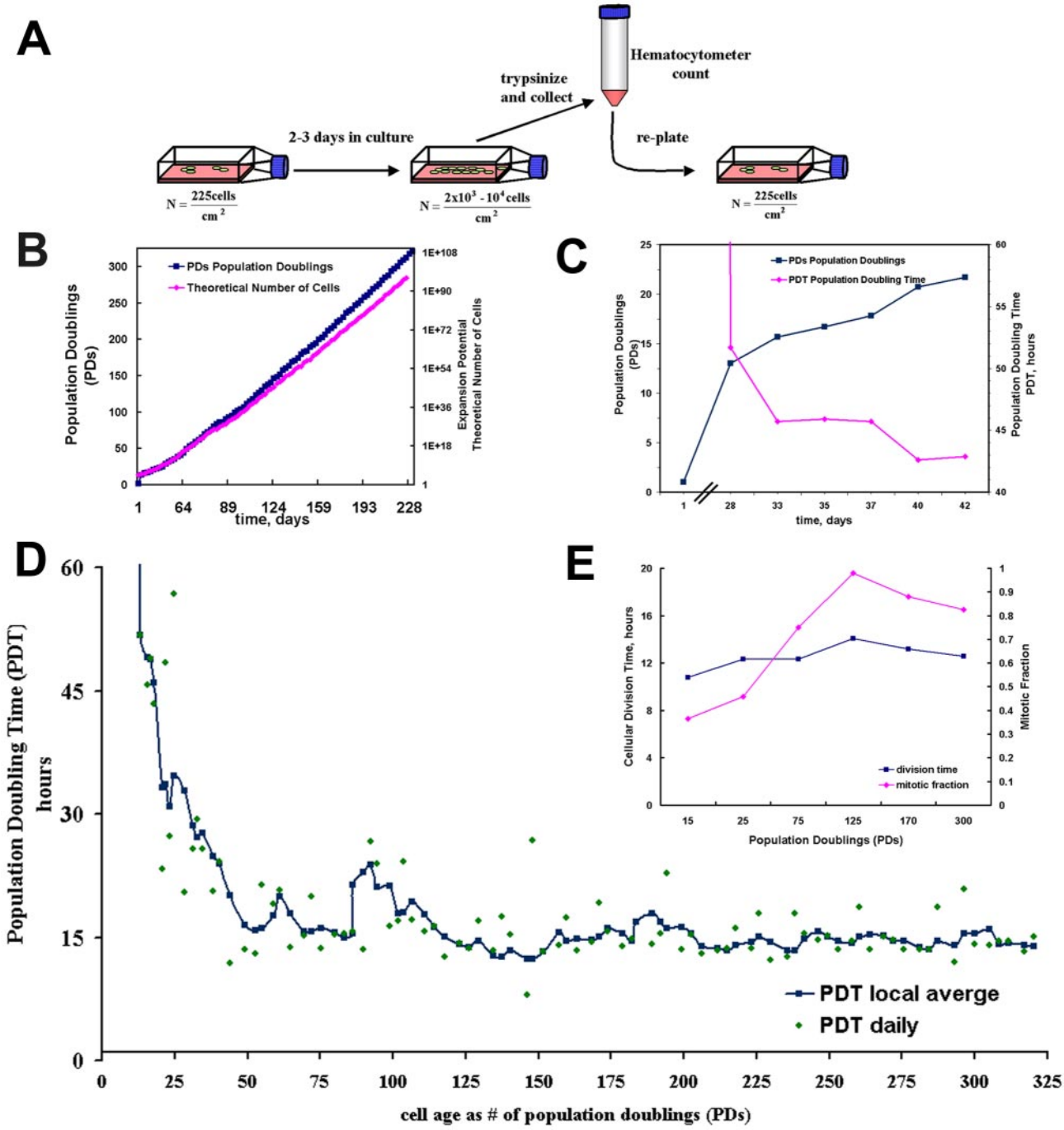


**Figure 1.** MDSC expansion. (A) Schematic representation of cell expansion method. Low growth density was maintained by routine passaging every 2 to 3 d. (B) MDSCs in culture were expanded for >300 PDs over a 6-mo period. (C) Closer examination of the cells during the first 6 wk (42 d) showed very slow growth. After ~4 wk, the number of PDs (blue ■) was ~12 and the PDT (red ♦) had dropped to 52 h. Before the 4-wk time point, the average PDT was much longer than 52 h and is not shown on the scale of this graph. After this period, cell death seemed to subside; the PDT at 6 wk was 42 h and the steadily increasing number of PDs had reached ~22 PDs. (D) Shown are the moving local average PDT (blue ■, smoothed line) and the individual PDT measurements taken every 2 or 3 d (green ♦). (E) Cellular DT did not change significantly during the expansion. Median division times (blue ■) are shown for MDSCs expanded for 15 PDs (13 h), 25 PDs (12 h), 75 PDs (14 h), 125 PDs (14 h), 170 PDs (14 h), and 300 PDs (14 h). Mitotic fractions (i.e., the fractions of daughter cells that were actively dividing) (red ♦) for MDSCs expanded for 15 PDs (0.37), 25 PDs (0.46), 75 PDs (0.75), 125 PDs (0.98), 170 PDs (0.88), and 300 PDs (0.83).

to 300 PDs ($p = 0.10$; one-way ANOVA). However, we observed a significant decrease in total CD34 expression after 200 PDs (65 ± 22% of MDSCs at 200 PDs vs. 94.7 ± 7% at 150–200 PDs; $p < 0.05$) and after 300 PDs (36 ± 22%; $p < 0.05$ vs. all other doubling levels; Figure 3A). Shifts in CD34 expression are apparent in the dot plots, but Sca-1 expression seems to be constant (Figure 3B). Stage-specific embryonic antigen 1 also was analyzed by flow cytometry,

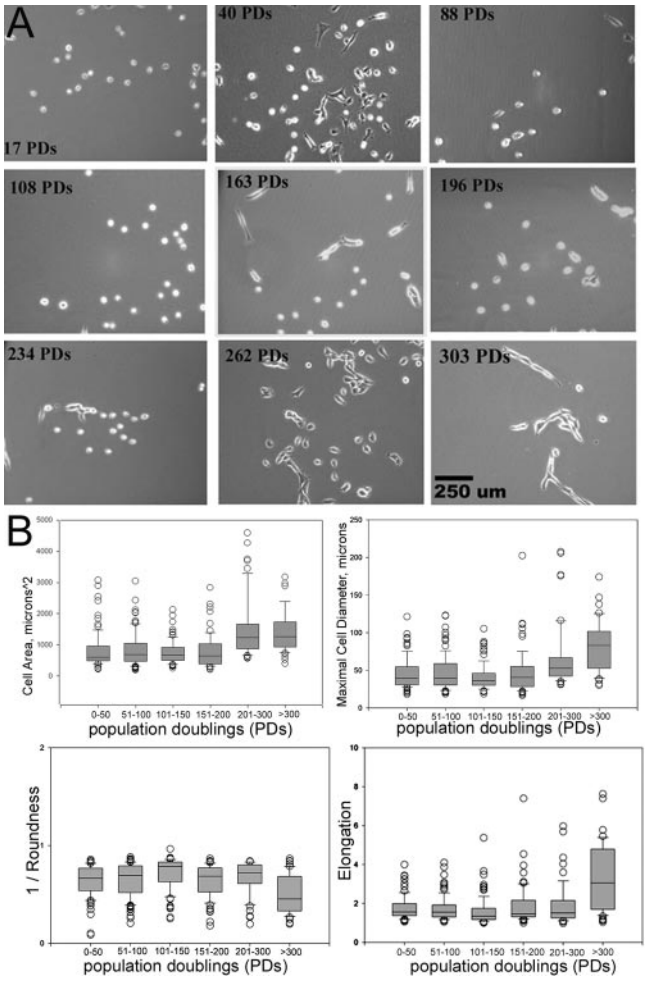


**Figure 2.** MDSC morphology. (A) Images illustrate MDSC morphology and the range of cellular densities at particular expansion levels (PDs) throughout the 6-mo period of in vitro expansion (100×; bar, 250 $\mu$m) (B) Morphological cellular features of MDSC populations during expansion were measured from phase contrast images. Box plots show the median, 10th, 25th, 75th, and 90th percentiles as vertical boxes with error bars. Highly expanded populations had a significantly larger area and diameter and were less round and more elongated ($p < 0.05$). Median cross-sectional area is as follows: 0–50 PDs (610 $\mu m^2$), 51–100 (690 $\mu m^2$), 101–150 (680 $\mu m^2$), 151–200 (644 $\mu m^2$), 201–300 (1230 $\mu m^2$), and >300 (1260 $\mu m^2$). Median diameter is as follows: 0–50 PDs (39 $\mu$m), 51–100 (39 $\mu$m), 101–150 (36 $\mu m^2$), 151–200 (40 $\mu$m), 201–300 (53 $\mu$m), and >300 (83 $\mu$m). Roundness values are as follows: 0–50 PDs (0.67), 51–100 (0.70), 101–150 (0.78), 151–200 (0.69), 201–300 (0.72), and >300 (0.45). Elongation values are as follows: 0–50 PDs (1.56), 51–100 (1.55), 101–150 (1.35), 151–200 (1.47), 201–300 (1.52), and >300 (3.06).

although MDSCs were negative for this marker throughout the expansion period (our unpublished data).

### *Myogenic Behavior*

***Myogenic Markers.*** Less than 20% of the MDSC population expressed the myogenic marker desmin upon analysis shortly after isolation (20 PDs), and the early MDSC population was negative for Pax-7 and m-cadherin expression, two markers of satellite cells (Irintchev *et al*., 1994; Seale *et al*., 2000). After expansion, we observed a slight increase in

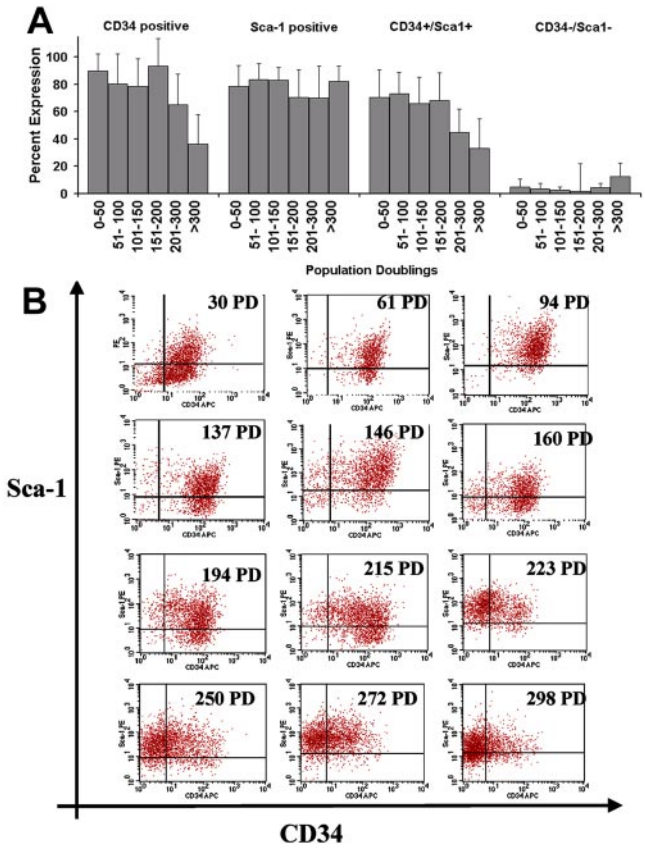


**Figure 3.** Stem cell marker expression. (A) CD34 and Sca-1 immunophenotyping after expansion. Total percentage of cells expressing CD34 is as follows: 0–50 PDs (85 ± 18; n = 9), 51–100 (81 ± 22; n = 12), 101–150 (78 ± 21%; n = 11), 151–200 (94 ± 7; n = 8), 201–300 (65 ± 22; n = 10), and >300 (37 ± 22; n = 5). Total percentage of cells expressing Sca-1 is as follows: 0–50 PDs (78 ± 15; n = 9), 51–100 (84 ± 12; n = 12), 101–150 (83 ± 9; n = 11), 151–200 (71 ± 17; n = 8), 201–300 (71 ± 23; n = 10), and >300 (76 ± 18; n = 5). The double-positive cell fraction (CD34+/Sca-1+) remained large for the first 200 PDs but significantly decreased in size after 200 PDs. There was no significant difference in the double-negative cell fraction (CD34−/Sca-1−) over time (ANOVA). (B) Flow cytometry dot plots from one representative expansion for 12 different time points throughout the expansion process.

desmin expression by MDSCs expanded beyond 200 PDs (19 ± 9%) compared with desmin expression by MDSCs evaluated at 61–200 PDs (range 4.5–7%; $p < 0.05$); however, there was no significant difference between desmin expression by MDSCs at 200 PDs, and desmin expression by MDSCs expanded for <60 PDs (7 ± 5%; Figure 4A). Immunocytochemical staining illustrates that only a few cells expressing desmin were present among a much larger number of desmin-negative cells (Figure 4B). MDSCs did not express Pax-7 or m-cadherin at any point during the expansion period (our unpublished data).

***Myogenic Differentiation.*** The extent of myogenic differentiation, i.e., myotube formation, declined with increased passaging of MDSCs. Cells at low doublings (<30 PDs) exhibited a high degree of differentiation, as indicated by the formation of multinucleated myotubes with 65% of the nuclei positive for myosin heavy chain (fast MyHC) after cul-

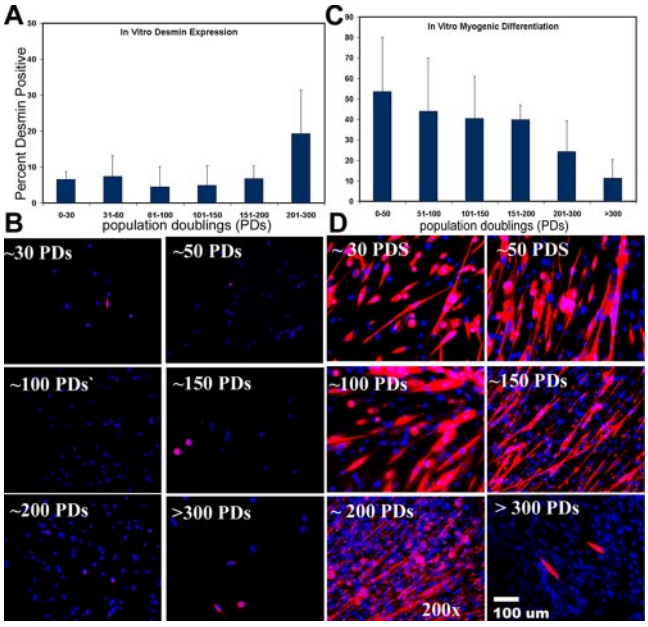


**Figure 4.** Immunochemical analysis of myogenic markers and differentiation. (A) Desmin expression by MDSCs expanded for various numbers of PDs (mean ± SD) is as follows: 0–30 PDs (6.5 ± 2%; n = 3), 31–60 (7.4 ± 7%; n = 4), 61–100 (4.5 ± 7%; n = 8), 101–150 (4.8 ± 5%; n = 5), 151–200 (6.8 ± 4%; n = 6), and 201–300 (19.2 ± 9%; n = 6). (B) Immunochemical staining of MDSCs at the different expansion levels. Desmin, red, Hoechst nuclei, blue (200×). (C) In vitro myogenic differentiation values (as percent myosin heavy chain positive) are as follows: 0–50 PDs (65 ± 4%; n = 4), 51–100 (44 ± 26%; n = 5), 101–150 (40 ± 20%; n = 5), 151–200 (40 ± 7%; n = 5), 201–300 (24 ± 15%; n = 4), and >300 (15 ± 8%; n = 4). ANOVA revealed a significant decrease between both the 201–300 PD time point and the >300 PDs time point compared with all earlier time points (ANOVA; $p < 0.05$). (D) Immunocytochemical staining for myogenic differentiation into myotubes expressing myosin heavy chain after incubation for 7 d in differentiation-inducing conditions. Myosin heavy chain, red; Hoechst nuclei, blue (200×).

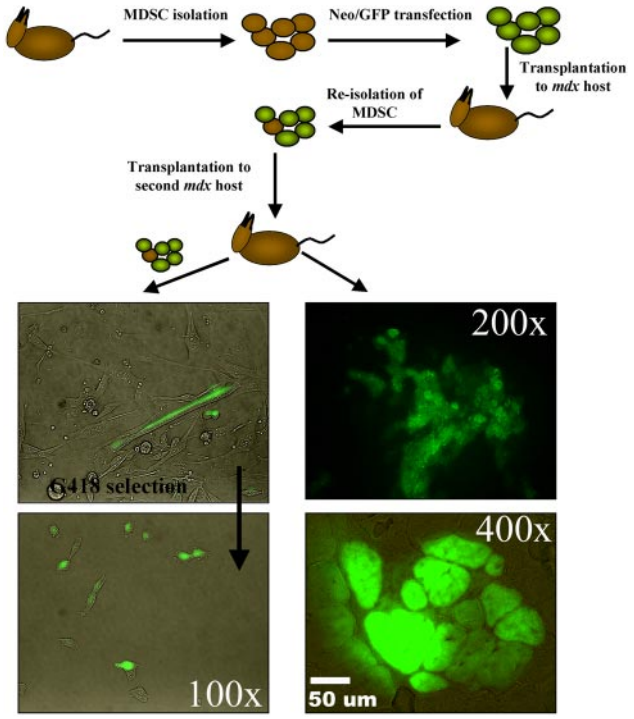


**Figure 5.** In vivo self-renewal. MDSCs were isolated and then were transduced with genes encoding for GFP and neomycin resistance. Two weeks after their injection, the labeled cells were reharvested, selected in G418 medium, and transplanted into secondary mdx recipients. Regeneration of muscle fibers was observed by green fluorescence, whereas contralateral muscles were used to reharvest MDSCs from the secondary recipients. Serially transplanted cells regenerated skeletal muscle fibers within the skeletal muscles of secondary recipients and differentiated into myotubes in vitro.

turing the MDSCs under low-serum and high-density conditions for 7 d (Figure 4C). Generally, the MDSCs began to fuse on day 3 or 4 under such differentiation-inducing conditions, before reaching 100% confluence in culture. A significantly smaller percentage of MDSCs underwent fusion or differentiation to form myotubes on day 7 at the 200 PD level (24 ± 15%; $p < 0.05$) and the 300 PD level (15 ± 8%; $p < 0.05$; Figure 4D) than at the <50 PD level (65 ± 4%).

### *In Vivo Self-Renewal*

The ability of MDSCs to undergo extensive proliferation while preserving their marker profile for at least 200 PDs is indicative of the high self-renewal ability of these cells in vitro. To examine in vivo self-renewal, we used the classic approach of serial transplantation. We were able to reisolate MDSCs that were previously genetically engineered to express neomycin-resistance gene and GFP and were transplanted into the skeletal muscles of dystrophic mice 14 d earlier. We selected the recovered cells in vitro and expanded the cell population for use in a second transplantation. These MDSCs regenerated GFP-positive myofibers within the secondary recipients (Figure 5, GFP-positive fibers), could be reharvested from the secondary recipients (Figure 5, GFP-positive cells in G418 sulfate), and demonstrated the ability to undergo myogenic differentiation in vitro (Figure 5, GFP-positive myotubes). These findings suggest that MDSCs are capable of self-renewal in vivo.

### *Muscle Regeneration*

MDSCs at low passages maintained the ability to regenerate large numbers of dystrophin-positive fibers after transplantation into the gastrocnemius muscles of mdx mice. We analyzed regeneration capacity in terms of the transplanted cells' regeneration index (RI)—the number of dystrophin-positive fibers per $10^5$ donor MDSCs. Fourteen days after transplantation, the average RI for MDSCs expanded for between 0 and 50 PDs was 829 ± 337 dystrophin-positive fibers. MDSCs maintained this high regeneration capacity for up to 195 PDs (RI = 800 ± 170; Figure 6A). Representative dystrophin engraftments are shown in Figure 6A. After 200 PDs, the engraftment efficiency decreased significantly; we observed a quantity of dystrophin-positive fibers comparable with the number of background revertant fibers (200–300 PDs, RI = 32 ± 47; >300 PDs, RI = 3 ± 3, $p < 0.001$; Figure 6D). Histological examination 14 d after transplantation of MDSCs expanded to 240 PDs revealed a large engraftment of mononuclear cells (Figure 6B). However, small numbers of dystrophin-positive fibers were visible at the graft site (Figure 6B). To confirm delivery of the MDSCs and identify the injection site, we used LacZ to retrovirally

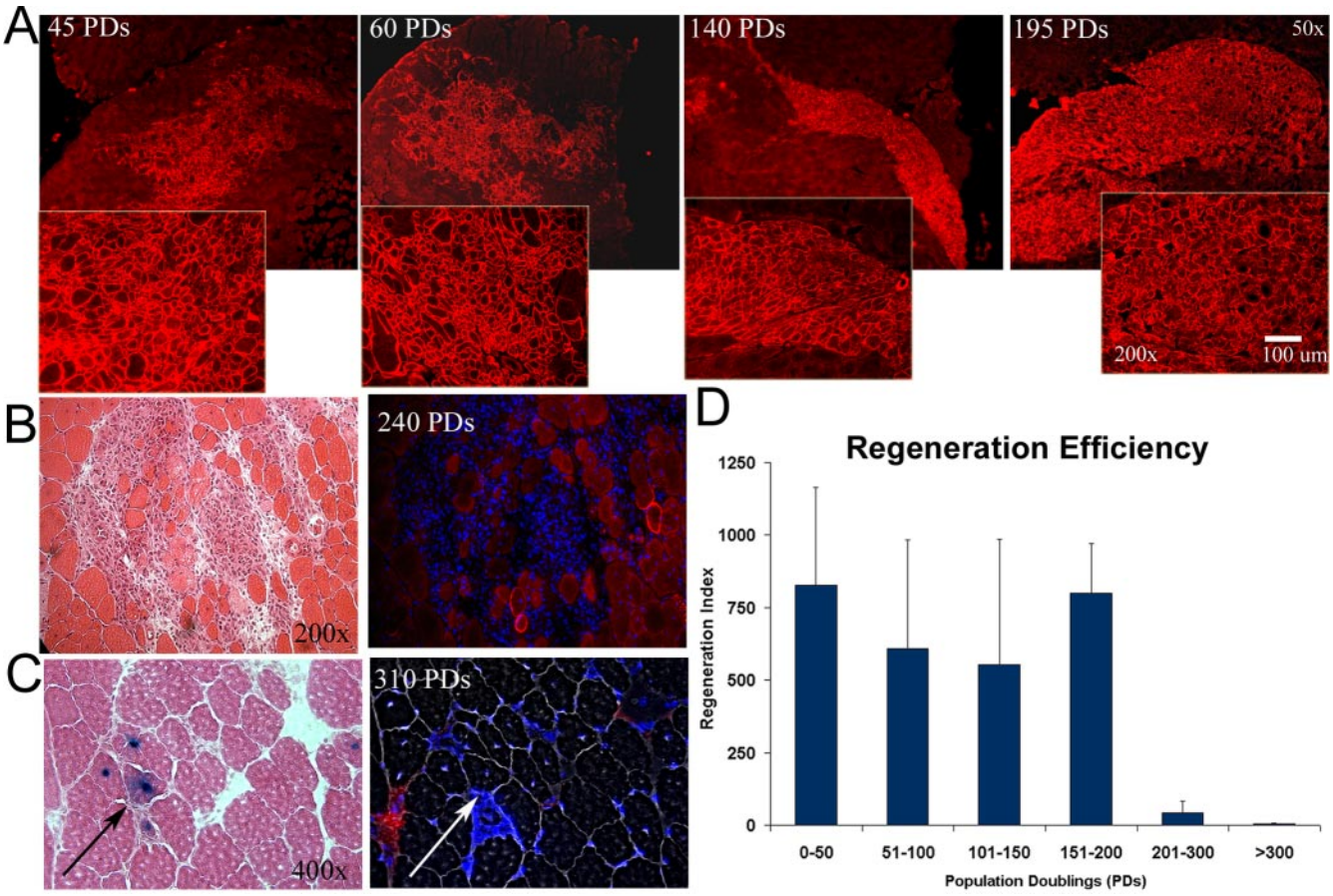


**Figure 6.** In vivo regeneration efficiency. (A) Regeneration of dystrophin-positive fibers within the skeletal tissue of mdx mice (harvested at 14 d), as indicated by immunostaining (red), by cells at 45, 60, 140, and 195 PDs (50× magnification in background, 200× magnification in foreground). (B) Eosin staining revealed numerous cells in the host mdx muscle transplanted with MDSCs expanded for 240 PDs. Serial sections contained very few dystrophin-positive fibers (200×). (C) LacZ-positive cells (arrows) enabled confirmation of the cell injection site, which serial sections again revealed to be negative for dystrophin (red, Hoechst blue). Image contrast to reveal fibers was performed on serial sections (400×). (D) Dystrophin-expressing muscle fibers present after cell transplantation were scored as the regeneration index (i.e., the number of dystrophin-positive fibers per 100,000 donor cells). Cells expanded for up to 200 PDs engrafted at a level comparable with that exhibited by newly isolated cells; after this point, however, regeneration efficiency dropped significantly (ANOVA; $p < 0.05$): 0–50 PDs (829 ± 336; n = 4), 51–100 (610 ± 376; n = 3), 101–150 (457 ± 272; n = 6), 151–200 (800 ± 170; n = 4), 201–300 (32 ± 47; n = 4), and >300 (3 ± 2.8; n = 8).

label MDSCs expanded for 310 PDs. We verified the site of cell delivery and observed <25 dystrophin-positive fibers in these regions (Figure 6C).

### *Transformation Analysis*

MDSCs at higher doublings demonstrated a heightened ability for anchorage-independent growth (Figure 7A) after 21 d in soft agar. We found that ~2.3% of MDSCs at 25 PDs initiated colonies, which did not progress beyond the four- or eight-cell stage (~30 $\mu$m in diameter) and that <1% formed colonies >60 $\mu$m in diameter (Figure 7B). Above 100 PDs, 12% of the plated cells formed colonies with diameters >30 $\mu$m. We detected several intriguing large colonies (>100 $\mu$m in diameter and comparable in size to the positive control, the rat 1A 412 transformed cell line) in the MDSCs expanded for 140 PDs (Figure 7B). No significant differences were detected among the five different PD groups expanded for <200 PDs (i.e., 0–30 PDs, 31–60 PDs, 61–100 PDs, 101–150 PDs, and 151–200 PDs; ANOVA; $p > 0.05$; Figure 7B). However, MDSCs expanded for 295 PDs formed significantly more colonies than did MDSCs expanded for <200 PDs (for MDSCs >295 PDs: 59% [590 ± 93 colonies per 1000 plated cells]; for MDSCs 0–200 PDs: <10%; $p < 0.001$).

We examined DNA content of MDSCs at different passages by performing flow cytometry to detect polyploidy. We observed no difference in the distribution of cells in the different phases of the cell cycle (Figure 7C), with the single exception of the percentage of cells in $G_2/M$ at the levels of 45 PDs (29 ± 2.5%) versus 300 PDs (21 ± 0.6%). These findings are consistent with the division time analysis that indicated no significant difference in the cell cycle time of expanded MDSCs (Figure 1E) and suggest normal durations of cell cycle phases ($G_0/G_1$: ~5–7 h, S: ~2–3 h, and $G_2/M$: ~3–4 h; Figures 1E and 7C). We also did not detect polyploidy or any increase in populations with >4N DNA content (Figure 7C). These results (Figures 1E and 7C) suggest that DNA content and cell cycle kinetics of MDSCs obtained through extensive expansion are similar to those of freshly isolated stem cells. Analysis of chromosomal number revealed that the cells continued to contain the modal diploid number of 40 chromosomes throughout the expansion process (Figure 7D); however, from one of the three expan-

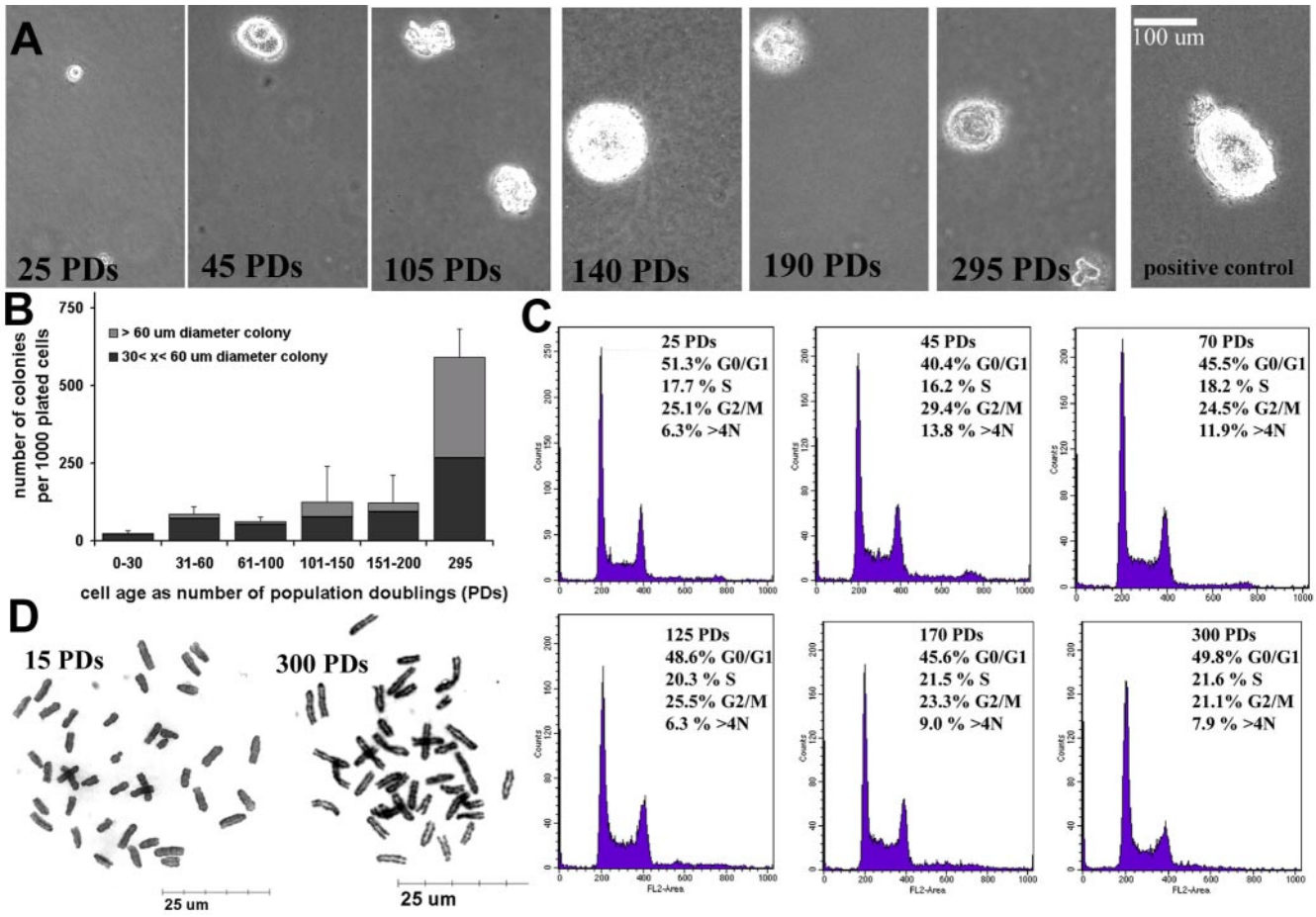


**Figure 7.** (A) Anchorage-independent growth on soft agar. Cells were plated at 2000 cells per 9.6-cm$^2$ well, and images were acquired 21 d after cell seeding. The positive control was the rat 1A cell line. Number of colonies formed per 1000 plated cells: 0–50 PDs (23 ± 10; n = 3), 51–100 (82 ± 24; n = 6), 101–150 (61 ± 13; n = 6), 151–200 (125 ± 116; n = 5), 201–300 (122 ± 88; n = 5), and >300 (590 ± 93; n = 5). The Northern Eclipse software package was used to score both large (>60 $\mu$m in diameter) and small colonies (<60 $\mu$m). (B) Representative images of colony growth (100×). (C) DNA content analysis by flow cytometry revealed a cell cycle distribution that did not differ significantly among the various doubling levels (ANOVA) with the single exception of the percentage of cells in $G_2$/M at 45 PDs (29 ± 2.5%) compared with the percentage of cells in $G_2$/M at 300 PDs (21 ± 0.6%). (D) Metaphase spreads of MDSCs at 15 PDs and 300 PDs (1000×).

sions, a population of cells expanded to ~295–310 PDs contained 76–80 chromosomes. It is interesting to note that the cell cycle analysis did not detect this as tetraploidy.

MDSCs at 15 PDs failed to give rise to tumors in either SCID or syngeneic animals. After implanting MDSCs at 300 PDs into mice, we detected one tumor (~0.75–1.0 cm in diameter) in a syngeneic mouse but no tumors in the SCID mice (Table 1 and Figure 8). The growth of the tumor in the syngeneic mouse was not detectable by radiography performed 30 or 60 d after injection, but it was slightly visible 150 d after injection; no other mice exhibited abnormal growths detectable by x-ray at any time points (Table 1). Pathological examination of tissue sections revealed neoplastic growth and the presence of reactive cells (Figure 8).

**Table 1.** Abnormal growth in SCID and syngeneic mice

| In vitro cell age | SCID mice (C57BL/6J-Prkdc) | Syngeneic mice (C57BL/6J) |
|---|---|---|
| MDSC-15 PDs | 0/4 | 0/4 |
| MDSC-300 PDs | 0/4 | 1/4 |

MDSCs at 15 PDs or at 300 PDs were subcutaneously injected into both SCID mice (0.3–0.4 × $10^6$ cells, mice sacrificed 130 d after injection) and syngeneic mice (0.75–1.0 × $10^6$ cells, mice sacrificed 150 d after injection) (number of growths observed/total number of injections).

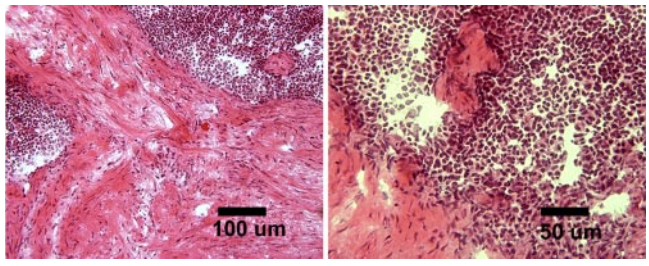


**Figure 8.** Histological examination of in vivo growth observed after transplantation of MDSC-300 PDs into syngeneic mice. Visible are cells with "strap"-like appearance, hypercellular areas containing cells of high nuclear-cytoplasm ratio, and extensive areas of connective tissue formation.

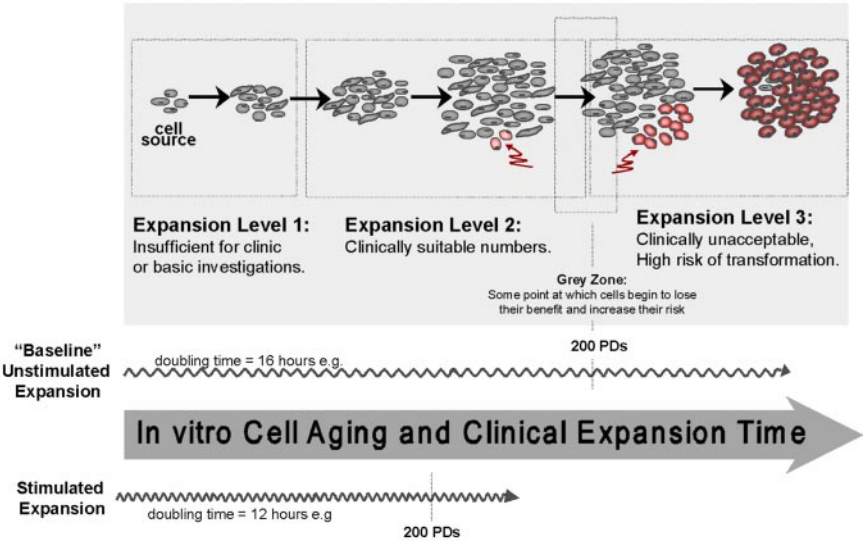


**Figure 9.** In vitro cell aging and clinical expansion of stem cells. Expansion of stem cells will involve generating quantities that are sufficient for basic investigation as well as future therapeutic applications. Identifying and controlling the appropriate expansion and self-renewal conditions represent a major focus in stem cell biology. It is necessary to know the limit of the expansion as it approaches cell transformation. In the study presented here, MDSC lost their stem cell phenotype after 200 PDs. Stimulated expansion, e.g., cytokine stimulation, can be expected to increase the rate at which a clinical dose is reached and also the rate at which cells may reach their limit.

The histomorphological appearance of the cells along with the infiltrative nature of the process suggest a neoplasia designation, whereas the appearance of numerous strap-like cells suggests that there are some areas of skeletal muscle differentiation that would indicate a rhabdomyosarcoma-like growth (Klein, personal communication). Although there was no statistical difference between the number of growths found in the two groups (Fisher's exact test; 15 vs. 300 PDs), our analysis of all the findings with the highly expanded cells, together with the incidence of one growth found with MDSC at 300 PDs, suggests that this may not be attributable to chance and should not be disregarded.

## DISCUSSION

Although it is theorized that several types of stem cells have extended replicative life spans, few studies have investigated the doubling potential of stem cell populations. MDSCs are postnatal stem cells identified and distinguished from satellite cells by their relatively low level of commitment to the myogenic lineage (Lee *et al*., 2000; Qu-Petersen *et al*., 2002). The origin of muscle stem cells isolated from skeletal tissue and their relationship to other stem cells (e.g., muscle satellite cells or blood-derived stem cells) remain unclear, but basic characterization studies have revealed many features of stem cell behavior (Seale *et al*., 2001; Zammit and Beauchamp, 2001; Deasy and Huard, 2002). Our study presented here reveals that MDSCs have an extended replicative lifetime and a substantial self-renewal capacity that previously has not been demonstrated for postnatal muscle-derived cells.

Freshly isolated MDSC exhibit high expression of CD34 and Sca-1 and low expression of myogenic markers. We were able to maintain this molecular profile for at least 200 PDs. After 200 PDs, MDSCs showed decreased CD34 expression that corresponded with the cells' decreased ability to generate dystrophin-positive muscle fibers after intramuscular transplantation. This finding is consistent with previous reports of CD34-sorted MDSCs, which indicate that, in comparison with CD34-negative populations, sorted CD34-positive populations exhibit a significantly greater ability to regenerate dystrophin-positive muscle fibers (Jankowski *et al*., 2002).

As with the majority of studies with stem cells, we did not solely use markers to define the MDSC populations; we also examined the behavior of the MDSCs as they differentiated toward the myogenic lineage in vitro and regenerated skeletal tissue in vivo. Changes in MDSCs' expression of molecular markers occurred concomitantly with decreases in the percentage of cells undergoing myogenic differentiation. MDSCs expanded for up to 195 PDs and subsequently transplanted into mdx mice demonstrated a remarkably high level of engraftment, comparable with that exhibited by freshly isolated MDSCs and significantly higher than that displayed by freshly isolated satellite cells (Jankowski *et al*., 2002; Qu-Petersen *et al*., 2002).

Few other postnatal stem cell populations have been observed to undergo such extensive expansion (http://www.nih.gov/news/stemcell/scireport.htm; Schwartz *et al*., 2002). It is interesting to note that the doubling level observed in our study is most similar to the doubling level reported for ES cells (Thomson *et al*., 1998; Amit *et al*., 2000; Smith, 2001; Xu *et al*., 2001). Other postnatal stem cell populations, such as hematopoietic and bone marrow-derived populations, have been expanded only to much lower levels, despite being cultured for several months (Piacibello *et al*., 1997; Colter *et al*., 2000; Gilmore *et al*., 2000; Jiang *et al*., 2002; Bianchi *et al*., 2003).

The MDSCs' high replicative potential, coupled with the ability to maintain their high regeneration capacity, provides evidence that these cells are capable of long-term self-renewal with preservation of the undifferentiated phenotype. However, the failure of MDSCs to engraft after expansion for >240 PDs (the first doubling level at which we observed a decline) indicates that their potential for extended in vitro self-renewal under the conditions used in our study is, in fact, limited. Several other groups of researchers have reported the loss of multipotency by expanded populations of postnatal stem cells. In comparison with unexpanded HSCs isolated from mice, HSCs expanded for only 2–7 d exhibited a decreased ability to perform hematopoietic reconstitution (Knobel *et al*., 1994; Peters *et al*., 1995; Traycoff *et al*., 1996). In another study, murine MSCs cultured for 24 or 48 h exhibited a decreased ability to home to the bone marrow and spleen (Rombouts and Ploemacher, 2003). Other researchers have reported that human MSC

populations expanded for 15 or 22 PDs have a decreased ability to differentiate toward osteogenic, chondrogenic, and adipogenic lineages (Digirolamo *et al*., 1999; Muraglia *et al*., 2000). By comparison, the MDSCs investigated in our study retained their phenotype and their ability to efficiently promote skeletal regeneration in vivo for up to 200 PDs, a remarkable property of these cells.

We also investigated whether the extended expansion process resulted in transformation of MDSCs, which is a concern for using stem cells in cell and gene therapy, and would be expected for culture-expanded populations (Figure 9). In comparison with earlier populations of MDSCs, the highly expanded MDSC population showed changes in morphology, a heightened ability to grow on soft agar, a decreased ability to exit the cell cycle, a loss of contact inhibition, and, in one case, the capacity to cause a neoplastic growth in vivo. After 200 PDs, MDSCs continued to proliferate even when cultured at high confluence within a reduced cytokine environment, conditions that normally stimulate MDSCs to fuse and form terminally differentiated multinucleated myotubes. Our assessment of MDSCs expanded for >200 PDs revealed dramatic increases in terms of cell growth on agar, with 59% of the cells able to grow on soft agar and form colonies. However, a region of mononuclear cells showing minimal to no cell fusion was visible 2 wk after the transplantation of these populations into the skeletal muscle of mdx mice. Furthermore, one of the eight mice injected subcutaneously with the highly expanded MDSC population developed a neoplastic growth. Together, these findings demonstrate a change in the phenotype of the MDSC population after extended expansion for 200 or more PDs. Although not investigated in our study, the development of structural chromosomal abnormalities due to excessive culturing of the MDSCs—perhaps by receiving multiple genetic hits—would not be surprising (Knudson, 2001).

These results also are particularly intriguing in light of recent studies indicating that stem cells share certain characteristics with cancer cells. Recent studies have investigated the hypothesis that cancer may be driven by cancer stem cells. Small populations of stem cells that share properties with normal cells but also have the ability to form cancer have been identified in cases of leukemia (Bonnet and Dick, 1997; Cobaleda *et al*., 2000; Miyamoto *et al*., 2000), breast cancer (Al-Hajj *et al*., 2003; Dick, 2003), and brain tumors (Hemmati *et al*., 2003; Singh *et al*., 2003). The obvious similarity between cancer cells and stem cells is their capacity for self-renewal. Our finding that MDSCs expanded for up to 200 PDs retain their stem cell properties in vitro and exhibit sustained in vivo engraftment efficiency suggests that MDSCs do not undergo transformation unless subjected to very extensive cell replication. It remains to be determined whether the loss of stem cell phenotype and apparent transformation observed here occurred due to chromosomal abnormalities resulting from cell culturing or to the selection of a small fraction of cancer-like stem cells within the MDSC population. Future sorting experiments to identify subpopulations within the expanded populations may help to answer this question.

Our study shows that expansion of MDSCs for up to 200 PDs will yield a large number of phenotypically comparable cells, which would theoretically be more than enough for any clinical application. The use of these cells may represent an alternative solution to the need of immortalization of human myogenic cells to obtain enough cells for transplantation (Berghella *et al*., 1999). In fact, the large yield suggests that one allogeneic donor could provide a sufficient number of cells for many recipients. Traditionally, whether the cells are being brought closer to senescence has been a central question of in vitro cytokine-stimulated expansion studies. Because we show that the "natural progression" of MDSCs cultured in 20% serum conditions for up to 200 PDs (>4 mo in culture) is to maintain their stem cell characteristics and regeneration capacity, we now can focus our efforts on reducing the initial lag period during MDSC expansion, in essence by decreasing the PDT (Figure 9).

This study clearly demonstrates that MDSCs at high expansion levels maintain their ability to efficiently regenerate skeletal muscle. Indeed, our study suggests that MDSCs' remarkable capacity for self-renewal and long-term expansion is comparable with that exhibited by ES cells. Our results also highlight the need to conduct more intensive investigations into basic stem cell behavior and its potential link to transformation before proceeding with the translation of cell therapies to clinical settings. Nevertheless, this is the first study to demonstrate that MDSCs exhibit a notable capacity for long-term proliferation and self-renewal.

## ACKNOWLEDGMENTS

We thank Drs. Ed Klein (Division of Laboratory Animal Resources University of Pittsburgh, Pittsburgh, PA) and Aaron Pollett (Mount Sinai Hospital, Toronto, Ontario, Canada) for histomorphological assessment of abnormal growth, Michael Mentzer and Marcelle Huard for technical assistance, Jim Cummins and Bruno Péault for scientific discussions, and Ryan Sauder for editorial assistance. This work was supported by the Muscular Dystrophy Association, National Institutes of Health Grants 1R01 AR49684-01 and P01 AR45925-05), the William F. and Jean W. Donaldson Chair at Children's Hospital of Pittsburgh, and the Henry J. Mankin Chair at the University of Pittsburgh. This investigation was conducted in a facility constructed with support from Research Facilities Improvement Program Grant No. C06 RR-14489 from the National Center for Research Resources, National Institutes of Health.

## REFERENCES

Al-Hajj, M., Wicha, M. S., Benito-Hernandez, A., Morrison, S. J., and Clarke, M. F. (2003). Prospective identification of tumorigenic breast cancer cells. Proc. Natl. Acad. Sci. USA *100*, 3983–3988.

Amit, M., Carpenter, M. K., Inokuma, M. S., Chiu, C. P., Harris, C. P., Waknitz, M. A., Itskovitz-Eldor, J., and Thomson, J. A. (2000). Clonally derived human embryonic stem cell lines maintain pluripotency and proliferative potential for prolonged periods of culture. Dev. Biol. *227*, 271–278.

Berghella, L., *et al*. (1999). Reversible immortalization of human myogenic cells by site-specific excision of a retrovirally transferred oncogene. Hum. Gene Ther. *10*, 1607–1617.

Bhardwaj, G., Murdoch, B., Wu, D., Baker, D. P., Williams, K. P., Chadwick, K., Ling, L. E., Karanu, F. N., and Bhatia, M. (2001). Sonic hedgehog induces the proliferation of primitive human hematopoietic cells via BMP regulation. Nat. Immunol. *2*, 172–180.

Bianchi, G., Banfi, A., Mastrogiacomo, M., Notaro, R., Luzzatto, L., Cancedda, R., and Quarto, R. (2003). Ex vivo enrichment of mesenchymal cell progenitors by fibroblast growth factor 2. Exp. Cell Res. *287*, 98–105.

Bonnet, D., and Dick, J. E. (1997). Human acute myeloid leukemia is organized as a hierarchy that originates from a primitive hematopoietic cell. Nat. Med. *3*, 730–737.

Cobaleda, C., Gutierrez-Cianca, N., Perez-Losada, J., Flores, T., Garcia-Sanz, R., Gonzalez, M., and Sanchez-Garcia, I. (2000). A primitive hematopoietic cell is the target for the leukemic transformation in human Philadelphia-positive acute lymphoblastic leukemia. Blood *95*, 1007–1013.

Colter, D. C., Class, R., DiGirolamo, C. M., and Prockop, D. J. (2000). Rapid expansion of recycling stem cells in cultures of plastic-adherent cells from human bone marrow. Proc. Natl. Acad. Sci. USA *97*, 3213–3218.

Deasy, B. M., and Huard, J. (2002). Gene therapy and tissue engineering based on muscle-derived stem cells. Curr. Opin. Mol. Ther. *4*, 382–389.

Deasy, B. M., Jankowski, R. J., Payne, T. R., Cao, B., Goff, J. P., Greenberger, J. S., and Huard, J. (2003). Modeling stem cell population growth: incorporating terms for proliferative heterogeneity. Stem Cells *21*, 536–545.

Dick, J. E. (2003). Breast cancer stem cells revealed. Proc. Natl. Acad. Sci. USA *100*, 3547–3549.

Digirolamo, C. M., Stokes, D., Colter, D., Phinney, D. G., Class, R., and Prockop, D. J. (1999). Propagation and senescence of human marrow stromal cells in culture: a simple colony-forming assay identifies samples with the greatest potential to propagate and differentiate. Br. J. Haematol. *107*, 275–281.

Gilmore, G. L., DePasquale, D. K., Lister, J., and Shadduck, R. K. (2000). Ex vivo expansion of human umbilical cord blood and peripheral blood CD34(+) hematopoietic stem cells. Exp. Hematol. *28*, 1297–1305.

Hayflick, L., and Moorhead, P. S. (1961). The serial cultivation of human diploid cell strains. Exp. Cell Res. *25*, 585–621.

Hemmati, H. D., Nakano, I., Lazareff, J. A., Masterman-Smith, M., Geschwind, D. H., Bronner-Fraser, M., and Kornblum, H. I. (2003). Cancerous stem cells can arise from pediatric brain tumors. Proc. Natl. Acad. Sci. USA *100*, 15178–15183.

Irintchev, A., Zeschnigk, M., Starzinski-Powitz, A., and Wernig, A. (1994). Expression pattern of M-cadherin in normal, denervated, and regenerating mouse muscles. Dev. Dyn. *199*, 326–337.

Jankowski, R. J., Deasy, B. M., Cao, B., Gates, C., and Huard, J. (2002). The role of CD34 expression and cellular fusion in the regeneration capacity of myogenic progenitor cells. J. Cell Sci. *115*, 4361–4374.

Jiang, Y., Henderson, D., Blackstad, M., Chen, A., Miller, R. F., and Verfaillie, C. M. (2003). Neuroectodermal differentiation from mouse multipotent adult progenitor cells. Proc. Natl. Acad. Sci. USA *100* (suppl 1), 11854–11860.

Jiang, Y., *et al*. (2002). Pluripotency of mesenchymal stem cells derived from adult marrow. Nature *418*, 41–49.

Karanu, F. N., Murdoch, B., Gallacher, L., Wu, D. M., Koremoto, M., Sakano, S., and Bhatia, M. (2000). The notch ligand jagged-1 represents a novel growth factor of human hematopoietic stem cells. J. Exp. Med. *192*, 1365–1372.

Knobel, K. M., McNally, M. A., Berson, A. E., Rood, D., Chen, K., Kilinski, L., Tran, K., Okarma, T. B., and Lebkowski, J. S. (1994). Long-term reconstitution of mice after ex vivo expansion of bone marrow cells: differential activity of cultured bone marrow and enriched stem cell populations. Exp. Hematol. *22*, 1227–1235.

Knudson, A. G. (2001). Two genetic hits (more or less) to cancer. Nat. Rev. Cancer *1*, 157–162.

Lee, J. Y., *et al*. (2000). Clonal isolation of muscle-derived cells capable of enhancing muscle regeneration and bone healing. J. Cell Biol. *150*, 1085–1100.

Miyamoto, T., Weissman, I. L., and Akashi, K. (2000). AML1/ETO-expressing nonleukemic stem cells in acute myelogenous leukemia with 8;21 chromosomal translocation. Proc. Natl. Acad. Sci. USA *97*, 7521–7526.

Molofsky, A. V., Pardal, R., and Morrison, S. J. (2004). Diverse mechanisms regulate stem cell self-renewal. Curr. Opin. Cell Biol. *16*, 700–707.

Muraglia, A., Cancedda, R., and Quarto, R. (2000). Clonal mesenchymal progenitors from human bone marrow differentiate in vitro according to a hierarchical model. J. Cell Sci. *113*, 1161–1166.

Peters, S. O., Kittler, E. L., Ramshaw, H. S., and Quesenberry, P. J. (1995). Murine marrow cells expanded in culture with IL-3, IL-6, IL-11, and SCF acquire an engraftment defect in normal hosts. Exp. Hematol. *23*, 461–469.

Piacibello, W., Sanavio, F., Garetto, L., Severino, A., Bergandi, D., Ferrario, J., Fagioli, F., Berger, M., and Aglietta, M. (1997). Extensive amplification and self-renewal of human primitive hematopoietic stem cells from cord blood. Blood *89*, 2644–2653.

Potten, C. S., and Morris, R. J. (1988). Epithelial stem cells in vivo. J. Cell Sci. (suppl) *10*, 45–62.

Qu-Petersen, *et al*. (2002). Identification of a novel population of muscle stem cells in mice: potential for muscle regeneration. J. Cell Biol. *157*, 851–864.

Reya, T., Morrison, S. J., Clarke, M. F., and Weissman, I. L. (2001). Stem cells, cancer, and cancer stem cells. Nature *414*, 105–111.

Reyes, M., Lund, T., Lenvik, T., Aguiar, D., Koodie, L., and Verfaillie, C. M. (2001). Purification and ex vivo expansion of postnatal human marrow mesodermal progenitor cells. Blood *98*, 2615–2625.

Rombouts, W. J., and Ploemacher, R. E. (2003). Primary murine MSC show highly efficient homing to the bone marrow but lose homing ability following culture. Leukemia *17*, 160–170.

Rubin, H. (1997). Cell aging in vivo and in vitro. Mech. Ageing Dev. *98*, 1–35.

Rubin, H. (2002). The disparity between human cell senescence in vitro and lifelong replication in vivo. Nat. Biotechnol. *20*, 675–681.

Seale, P., Asakura, A., and Rudnicki, M. A. (2001). The potential of muscle stem cells. Dev. Cell. *1*, 333–342.

Seale, P., Sabourin, L. A., Girgis-Gabardo, A., Mansouri, A., Gruss, P., and Rudnicki, M. A. (2000). Pax7 is required for the specification of myogenic satellite cells. Cell *102*, 777–786.

Sherley, J. L., Stadler, P. B., and Stadler, J. S. (1995). A quantitative method for the analysis of mammalian cell proliferation in culture in terms of dividing and non-dividing cells. Cell Prolif. *28*, 137–144.

Singh, S. K., Clarke, I. D., Terasaki, M., Bonn, V. E., Hawkins, C., Squire, J., and Dirks, P. B. (2003). Identification of a cancer stem cell in human brain tumors. Cancer Res. *63*, 5821–5828.

Smith, A. G. (2001). Embryo-derived stem cells: of mice and men. Annu. Rev. Cell. Dev. Biol. *17*, 435–462.

Stiles, B., Groszer, M., Wang, S., Jiao, J., and Wu, H. (2004). PTENless means more. Dev. Biol. *273*, 175–184.

Thomson, J. A., Itskovitz-Eldor, J., Shapiro, S. S., Waknitz, M. A., Swiergiel, J. J., Marshall, V. S., and Jones, J. M. (1998). Embryonic stem cell lines derived from human blastocysts. Science *282*, 1145–1147.

Traycoff, C. M., Cornetta, K., Yoder, M. C., Davidson, A., and Srour, E. F. (1996). Ex vivo expansion of murine hematopoietic progenitor cells generates classes of expanded cells possessing different levels of bone marrow repopulating potential. Exp. Hematol. *24*, 299–306.

van Noort, M., and Clevers, H. (2002). TCF transcription factors, mediators of Wnt-signaling in development and cancer. Dev. Biol. *244*, 1–8.

Varnum-Finney, B., Xu, L., Brashem-Stein, C., Nourigat, C., Flowers, D., Bakkour, S., Pear, W. S., and Bernstein, I. D. (2000). Pluripotent, cytokine-dependent, hematopoietic stem cells are immortalized by constitutive Notch1 signaling. Nat. Med. *6*, 1278–1281.

Xu, C., Inokuma, M. S., Denham, J., Golds, K., Kundu, P., Gold, J. D., and Carpenter, M. K. (2001). Feeder-free growth of undifferentiated human embryonic stem cells. Nat. Biotechnol. *19*, 971–974.

Zammit, P., and Beauchamp, J. (2001). The skeletal muscle satellite cell: stem cell or son of stem cell? Differentiation *68*, 193–204.

Zipori, D. (2004). The nature of stem cells: state rather than entity. Nat. Rev. Genet. *5*, 873–878.

JCB: ARTICLE

# A role for cell sex in stem cell–mediated skeletal muscle regeneration: female cells have higher muscle regeneration efficiency

Bridget M. Deasy,[1,2,3] Aiping Lu,[3] Jessica C. Tebbets,[3] Joseph M. Feduska,[3] Rebecca C. Schugar,[3] Jonathan B. Pollett,[2,3] Bin Sun,[3] Kenneth L. Urish,[1,3] Burhan M. Gharaibeh,[2,3] Baohong Cao,[2,3] Robert T. Rubin,[5] and Johnny Huard[1,2,3,4]

[1]Department of Bioengineering, [2]Department of Orthopaedic Surgery, [3]Stem Cell Research Center, Children's Hospital of Pittsburgh, University of Pittsburgh Medical Center, and [4]Department of Molecular Genetics and Biochemistry, University of Pittsburgh, Pittsburgh, PA 15260
[5]Department of Psychiatry and Biobehavioral Sciences, University of California, Los Angeles, Los Angeles CA 90095

We have shown that muscle-derived stem cells (MDSCs) transplanted into dystrophic (*mdx*) mice efficiently regenerate skeletal muscle. However, MDSC populations exhibit heterogeneity in marker profiles and variability in regeneration abilities. We show here that cell sex is a variable that considerably influences MDSCs' regeneration abilities. We found that the female MDSCs (F-MDSCs) regenerated skeletal muscle more efficiently. Despite using additional isolation techniques and cell cloning, we could not obtain a male subfraction with a regeneration capacity similar to that of their female counterparts. Rather than being directly hormonal or caused by host immune response, this difference in MDSCs' regeneration potential may arise from innate sex-related differences in the cells' stress responses. In comparison with F-MDSCs, male MDSCs have increased differentiation after exposure to oxidative stress induced by hydrogen peroxide, which may lead to in vivo donor cell depletion, and a proliferative advantage for F-MDSCs that eventually increases muscle regeneration. These findings should persuade researchers to report cell sex, which is a largely unexplored variable, and consider the implications of relying on cells of one sex.

## Introduction

We previously reported that the transplantation of muscle-derived stem cells (MDSCs) into diseased muscle results in a large number of regenerated myofibers (Qu-Petersen et al., 2002; Deasy et al., 2005). These studies were initiated to understand the broad heterogeneity in phenotype and performance that has been reported for MDSCs and other muscle stem cell populations (Molnar et al., 1996; Schultz, 1996; Zammit and Beauchamp, 2001; Mueller et al., 2002; Deasy et al., 2004; Collins et al., 2005; Mitchell et al., 2005; Wagers and Conboy, 2005). In our laboratory, we also have observed a high degree of variability in the ability of different populations of MDSCs to regenerate skeletal muscle. While investigating MDSC population heterogeneity and characteristics that define efficient in vivo skeletal muscle regeneration, we have found that cell sex, a rarely considered variable, has a considerable effect on in vivo outcome. Compared with the transplantation of male MDSCs (M-MDSCs), the transplantation of female MDSCs (F-MDSCs) leads to substantially more regeneration of the diseased skeletal muscle of *mdx* mice, which model Duchenne muscular dystrophy.

More than 2,000 yr ago, Aristotle speculated that sexual dimorphism existed at the earliest stage of embryonic growth; he believed that male embryos became animated 40 d after conception, whereas female animation required 90 d (Aristotle, 350 BC). Recent studies support this notion (Avery et al., 1992; Xu et al., 1992; Pergament et al., 1994; Kochhar et al., 2003;). Male embryos created by in vitro fertilization grow faster before implantation than female embryos, and these findings support a genetic cellular difference between the sexes that exists before the induction of hormonal stimulation (Avery et al., 1992; Xu et al., 1992; Pergament et al., 1994; Kochhar et al., 2003). Sex-related differences in the expression of genes during early embryo development have also been observed: females exhibit higher mRNA levels of *glucose-6-phosphate dehydrogenase* and *hypoxanthine*

Correspondence to Johnny Huard: jhuard@pitt.edu

Abbreviations used in this paper: ANOVA, analysis of variance; F-MDSC, female MDSC; GM, growth medium; MDSC, muscle-derived stem cell; M-MDSC, male MDSC; MyHC, myosin heavy chain; PD, population doubling; PDT, PD time; RI, regeneration index; ROS, reactive oxygen species; SCID, severe combined immunodeficiency.

The online version of this article contains supplemental material.


The Journal of Cell Biology, Vol. 177, No. 1, April 9, 2007 73–86
http://www.jcb.org/cgi/doi/10.1083/jcb.200612094

Supplemental Material can be found at:
http://www.jcb.org/cgi/content/full/jcb.200612094/DC1

*phosphoribosyl transferase*, which are two genes involved in the detoxification of reactive oxygen species (ROS; Gutierrez-Adan et al., 2000; Peippo et al., 2002). Male and female embryonic neurons (isolated from rats before gonad differentiation or hormonal stimulation) also display different cellular responses. The female cells are more sensitive to apoptosis-inducing agents, whereas male neurons are more sensitive to ischemia and nitrosative stress, and they cannot maintain the proper level of glutathione, which regulates ROS levels (Du et al., 2004).

Few studies have investigated whether sex-related differences affect tissue or organ regeneration by progenitor cells. Blankenhorn et al. (2003) demonstrated that the regrowth of cartilage, skin, and hair follicles in an ear pinna wound occurred faster and more completely in female mice as compared with male mice. Another study has shown that female mice modeling living donor liver transplantation with ischemia and reperfusion exhibit more efficient liver regeneration than their male counterparts (Harada et al., 2003). Similarly, male rats show more tissue growth than female rats after nephroctomy (Mulroney et al., 1999). Chau et al. (2002) found that blocking antiapoptotic activity in male animals resulted in sex-related differences in the animals' survival after endotoxic stress; the males recovered, but there was no advantage for females. Finally, in a study of human hematopoietic stem cell transplantations, superior survival was observed with maternally donated recipients as compared with recipients of paternal transplantations (Tamaki et al., 2001).

Several theories have been designed to unify cell and tissue aging with the overall aging of organisms and, thereby, explain females' longer life spans. Telomeres, whose length is believed to act as the mitotic clock of cells, are shorter in older males than in older females, which suggests that male cells undergo more rounds of division than female cells (Aviv et al., 2005; Vina et al., 2005). This finding supports a possible link between growth rate and aging (Rollo, 2002). Stindl (2004) has proposed that cells that have finite replicative lifespans must undergo more rounds of division to build the larger bodies of male organisms. Other research has shown that estrogen stimulates telomerase, which slows the rate of telomere attrition (for review see Aviv, 2002). This finding has ties with the free radical theory of cell aging, according to which ROS causes aging by damaging DNA, lipids, and proteins. Estrogens also up-regulate pathways that induce the expression of antioxidants (such as glutathione peroxidase) that reduce damage by ROS (for example, the MAPK pathway; Vina et al., 2005). Together, these findings suggest that sex-related differences in the health of the stem cell compartment could partially explain different rates of aging and disease. Stem and progenitor cells are believed to persist throughout life and contribute to the repair and maintenance of tissue. Therefore, investigations of sex-related differences shown by stem cells, as presented in this study, could lead to an improved understanding of sex-related differences in aging and disease.

## Results

### MDSC isolation and in vitro characterization

To determine whether any of the standard markers for MDSC characterization are predictive of high in vivo muscle regeneration, we examined 25 populations of MDSCs in terms of five variables: in vivo muscle regeneration efficiency, expression of CD34, expression of Sca-1, expression of desmin, and cell sex. Analysis of these variables revealed a large degree of heterogeneity in the MDSC populations. The distribution of the populations' regeneration indexes (RIs) and CD34, Sca-1, and desmin expression are shown in Fig. 1 A. The RI is a measure of how efficiently stem cells participate in skeletal muscle regeneration (Jankowski et al., 2002; Deasy et al., 2005), whereas CD34 and Sca-1 are stem cell markers, and desmin is a myogenic marker.

We performed a Pearson product moment correlation analysis to identify significant relationships between any two variables and, in particular, to determine whether any of the markers correlate with high in vivo muscle regeneration. Fig. 1 B shows the correlation scatter matrix comprising scatter plots for all possible combinations of variables. Only cell sex correlated with the RI ($P = 0.070$); M-MDSC populations had a significantly lower RI on average than F-MDSC populations ($P = 0.035$; *t* test). We also detected a significant correlation between cell sex and Sca-1 expression ($P = 0.014$): the mean expression of Sca-1 for all M-MDSC populations was significantly higher (M-MDSCs, 73 ± 16%; F-MDSCs, 52 ± 22%; mean ± SD; $P = 0.001$; *t* test). We next separated the correlation matrices on the basis of sex; Fig. 1 C shows the scatter plots for M-MDSCs (10 populations are shown in each plot), and Fig. 1 D shows the scatter plots for F-MDSCs (15 populations are shown in each plot). The scatter plot of the RI versus Sca-1 for M-MDSCs indicates that a higher level of Sca-1 expression by M-MDSCs positively correlated with a higher RI ($P = 0.021$; Fig. 1 C). This demonstrates that the significantly higher levels of Sca-1 expression by M-MDSCs (as compared with F-MDSCs) are not directly related to their low RIs (as compared with the RIs of F-MDSCs). The scatter plots of the F-MDSC populations did not reveal such a relationship (Fig. 1 D). Significant correlations between variables other than RIs are also indicated in Fig. 1 (C and D), and correlation coefficients are listed in Table S1 (available at http://www.jcb.org/cgi/content/full/jcb.200612094/DC1). We focused our subsequent analysis on the sex-related differences exhibited by MDSCs because cell sex was the only variable that correlated with the RI.

We used identical methods to isolate M- and F-MDSCs, and both exhibited stem cell characteristics in vitro (Fig. 2 and Fig. S1, available at http://www.jcb.org/cgi/content/full/jcb.200612094/DC1). Morphological comparison of the M- and F-MDSC populations revealed no significant differences in cell size or cell shape (Fig. S1, A and B). Analysis of the cells' multilineage differentiation potential showed that with appropriate stimulation in vitro, both male and female cells expressed markers of myogenic (Fig. 2 A), osteogenic (Fig. S1 C), and adipogenic lineages (Fig. S1 C), although they did so at different rates and to different extents. On average, there was no significant difference in the mean amount of fast myosin heavy chain (MyHC) in M- versus F-MDSCs (Fig. 2 B).

Our analysis of short-term kinetics showed that M-MDSC and F-MDSC populations had similar population doubling (PD) times (PDTs; 13 ± 1.4 h and 14.2 ± 3.1 h, respectively), cell cycle times (12 ± 1.3 h and 12 ± 1.3 h, respectively), and mitotic

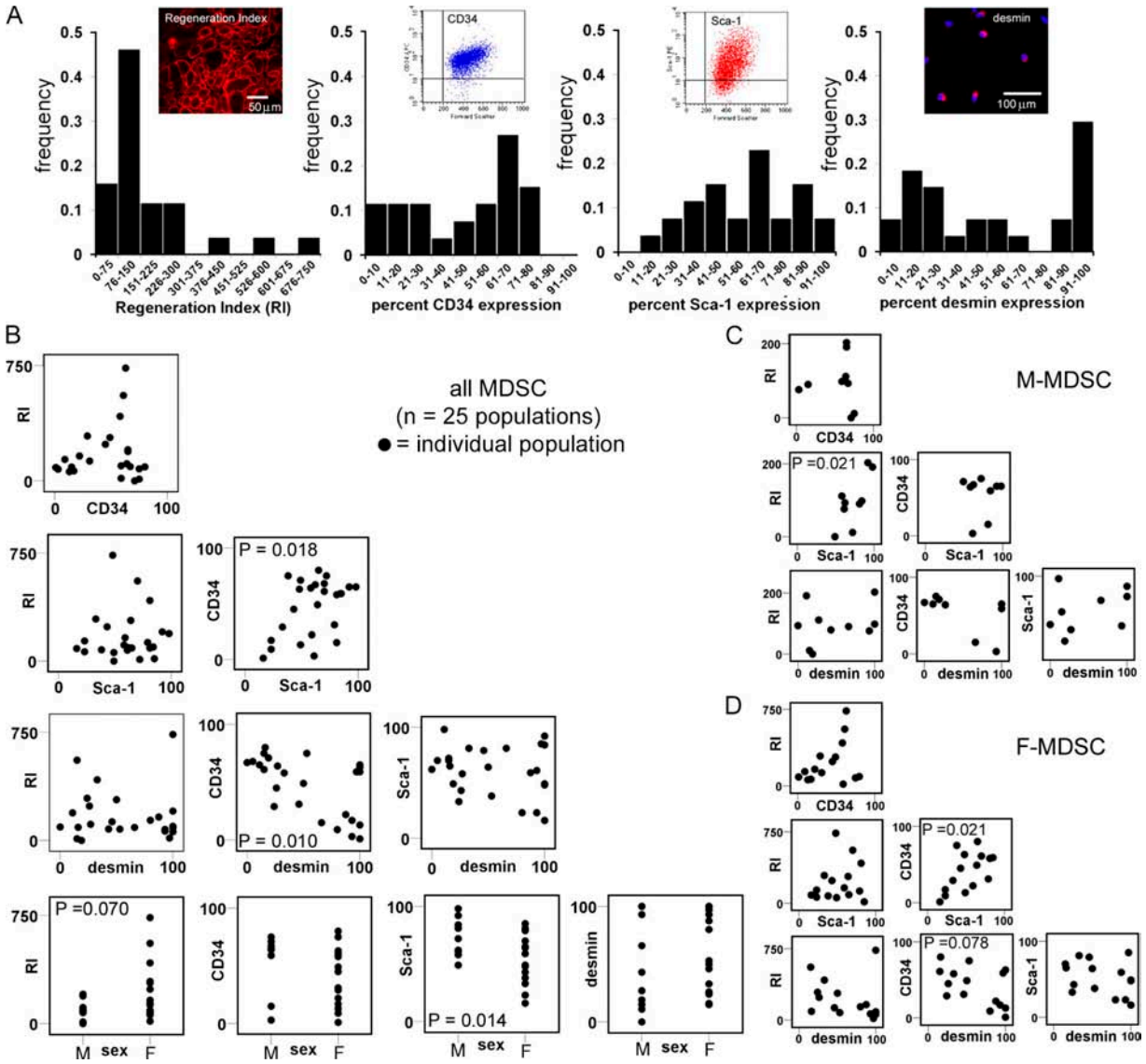


Figure 1. **Variability among muscle-derived cell populations.** (A) We examined 25 populations of MDSCs for five variables: in vivo muscle regeneration efficiency (RI), CD34 expression, Sca-1 expression, desmin expression, and cell sex. Histograms show the distribution of each parameter for the 25 different populations. In vivo regeneration was quantified as the number of dystrophin-positive myofibers (red) present in the skeletal muscle of dystrophin-deficient *mdx* mice after the transplantation of MDSCs. Flow plots are shown for CD34 and Sca-1 expression, and immunofluorescence is shown for desmin (desmin, red; nuclei, blue). (B) We performed correlation analysis to identify significant relationships between variables. The scatter plots are shown. Each population is represented as a dot on the scatter plots. P-values are shown for the correlation coefficient when a linear relationship was found to exist between the two given variables. Only cell sex correlated with in vivo regeneration efficiency ($R = 0.367$; $P = 0.070$; M, male; F, female); our subsequent *t* test comparison of the regeneration efficiency of M-MDSCs with that of F-MDSCs revealed a significant difference ($P = 0.035$). We also detected a significant correlation between Sca-1 expression and cell sex ($R = -0.490$; $P = 0.014$), with significantly more M- than F-MDSCs expressing Sca-1 ($P = 0.001$; *t* test). (C and D) Examination of the correlation matrices for M- (C) and F-MDSCs (D) again revealed the heterogeneity of the populations. In particular, the higher level of Sca-1 expression by M-MDSCs correlated positively with a higher RI ($P = 0.021$), which suggests that the significantly higher levels of Sca-1 expression by M-MDSCs were not directly related to their low in vivo RI (see plot of RI vs. Sca-1 for M-MDSCs in D).

fractions ($0.91 \pm 0.10$ and $0.85 \pm 0.08$, respectively; $P = 0.28$; *t* test) over a 3-d period (mean ± SD; Fig. 2, C and D). However, after moderate expansion over 14 d or extended expansion over 3 mo (>150 PDs), M-MDSC populations exhibited higher growth rates than F-MDSC populations (M-MDSCs: PDT = ∼13 h and mitotic fraction = 0.87–0.97; F-MDSCs: PDT = ∼15 h and mitotic fraction = 0.81–0.87; Fig. 2 E and not depicted). After extended expansion, there was no significant difference in telomere length (Fig. S1 D) or telomerase activity (Fig. S1 E) as measured by flow cytometry. In addition, we observed a normal modal chromosome number for M- and F-MDSCs that were expanded to 90 PDs (unpublished data); this is consistent with our previous study of F-MDSCs (Deasy et al., 2005).

### In vivo skeletal muscle regeneration

After transplanting M- and F-MDSCs into the skeletal muscle of dystrophic *mdx* mice (i.e., mice that lack dystrophin at the sarcolemma of muscle fibers), we investigated the cells' abilities to regenerate dystrophin-expressing myofibers. Sex-matched experiments involving several cell populations obtained from

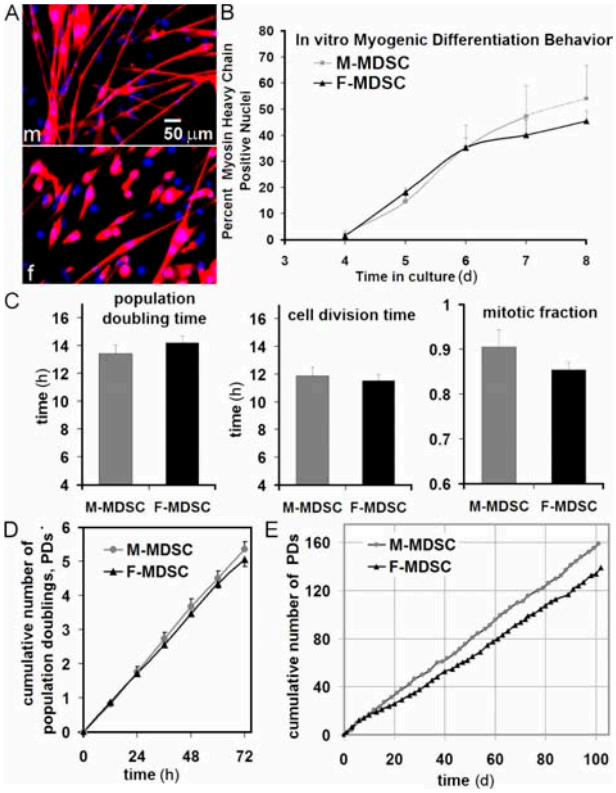


Figure 2. **M- and F-MDSCs demonstrate similar in vitro stem cell characteristics.** (A) M- and F-MDSCs underwent myogenic differentiation, as shown by MyHC expression (red; m, M-MDSC; f, F-MDSC). (B) We did not detect a significant difference in the extent or rate of myogenic differentiation as measured by the percentage of nuclei that colocalized with MyHC in low serum–containing medium ($P > 0.05$). (C) PDT, cell division time, and mitotic fraction were similar for M- and F-MDSCs. (D) Short-term proliferation kinetics were similar for M- and F-MDSCs. (E) Long-term proliferation kinetics showed that both M- and F-MDSCs can be expanded for >150 PDs in vitro. However, we observed a trend toward faster proliferation by M-MDSCs cultured for longer periods of time. Error bars represent SD.

various isolations revealed that the implantation of F-MDSC populations led to significantly better skeletal muscle regeneration in vivo, as determined by calculating each population's RI (the ratio of dystrophin$^+$ fibers per $10^5$ donor cells; Fig. 3 A). Female cell populations regenerated significantly more dystrophin-positive myofibers ($n = 15$ F-MDSC populations; two to six muscles per population; RI = 230 ± 52; mean ± SEM) as compared with male populations ($n = 10$ M-MDSC populations; two to six muscles per population; RI = 95 ± 20; $P = 0.035$). Representative images of dystrophin-expressing myofibers within the *mdx* muscle tissue are shown in Fig. 3 B. Although the RIs of both M- and F-MDSC populations varied, no M-MDSCs exhibited high regeneration efficiency (i.e., RI > 203). In vitro immunostaining of myotubes after MDSC differentiation demonstrated that both M- and F-MDSCs are able to express dystrophin in myotubes containing a similar number of nuclei (Fig. 3 C).

We performed both sex-matched and sex-mismatched transplantations to determine whether the sex of the host tissue might play a role in the cells' differing regeneration abilities. We used two F- and two M-MDSC populations that had similar expression profiles for CD34, Sca-1, and desmin and exhibited similar short-term proliferation characteristics. Regardless of host sex, M-MDSC transplantation resulted in a low RI (160 ± 75 in female hosts and 105 ± 25 in male hosts; Fig. 3 D). Two-way analysis of variance (ANOVA) confirmed these findings and revealed both a significant difference as a result of host sex ($P = 0.048$) and a significant effect as a result of cell sex ($P < 0.001$). These results are consistent with those observed in previous studies using sorted populations of M-MDSCs (Jankowski et al., 2002; Jankowski and Huard, 2004a,b) or using male hosts (Mueller et al., 2002). M-MDSCs had a significantly lower RI than F-MDSCs ($P < 0.05$), and there was a significantly lower RI with the male host as compared with the female host ($P < 0.01$).

The difference caused by host sex suggests that the female microenvironment might be a more receptive environment for skeletal muscle regeneration by MDSCs and might play a role in RI variability. Hormonal differences between male and female hosts may influence the regeneration process; previous studies have described such differences in the responses of progenitor and stem cells to hormones (Jilka et al., 1992; Steinlein et al., 1995). We first tested the possibility that the low RI of M-MDSCs implanted in female *mdx* hosts (as compared with female to female transplantations) might be caused by the immune rejection of the M-MDSCs as a result of H-Y antigenicity. We examined the immune response at the site of cell delivery by measuring the total cross-sectional area of CD4 expression after sex-matched and sex-crossed transplantations. We observed a larger area containing CD4-positive cells after sex-crossed transplantations (Fig. 3 E).

We next investigated the effect of host sex in the absence of an immune response by performing sex-crossed and sex-matched transplantations in immune-compromised animals. M-MDSC to female *mdx*/severe combined immunodeficiency (SCID) mouse transplantations again resulted in a low level of skeletal muscle regeneration (RI = 216 ± 39), which is similar to what we observed in the female *mdx* host. We observed no significant difference as a result of host sex ($P = 0.235$), yet the significant difference as a result of cell sex remained ($P = 0.018$; two-way ANOVA; Fig. 3 F).

### Hormonal stimulation

To determine whether estrogen stimulation improves the in vivo regeneration efficiency of MDSCs, we stimulated M- and F-MDSCs with two doses of 17-β-estradiol (10 or 100 nM; physiologic range of 10–100 nM; Maeda et al., 2000). We confirmed the expression of estrogen receptors in M- and F-MDSCs by immunocytochemistry (Fig. S2 A, available at http://www.jcb.org/cgi/content/full/jcb.200612094/DC1) and by microarray analysis (not depicted). After 2 wk in vitro with estradiol, M-MDSCs displayed lower proliferation rates than unstimulated M-MDSCs (although the decrease was not significant). Consistent with other results, comparison of the proliferation rates of the unstimulated cells showed that F- MDSCs proliferated more slowly than unstimulated M-MDSCs at all time points after 7 d (9 d, $P = 0.070$; 12 and 14 d, $P < 0.05$; *t* test; Fig. S2 B). We compared the in vivo regeneration efficiency of stimulated and unstimulated M- and F-MDSCs. 2 wk after transplantation,

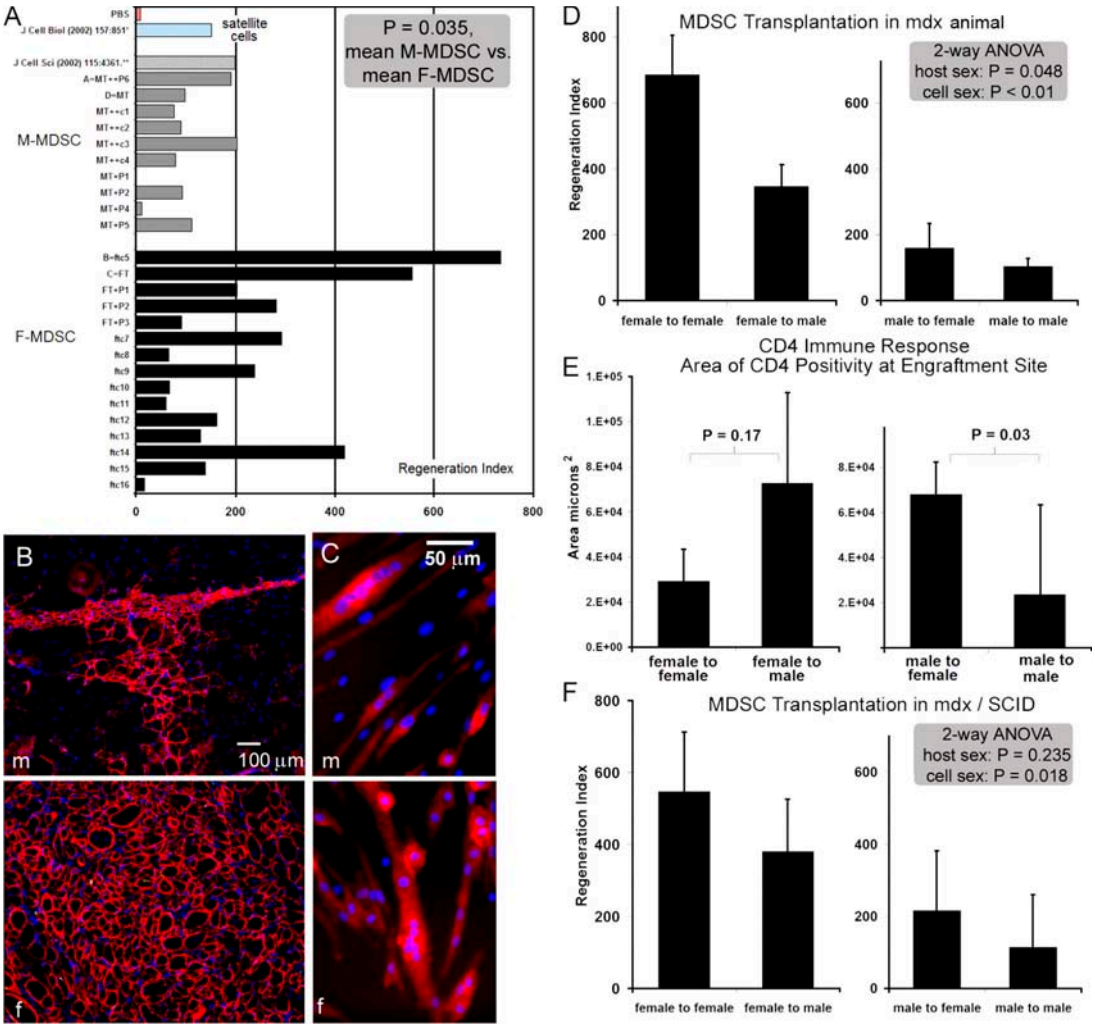


Figure 3. **F-MDSCs induce more efficient skeletal muscle regeneration than M-MDSCs.** (A) Quantitation of engraftment in terms of the RI (RI = number of dystrophin-positive fibers per $10^5$ donor cells). The overall mean RI is significantly higher for F-MDSCs (black bars; RI = 230 ± 52; $n$ = 15 F-MDSC populations; two to six muscles per population) than for M-MDSCs (gray bars; RI = 109 ± 18; mean ± SEM; $n$ = 10 M-MDSC populations; two to six muscles per population; P = 0.035; $t$ test). Sham-injected muscles (PBS; red bar) and RI values from previous studies of myoblasts (Qu-Petersen et al., 2002) and male myogenic progenitor cells (Jankowski et al., 2002) are also shown. (B) Representative engraftments of transplanted cells to mouse *mdx* skeletal muscle show dystrophin-positive fibers (red) within dystrophic muscle (nuclei stained with Hoechst). M-MDSCs produced fewer dystrophin-positive fibers than did F-MDSCs. (C) Dystrophin expression in vitro confirms the ability of both M- and F-MDSCs to express the dystrophin gene after cell fusion. (D)We performed sex-matched and sex-crossed transplantations. Two-way parametric ANOVA indicated significant differences in the RI associated with the sex of the donor cells (P < 0.001) and the sex of the host (P = 0.048). Mean RI and SEM (error bars) are shown (female to female, RI = 686 ± 120; female to male, RI = 347 ± 69; male to female, RI = 160 ± 75; male to male, RI = 105 ± 25; $n$ = 6–12 per group). (E) Immune response at the site of transplantation in immune-competent *mdx* mice was quantified as the cross-sectional area (micrometers squared) of CD4 expression in tissue sections. There was significantly more CD4 positivity after male to female cross transplantation than after sex-matched male to male transplantation (mean ± SEM; $t$ test; $n$ = 4). (F) Transplantation of MDSCs into *mdx*/SCID mice. Two-way nonparametric ANOVA revealed no effect on the RI as a result of the sex of the host (P = 0.235), but there was a significant effect as a result of the sex of the cells (P = 0.018). RIs are reported as mean ± SEM (female to female, RI = 546 ± 166; female to male, RI = 381 ± 145; male to female, RI = 216 ± 39; male to male, RI = 115 ± 11; $n$ = 4 per group).

F-MDSCs cultured in control conditions of 0 nM estradiol had a higher RI than similarly cultured M-MDSCs (557 ± 229 vs. 115 ± 36; P = 0.06). Stimulation with estradiol had no significant effect on the RIs of M-MDSCs; however a trend toward a decreased RI was detected in F-MDSCs stimulated with 10 or 100 nM estradiol (P = 0.09 and P = 0.07; $n$ = 3; $t$ test; Fig. S2 C).

### Exploring alternate M-MDSC donor sources

Based on cell adhesion characteristics, the preplate technique or variations of this technique have been used to isolate cells from adult skeletal muscle tissue (Rando and Blau, 1994; Qu et al., 1998). These cells have demonstrated multilineage differentiation potential ( Lee et al., 2000; Winitsky et al., 2005; Sarig et al., 2006; Nomura et al., 2007). To determine whether M-MDSCs are a rare subpopulation with particular adhesion or isolation characteristics, we attempted to isolate potent M- MDSCs from three other methods: (1) other preplates or other subfractions of myogenic progenitors, (2) a defined FACS subfraction expressing the stem cell marker CD34, and (3) clonal populations.

The preplate technique used to isolate MDSCs from a skeletal muscle biopsy involves serial preplating of low-adherence

cells found within the primary medium supernatant to separate these cells from cells adhered to the collagenated surface of the flask (Fig. 4 A). Usually, myogenic precursors with characteristics of myoblasts or satellite cells are found within the early preplates (pp3–6), whereas cells isolated from the later preplates (≥pp6) have stem cell characteristics. We compared the in vivo regeneration efficiency (RI) of M-MDSCs with that of male myoblasts obtained from pp3–6 but identified no significant differences (Fig. 4 A).

To determine the effect of the expression of CD34 on regeneration efficiency, we used FACS to purify M- and F-MDSCs and obtain $CD34^+$ fractions. The expression of Sca-1 and CD34 by unsorted M- and F-MDSCs was comparable (Fig. 4 B), and, in both populations, <15% of the cells were desmin positive. Our comparison of the RI of CD34-positive F-MDSCs (RI = 417 ± 56) with that of similarly sorted M-MDSCs (RI = 266 ± 61) revealed that the latter RI was significantly lower (P = 0.053; Fig. 4 B).

To test whether there are fewer cells within the M-MDSC populations that are capable of contributing to muscle regeneration, we performed in vitro and in vivo clonal analysis of myogenic behavior. We used FACS to single-cell sort and obtain clones to determine the percentage of clones with myogenic potential in the M- and F-MDSC populations. Because some populations already had a high level of expression of the myogenic marker desmin, we analyzed the clones from these populations separately. At 2 wk after single-cell cloning, there was no significant difference in the percentage of clones among male or female cells derived from MDSC populations (with high or low desmin expression), which yielded myogenic colonies as defined by myotube formation (P = 0.776; one-way ANOVA; Fig. 4 C). When we compared all three factors (cell sex, desmin expression, and week of analysis), we detected a significant effect (P = 0.066, P = 0.003, and P = 0.756, respectively) as a result of the desmin level and week of myogenic analysis but no effect as a result of the cell sex (three-way ANOVA). We transplanted eight representative clonal populations of MDSCs (four male and four female clones) into *mdx* animals to determine whether a clonal population could be identified within the M-MDSC populations that demonstrated a high RI. We confirmed that the overall trend we observe in Fig. 2 (using 25 populations) is consistent with results obtained from clonal populations (Fig. 4 C). Although we did observe an F-MDSC clone that exhibited a lower RI as compared with its parent population (F3 vs. C parent population), we did not observe any male clone that exhibited a higher RI as compared with the parent population.



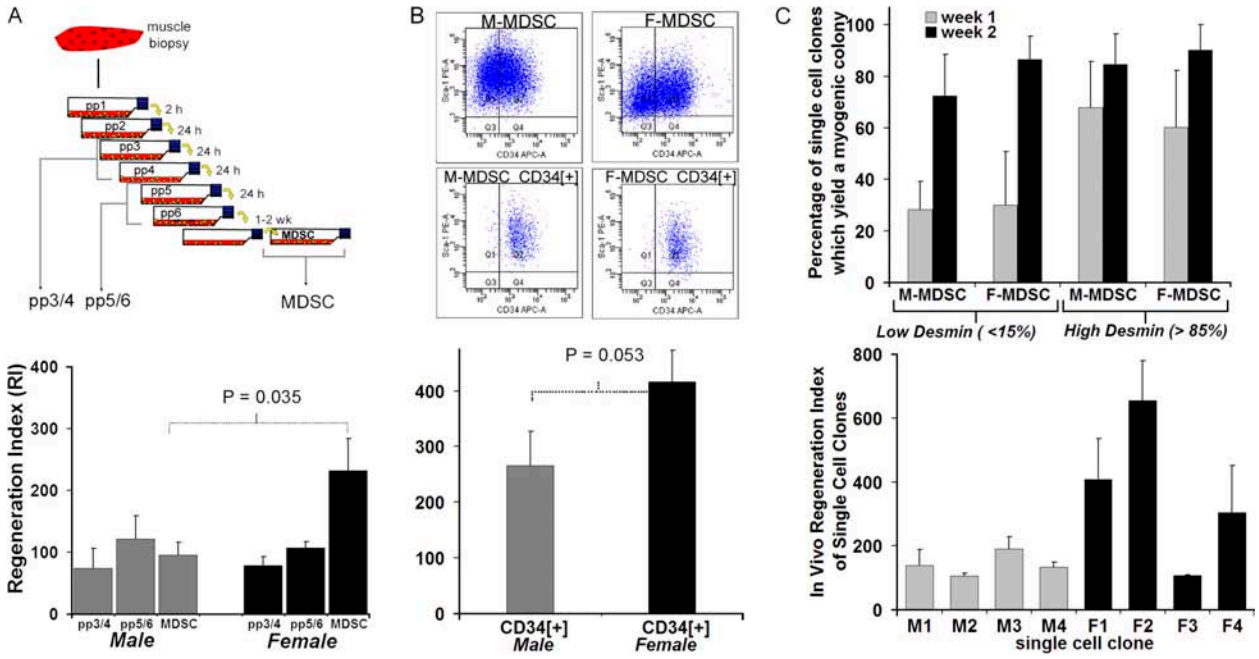


Figure 4. **Examination of alternate M-MDSC sources.** (A) The preplate technique to isolate subfractions of muscle-derived cells is based on their adhesion characteristics from muscle biopsy. Male myoblast subfractions also demonstrated low regeneration efficiency. There was no significant difference between the RIs of male pp3/4 (74 ± 32; *n* = 4) and pp5/6 (122 ± 38; *n* = 3) when compared with the RI of M-MDSCs (109 ± 18; *n* = 10 for all M-MDSC populations shown in Fig. 2). There also was no significant difference between the RIs of male myoblasts and female myoblasts (female pp3/4 RI = 79 ± 14, *n* = 4; female pp5/6 RI = 107 ± 10, *n* = 3; P > 0.05). The bars for the M- and F-MDSCs represent the mean RIs for all male and female populations shown in Fig. 2 (95 ± 21 [*n* = 10] and 230 ± 52 [*n* = 15], respectively). (B) M- and F-MDSCs were sorted by FACS to obtain a subpopulation expressing the stem cell marker CD34. The presorted population had similar expression levels for desmin/Sca-1 and CD34. Cells were purified to contain >96% $CD34^+$ cells only. Transplantation of purified M-MDSCs expressing CD34 resulted in a significantly lower RI (266 ± 61) than did transplantation of F-MDSCs expressing CD34 (417 ± 56; P = 0.052; *t* test). All RIs are reported as means ± SEM (error bars), and p-values are for *t* test comparisons. (C, top) 2 wk after single-cell cloning, there was no significant difference in the percentage of single-cell clones derived from M- or F-MDSC populations that yielded myogenic colonies as defined by myotube formation (73–90%; P = 0.776). We detected no effect as a result of the cell sex (P = 0.756). Parent populations were either low in desmin expression (<15% positive cells within the population) or high in desmin expression (>85% positive). (C, bottom) We did not observe any male clone that exhibited a higher RI as compared with the parent population. We transplanted four M-MDSC clonal populations (M1, M2, M3, and M4) and four F-MDSC clonal populations (F1, F2, F3, and F4; mean ± SEM is shown; *n* = 3 muscle transplantations per clone). In contrast, we found that three of the four F-MDSCs display a high-regenerating potential as observed with their parent population.

### Microarray analysis and cell stress response

We next performed microarray gene ontology analysis of M- and F-MDSCs to explore global gene expression differences between the populations. We identified the expression of more general cell stress–related genes, including oxidative stress and antiapoptotic genes, in F-MDSCs than in M-MDSCs (Fig. 5 A) using both gene ontology based on the NetAffx annotation database and GeneSifter. Of 45 general cellular stress–related genes, 29% of the genes were significantly increased in females, 7% were significantly higher in males ($P < 0.05$), and 64% showed no significant difference. There were also sexual dimorphisms in genes that were involved in responses to hypoxia and oxidative stress between M- and F-MDSCs. Of 99 apoptosis-related genes, 23% of the genes were significantly increased in females, 4% were higher in males, and 72% showed no significant difference. We confirmed the sex-related differences in the expression levels of several of these genes using RT-PCR (Fig. 5 B). We also compared microarray data of F-MDSCs that yielded a low level of regeneration with F-MDSCs that yielded a high level of regeneration. We found two stress-related genes (*TRP53inp1* and *SOD1*) that showed significant trends in a direction opposite to what we expected. For example, SOD1 was significantly higher in F-MDSCs as compared with M-MDSCs; however, when we explored the data of F-MDSCs with low RIs versus those with high RIs, we observed that SOD1 was higher in F-MDSCs that had only a low level of regeneration ($P < 0.05$). Similarly, TRP53Inp1 was significantly higher in the low-regenerating M-MDSCs, but, when we examined the low- versus high-regenerating F-MDSCs, we observed significantly higher

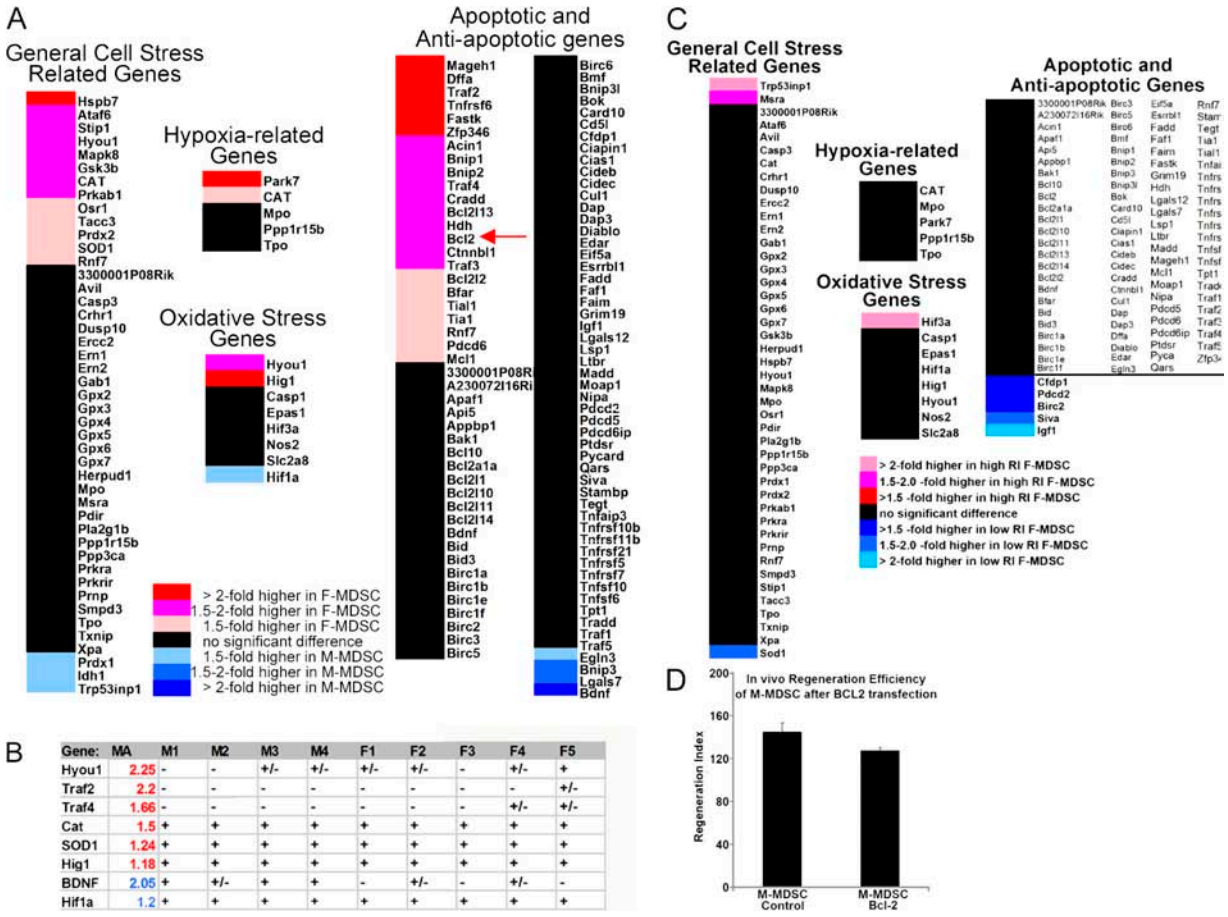


Figure 5. **Differences in hypoxic and oxidative stress genes.** (A) Microarray gene ontology analysis of M- and F-MDSCs. An increase in the expression of cell stress–related genes, including oxidative stress and antiapoptotic genes, was identified for F-MDSCs in comparison with M-MDSCs (colored bars represent significant differences; $P < 0.05$). Of 45 general cellular stress–related genes, 29% of the genes were significantly increased in F-MDSCs, 7% were significantly higher in M-MDSCs, and 64% showed no significant difference. Of 99 apoptosis-related genes, 23% of the genes were significantly increased in F-MDSCs, 4% were higher in M-MDSCs, and 72% showed no significant difference. (B) Gene levels of several key genes were examined using RT-PCR analysis. The results of several rounds of RT-PCR showing the gene symbol (Gene), the increase as seen by microarray analysis (MA; blue indicates that it is higher in M-MDSCs, and red indicates that it is higher in F-MDSCs), and the results of nine screened populations (four male populations, M1–M4, and five female populations, F1–F5; + indicates detection at 25 or 28 cycles, +/− denotes genes that were only observed at 30 cycles, and – represents genes that were not observed at 30 cycles). (C) We also examined the microarray data for differences in F-MDSCs that yielded a high level of muscle regeneration (high RI) as compared with F-MDSCs that yielded a low level of regeneration (low RI). High RIs are shown as red bars, and low RIs are shown blue bars. $P < 0.05$. (D) We found that the antiapoptotic factor *Bcl2* was twofold higher in F-MDSCs than in M-MDSCs (A, arrow). We hypothesized that low *Bcl2* expression may be related to reduced survival after cell transplantation, and we transfected M-MDSCs to overexpress *Bcl2* (M-MDSC–*Bcl2*). However, we did not observe a significant difference in the RI of M-MDSC–*Bcl2* (RI = 128 ± 17) as compared with the M-MDSC control (RI = 145 ± 48) at 2 wk after transplantation into dystrophic muscle ($P = 0.415$).

levels of TRP53Inp1 in the female populations with the best in vivo regeneration (Fig. 5 C). Although these trends are interesting, this analysis did not provide any clear indicators for genes of importance.

In particular, we found that the antiapoptotic factor *Bcl2* was twofold higher in F-MDSCs than in M-MDSCs by microarray analysis (Fig. 5 A, arrow) and Western blotting (not depicted). To test whether the overexpression of *Bcl2* in M-MDSCs could provide a gain of function in terms of in vivo skeletal muscle regeneration, we transfected the M-MDSCs with a *Bcl2* plasmid. Western blot analysis and quantification showed higher levels of Bcl2 in M-MDSCs that were transfected to overexpress *Bcl2* as compared with control M- or F-MDSCs (unpublished data). However, we did not observe a change in the RI of *Bcl2*-engineered M-MDSCs as compared with M-MDSC controls (Fig. 5 D).

### Examination of cell fate at early time points

We transplanted M- and F-MDSCs, which were transduced with a *lacZ*-encoding retroviral vector, into the gastrocnemius muscles of sex-matched mice, and we harvested at several time points between 16 h and 14 d. We quantified the number of *lacZ*-expressing nuclei that were detected at the transplantation site. At 16, 24, 48, and 72 h, there were significantly more *lacZ* nuclei detected in muscles of M-MDSC transplantations as compared with F-MDSC transplantations ($P < 0.05$; Fig. 6 A). In separate experiments, we digested the skeletal muscle 24 and 48 h after the transplantation of M- and F-MDSCs, and we quantified the amount of *lacZ* gene by quantitative RT-PCR. Similar to the histological analysis, we found more *lacZ* in muscles transplanted with M-MDSCs as compared with F-MDSC transplantations, although this was not statistically significant ($P > 0.05$; Fig. 6 B). In support of the finding of more M-MDSCs after transplantation, we detected higher levels of reduced glutathione, an antioxidant peptide whose levels are reported to be maximal in mitotic cells (Li and Oberley, 1998). We used flow cytometry and monochlorobimane labeling to detect glutathione levels and found significantly more glutathione in M-MDSCs as compared with F-MDSCs ($P < 0.01$; Fig. 6 C).

We also examined the amount of donor cell fusion or differentiation at the engraftment site by quantifying the percentage of *lacZ* nuclei that were located within muscle fibers. We examined the transplantation sites at 1, 2, and 5 d after cell injection. At 5 d after transplantation, we observed a trend toward significantly more donor cell fusion or differentiation with M-MDSCs as compared with F-MDSC transplantation to *mdx* muscle ($P = 0.068$; Fig. 6 D).

### Response to cell stress

To evaluate the effect of low oxygen conditions and oxidative stress on M- and F-MDSCs, we examined MDSC viability, phenotype, and myogenic differentiation under these conditions. We hypothesize that after MDSC transplantation, the transplanted cells will experience conditions of low physiologic oxygen environment and oxidative stress. Previous studies have demonstrated that inflammation occurs at the local microenvironment after cell transplantation (Guerette et al., 1997a; Qu et al., 1998; Bottino et al., 2002; Suzuki et al., 2004) and that oxidative stress occurs after an inflammation response and in the presence of low oxygen (Gute et al., 1998; Dhalla et al., 1999).

After exposure to physiologic oxygen for 24 h (2.5% $O_2$), we observed a trend toward reduced proliferation in both M-MDSCs and F-MDSCs as compared with their controls ($P = 0.18$ and $P = 0.079$, respectively; Fig. 7 A). There was no significant difference in the amount of cell viability or cell death in M-MDSCs as compared with F-MDSCs under conditions of

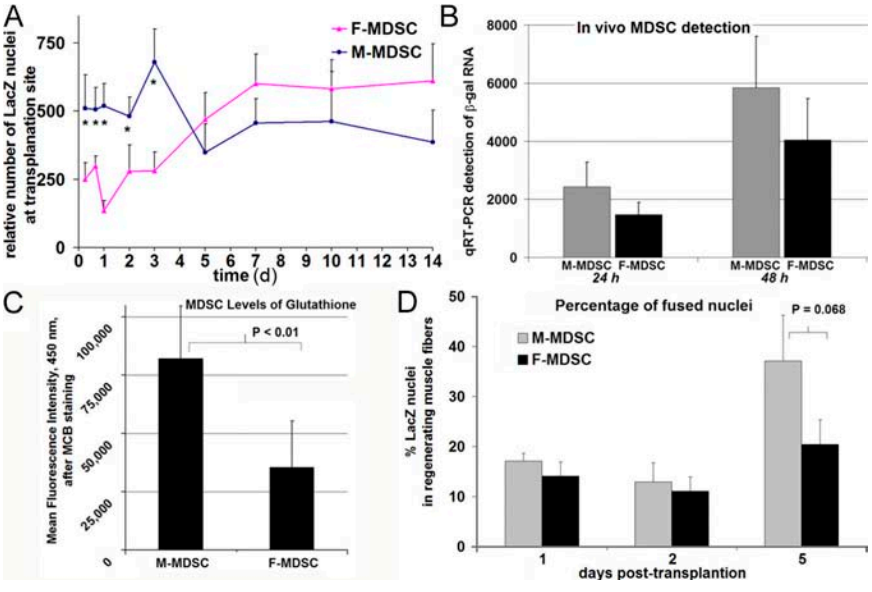


Figure 6. **Examination of the transplantation site at early time points.** (A) M- and F-MDSCs were transduced with the retroviral *lacZ* gene and transplanted into the gastrocnemius muscles of sex-matched mice, and the muscles were harvested at several time points between 16 h and 14 d. We quantified the number of *lacZ* nuclei that were detected at the transplantation site. At 16, 24, 48, and 72 h, there were significantly more nuclei detected in M-MDSC transplantations as compared with F-MDSC transplantations (*, $P < 0.05$ at all time points). (B) We digested the skeletal muscle after 24 and 48 h after transplantation, and we quantified the amount of *lacZ* gene by RT-PCR to support the histological staining results. Similar to the histological analysis, we detected more β-gal transcripts in muscles transplanted with M-MDSCs as compared with F-MDSC transplantations. (C) We stained M- and F-MDSCs using monochlorobimane (MCB) and found significantly more intracellular glutathione in M-MDSCs as compared with F-MDSCs ($P < 0.01$). (D) We quantified the percentage of $lacZ^+$ donor cells that are located within regenerating muscle fibers at 1, 2, and 5 d after MDSC transplantation. At 5 d after transplantation, we observed a trend toward significantly more donor cell fusion or differentiation with M-MDSCs as compared with F-MDSC transplantations to *mdx* muscle ($P = 0.068$). Error bars represent SD.

low oxygen ($P = 0.652$; Fig. 7 A). After exposure to oxidative stress (100 μM $H_2O_2$), we observed a significant decrease in cell numbers of both M-MDSCs and F-MDSCs ($P = 0.039$ and $P = 0.001$, respectively; Fig. 7 B). However, when we compared the response of M- with F-MDSCs in terms of cell proliferation or total cell numbers after stress, we observed no difference between the populations; there was no difference in the percent change in cell viability for M- vs. F-MDSCs after oxidative stress (41 vs. 55% decrease; $P = 0.325$; Fig. 7 B).

We examined the expression of CD34, Sca-1, and desmin in the populations after exposure to cell stress. We did not observe a change in CD34 or Sca-1 expression in M- or F-MDSCs that were exposed to 2.5% $O_2$ as compared with cells cultured in atmospheric $O_2$. We did observe a trend in increased desmin expression in M-MDSCs that had initially low levels of desmin ($P = 0.065$; Fig. 7 C). There was no similar change in desmin expression in a comparable population of F-MDSCs. After treatment with hydrogen peroxide, we observed trends toward an increase in CD34 and Sca-1 in all populations; however, after oxidative stress, there was no significant difference in the phenotype of M-MDSCs as compared with F-MDSCs (Fig. 7 D).

Next, we tested the ability of the cells to undergo myogenic differentiation after exposure to low oxygen or hydrogen peroxide. We plated M- and F-MDSCs at high density. After 4 d in culture, we transferred cells to either low oxygen or applied 100 μM $H_2O_2$ growth media. Control MDSCs were maintained at atmospheric oxygen with no $H_2O_2$. After 24 and 48 h, we performed immunochemistry for fast MyHC expression.

Under control conditions, there was no significant difference in the percentage of nuclei that colocalized with MyHC in M- or F-MDSC populations at 24 or 48 h (27–45% of the nuclei colocalized with MyHC). We observed a trend toward increased myogenic differentiation in M-MDSCs as compared with F-MDSCs after 48 h in low oxygen (Fig. 7 E). The sex-related difference in the differentiation response was also observed after exposure to hydrogen peroxide for 24 ($P = 0.060$) and 48 h (Fig. 7 F). In comparison with F-MDSCs, we observed an increase in myogenic differentiation with M-MDSCs as compared with their untreated controls (Fig. 7 F).

## Discussion

We show here that the sex of MDSCs influences their ability to promote skeletal muscle regeneration. These studies were initiated to understand the broad heterogeneity that has been reported for MDSCs and other muscle stem cell populations (Molnar et al., 1996; Schultz, 1996; Zammit and Beauchamp, 2001; Mueller et al., 2002; Deasy et al., 2004; Collins et al., 2005; Mitchell et al., 2005; Wagers and Conboy, 2005). The use of different isolation techniques, culture techniques, and tools for stem cell characterization complicates cross comparisons among cell populations isolated in different research laboratories.



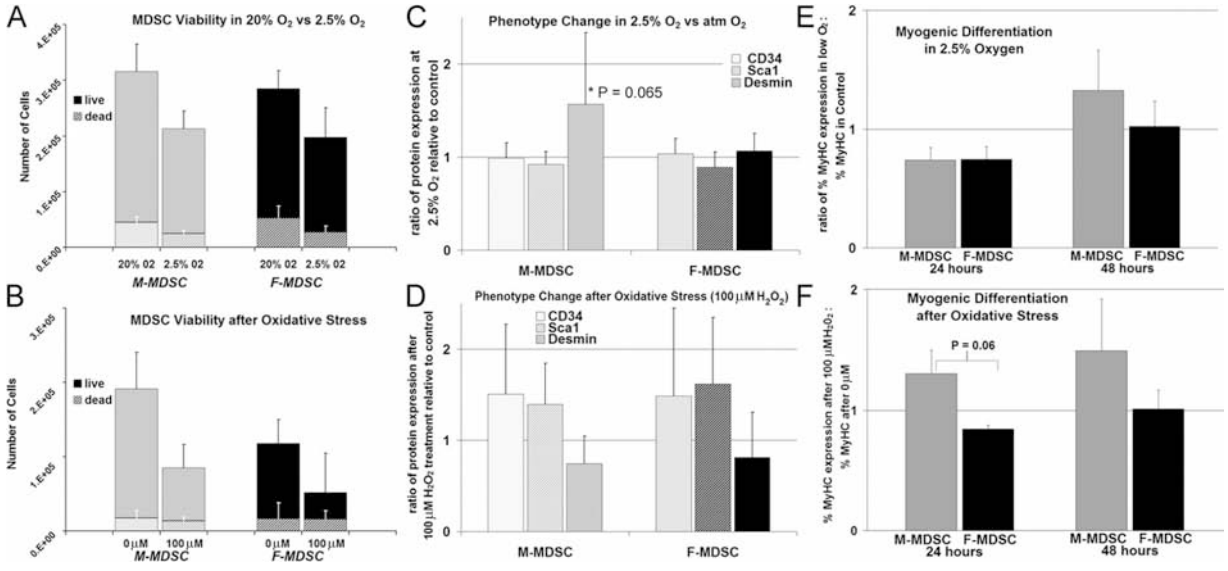


Figure 7. **Behavioral response to low oxygen and oxidative stress.** (A) After exposure to physiologic oxygen for 24 h (2.5% $O_2$), we observed a trend toward reduced cell numbers in both M-MDSCs and F-MDSCs ($P = 0.18$ and $P = 0.079$, respectively). There was no significant difference in the amount of cell viability or cell death in M-MDSCs as compared with F-MDSCs (ratio of the percentage of cells in low oxygen to atmospheric oxygen; $P = 0.652$). (B) After exposure to oxidative stress (100 μM $H_2O_2$), we observed a significant decrease in cell numbers of both M-MDSCs and F-MDSCs ($P = 0.039$ and $P = 0.001$, respectively). There was no difference in the percent change in cell viability for M-MDSCs vs. F-MDSCs after oxidative stress (ratio of the percentage of cells in 100 μM to atmospheric oxygen; $P = 0.325$). Bars are means ± SEM (error bars). (C) We examined the expression of CD34, Sca-1, and desmin in the populations after exposure to low oxygen. We did not observe a change in CD34 or Sca-1 expression in M- or F-MDSCs that were exposed to 2.5% $O_2$ as compared with cells cultured in atmospheric $O_2$. We observed a trend in increased desmin expression in M-MDSCs that had initially low levels of desmin ($P = 0.065$). There was no similar change in desmin expression in a comparable population of F-MDSCs. (D) After treatment with hydrogen peroxide, we observed trends toward an increase in CD34 and Sca-1 in all populations; however, there was no significant difference in the phenotype of M-MDSCs as compared with F-MDSCs ($P > 0.05$). Bars are means ± SD. (E) We induced myogenic differentiation and subsequently exposed cells to 2.5% oxygen for 24 and 48 h. We quantified the percentage of nuclei that colocalized with cells expressing the myogenic marker fast MyHC. We observed a trend toward more myogenic differentiation with M-MDSCs as compared with F-MDSCs. (F) We observed an increase in myogenic differentiation with M-MDSCs that were treated with 100 μM $H_2O_2$ as compared with their untreated controls at both 24 and 48 h. In comparison with their female counterparts, this change was significant at 24 h ($P = 0.06$). Bars are means ± SEM.

This study identifies sex-related differences as a factor in MDSC variability in skeletal muscle regeneration.

The M- and F-MDSC populations isolated by the preplate technique shared stem cell characteristics; however, extensive in vivo screening showed that only 2/10 male populations had an in vivo RI near 200. In comparison, 60% of the 15 female populations had an RI higher than the mean RI of M-MDSCs (RI = 95), and 40% of the F-MDSCs had an RI higher than the maximal male RI (RI = 203). After transplantation into the skeletal muscle of dystrophic mice, F-MDSCs transplanted into hosts of either sex consistently regenerated more dystrophin-positive myofibers than did M-MDSCs transplanted into hosts of either sex.

### Searching for a robust M-MDSC

To determine whether the M-MDSC population is more elusive than the F-MDSC population, we attempted to isolate cells with the M-MDSC phenotype from other isolation subfractions. First, we investigated whether preplate isolation might result in the inadvertent removal of potent M-MDSCs. To determine whether viable M-MDSCs reside in an earlier preplate passage than previously believed, we transplanted male pp3, 4, 5, and 6 cells into dystrophic mice. However, the RIs of these male cells were no higher than that of their parent M-MDSCs. We examined clones of M- and F-MDSCs and did not observe any male clones that participated in muscle regeneration to a level similar to that of F-MDSCs. We also compared M- and F-MDSC populations sorted on the basis of their expression of CD34, an established muscle stem cell marker whose expression decreases as cells differentiate. In side by side experiments, male $CD34^+$ cells led to substantially less skeletal muscle regeneration than did female $CD34^+$ cells.

A retrospective analysis of our previous work with muscle-derived cells provided further evidence that M-MDSCs exhibit lower regeneration efficiency than F-MDSCs (Jankowski et al., 2002; Jankowski and Huard, 2004a,b). Two previous studies performed by members of our laboratory involved the use of Y-chromosome in situ hybridization to track male cells injected into female hosts (before our notion of sex-related differences; Jankowski et al., 2002; Jankowski and Huard, 2004b). The authors of both studies calculated RIs to assess the efficiency with which the donor cells regenerated dystrophin-positive fibers in dystrophic mice. These studies found that male populations, which were sorted for CD34 expression by magnetic antibody cell sorting (Jankowski et al., 2002) or by FACS (Jankowski and Huard, 2004b), exhibited RIs $<200$, which is a level consistent with the RIs reported in this study. In addition, because those studies used freshly isolated populations, the authors performed $>20$ separate isolations from male animals to generate a sufficient sample size; none of the male populations had an RI $>200$ (the authors scaled their RI to the percentage of myogenic [$desmin^+$] donor cells; we have adjusted for the authors' reported values for desmin expression). A third study using female cells obtained from rats demonstrated a high RI ($>200$) after transplantation of the F-MDSCs into *mdx*/SCID mice (RI = 392 ± 55 dystrophin-positive fibers/$10^5$ myogenic donor cells; Jankowski and Huard, 2004a). In a study performed by another group, Mueller et al. (2002) used MDSCs derived from our group and found a low efficiency of muscle regeneration when the MDSCs were transplanted to male hosts, as we observe here. Collectively, these findings provide compelling evidence that MDSCs and host animals exhibit sex-related differences.

We tested whether hormones play a role in this process. We failed to observe increased regeneration by normal M-MDSCs transplanted into female mice or M-MDSCs prestimulated with physiologic estrogen levels. This finding parallels the results of other studies indicating that sex-related differences might not be exclusively hormonal (Xu et al., 1992; Gutierrez-Adan et al., 2000; Du et al., 2004). Indeed, other dosing regimes and other sex steroids such as progesterone or testosterone should be considered in conjunction with studying the various receptor isoforms to fully evaluate the potential role of hormones in the sex-related differences exhibited by MDSCs.

### Sex-related differences in cell stress response

By microarray analysis, we observed trends in sex differences in genes related to apoptosis, hypoxia, oxidative stress, and general cell stress response. In particular, the RNA and protein levels of the antiapoptotic gene *Bcl2* were lower in M-MDSCs as compared with F-MDSCs. The rapid cell death in muscle cell transplantation has been previously reported (Beauchamp et al., 1994, 1999; Fan et al., 1996). Therefore, we attempted a gain of function in M-MDSCs by the overexpression of *Bcl2*. We did not, in fact, observe an increase in muscle regeneration after *Bcl2* gene transfer. Indeed, subsequent experiments surprisingly demonstrated that there were more M-MDSCs than F-MDSCs at the transplantation site up to 3 d after transplantation. We also detected higher levels of reduced glutathione in the M-MDSC than in the F-MDSC. Glutathione's role in protecting cells from antioxidants could explain a better survival of M-MDSCs after transplantation. In addition, it has also been shown that glutathione levels are elevated during mitosis (Li and Oberley, 1998; Menon et al., 2003). This finding, along with the finding of differences in the mitotic fraction of M- and F-MDSCs, could also suggest that the M-MDSCs were more mitotic than the F-MDSCs after transplantation.

We also tested the cells' abilities to undergo myogenic differentiation after exposure to low oxygen environment or oxidative stress, two conditions that are expected to be present in the microenvironment after transplantation. We found an increase in the percentage of cells that expressed the myogenic marker desmin in M-MDSCs grown in low oxygen. We also found more MyHC expression by M-MDSCs after exposure to oxidative stress for 24 h and a similar trend after 48 h.

We hypothesize that the effect of cell stress on myogenic differentiation leads to in vivo sex-related differences in skeletal muscle regeneration (Fig. 8). F-MDSCs respond to low oxygen or oxidative stress by maintaining a low level of proliferation. In a myogenic environment with low oxygen or oxidative stress, F-MDSCs do not readily differentiate. Conversely, M-MDSCs demonstrate increased myogenic differentiation in the presence of low oxygen or oxidative stress. In vivo, we hypothesize that

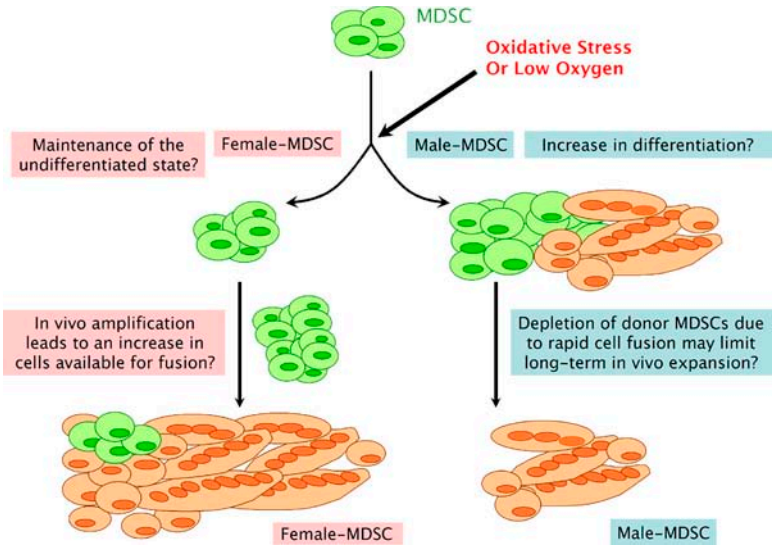


Figure 8. **Schematic of proposed sex-related differences in response to cell stress and role in skeletal muscle regeneration.** Sex-related differences affect the response of MDSCs to low oxygen or oxidative stress. F-MDSCs may respond by maintaining a low level of proliferation. In a myogenic environment with low oxygen or oxidative stress, F-MDSCs do not appear to readily differentiate. Conversely, M-MDSCs demonstrate increased myogenic differentiation in the presence of low oxygen or oxidative stress. In vivo, we hypothesize that the increased differentiation will result in the rapid depletion of donor M-MDSCs as cells fuse to form terminally differentiated multinucleated myotubes/fibers. F-MDSCs may be less proliferative at early time points after implantation and demonstrate an increase in cell numbers starting at 3 d after implantation. Ultimately, the tendency to maintain the undifferentiated phenotype or resist differentiation would be a mechanism that allows for in vivo expansion of F-MDSCs that are subsequently available at later time points for muscle regeneration.

the increased differentiation will result in the rapid depletion of donor M-MDSCs as cells undergo myogenic differentiation, including transient amplification and fusion to form terminally differentiated multinucleated myotubes/fibers. F-MDSCs may be less proliferative, or we speculate that they may enter quiescence in response to oxidative stress at early time points after implantation. Subsequently, F-MDSCs demonstrate an increase in cell numbers starting at 3 d after implantation, a point at which acute inflammation subsides (Guerette et al., 1997a,b). Ultimately, the tendency to maintain the undifferentiated phenotype allows for in vivo expansion of F-MDSCs that are consequently available at later time points for muscle regeneration. These results both strongly support the notion that MDSCs exhibit sex-related differences at the cellular level and suggest that pathways involved with cellular responses to stress may differ in M- and F-MDSCs.

It will be interesting to determine whether other stem cell types also exhibit sex-related differences. In addition, stem cell experiments could have skewed results if male cells are selectively used for the purpose of in vivo cell tracking via the Y chromosome. This evidence that innate cellular sex differences may influence stem and progenitor biology should influence how researchers report and investigate the use of progenitor cells for regenerative medicine and the treatment of diseases.

## Materials and methods

### MDSC isolation and in vitro characterization

A modified preplate technique was used to isolate a low-adhering fraction of MDSCs from skeletal muscle biopsies obtained from 3-wk-old normal C57BL mice (Rando and Blau, 1994; Qu-Petersen et al., 2002). Six isolations were performed using anatomically sexed animals, and cell sex was later confirmed by FISH analysis. All populations were negative for CD45 expression (<0.1% of cells). Both M- and F-MDSCs were cultured in normal growth medium (GM): DME (supplemented with 10% FBS; Invitrogen), 10% horse serum, 1% penicillin/streptomycin, and 0.5% chick embryo extract (Accurate Chemical).

Cell populations were characterized by flow cytometry for CD34 and Sca-1 expression. MDSCs were labeled with rat anti–mouse Sca-1 (phycoerythrin) and CD34 (biotin) mAbs (BD Biosciences). A separate portion of cells was treated with equivalent amounts of isotype control antibodies. Both fractions were washed and labeled with streptavidin-allophycocyanin. We added 7-amino-actinomycin D to exclude nonviable cells from the analysis. Sca-1 and CD34 expression was determined by flow cytometry with a cell sorter (FACStar Plus or FACSAria; Becton Dickinson). Desmin expression was assessed via immunocytochemistry. After cold methanol fixation, cells were blocked in 5% horse serum and were incubated with mouse monoclonal IgG desmin (1:250; Sigma-Aldrich), secondary biotinylated IgG (1:250; Vector Laboratories), and streptavidin-Cy3 (1:500; Sigma-Aldrich) to fluorescently label the cells and determine the percentage of myogenic cells within the population. Cell sex was confirmed by FISH. Degenerate oligonucleotide-primed PCR-labeled Y probes were used to determine cell sex. Populations were screened for their in vivo regeneration efficiency after transplantation into skeletal muscle (see Cell transplantation to skeletal muscle).

### In vitro characterization

To measure morphology, phase-contrast light microscopy images were acquired for several M- and F-MDSC isolations. Northern Eclipse software (Sun Systems) was used to collect morphometric data by outlining or tracing individual cells. A rank sum test was performed to compare quantitative measurements of F- and M-MDSC area (number of pixels calibrated to micrometers squared), cell diameter (maximal length in micrometers), cell elongation (ratio of the major axis to the minor axis), and cell roundness (perimeter squared/$4 \times \pi \times$ area).

To examine multipotency, MDSCs were induced to undergo myogenic, osteogenic, and adipogenic differentiation. To promote myogenic differentiation, MDSCs were plated at high confluence (1,500 cells/cm$^2$) in GM for 3 d, transferred to low serum–containing medium (2% horse serum/FBS in DME) for 4 d, and examined for myotube formation by MyHC expression (1:250; Sigma-Aldrich), biotinylated IgG (1:250; Vector Laboratories), and streptavidin-Cy3 (1:500) or dystrophin immunocytochemistry. Osteogenic differentiation was induced by stimulation with 10 ng/ml of bone morphogenetic protein 4 for 10 d and was evaluated by AP and von Kossa staining (Lee et al., 2000). Adipogenic differentiation was induced after cells reached confluency by adding adipogenic medium to the cells (dexamethasone, insulin, indomethacin, and 3-isobutyl-1-methylxanthinine; Cambrex) as previously described (Pittenger et al., 1999). Lipid vacuole formation was assessed by Oil Red O staining.

To examine short-term growth kinetics, the division time, PDT, and mitotic or dividing fraction were determined from time-lapsed microscopy as previously described (Sherley et al., 1995; Deasy et al., 2003). To examine long-term proliferation potential, M- and F-MDSCs were plated in 25-cm$^2$ collagen-coated flasks, and routine cell passaging was performed every 2–3 d (Deasy et al., 2005). At each passage, cells were replated to a density of 225 cells/cm$^2$. The number of PDs for each subculturing was calculated as the $\log_2 (N/N_0)$. This process was repeated for >150 PDs. Karyotyping was performed as previously described (Deasy et al., 2005) for the two M-MDSC populations (A and D) and two F-MDSC populations (B and C).

**Acquisition and processing of images.** Immunofluorescent images of dystrophin, desmin, and MyHC were acquired at RT on a microscope (DM IRB; Leica) using a 20× NA 0.04 objective (CorrPh1 α/0–2/C; Leica). No imaging medium was used, and the fluorochromes used are as indicated. Digital images were acquired using a camera (Regita; QImaging) and Northern Eclipse software (version 6.0; Sun Systems). Images were acquired at exposures that were based on unstained controls. The final presentation of images was prepared in Photoshop versions 5.0–7.0 (Adobe), and, in some cases, only uniform brightness or contrast adjustments were performed.

### Telomerase activity and telomere length

Telomerase activity was determined using the TeloTAGGG Telomerase PCR ELISA PLUS kit (Roche) according to the manufacturer's protocol. $2 \times 10^5$ cells were lysed in 200 μl of lysis reagent, and 10 μl of the lysate was used for the telomere repeat amplification protocol reaction. The experiment was performed in triplicate, and relative telomerase activity was recorded and plotted. For the flow cytometry–based measurement of telomere length, telomeres in M- and F-MDSCs were detected with the PNA Kit for Flow Cytometry (DakoCytomation) according to the manufacturer's protocol. $2 \times 10^6$ male or female cells were divided into four 1.5-ml tubes. The cellular DNA was denatured for 10 min at 82°C and hybridized with the telomere PNA probe (FITC) at RT overnight. The cells were then analyzed by flow cytometry, and the relative telomere length was calculated.

### Cell transplantation to skeletal muscle

The use of animals and the surgical procedures performed in this study were approved by the Institutional Animal Care and Use Committee of the Children's Hospital of Pittsburgh (University of Pittsburgh Medical Center). *mdx* mice (C57BL/10ScSn-*Dmd*$^{mdx}$) were obtained from The Jackson Laboratory or bred at the institution's animal facility. *mdx*/SCID mice were bred by crossing C57BL/10ScSn-*Dmd*$^{mdx}$ and C57BL/6J-*Prkdc*$^{scid}$/SzJ mice.

For all experiments involving the transplantation of MDSCs, satellite cells, or CD34-sorted populations, $1–2 \times 10^5$ cells were transplanted into the gastrocnemius muscles of male or female mice as indicated and harvested after 2 wk. For sex-mismatched experiments, two M-MDSCs (populations A and D) were transplanted into female hosts, and two F-MDSCs (populations B and C) were transplanted into male hosts. The populations had similar phenotypes: populations A and C (CD34 [60–80% positive], Sca-1 [70–100% positive], and desmin [>95% positive]), populations B and D (CD34 [60–80% positive] and Sca-1 [40–80% positive], and desmin [<15% positive]). For CD34-sorting experiments, populations A and C were used.

Tissues were harvested and snap frozen in liquid nitrogen–cooled 2-methyl butane and cryosectioned at 10 μm. Either the MOM (mouse on mouse) kit (Vector Laboratories) with DYS2 antibody (1:50; Novocastra) or a donkey anti–rabbit dystrophin (1:300; Abcam) antibody was used to stain tissue sections for dystrophin. For the DYS2 antibody, the sections were fixed with cold methanol, and the MOM kit protocol was followed (DYS2 at 1:50, biotinylated anti–mouse IgG at 1:250, and streptavidin-Cy3 T at 1:500; Sigma-Aldrich). For anti–rabbit dystrophin, sections were fixed with 5% formalin, blocked with donkey serum, incubated with primary antibody, and incubated with AlexaFluor594 donkey anti–rabbit (1:500; Invitrogen). For CD4 staining, tissue was blocked with goat serum and was incubated with rat anti–mouse CD4 (1:100; BD Biosciences), biotin goat anti–rat (1:400; Vector Laboratories), and peroxidase-streptavidin (1:800; DakoCytomation).

A previously described technique (Jankowski et al., 2002; Deasy et al., 2005) was used to measure the cells' RIs. The RI is the ratio of the number of dystrophin-positive fibers per $10^5$ donor cells (RI is scored at the cross section of maximal engraftment). The large majority of the >150 muscle transplantations of this study were quantitated for the RI in a blind manner by more than one investigator.

The RIs or areas containing CD4-positive cells were compared by two-way ANOVA or a *t* test to assess the effects of cell sex and host sex. For transplantations of *lacZ* MDSCs, cells were first labeled with retrovirus encoding for the *lacZ* gene as previously described (Lee et al., 2000). We performed X-gal staining to visualize β-gal activity and quantified the total number of these *lacZ*-positive nuclei and the number that were located within muscle fibers.

### Single-cell cloning and clonal analysis

We used FACS to obtain single-cell clones (FACSAria and visual confirmation) of M- and F-MDSCs (populations A–D) on 96-well plates. Clones were cultured in 50 μl GM. At 1 wk after sorting, we identified viable colonies and scored these clones as myogenic or not myogenic based on the presence of distinct multinucleated myotubes. At 2 wk after cloning, we again determined the cumulative number of myogenic colonies based on the presence of distinct myotubes. For transplantation experiments using clonal populations, we similarly obtained single-cell clones from M- and F-MDSCs (populations A–D). After culture expansion, we selected eight representative populations and performed transplantations as described above (Cell transplantation to skeletal muscle) to determine the RI of each clone.

### Estrogen stimulation

M- and F-MDSCs (populations A–D) were cultured in GM without phenol red and supplemented with 0, 10, or 100 nM 17-β-estradiol (Sigma-Aldrich). Cells were replated in fresh medium every 2–3 d for 14 d. After in vitro stimulation, $10^5$ cells per muscle were transplanted into the gastrocnemius of female *mdx*/SCID mice ($n = 3$ muscles per group). 2 wk after transplantation, the muscles were harvested, sectioned, and immunostained for dystrophin, and the RI was analyzed as described above (Cell transplantation to skeletal muscle).

### Microarray analysis

RNA was isolated from five M- and five F-MDSC populations using an RNeasy kit (QIAGEN) and analyzed on a GeneChip Mouse Genome 430A 2.0 array (Affymetrix, Inc.). Fold increase was determined using previously established techniques (Perez-Iratxeta et al., 2005). Gene ontology was determined using the NetAffx (Affymetrix, Inc.) annotation database (Liu et al., 2003; Harris et al., 2004). All results were confirmed using GeneSifter (VizX Labs), a certified GeneChip-compatible web-based analysis tool. The resulting data on fold increase for each population were analyzed using a *t* test to determine significant differences ($P < 0.05$) between the M- and F-MDSC populations.

### RT-PCR and real-time quantitative PCR

Several genes of interest from the microarray were confirmed with RT-PCR analysis. Total RNA was extracted from $5 \times 10^5$ cells using the Nucleospin RNA kit (CLONTECH Laboratories, Inc.). cDNA was synthesized with SuperScript II reverse transcriptase (Invitrogen) according to the manufacturer's instructions. PCR was performed with Taq polymerase (Invitrogen) according to the manufacturer's instructions for 25, 28, and 30 cycles at 58°C annealing temperature, and PCR products were separated by electrophoresis on 1% agarose gels. The primers used are listed in Table S2 (available at http://www.jcb.org/cgi/content/full/jcb.200612094/DC1).

For quantitative PCR, we used 50 ng cDNA. cDNA and β-gal primers (forward, ACAGTACGCGTAG; reverse, CCATCAATCCGGTAGGTTTTCCGG) were added to SYBR green PCR master mix (Applied Biosystems) according to the manufacturer's instructions. All *lacZ* data were normalized to 18S, which was used as the internal control.

### Overexpression of *Bcl2*

M- and F-MDSCs were plated at 2,500 cells/9.6 cm$^2$ in GM. The following day, the medium was replaced with 500 μl DME (without serum or antibiotics) containing 4.0 μg *Bcl2* plasmid, which also encoded for the neomycin resistance gene, and 5 μl LipofectAMINE 2000 reagent (Invitrogen). MDSCs were incubated at 37°C for 6 h in this medium, and then medium was removed and replaced with normal GM. After 5 d in culture, we began a selection process. For the next 2 wk, MDSCs were cultured in GM containing 1.5 mg/ml G418 sulfate (Cellgro). Controls were also transfected with GFP plasmid to confirm transfection. Cells were maintained in GM and transplanted to male *mdx*/SCID mice as described above (Cell transplantation to skeletal muscle). Western blot analysis was performed using standard molecular biological techniques. Cells were lysed in Laemmli sample buffer (Bio-Rad Laboratories) and resolved on 4–20% precast gradient gels. Mouse *Bcl2* was detected with anti-*Bcl2* (1:1,000; BD Biosciences) with goat anti–rabbit HRP (1:2,500; BD Biosciences) and imaged using SuperSignal (Pierce Chemical Co.). β-actin levels were detected with anti–β-actin (1:5,000; Sigma-Aldrich) and goat anti–mouse HRP (1:5,000; Pierce Chemical Co.).

### Response to cell stress

**Viability.** For the low oxygen environment, M- and F-MDSCs (populations A–D) were plated at a density of 500 cells/cm$^2$ on collagen-coated flasks with normal GM. After cell adherence (4–6 h), MDSCs were incubated for 24 h in either atmospheric (~20%) or 2.5% $O_2$ conditions (HERAcell 150 incubator; MidAtlantic Diagnostics). For oxidative stress, M- and F-MDSCs (populations A–D) were plated at a density of 700 cells/cm$^2$. After cell adherence, MDSCs were incubated for 24 h with either 0 or 100 μM $H_2O_2$ (under atmospheric oxygen). After 24 h in low $O_2$ or after 24 h with 100 μM $H_2O_2$, MDSCs from the supernatant and adherent cells were collected

(0.25% trypsin-EDTA). Cells were counted using a Neubauer hemacytometer (Fisher Scientific), and trypan blue staining was used to identify the live and dead cells.

**Phenotype after cell stress.** We examined CD34, Sca-1, and desmin expression as described above (MDSC isolation and in vitro characterization).

**Myogenic differentiation after cell stress.** The ability of MDSCs to form myotubes under low oxygen conditions or after exposure to hydrogen peroxide was determined by fast MyHC staining. M- and F-MDSCs (populations A–D) were plated at a density of 1,000 cells/$cm^2$ on collagen-coated plates with normal GM. For low oxygen stress, after 4 d of growth in atmospheric conditions, growth media was refreshed, and cells were transferred to a 2.5% oxygen incubator. Control flasks were maintained in atmospheric $O_2$ incubators. For oxidative stress, after 4 d of growth in atmospheric conditions with normal media, growth media was refreshed (control), or MDSCs received media with 100 μM $H_2O_2$. After 24 and 48 h of exposure to low oxygen or incubation with $H_2O_2$, MDSC cultures were fixed and immunostained for MyHC as described above (In vitro characterization).

Reduced glutathione levels were determined for M- and F-MDSC populations by flow cytometry. Cells were plated at 1,600 cells/$cm^2$ on collagen-coated flasks with normal GM. After 24 h, cells were incubated in 5 μM monochlorobimane (Invitrogen) in normal growth media for 20 min at 37°C. The cells were then washed twice with PBS and harvested in 0.25% trypsin-EDTA. Intracellular glutathion levels were determined with a FACSAria machine (monochlorobimane excitation of 380 nm and emission of 461 nm).

**Online supplemental material**

Fig. S1 shows M- and F-MDSC similarities in cell morphology comparisons, multilineage marker expression, telomerase activity, and telomere length. Fig. S2 shows the in vitro and in vivo effects of estrogen stimulation on M- and F-MDSCs. Table S1 presents the correlation coefficients for relations between variables. Table S2 presents the primers for RT-PCR. Online supplemental material is available at http://www.jcb.org/cgi/content/full/jcb.200612094/DC1.

We would like to thank Samantha Sanford, Seiji Kubo, Michele Jones, Michael Mentzer, Patrick Blake, Chris Scelfo, Michelle Wiit, and Maria Branca for technical assistance, Ryan Sauder for excellent editorial assistance, and Dr. Bruno Péault (University of Pittsburgh, Pittsburgh, PA) and Dr. Art Levine (University of Pittsburgh School of Medicine, Pittsburgh, PA) for insightful discussions.

This work was supported by the Jesse's Journey Foundation, the Muscular Dystrophy Association, the National Institutes of Health (grant R01 AR49684-01), the William F. and Jean W. Donaldson Chair at the Children's Hospital of Pittsburgh, and the Henry J. Mankin Chair at the University of Pittsburgh.

Submitted: 18 December 2006
Accepted: 11 March 2007

## References

Aristotle. 350 BC. Historia Animalium: Books VII–X. 1991 edition. D.M. Balme, editor. Harvard University Press, Cambridge, MA. 435–437.

Avery, B., C.B. Jorgensen, V. Madison, and T. Greve. 1992. Morphological development and sex of bovine in vitro-fertilized embryos. *Mol. Reprod. Dev.* 32:265–270.

Aviv, A. 2002. Telomeres, sex, reactive oxygen species, and human cardiovascular aging. *J. Mol. Med.* 80:689–695.

Aviv, A., J. Shay, K. Christensen, and W. Wright. 2005. The longevity gender gap: are telomeres the explanation? *Sci. Aging Knowledge Environ*. 2005: pe16.

Beauchamp, J.R., J.E. Morgan, C.N. Pagel, and T.A. Partridge. 1994. Quantitative studies of efficacy of myoblast transplantation. *Muscle Nerve*. 1:S261.

Beauchamp, J.R., J.E. Morgan, C.N. Pagel, and T.A. Partridge. 1999. Dynamics of myoblast transplantation reveal a discrete minority of precursors with stem cell-like properties as the myogenic source. *J. Cell Biol.* 144:1113–1122.

Blankenhorn, E.P., S. Troutman, L.D. Clark, X.M. Zhang, P. Chen, and E. Heber-Katz. 2003. Sexually dimorphic genes regulate healing and regeneration in MRL mice. *Mamm. Genome*. 14:250–260.

Bottino, R., A.N. Balamurugan, S. Bertera, M. Pietropaolo, M. Trucco, and J.D. Piganelli. 2002. Preservation of human islet cell functional mass by anti-oxidative action of a novel SOD mimic compound. *Diabetes*. 51:2561–2567.

Chau, B.N., H.L. Borges, T.T. Chen, A. Masselli, I.C. Hunton, and J.Y. Wang. 2002. Signal-dependent protection from apoptosis in mice expressing caspase-resistant Rb. *Nat. Cell Biol.* 4:757–765.

Collins, C.A., I. Olsen, P.S. Zammit, L. Heslop, A. Petrie, T.A. Partridge, and J.E. Morgan. 2005. Stem cell function, self-renewal, and behavioral heterogeneity of cells from the adult muscle satellite cell niche. *Cell*. 122:289–301.

Deasy, B.M., R.J. Jankowski, T.R. Payne, B. Cao, J.P. Goff, J.S. Greenberger, and J. Huard. 2003. Modeling stem cell population growth: incorporating terms for proliferative heterogeneity. *Stem Cells*. 21:536–545.

Deasy, B.M., Y. Li, and J. Huard. 2004. Tissue engineering with muscle-derived stem cells. *Curr. Opin. Biotechnol.* 15:419–423.

Deasy, B.M., B.M. Gharaibeh, J.B. Pollett, M.M. Jones, M.A. Lucas, Y. Kanda, and J. Huard. 2005. Long-term self-renewal of postnatal muscle-derived stem cells. *Mol. Biol. Cell*. 16:3323–3333.

Dhalla, N.S., L. Golfman, S. Takeda, N. Takeda, and M. Nagano. 1999. Evidence for the role of oxidative stress in acute ischemic heart disease: a brief review. *Can. J. Cardiol.* 15:587–593.

Du, L., H. Bayir, Y. Lai, X. Zhang, P.M. Kochanek, S.C. Watkins, S.H. Graham, and R.S. Clark. 2004. Innate gender-based proclivity in response to cytotoxicity and programmed cell death pathway. *J. Biol. Chem.* 279:38563–38570.

Fan, Y., M. Maley, M. Beilharz, and M. Grounds. 1996. Rapid death of injected myoblasts in myoblast transfer therapy. *Muscle Nerve*. 19:853–860.

Guerette, B., I. Asselin, D. Skuk, M. Entman, and J.P. Tremblay. 1997a. Control of inflammatory damage by anti-LFA-1: increase success of myoblast transplantation. *Cell Transplant.* 6:101–107.

Guerette, B., D. Skuk, F. Celestin, C. Huard, F. Tardif, I. Asselin, B. Roy, M. Goulet, R. Roy, M. Entman, and J.P. Tremblay. 1997b. Prevention by anti-LFA-1 of acute myoblast death following transplantation. *J. Immunol.* 159:2522–2531.

Gute, D.C., T. Ishida, K. Yarimizu, and R.J. Korthuis. 1998. Inflammatory responses to ischemia and reperfusion in skeletal muscle. *Mol. Cell. Biochem.* 179:169–187.

Gutierrez-Adan, A., M. Oter, B. Martinez-Madrid, B. Pintado, and J. De La Fuente. 2000. Differential expression of two genes located on the X chromosome between male and female in vitro-produced bovine embryos at the blastocyst stage. *Mol. Reprod. Dev.* 55:146–151.

Harada, H., K.P. Pavlick, I.N. Hines, D.J. Lefer, J.M. Hoffman, S. Bharwani, R.E. Wolf, and M.B. Grisham. 2003. Sexual dimorphism in reduced-size liver ischemia and reperfusion injury in mice: role of endothelial cell nitric oxide synthase. *Proc. Natl. Acad. Sci. USA*. 100:739–744.

Harris, T.W., N. Chen, F. Cunningham, M. Tello-Ruiz, I. Antoshechkin, C. Bastiani, T. Bieri, D. Blasiar, K. Bradnam, J. Chan, et al. 2004. WormBase: a multi-species resource for nematode biology and genomics. *Nucleic Acids Res.* 32:D411–D417.

Jankowski, R.J., and J. Huard. 2004a. Establishing reliable criteria for isolating myogenic cell fractions with stem cell properties and enhanced regenerative capacity. *Blood Cells Mol. Dis.* 32:24–33.

Jankowski, R.J., and J. Huard. 2004b. Myogenic cellular transplantation and regeneration: sorting through progenitor heterogeneity. *Panminerva Med.* 46:81–91.

Jankowski, R.J., B.M. Deasy, B. Cao, C. Gates, and J. Huard. 2002. The role of CD34 expression and cellular fusion in the regeneration capacity of myogenic progenitor cells. *J. Cell Sci.* 115:4361–4374.

Jilka, R.L., G. Hangoc, G. Girasole, G. Passeri, D.C. Williams, J.S. Abrams, B. Boyce, H. Broxmeyer, and S.C. Manolagas. 1992. Increased osteoclast development after estrogen loss: mediation by interleukin-6. *Science*. 257:88–91.

Kochhar, H.S., K.P. Kochhar, P.K. Basrur, and W.A. King. 2003. Influence of the duration of gamete interaction on cleavage, growth rate and sex distribution of in vitro produced bovine embryos. *Anim. Reprod. Sci.* 77:33–49.

Lee, J.Y., Z. Qu-Petersen, B. Cao, S. Kimura, R. Jankowski, J. Cummins, A. Usas, C. Gates, P. Robbins, A. Wernig, and J. Huard. 2000. Clonal isolation of muscle-derived cells capable of enhancing muscle regeneration and bone healing. *J. Cell Biol.* 150:1085–1100.

Li, N., and T.D. Oberley. 1998. Modulation of antioxidant enzymes, reactive oxygen species, and glutathione levels in manganese superoxide dismutase-overexpressing NIH/3T3 fibroblasts during the cell cycle. *J. Cell. Physiol.* 177:148–160.

Liu, G., A.E. Loraine, R. Shigeta, M. Cline, J. Cheng, V. Valmeekam, S. Sun, D. Kulp, and M.A. Siani-Rose. 2003. NetAffx: Affymetrix probesets and annotations. *Nucleic Acids Res.* 31:82–86.

Maeda, K.-I., S. Ohkura, and H. Tsukamura. 2000. Physiology of reproduction. *In* The Laboratory Rat: the Handbook of Experimental Animals. G.J. Krinke, editor. Academic Press, San Diego. 756 pp.

Menon, S.G., E.H. Sarsour, D.R. Spitz, R. Higashikubo, M. Sturm, H. Zhang, and P.C. Goswami. 2003. Redox regulation of the G1 to S phase transition in the mouse embryo fibroblast cell cycle. *Cancer Res.* 63:2109–2117.

Mitchell, P.O., T. Mills, R.S. O'Connor, T. Graubert, E. Dzierzak, and G.K. Pavlath. 2005. Sca-1 negatively regulates proliferation and differentiation of muscle cells. *Dev. Biol.* 283:240–252.

Molnar, G., M.L. Ho, and N.A. Schroedl. 1996. Evidence for multiple satellite cell populations and a non-myogenic cell type that is regulated differently in regenerating and growing skeletal muscle. *Tissue Cell*. 28:547–556.

Mueller, G.M., T. O'Day, J.F. Watchko, and M. Ontell. 2002. Effect of injecting primary myoblasts versus putative muscle-derived stem cells on mass and force generation in mdx mice. *Hum. Gene Ther.* 13:1081–1090.

Mulroney, S.E., C. Woda, M. Johnson, and C. Pesce. 1999. Gender differences in renal growth and function after uninephrectomy in adult rats. *Kidney Int.* 56:944–953.

Nomura, T., E. Ashihara, K. Tateishi, S. Asada, T. Ueyama, T. Takahashi, H. Matsubara, and H. Oh. 2007. Skeletal myosphere-derived progenitor cell transplantation promotes neovascularization in delta-sarcoglycan knockdown cardiomyopathy. *Biochem. Biophys. Res. Commun*. 352:668–674.

Peippo, J., A. Farazmand, M. Kurkilahti, M. Markkula, P.K. Basrur, and W.A. King. 2002. Sex-chromosome linked gene expression in in-vitro produced bovine embryos. *Mol. Hum. Reprod.* 8:923–929.

Perez-Iratxeta, C., G. Palidwor, C.J. Porter, N.A. Sanche, M.R. Huska, B.P. Suomela, E.M. Muro, P.M. Krzyzanowski, E. Hughes, P.A. Campbell, et al. 2005. Study of stem cell function using microarray experiments. *FEBS Lett.* 579:1795–1801.

Pergament, E., M. Fiddler, N. Cho, D. Johnson, and W.J. Holmgren. 1994. Sexual differentiation and preimplantation cell growth. *Hum. Reprod.* 9:1730–1732.

Pittenger, M.F., A.M. Mackay, S.C. Beck, R.K. Jaiswal, R. Douglas, J.D. Mosca, M.A. Moorman, D.W. Simonetti, S. Craig, and D.R. Marshak. 1999. Multilineage potential of adult human mesenchymal stem cells. *Science*. 284:143–147.

Qu, Z., L. Balkir, J.C. van Deutekom, P.D. Robbins, R. Pruchnic, and J. Huard. 1998. Development of approaches to improve cell survival in myoblast transfer therapy. *J. Cell Biol.* 142:1257–1267.

Qu-Petersen, Z., B. Deasy, R. Jankowski, M. Ikezawa, J. Cummins, R. Pruchnic, J. Mytinger, B. Cao, C. Gates, A. Wernig, and J. Huard. 2002. Identification of a novel population of muscle stem cells in mice: potential for muscle regeneration. *J. Cell Biol.* 157:851–864.

Rando, T.A., and H.M. Blau. 1994. Primary mouse myoblast purification, characterization, and transplantation for cell-mediated gene therapy. *J. Cell Biol.* 125:1275–1287.

Rollo, C.D. 2002. Growth negatively impacts the life span of mammals. *Evol. Dev.* 4:55–61.

Sarig, R., Z. Baruchi, O. Fuchs, U. Nudel, and D. Yaffe. 2006. Regeneration and transdifferentiation potential of muscle-derived stem cells propagated as myospheres. *Stem Cells*. 24:1769–1778.

Schultz, E. 1996. Satellite cell proliferative compartments in growing skeletal muscles. *Dev. Biol.* 175:84–94.

Sherley, J.L., P.B. Stadler, and J.S. Stadler. 1995. A quantitative method for the analysis of mammalian cell proliferation in culture in terms of dividing and non-dividing cells. *Cell Prolif.* 28:137–144.

Steinlein, P., O. Wessely, S. Meyer, E.M. Deiner, M.J. Hayman, and H. Beug. 1995. Primary, self-renewing erythroid progenitors develop through activation of both tyrosine kinase and steroid hormone receptors. *Curr. Biol.* 5:191–204.

Stindl, R. 2004. Tying it all together: telomeres, sexual size dimorphism and the gender gap in life expectancy. *Med. Hypotheses*. 62:151–154.

Suzuki, K., B. Murtuza, J.R. Beauchamp, R.T. Smolenski, A. Varela-Carver, S. Fukushima, S.R. Coppen, T.A. Partridge, and M.H. Yacoub. 2004. Dynamics and mediators of acute graft attrition after myoblast transplantation to the heart. *FASEB J.* 18:1153–1155.

Tamaki, S., T. Ichinohe, K. Matsuo, N. Hamajima, N. Hirabayashi, and H. Dohy. 2001. Superior survival of blood and marrow stem cell recipients given maternal grafts over recipients given paternal grafts. *Bone Marrow Transplant.* 28:375–380.

Vina, J., C. Borras, J. Gambini, J. Sastre, and F.V. Pallardo. 2005. Why females live longer than males: control of longevity by sex hormones. *Sci. Aging Knowledge Environ*. 2005:pe17.

Wagers, A.J., and I.M. Conboy. 2005. Cellular and molecular signatures of muscle regeneration: current concepts and controversies in adult myogenesis. *Cell*. 122:659–667.

Winitsky, S.O., T.V. Gopal, S. Hassanzadeh, H. Takahashi, D. Gryder, M.A. Rogawski, K. Takeda, Z.X. Yu, Y.H. Xu, and N.D. Epstein. 2005. Adult murine skeletal muscle contains cells that can differentiate into beating cardiomyocytes in vitro. *PLoS Biol.* 3:e87.

Xu, K.P., B.R. Yadav, W.A. King, and K.J. Betteridge. 1992. Sex-related differences in developmental rates of bovine embryos produced and cultured in vitro. *Mol. Reprod. Dev.* 31:249–252.

Zammit, P., and J. Beauchamp. 2001. The skeletal muscle satellite cell: stem cell or son of stem cell? *Differentiation*. 68:193–204.

# STEM CELL-MEDIATED MUSCLE HEALING: EFFECT OF CELL AGE AND SEX ON FIBROSIS AND REGENERATION

*Liu, T; *Deasy, B; *Li, Y; +*Huard, J
+*Growth and Development Laboratory, Children's Hospital of Pittsburgh and Department of Orthopaedic Surgery, University of Pittsburgh, Pittsburgh, PA
jhuard@pitt.edu

## INTRODUCTION

Muscle-derived stem cells (MDSCs) are a potential cell source for many tissue engineering and cell therapy applications in orthopaedics. Members of our laboratory are working to identify the optimal cell phenotype for particular applications. While working with our model of muscle injury and fibrosis, we have identified 2 important variables—cell age and cell sex—that researchers should consider when developing cell therapies for fibrosis prevention. Fibrosis, or fibrous scar tissue formation, involves the deposition of extracellular matrix that disrupts the healing of muscle tissue and restoration of its healthy architecture. Our findings here demonstrate a statistical relationship between fibrosis and muscle regeneration, which appear to be mutually exclusive. Our results also reveal relationships of both cell age and cell sex with both fibrosis and muscle regeneration.

## MATERIALS AND METHODS

***MDSC isolation.*** MDSCs were isolated from normal 3- week-old mice by the preplate technique. ***Cell age:*** To obtain aged cells, MDSCs were expanded in culture as previously described; routine subculturing techniques were used to culture the cells continuously for 6 months. Quantitation was performed to record the population doubling (PD) level as a measure of cell age. ***Cell sex:*** Both male MDSCs (M-MDSCs) and female MDSCs (F-MDSCs) were obtained; cell sex was confirmed by fluorescent in situ hybridization for the X and Y chromosomes.

***Fibrosis and muscle regeneration:*** MDSCs were transplanted into the gastrocnemius of *mdx* mice, which lack the dystrophin protein. Mice were sacrificed 2 weeks after transplantation, and the muscles were isolated, frozen, and sectioned. Sections were immunostained to detect dystrophin expression. The degree of muscle regeneration was determined by calculating a regeneration index (RI): the number of dystrophin-positive fibers/$10^5$ donor cells. Trichrome staining was performed on tissue sections to assess the degree of muscle fibrosis. Trichrome staining reveals the collagen content of the muscle tissue by staining cell nuclei black, muscle fibers red, and collagen blue. Five nonconsecutive sections throughout the muscles were analyzed for fibrosis by a blinded investigator. Northern Eclipse imaging software was used to quantify the area of fibrosis. Statistical relationships between the degree of regeneration and fibrosis and between both of those variables and cell age and cell sex were determined by linear regression and correlation analyses. Statistically significant differences were identified by a Student's *t* test and 2-way ANOVA (SigmaStat version 2.0).

## RESULTS

The degree of muscle regeneration and that of fibrosis were inversely proportional (Fig. 1). In muscles exhibiting increased fibrosis, there was a clear trend toward lower regeneration, regardless of donor cell sex or donor cell age.

Our analysis of the effect of in vitro cell age on the RI revealed a large drop in the RIs as the cells aged in vitro (Fig. 2A and *Mol Biol Cell, 7: 3323, 2005*). We also observed a large amount of skeletal muscle fibrosis in the muscles that received donor cells of higher in vitro ages (Fig. 2B).

Other members of our laboratory have observed that the transplantation of M-MDSCs results in a lower level of skeletal muscle regeneration than does the transplantation of F-MDSCs (Fig. 3A). We found that the muscle injected with M-MDSCs displayed more fibrosis than did muscle injected with F-MDSCs.

These findings support the notion that skeletal muscle fibrosis might prevent proper skeletal muscle healing and could explain the lower RIs exhibited by M-MDSCs and MDSCs expanded in culture.

## CONCLUSION

Both age and sex are major determinants in the ability of MDSCs to promote tissue repair and regeneration. The results presented here indicate that increased fibrosis might explain the reduced in vivo muscle regeneration capacity of M-MDSCs and MDSCs subjected to long-term expansion in culture. Our findings indicate that the prevention of fibrosis will increase the regeneration capacity of stem cells injected in skeletal muscle.

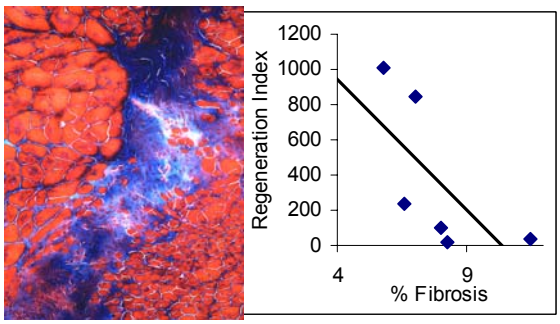


**Figure 1:** A) Fibrosis analysis by Trichrome staining. B) Plot of percent fibrosis vs. regeneration.

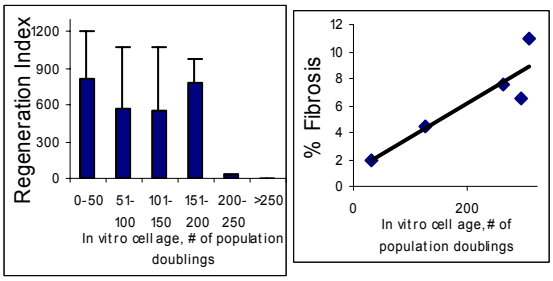


**Figure 2**

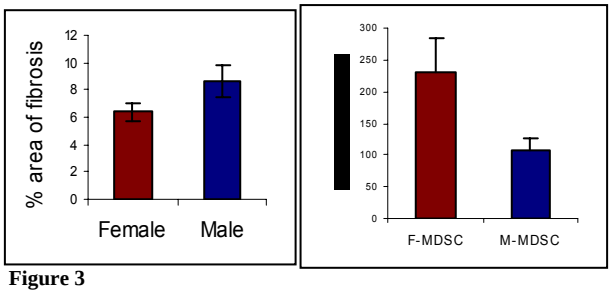


**Figure 3**

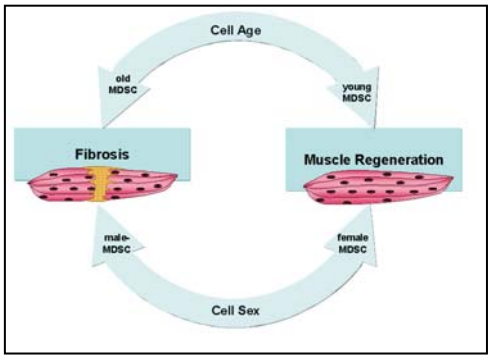


**Figure 4:** Schematic of the relationship between fibrosis and muscle regeneration and the roles of cell age and cell sex.

## ACKNOWLEDGMENTS

The authors are grateful for the funding support provided by the Jesse Journey Foundation, the Muscular Dystrophy Association, the NIH (R01 AR049684), the Hirtzel Foundation, the Henry J. Mankin Endowed Chair for Orthopaedic Research at the University of Pittsburgh, and the William F. and Jean W. Donaldson Chair at Children's Hospital of Pittsburgh.

Appendix 7

# Decorin Gene Transfer Promotes Muscle Cell Differentiation and Muscle Regeneration

Yong Li[1,2,3], Juan Li[2], Jinghong Zhu[1], Bin Sun[1], Maria Branca[1], Ying Tang[1], William Foster[1], Xiao Xiao[2] and Johnny Huard[1,2,4]

[1]*Stem Cell Research Center, Children's Hospital of Pittsburgh, Pittsburgh, Pennsylvania, USA;* [2]*Department of Orthopaedic Surgery, University of Pittsburgh, Pittsburgh, Pennsylvania, USA;* [3]*Department of Pathology, University of Pittsburgh, Pittsburgh, Pennsylvania, USA;* [4]*Department of Molecular Genetics and Biochemistry, University of Pittsburgh, Pittsburgh, Pennsylvania, USA*

We have shown that decorin, a small leucine-rich proteoglycan, can inhibit transforming growth factor (TGF)-$\beta$1 to prevent fibrous scar formation and improve muscle healing after injury. In the decorin-treated muscle, an enhancement of muscle regeneration is observed through histological examination. In this article, we report our determination of whether decorin has a direct effect on myogenic cells' differentiation. Our results indicate that myoblasts genetically engineered to express decorin (CD cells) differentiated into myotubes at a significantly higher rate than did control myoblasts (C2C12). This enhanced differentiation led to the up-regulation of myogenic genes (*Myf5*, *Myf6*, *MyoD*, and myogenin) in CD cells in vitro. We speculate that the higher rate of differentiation exhibited by the CD cells is due to the up-regulation of follistatin, peroxisome-proliferator-activated receptor-gamma co-activator-1$\alpha$ (PGC-1$\alpha$), p21, and the myogenic genes, and the down-regulation of TGF-$\beta$1 and myostatin. Decorin gene transfer *in vivo* promoted skeletal muscle regeneration and accelerated muscle healing after injury. These results suggest that decorin not only prevents fibrosis but also improves muscle regeneration and repair.

*Received 13 November 2006; accepted 20 May 2007; published online 3 July 2007. doi:10.1038/sj.mt.6300250*

## INTRODUCTION

Decorin, a small leucine-rich proteoglycan, is a component of the extracellular matrix of all collagen-containing tissues.[1] Decorin is pivotal in regulating the proper assembly of collagenous matrices and in controlling cell proliferation under various conditions.[2] On the basis of its ability to bind fibrillar collagen and delay *in vitro* fibrillogenesis, decorin is regarded as a key modulator of matrix assembly.[3,4] This proteoglycan can modulate the bioactivity of growth factors and act as a direct signaling molecule to different cells.[5] Decorin, which is expressed at high levels in skeletal muscle during early development,[6] also interferes with muscle cell differentiation and migration and regulates connective tissue formation in skeletal muscle.[7–9]

Because terminal differentiation is critical for initial skeletal muscle development and regeneration after injury and disease,[10] we examined decorin's role in remodeling healing skeletal muscle. We have shown that the direct injection of bovine decorin decreased muscle fibrosis and provided nearly complete functional recovery.[11] Decorin blocks fibrosis (mostly by inhibiting transforming growth factor (TGF)-$\beta$ activity), which improves muscle healing. However, the role of decorin in muscle cell differentiation and regeneration is still unknown. Although we hypothesize that decorin's effect on muscle fibrosis may indirectly impact regeneration, we were unable to exclude the possibility that decorin promotes regeneration independent of its effects on fibrosis formation.

Many studies have investigated the mechanism behind the antifibrotic effect of decorin.[3,12–14] Others have shown that hepatocyte growth factor increases decorin production by fibroblasts through the extracellular signal–regulated kinase 1/2, and p38 mitogen-activated protein kinase–mediated pathways.[14] Decorin stimulates the growth of smooth muscle cells under specific conditions and influences the growth of epidermal cells by interacting with epidermal growth factor and its receptors.[15,16] Recent research has shown that decorin can bind both insulin-like growth factor-I and its receptor; this interaction leads to the phosphorylation of protein kinase B (Akt) and p21 expression in endothelial cells.[17]

Decorin also influences muscle cell behavior by interacting with p21, an important cyclin-dependent kinase inhibitor.[18,19] Follistatin and myostatin are involved in the control of muscle mass during development. These two proteins have opposite effects on muscle growth, as documented by genetic models.[21,22] Recent studies have shown that myostatin action is inhibited by decorin,[23] resulting in enhanced healing and reduced fibrosis within myostatin-null mice compared with wild-type mice.[24] A recent study indicates that peroxisome-proliferator-activated receptor-gamma co-activator-1$\alpha$ (PGC-1$\alpha$), is also involved in the muscle healing process and influences muscle fiber–type determination.[25,26] Decorin may also interact with PGC-1$\alpha$ expression in skeletal muscle after injury.

In this study, we investigated the *in vitro* effect of decorin on the differentiation of myoblasts (C2C12) and characterized the *in vitro* and *in vivo* behavior of myoblasts transfected with the

***Correspondence:*** *Johnny Huard, Stem Cell Research Center (SCRC), 4100 Rangos Research Center, 3460 Fifth Avenue, Pittsburgh, Pennsylvania 15213-2583, USA. E-mail: jhuard@pitt.edu*

decorin gene (CD cells). We also studied the influence that decorin over-expression had on myostatin, follistatin, PGC-1$\alpha$, and p21 expression. Using an adeno-associated virus (AAV) vector, we transduced the decorin gene into injured skeletal muscle to further investigate its function on muscle healing. Our overall goal in this study was to determine whether decorin could improve skeletal muscle healing by enhancing muscle regeneration independently of its antifibrotic action.

## RESULTS

### Genetic engineering of myogenic cells to over-express decorin

We used lipofectin to transfect a pAAV-CMV-decorin plasmid (**Figure 1a**) into both 293 cells (packaging cell line) and C2C12 cells (myoblast cell line). The results of western blot analysis (**Figure 1b**) showed decorin in both the supernatant (culture media) and the lysate of the 293 cells 48 hours after transfection. The transfected C2C12 cells (CD clone cells) expressed decorin (**Figure 1c:** lane 2, 24 hours; lane 4, 48 hours; lane 5, decorin-positive control), whereas non-transfected C2C12 cells did not (**Figure 1c:** lane 1, 24 hours; lane 3, 48 hours). We also detected decorin in both myoblasts (C2C12) and muscle-derived stem cells after mDecorin-AAV (mDec-AAV) gene transfer *in vitro* (**Figure 1d** and **e**).

### Decorin stimulates myoblast differentiation *in vitro*

To investigate myoblast differentiation, we compared decorin-co-cultured C2C12 cells with non-treated C2C12 cells *in vitro*. C2C12 cells cultured with decorin (10 μg/mL) and grown in differentiation/fusion medium exhibited significantly enhanced differentiation and fusion *in vitro*. After 3 and 4 days of stimulating C2C12 cells with decorin, we observed a significant increase in the number of myotubes when compared with un-stimulated C2C12 (control) cells ($P < 0.01$ at 3 days and $P < 0.05$ at 4 days, respectively). However, the numbers of myotubes 5 days after treatment were not significantly different (**Figure 2a**). We then evaluated whether CD cells exhibited a greater propensity to undergo myogenic differentiation than did non-transfected C2C12 cells. As shown in **Figure 2b** (myotubes stained in mouse anti-myosin heavy chain are red) and **Figure 2c**, CD cells generated significantly more myotubes overall and created significantly larger myotubes than did non-transfected C2C12 cells.

### Decorin increases myoblast differentiation and induces myogenic gene expression *in vitro*

We investigated whether the CD cells expressed higher levels of myogenic genes than did non-transfected C2C12 (control) cells. Our results, shown in **Figure 3a**, demonstrate that decorin gene transfer led to higher expression of the myogenic genes *Myf5*, *Myf6*, *MyoD*, and *myogenin*. Desmin expression levels in CD and C2C12 cells remained similar.

### Decorin up-regulates p21, follistatin, and PGC-1$\alpha$, but down-regulates TGF-$\beta$1 and myostatin in C2C12

We also performed experiments designed to investigate the mechanism by which decorin influences the differentiation of muscle cells. We found that CD cells exhibited increased p21 expression and decreased myostatin expression (**Figure 3b**). The C2C12 cells can be induced to express TGF-$\beta$1 in an autocrine manner, as we have previously determined;[27] however, the CD cells do not show any detectable expression of TGF-$\beta$1 after

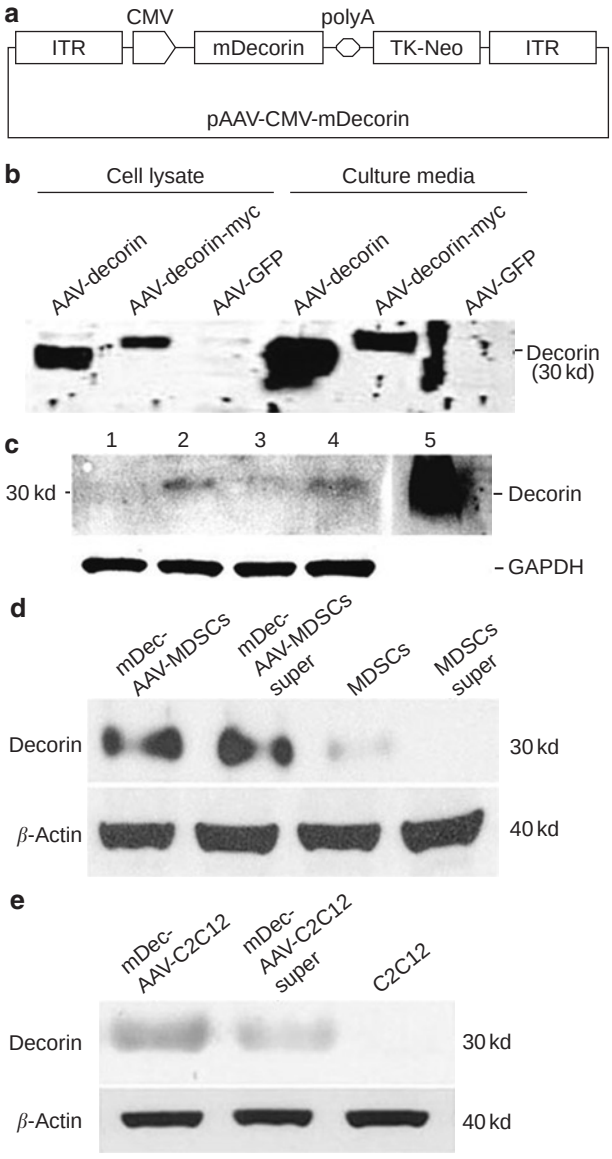


**Figure 1 Decorin plasmid construction and initial transfection *in vitro*.** (**a**) The decorin plasmid used for the study contained the full sequence of a mouse decorin gene inserted at the *Not*I site, which placed it under the control of a cytomegalovirus (CMV) promoter. (**b**) We transfected the plasmid into 293 cells. We observed decorin expression in both the 293 cells and their supernatant, but not in the control adeno-associated virus (AAV)–transfected (green fluorescent protein, GFP) cells. (**c**) Western blot analysis also revealed decorin expression in CD clone cells within different time period cultures (lane 2, 24 hours; lane 4, 48 hours), but not in C2C12 (lane 1, 24 hours; lane 3, 48 hours). We used 5 μg of decorin as a positive control (lane 5). GAPDH, glyceraldehyde-3-phosphate dehydrogenase is used as a control. (**d**) Decorin expression in muscle-derived stem cells (MDSCs) in pellet form was low, but this was not the case in the supernatant. Both MDSCs and their cultured supernatant strongly expressed decorin after mDec-AAV gene transfer. $\beta$-actin is used as a control. (**e**) We did not detect decorin in normal C2C12 cells, but C2C12 cells and their cultured supernatant both expressed decorin after mDec-AAV gene transfer.

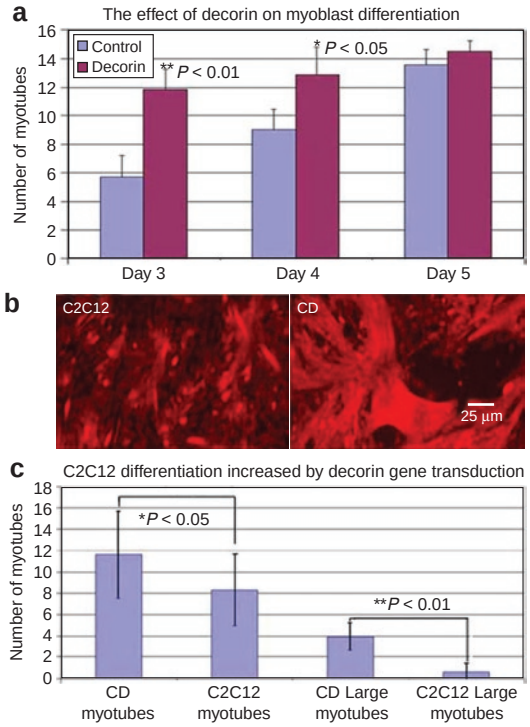


**Figure 2 Decorin stimulates C2C12 differentiation *in vitro*.** (**a**) Decorin treatment accelerated the differentiation and fusion of myoblasts (C2C12 cells) compared with non-treated myoblasts (C2C12 cells). (**a**) The cultures of decorin-treated C2C12 cells contained more myotubes at the 3- and 4-day time points than control cells. (**b**, **c**) Similarly, decorin-transfected C2C12 clone cells (CD cells) produced more myotubes than did C2C12 cells, including larger myotubes (containing more than three nuclei) *in vitro*. Red staining shows myosin heavy chain fluorescence after immunostaining (**b**).

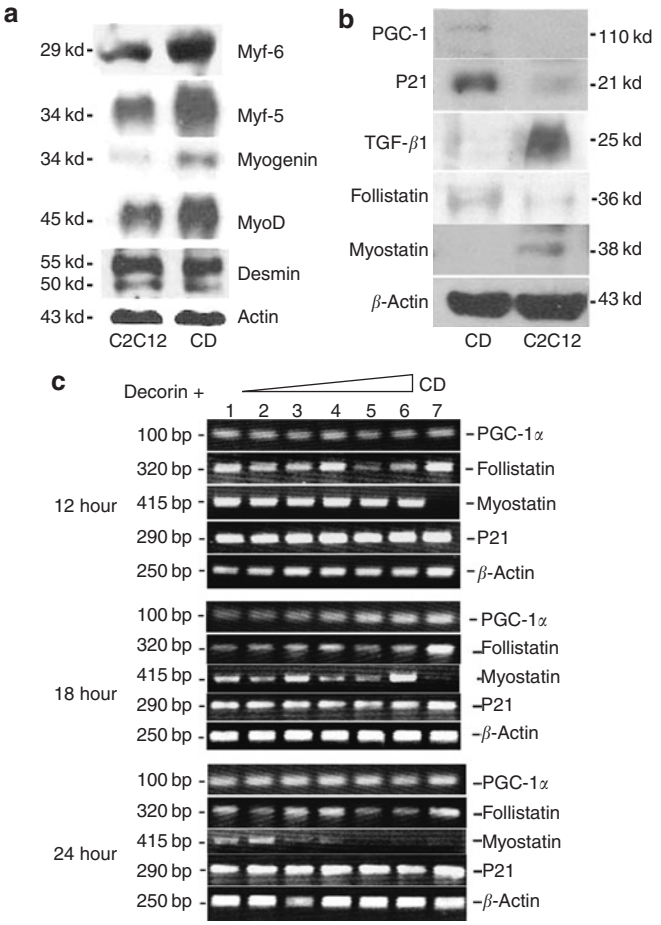


**Figure 3 Decorin gene transfer up-regulates myogenic proteins and p21 and down-regulates myostatin during muscle cell differentiation.** (**a**) Genetic engineering of myoblasts to express decorin influenced the expression of myogenic proteins (including Myf5/6, Myogenin, and MyoD), as shown by western blot results. However, C2C12 cells and CD clone cells expressed comparable levels of desmin. (**b**) We detected the presence of p21 expressed in CD clone cells. We also detected peroxisome-proliferator-activated receptor-gamma co-activator-1α (PGC-1α) and follistatin expressed in CD, but not C2C12, cells. In addition, CD cells exhibited lower levels of myostatin, a negative regulator of muscle mass. The induction of tumor growth factor (TGF)-β1 auto-expression was also inhibited by decorin over-expression in CD cells. (**c**) Similar results were obtained by real-time polymerase chain reaction. Lanes 1–6 show results for C2C12 cells exposed to different concentrations of decorin (0, 0.001, 0.01, 0.1, 1.0, and 5.0 ng/ml, respectively). Lane 7 displays the test results for CD cells, which served as the positive control. We did not detect a visible change in the expression of PGC-1α, follistatin, myostatin, or p21 after 12 hours of stimulation with different concentrations of decorin. PGC-1α and follistatin were up-regulated in C2C12 cells in a dose-dependent manner after 18 hours of stimulation with decorin. Myostatin was down-regulated in C2C12 cells in a dose-dependent manner after 24 hours of decorin stimulation. The concentration of p21 did not visibly change after cell stimulation with any experimental concentration of decorin over all time points. With decorin gene transfer, we found that CD cells consistently expressed follistatin, p21, and PGC-1α but were negative for myostatin. Note that β-actin was selected as a positive gene control.

TGF-β1 stimulation. More importantly, we detected that both follistatin and PGC-1α (**Figure 3b**) had been up-regulated when compared with C2C12 cells. We also discovered that follistatin and PGC-1α messenger RNA were altered in C2C12 cells after decorin stimulation, as determined by real-time polymerase chain reaction. Specifically, we found that PGC-1α and follistatin increased in a dose-dependent manner after 18 hours of stimulation with decorin, and that myostatin was decreased in a dose-dependent manner after 24 hours of stimulation with decorin (**Figure 3c**). In CD cells, we also observed increased amounts of all three genes (*p21*, *follistatin*, and *PGC-1α*), but a decrease in myostatin was observed (**Figure 3c**).

The up-regulation of *follistatin*, *PGC-1α*, *p21*, and myogenic genes, including *MyoD* (**Figure 3a**), in CD cells could at least partially explain how decorin promotes muscle cell differentiation. Alternatively, the down-regulation of myostatin, a well-known negative regulator of muscle growth during muscle regeneration, could also benefit muscle cell differentiation.

## The implantation of CD cells in skeletal muscle results in improved muscle regeneration

The implantation of CD cells within skeletal muscle resulted in significantly better muscle regeneration than that observed for control C2C12 cells, as determined 4 weeks after injection of the cells into *MDX*/SCID mice. Although the number of LacZ-positive muscle fibers (*i.e.*, regenerating muscle fibers) did not differ between the groups (**Figure 4a**, **c**, and **d**), the diameters of the regenerating muscle fibers (*e.g.*, dystrophin-positive myofibers) in the muscles injected with CD cells were significantly larger than those of the regenerating muscle fibers in the control muscles

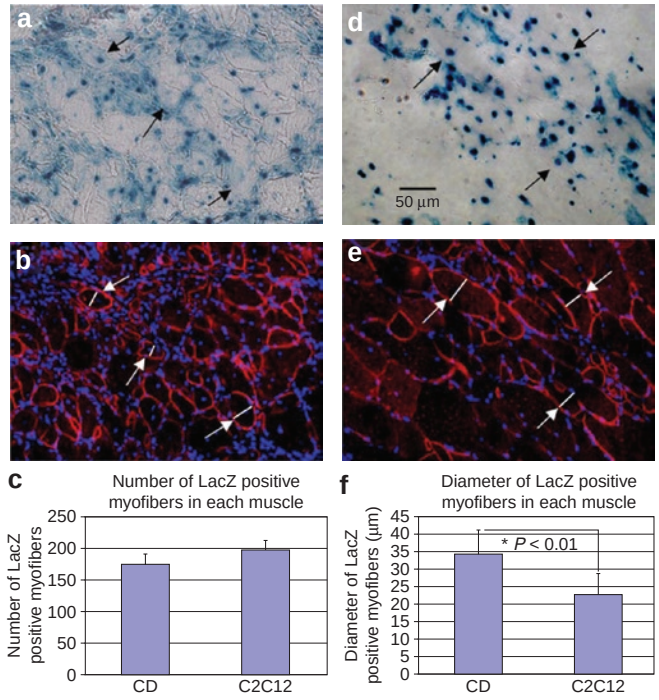


**Figure 4 Decorin gene transfer stimulates muscle regeneration *in vivo*.** C2C12 cells regenerated muscle fibers after transplantation into skeletal muscle of *MDX*/SCID mice, as shown on both (**a**) LacZ- and (**b**) dystrophin-expressing myofibers. However, transplantation of CD clone cells, rather than C2C12 cells, resulted in larger muscle fibers in *MDX*/SCID mice, as shown in some of the (**d**) LacZ- and (**e**) dystrophin-positive myofibers. (**c**) Although there was no significant difference between the number of LacZ-labeled muscle fibers that formed in muscles transplanted with C2C12 or CD cells, (**f**) the transplantation of CD cells resulted in the regeneration of larger-diameter myofibers ($P < 0.01$).

(**Figure 4b**, **e**, and **f**; dystrophin is red). The larger diameters of the dystrophin-positive muscle fibers generated by CD cells could indicate that implantation of CD cells accelerated muscle regeneration; however, we were unable to exclude the possibility that the CD cells may have a greater propensity to fuse in host myofibers than C2C12 control cells.

## mDec-AAV gene transfer promotes muscle regeneration and reduces fibrosis

Better muscle regeneration was observed within mDec-AAV-treated muscle (**Figure 5a** and **b**) than within non-mDec-AAV-treated muscle at 2 weeks after injury (**Figure 5c** and **d**). Histological analysis of total collagen deposition 4 weeks after injury revealed that mDec-AAV-injected muscles contained less fibrous scar tissue in the injured area than did non-treated control muscles (**Figure 5f**, **h**, and **j**; collagen deposition areas are blue). We also observed that decorin stimulated skeletal muscle regeneration 4 weeks after laceration injury. We found that mDec-AAV-injected muscles contained more centronucleated (regenerating) myofibers and less scar tissue 4 weeks after injury than did control muscles (**Figure 5e**, **g**, and **i**).

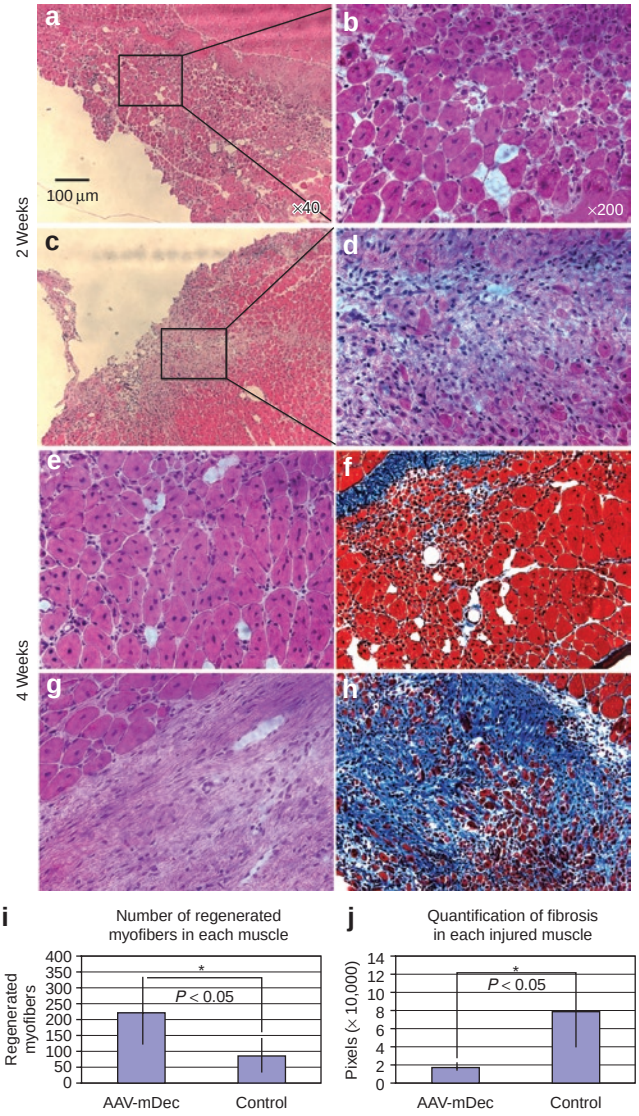


**Figure 5 mDec-AAV vector gene therapy in injured muscle prevents fibrosis and promotes muscle regeneration.** Decorin-treated muscle exhibits a greater number of regenerating myofibers than the control muscle at all time points (**a–d** 2 weeks; **e–h** 4 weeks). (**i**) The mDec-AAV-injected muscle contained significantly higher numbers of centronucleated (regenerated) myofibers than did control (sham-injected) muscle at 4 weeks after therapy. We also found that decorin gene therapy minimized fibrosis in injured skeletal muscle. We used Masson's trichrome staining to reveal collagen in injured skeletal muscle, the results of which show that (**f**) mDec-AAV-injected muscle contained significantly less fibrosis in the injured area than did the (**h**) control muscle at (**j**) 4 weeks after injury.

## DISCUSSION

Results from these experiments show that decorin is able to activate the differentiation of skeletal muscle cells (C2C12) *in vitro* and enhances muscle regeneration in two mouse models *in vivo*. The mechanism behind decorin's accelerated muscle healing is not yet known; however, our results demonstrate that decorin up-regulates the expression of PGC-1$\alpha$, follistatin, p21, and a variety of myogenic proteins (including MyoD) but down-regulates myostatin expression. These results, in addition to decorin's ability to neutralize the effects of TGF-$\beta$1, likely explain the beneficial action that decorin has on muscle cell differentiation and muscle regeneration.

Our previous studies have demonstrated that myogenic cells (including muscle-derived stem cells) in injured muscle can

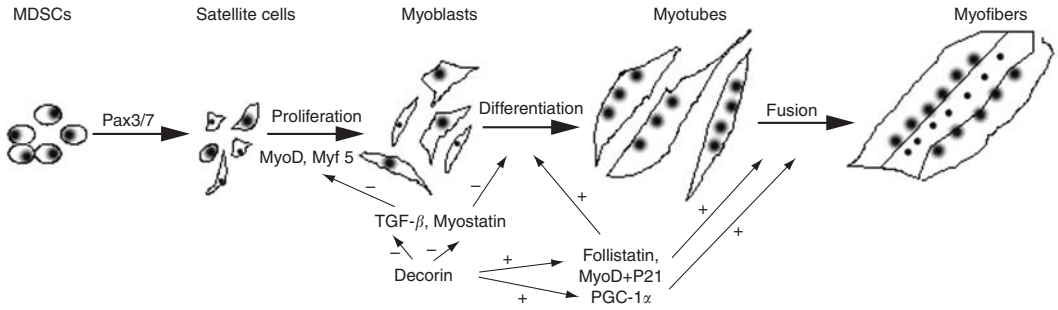


**Figure 6 Schematic of the potential effect of decorin on muscle healing.** Decorin may improve muscle healing through various pathways: inhibition of tumor growth factor (TGF)-$\beta$1, up-regulation of follistatin, peroxisome-proliferator-activated receptor-gamma co-activator-1$\alpha$ (PGC-1$\alpha$), p21, and myogenic genes (such as *MyoD*), and down-regulation of myostatin expression. MDSCs, muscle-derived stem cells.

differentiate into fibrotic cells and that TGF-$\beta$1 is a major stimulator of this differentiation.[27,28] Using different animal models of muscle injury, we have investigated biological approaches to prevent fibrosis and thereby improve muscle healing.[11,27,29–31] We have used various molecules, such as decorin, that impede fibrosis by blocking TGF-$\beta$1 to facilitate the near-complete recovery of injured skeletal muscle.[11] The ability of decorin to inhibit TGF-$\beta$1 activity is the likely mechanism by which this molecule blocks fibrosis formation. However, our results indicate that the improved muscle healing observed after decorin treatment is due to both its inhibiting effect on fibrosis and its stimulating effect on muscle regeneration. **Figure 6** summarizes the potential effect of decorin on muscle healing.

The repair of injured skeletal muscle occurs through the activation of muscle precursor cells located between the basal lamina and the sarcolemma, including satellite cells and stem cells.[32] The activation and growth of these cells are regulated by various growth factors released by infiltrating lymphocytes, injured myofibers, and the extracellular matrix.[10,32] Some growth factors, such as insulin-like growth factor-1 and hepatocyte growth factor, can stimulate precursor cell proliferation and differentiation by increasing the transcriptional activity of the muscle basic helix–loop–helix.[33–36] Healing and organizational processes are dependent upon the extra- and intracellular signaling that induces the expression of myogenic genes, including *MyoD*, *Myf5*, and *myosin*.[37,38] When properly stimulated, precursor cells fuse with one another or with local myofibers to repair the damaged muscle.[39]

Muscle regeneration, the key event in muscle healing, is often incomplete, particularly in severely injured muscle.[10,11,27,28,32,40] The overgrowth of the extracellular matrix leads to significant local fibrosis (*i.e.*, fibrous scar formation) in the injured area, which can impede the formation of normal muscle fibers. The presence of fibrous scar tissue in injured muscle results in incomplete functional recovery and a propensity for re-injury.[41] Muscle regeneration and fibrosis in injured muscle often occur simultaneously and thus compete with one another during the muscle healing process.[32,36,40] A persistent imbalance between collagen biosynthesis and degradation contributes to hypertrophic scar formation and fibrosis in many tissues.[42,43] Several studies have revealed high levels of collagen in injured regions of skeletal muscle, and shown that inhibition of collagen deposition reduced the formation of scar tissue in injured skeletal muscle.[27,28,30,31]

Interactions between decorin and TGF-$\beta$1 have been observed in many tissues, and researchers have used various animal models to study the antifibrotic effect of decorin.[3,11,13,44] Researchers have also shown that hepatocyte growth factor can increase the level of decorin expression in fibroblasts, perhaps by activating the extracellular signal–regulated kinase 1/2 and p38 mitogen-activated protein kinase–mediated pathways.[14] Such findings could explain the antifibrotic effect of hepatocyte growth factor in a variety of tissues.[14,45–47] In endothelial cells, decorin binds with both insulin-like growth factor-I and its receptor to influence cell behavior.[17] Decorin can also control and suppress cancer growth and invasion, presumably by influencing the biological activity of growth factors such as TGF-$\beta$1, platelet-derived growth factor, vascular endothelial growth factor, and epidermal growth factor, all of which are released by cancer cells.[5,15] These decorin-induced effects appear to be mediated, at least in part, by a specific interaction between the decorin protein core and the epidermal growth factor receptor.[15,16] This interaction triggers a signal cascade that results in activation of mitogen-activated protein kinase, mobilization of intracellular calcium, up-regulation of p21, and, ultimately, the suppression of tumor growth.[18,19]

Cell cycle exit and the differentiation of muscle cells are coordinated by p21, which is essential for normal myogenic progenitor cell differentiation and skeletal muscle regeneration. Studies have indicated that p21 is necessary for MyoD-induced activity in cells, allowing them to enter into and be stabilized in a postmitotic state. Since MyoD plays a central role in the differentiation of muscle cells, TGF-$\beta$1 controls myostatin-related regulation of myogenesis in muscle cells by down-regulating both p21 and MyoD. In this study, we determined that the treatment of myoblasts with decorin down-regulated the expression of myostatin, which might influence p21 and myogenic protein expression. In addition, myostatin and follistatin interact directly in the skeletal muscle system. Follistatin can inhibit myostatin, leading to muscle differentiation in a concentration-dependent manner.[21] PGC-1$\alpha$, which is expressed in several tissues, including brown fat and the skeletal muscle of mammals, activates mitochondrial biogenesis and oxidative metabolism.[26] PGC-1$\alpha$ is a principal factor involved in determining muscle fiber type in injured skeletal muscle and is involved in exercise-induced mitochondrial biogenesis.[48] In this experiment, we observed that decorin treatment increased PGC-1$\alpha$ expression in skeletal muscle cells. Combined with our previous research results, our current findings suggest that decorin not

only acts as an antifibrotic agent but also enhances muscle regeneration in skeletal muscle.

Successful muscle differentiation during limb development requires decorin expression.[6] Previous findings have shown that decorin can improve muscle healing by inhibiting fibrosis and that myoblasts and muscle satellite cells expressing decorin in an injured site regenerated damaged myofibers faster than the controls.[11,27] The results of this study demonstrate that decorin is also a potent stimulator of skeletal muscle regeneration. Myoblasts expressing decorin differentiated and fused to form myotubes and myofibers at a significantly higher rate than did normal myoblasts *in vitro* and *in vivo*. We attribute this enhanced differentiation to the up-regulation of p21, follistatin, PGC-1$\alpha$, and myogenic gene expression and the down-regulation of TGF-$\beta$1 and myostatin. These results provide at least a partial explanation of the way in which decorin promotes muscle regeneration and may explain why there is such a high level of decorin expression in developing skeletal muscle. It is possible that decorin increases muscle fiber growth and limits the overgrowth of connective tissues. These findings indicate that decorin could be very useful in promoting the healing of muscles damaged by injury or disease.

## MATERIALS AND METHODS

***Gene transfection and transfer.*** An AAV-mDecorin plasmid, which encodes for a mouse decorin sequence under the control of the cytomegalovirus promoter (**Figure 1**), was used for gene transfection. This plasmid also contains a neomycin resistance gene to enable G418 selection. The AAV-mDecorin plasmid was transfected into 293 packaging cells and C2C12 cells with lipofectin; clone cells were selected for treatment of the cells with G418 (500 μg/mL) (Gibco BRL, Grand Island, NY) for 2 weeks. The selected decorin-transfected C2C12 clone cells (CD cells) were cultured in Dulbecco's modified Eagle's medium (Gibco BRL, Grand Island, NY) containing the same concentration of G418 for the remainder of the project.

The mDec-AAV vector was produced by co-transfection methods described previously by Dr. Xiao.[49] Muscle-derived stem cells and myoblasts (C2C12 cells) were each grown to 50–60% confluency. Fresh Dulbecco's modified Eagle's medium (without fetal bovine serum or penicillin/streptomycin) containing the mDec-AAV vector ($5 \times 10^4$ particles/cell) was then added directly to the cells. The cultures were incubated at 37 °C in a 5% $CO_2$ incubator for 1 hour. Normal culture medium (Dulbecco's modified Eagle's medium supplemented with 10% fetal bovine serum and 1% Abs) was then added for another 24 hours, at which point the cells were collected for analysis of decorin expression by western blotting.

***Differentiation of myoblasts and immunocytochemistry.*** Three different groups of cells (C2C12 cells, C2C12 cells cultured with decorin, and CD cells) were seeded into 12-well plates containing proliferation medium.[28] All cells were transferred into serum-free medium 12 hours later to induce differentiation. The myotubes that formed in the cultures were counted daily for 5 days, and the numbers were compared among the groups. We considered myotubes containing three or more nuclei to be large myotubes *in vitro*. At different time points, the cells were fixed with cold acetone (3 minutes) for immunostaining. Mouse anti-myosin heavy chain antibody (Novocastra Lab) at a 1:200 dilution was applied for 1 hour at room temperature (RT). The primary antibody was detected using anti-mouse-Cy3, 1:250 for 45 minutes at RT. Results were analyzed by fluorescent microscopy (Nikon microscope, Nikon, Melville, New York).

***Real-time polymerase chain reaction.*** Total RNA was extracted from the treated and non-treated C2C12 cells using a Nucleospin column (Clontech, Mountan View, CA), and the complementary DNA was synthesized with SuperScript II reverse transcriptase (Invitrogen, Carlsbad, CA), both according to manufacturer's instructions. Primers specific for *myostatin*, *follistatin*, *p21*, and *PGC-1α* were designed using Oligo software (OligoPerfect Designer; Invitrogen, Carlsbad, CA). The protocol for amplification was as follows: 94 °C for 30 seconds, 58 °C for 30 seconds, and 72 °C for 30 seconds for 30 cycles. Polymerase chain reaction products were separated by size in a 1.5% agarose gel.

***Western blot analysis.*** C2C12 and CD cells were lysed when cell density reached 70% confluency. The samples were separated on a 12% sodium dodecyl sulfate–polyacrylamide electrophoresis gel and transferred to nitrocellulose membranes used to perform immunostaining. The primary antibodies were anti-decorin (a gift from Dr. Fisher of the National Institutes of Health), anti-TGF-$\beta$1 (4 μg/mL; BD Pharmingen, San Diego, CA), anti-p21 (BD Pharmingen, San Diego, CA), anti-myf5, anti-myf6, anti-MyoD, and anti-myogenin (Santa Cruz Bio, Santa Cruz, CA), all at concentrations of 1:1,000, and anti-myostatin, anti-follistatin (Chemicon, Temecula, CA), and anti-desmin (Sigma, St. Louis, MO), all at concentrations of 1:2,000 for 1 hour at RT. Mouse anti-$\beta$-actin and anti-glyceraldehyde-3-phosphate dehydrogenase (Sigma, St. Louis, MO) were used for protein quantification and were diluted to 1:8,000. The secondary anti-rat horseradish peroxidase or anti-rabbit horseradish peroxidase (Pierce, Rockford, IL) was used at a concentration of 1:5,000 for 1 hour. Peroxidase activity was determined by enhanced chemiluminescence (Amersham Pharmacia Biotech, Piscataway, NJ), and the positive bands were detected on X-ray film. Northern Eclipse software v.6.0 (Empix Imaging, Mississauga, Canada) was used to evaluate all results.

***Animal experiments.*** All animal experiments were approved by the Children's Hospital of Pittsburgh. The Animal Research Committee at the authors' institution approved all experimental protocols (No. 15/03).

*Group 1: C2C12 and CD cell transplantation.* Twenty-four female *MDX*/SCID mice (C57BL/10ScSn-*Dmd*$^{mdx}$ crossed with C57BL/6J-*Prkdc*$^{scid}$/SzJ, 6–8 weeks of age) were used for the C2C12 and CD cell transplantation. C2C12 and CD clone cells were transduced with a retrovirus vector encoding for LacZ.[27] LacZ-positive CD cells ($1 \times 10^6$) were injected into the left gastrocnemius muscles (GMs); the same quantity of LacZ-positive C2C12 cells were injected into the right GMs as a control. At various times after injection, mice were killed, and the GMs were collected for histological analysis by LacZ staining and immunohistochemistry to stain for dystrophin-positive myofibers.

*Group 2: mDec-AAV gene therapy administered to injured skeletal muscle.* Twenty mice (C57BL6J$^{+/+}$, 6 weeks old; Jackson Laboratory, Bar Harbor, ME) were used for these experiments. The mDec-AAV vector ($2 \times 10^{11}$ particles in 20 μL of Dulbecco's modified Eagle's medium) was injected directly into the left GM of each mouse; the contralateral leg was injected with the same volume of phosphate-buffered saline (20 μL) as a control. One week after injection, both GMs were lacerated in accordance with our previously described muscle injury model.[11,27,28,40] Mice were killed at different time points (5 days and 1, 2, 3, and 4 weeks after injury), and the GMs were collected for histological analysis by either hematoxylin and eosin or Masson's trichrome staining. The regeneration and fibrous scar tissue formation in the two groups were compared.

***Immunohistochemical analysis.*** Serial 10-μm cryostat sections were prepared using standard techniques.[27,28] For immunohistochemistry, the slides were fixed with formalin (4%) for 5 minutes after LacZ staining, and then blocked with donkey serum (10%) for 1 hour. Rabbit anti-dystrophin antibody (Abcam, Cambridge, MA) was applied to the slides at a 1:300 dilution for 60 minutes at RT. The second antibody, goat anti-rabbit IgG (Alexa Fluor® 488; Molecular Probes, Eugene, OR), was used at a concentration of 1:200 for 45 minutes at RT. Negative controls were performed concurrently with all immunohistochemical staining. The nuclei of the sections were revealed using 4′,6′-diamidino-2-phenylindole hydrochloride

staining (Sigma, St. Louis, MO), and fluorescent microscopy was used to visualize the results as described above.

***Statistical analysis.*** LacZ-positive myofibers were counted in 10 representative sections. Both the diameter and number of LacZ- and dystrophin-positive myofibers were assessed at different time points in each group. The statistical significance of differences between the various groups was determined using a *t*-test or one-way or two-way analysis of variance.

## ACKNOWLEDGMENTS

The authors wish to thank James Cummins, Marcelle Pellerin, and Jing Zhou (Stem Cell Research Center, Children's Hospital of Pittsburgh, Pittsburgh, PA) for their technical assistance, Paul Robbins (Department of Molecular Genetics and Biochemistry, University of Pittsburgh School of Medicine, Pittsburgh, PA) for his contribution of the LacZ retrovirus vector, and Ryan Sauder, Shannon Bushyeager, and David Humiston (Stem Cell Research Center) for their excellent editorial assistance with this manuscript. The authors also gratefully acknowledge the financial support of the Department of Defense in the form of grant W81XWH-06-01-0406 and the National Institutes of Health in the form of NIH grant R01 AR47973.

## REFERENCES

1. Hocking, AM, Shinomura, T and McQuillan, DJ (1998). Leucine-rich repeat glycoproteins of the extracellular matrix. *Matrix Biol* **17**: 1–19.
2. Sottile, J, Hocking, DC and Swiatek, PJ (1998). Fibronectin matrix assembly enhances adhesion-dependent cell growth. *J Cell Sci* **111**: 2933–2943.
3. Giri, SN, Hyde, DM, Braun, RK, Gaarde, W, Harper, JR and Pierschbacher, MD (1997). Antifibrotic effect of decorin in a bleomycin hamster model of lung fibrosis. *Biochem Pharmacol* **54**: 1205–1216.
4. Noble, NA, Harper, JR and Border, WA (1992). *In vivo* interactions of TGF-beta and extracellular matrix. *Prog Growth Factor Res* **4**: 369–382.
5. Stander, M, Naumann, U, Dumitrescu, L, Heneka, M, Loschmann, P, Gulbins, E *et al.* (1998). Decorin gene transfer-mediated suppression of TGF-beta synthesis abrogates experimental malignant glioma growth *in vivo*. *Gene Ther* **5**: 1187–1194.
6. Nishimura, T, Futami, E, Taneichi, A, Mori, T and Hattori, A (2002). Decorin expression during development of bovine skeletal muscle and its role in morphogenesis of the intramuscular connective tissue. *Cells Tissues Organs* **171**: 199–214.
7. Brandan, E, Fuentes, ME and Andrade, W (1991). The proteoglycan decorin is synthesized and secreted by differentiated myotubes. *Eur J Cell Biol* **55**: 209–216.
8. Casar, JC, McKechnie, BA, Fallon, JR, Young, MF and Brandan, E (2004). Transient up-regulation of biglycan during skeletal muscle regeneration: delayed fiber growth along with decorin increase in biglycan-deficient mice. *Dev Biol* **268**: 358–371.
9. Yoshida, N, Yoshida, S, Koishi, K, Masuda, K and Nabeshima, Y (1998). Cell heterogeneity upon myogenic differentiation: down-regulation of MyoD and Myf-5 generates 'reserve cells'. *J Cell Sci* **111**: 769–779.
10. Li, Y, Cummins, J and Huard, J (2001). Muscle injury and repair. *Curr Opin Orthop* **12**: 409–415.
11. Fukushima, K, Badlani, N, Usas, A, Riano, F, Fu, F and Huard, J (2001). The use of an antifibrosis agent to improve muscle recovery after laceration. *Am J Sports Med* **29**: 394–402.
12. Harper, JR, Spiro, RC, Gaarde, WA, Tamura, RN, Pierschbacher, MD, Noble, NA *et al.* (1994). Role of transforming growth factor beta and decorin in controlling fibrosis. *Methods Enzymol* **245**: 241–254.
13. Isaka, Y, Brees, DK, Ikegaya, K, Kaneda, Y, Imai, E, Noble, NA *et al.* (1996). Gene therapy by skeletal muscle expression of decorin prevents fibrotic disease in rat kidney. *Nat Med* **2**: 418–423.
14. Kobayashi, E, Sasamura, H, Mifune, M, Shimizu-Hirota, R, Kuroda, M, Hayashi, M *et al.* (2003). Hepatocyte growth factor regulates proteoglycan synthesis in interstitial fibroblasts. *Kidney Int* **64**: 1179–1188.
15. Csordas, G, Santra, M, Reed, CC, Eichstetter, I, McQuillan, DJ, Gross, D *et al.* (2000). Sustained down-regulation of the epidermal growth factor receptor by decorin. A mechanism for controlling tumor growth *in vivo*. *J Biol Chem* **275**: 32879–32887.
16. Iozzo, RV, Moscatello, DK, McQuillan, DJ and Eichstetter, I (1999). Decorin is a biological ligand for the epidermal growth factor receptor. *J Biol Chem* **274**: 4489–4492.
17. Schonherr, E, Sunderkotter, C, Iozzo, RV and Schaefer, L (2005). Decorin, a novel player in the insulin-like growth factor system. *J Biol Chem* **280**: 15767–15772.
18. De Luca, A, Santra, M, Baldi, A, Giordano, A and Iozzo, RV (1996). Decorin-induced growth suppression is associated with up-regulation of p21, an inhibitor of cyclin-dependent kinases. *J Biol Chem* **271**: 18961–18965.
19. Schonherr, E, Levkau, B, Schaefer, L, Kresse, H and Walsh, K (2001). Decorin-mediated signal transduction in endothelial cells. Involvement of Akt/protein kinase B in up-regulation of p21(WAF1/CIP1) but not p27(KIP1). *J Biol Chem* **276**: 40687–40692.
20. Budasz-Rwiderska, M, Jank, M and Motyl, T (2005). Transforming growth factor-beta1 upregulates myostatin expression in mouse C2C12 myoblasts. *J Physiol Pharmacol* **56** (suppl. 3): 195–214.
21. Amthor, H, Nicholas, G, McKinnell, I, Kemp, CF, Sharma, M, Kambadur, R *et al.* (2004). Follistatin complexes Myostatin and antagonises Myostatin-mediated inhibition of myogenesis. *Dev Biol* **270**: 19–30.
22. Lee, SJ and McPherron, AC (2001). Regulation of myostatin activity and muscle growth. *Proc Natl Acad Sci USA* **98**: 9306–9311.
23. Miura, T, Kishioka, Y, Wakamatsu, J, Hattori, A, Hennebry, A, Berry, CJ *et al.* (2006). Decorin binds myostatin and modulates its activity to muscle cells. *Biochem Biophys Res Commun* **340**: 675–680.
24. McCroskery, S, Thomas, M, Platt, L, Hennebry, A, Nishimura, T, McLeay, L *et al.* (2005). Improved muscle healing through enhanced regeneration and reduced fibrosis in myostatin-null mice. *J Cell Sci* **118**: 3531–3541.
25. Duguez, S, Feasson, L, Denis, C and Freyssenet, D (2002). Mitochondrial biogenesis during skeletal muscle regeneration. *Am J Physiol Endocrinol Metab* **282**: E802–E809.
26. Lin, J, Wu, H, Tarr, PT, Zhang, CY, Wu, Z, Boss, O *et al.* (2002). Transcriptional co-activator PGC-1 alpha drives the formation of slow-twitch muscle fibres. *Nature* **418**: 797–801.
27. Li, Y, Foster, W, Deasy, BM, Chan, Y, Prisk, V, Tang, Y *et al.* (2004). Transforming Growth Factor-beta1 Induces the Differentiation of Myogenic Cells into Fibrotic Cells in Injured Skeletal Muscle: A Key Event in Muscle Fibrogenesis. *Am J Pathol* **164**: 1007–1019.
28. Li, Y and Huard, J (2002). Differentiation of muscle-derived cells into myofibroblasts in injured skeletal muscle. *Am J Pathol* **161**: 895–907.
29. Chan, YS, Li, Y, Foster, W, Fu, FH and Huard, J (2005). The use of suramin, an antifibrotic agent, to improve muscle recovery after strain injury. *Am J Sports Med* **33**: 43–51.
30. Chan, YS, Li, Y, Foster, W, Horaguchi, T, Somogyi, G, Fu, FH *et al.* (2003). Antifibrotic effects of suramin in injured skeletal muscle after laceration. *J Appl Physiol* **95**: 771–780.
31. Sato, K, Li, Y, Foster, W, Fukushima, K, Badlani, N, Adachi, N *et al.* (2003). Improvement of muscle healing through enhancement of muscle regeneration and prevention of fibrosis. *Muscle Nerve* **28**: 365–372.
32. Huard, J, Li, Y and Fu, FH (2002). Muscle injuries and repair: current trends in research. *J Bone Joint Surg Am* **84-A**: 822–832.
33. Engert, JC, Berglund, EB and Rosenthal, N (1996). Proliferation precedes differentiation in IGF-I-stimulated myogenesis. *J Cell Biol* **135**: 431–440.
34. McFarland, DC, Pesall, JE and Gilkerson, KK (1993). The influence of growth factors on turkey embryonic myoblasts and satellite cells *in vitro*. *Gen Comp Endocrinol* **89**: 415–424.
35. Sheehan, SM and Allen, RE (1999). Skeletal muscle satellite cell proliferation in response to members of the fibroblast growth factor family and hepatocyte growth factor. *J Cell Physiol* **181**: 499–506.
36. Tatsumi, R Anderson, JE, Nevoret, CJ, Halevy, O and Allen, RE (1998). HGF/SF is present in normal adult skeletal muscle and is capable of activating satellite cells. *Dev Biol* **194**: 114–128.
37. Beauchamp, JR, Heslop, L, Yu, DS, Tajbakhsh, S, Kelly, RG, Wernig, A *et al.* (2000). Expression of CD34 and Myf5 defines the majority of quiescent adult skeletal muscle satellite cells. *J Cell Biol* **151**: 1221–1234.
38. Chambers, RL and McDermott, JC (1996). Molecular basis of skeletal muscle regeneration. *Can J Appl Physiol* **21**: 155–184.
39. Bischoff, R (1994). The satellite cell and muscle regeneration. In Engel, AG and Franzini-Armstrong, C (eds). *Myology: Basic and Clinical.* McGraw-Hill, New York. pp. 97–118.
40. Shen, W, Li, Y, Tang, Y, Cummins, J and Huard, J (2005). NS-398, a cyclooxygenase-2-specific inhibitor, delays skeletal muscle healing by decreasing regeneration and promoting fibrosis. *Am J Pathol* **167**: 1105–1117.
41. Jarvinen, TA, Jarvinen, TL, Kaariainen, M, Kalimo, H and Jarvinen, M (2005). Muscle injuries: biology and treatment. *Am J Sports Med* **33**: 745–764.
42. Branton, MH and Kopp, JB (1999). TGF-$\beta$ and fibrosis. *Microbes Infect* **1**: 1349–1365.
43. Franklin, TJ (1997). Therapeutic approaches to organ fibrosis. *Int J Biochem Cell Biol* **29**: 79–89.
44. Zhao, J, Sime, PJ, Bringas, P, Gauldie, J and Warburton, D (1999). Adenovirus-mediated decorin gene transfer prevents TGF-beta-induced inhibition of lung morphogenesis. *Am J Physiol* **277**: L412–L422.
45. Gong, R, Rifai, A, Tolbert, EM, Centracchio, JN and Dworkin, LD (2003). Hepatocyte growth factor modulates matrix metalloproteinases and plasminogen activator/plasmin proteolytic pathways in progressive renal interstitial fibrosis. *J Am Soc Nephrol* **14**: 3047–3060.
46. Taniyama, Y, Morishita, R, Nakagami, H, Moriguchi, A, Sakonjo, H, Shokei, K *et al.* (2000). Potential contribution of a novel antifibrotic factor, hepatocyte growth factor, to prevention of myocardial fibrosis by angiotensin II blockade in cardiomyopathic hamsters. *Circulation* **102**: 246–252.
47. Yang, J, Dai, C and Liu, Y (2002). Hepatocyte growth factor gene therapy and angiotensin II blockade synergistically attenuate renal interstitial fibrosis in mice. *J Am Soc Nephrol* **13**: 2464–2477.
48. Norrbom, J, Sundberg, CJ, Ameln, H, Kraus, WE, Jansson, E and Gustafsson, T (2004). PGC-1alpha mRNA expression is influenced by metabolic perturbation in exercising human skeletal muscle. *J Appl Physiol* **96**: 189–194.
49. Xiao, X, Li, J and Samulski, RJ (1998). Production of high-titer recombinant adeno-associated virus vectors in the absence of helper adenovirus. *J Virol* **72**: 2224–2232.

**Appendix 8**

## Stable transduction of rAAV-GFP in cultured dividing myo-endo cells

Michael Y. Mi, Ying Tang, Bo Zheng, Johnny Huard, Bing Wang*
Stem Cell Research Center, Department of Orthopaedic Surgery
University of Pittsburgh School of Medicine, Pittsburgh, PA 15261
*bingwang@pitt.edu

Myogenic endothelial (myo-endo) cells, isolated from adult human skeletal muscle, posses the capacity for self-renewal and the multilineage potential to regenerate tissues of the musculoskeletal system such as myofibers in the injured skeletal muscle of SCID mice (Bo Zheng et al. 2007, *Nature Biotechnology*). Viral vectors are commonly used in *ex vivo* approaches for stem cell therapy modalities. The potential for insertional mutagenesis by random DNA integration limits the application of retro-and lenti-viral vectors for stem cell therapy *in vivo*. On the other hand, rAAV vectors that have all of their viral replication (Rep) genes deleted exist as extrachromosomal episomes rather than as DNA integrated genomes, which ensures that the rAAV transduction remains innocuous. In order to develop rAAV-based, myo-endo progenitor cell gene therapy to treat musculoskeletal degenerative diseases, we investigated the efficiency of transduction of an AAV2 vector in myo-endo cells cultured over 10 passages. In this study, we infected myo-endo cells (Passage 3) with AAV2-GFP and continuously split the cells (1:3) to keep them at a cellular confluency of approximately 50%. The results demonstrated that over 50% of cells remained GFP positive through each passage examined by fluorescence microscopy and flow cytometry, which is similar to the transduction efficiency observed by the Lenti-GFP viral vector (**Figure**). These results indicate that rAAV mediated transduction is not affected by the splitting of the cell cultures. It is evidenced by the current study that the rAAV genome, in its episomal form, can be evenly distributed into the daughter cell nuclei after mitotic division, with no appreciable loss of the episomic transgene. This observation will help us to further our understanding of AAV-based *ex vivo* stem cell therapy and allow us to better engineer these systems to treat musculoskeletal degenerative diseases.

Keyword: Recombinant adeno-associated virus (rAAV), GFP, transduction, myogenic endothelial (myo-endo) cells

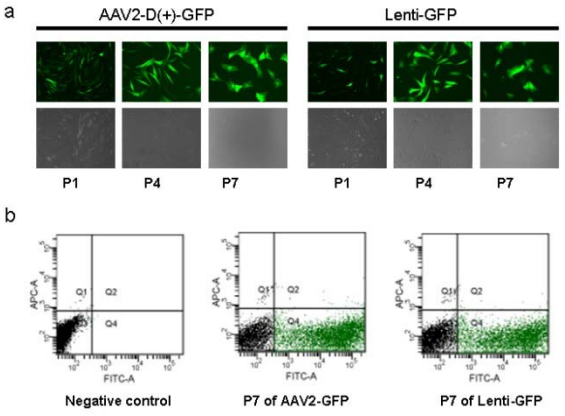


**Fig. Stable transduction of rAAV-GFP in cultured dividing myo-endo cells.** The efficient transduction of both rAAV-GFP and Lenti-GFP has shown in the passage 1, 4 and 7 by fluorescent microscopy (a). The flow cytometry analysis showed that 51% of AAV2-GFP and 45% of Lenti-GFP in the passage 7 (b).

nature biotechnology

Appendix 9



# Prospective identification of myogenic endothelial cells in human skeletal muscle

Bo Zheng[1], Baohong Cao[1], Mihaela Crisan[1], Bin Sun[1], Guangheng Li[1], Alison Logar[2], Solomon Yap[1], Jonathan B Pollett[1,3], Lauren Drowley[1], Theresa Cassino[1], Burhan Gharaibeh[1], Bridget M Deasy[1], Johnny Huard[1,4,5] & Bruno Péault[1,2,5]

**We document anatomic, molecular and developmental relationships between endothelial and myogenic cells within human skeletal muscle. Cells coexpressing myogenic and endothelial cell markers (CD56, CD34, CD144) were identified by immunohistochemistry and flow cytometry. These myoendothelial cells regenerate myofibers in the injured skeletal muscle of severe combined immunodeficiency mice more effectively than CD56$^+$ myogenic progenitors. They proliferate long term, retain a normal karyotype, are not tumorigenic and survive better under oxidative stress than CD56$^+$ myogenic cells. Clonally derived myoendothelial cells differentiate into myogenic, osteogenic and chondrogenic cells in culture. Myoendothelial cells are amenable to biotechnological handling, including purification by flow cytometry and long-term expansion *in vitro*, and may have potential for the treatment of human muscle disease.**

Upon muscle injury, intense activity or aging, normally quiescent myoblasts, or 'satellite cells', can reenter the cell cycle, differentiate and fuse to generate myofibers[1,2]. Injection of myoblasts has been shown to improve skeletal and heart muscle performance to some extent in animals and humans, but success has been limited, probably owing to the lower position of myoblasts in the myogenic cell hierarchy, implying poor cell survival and limited proliferation after implantation[3–7]. By contrast, the use of self-renewable, more primitive stem cells, for instance, muscle-derived stem cells, may permit more robust muscle regeneration in patients with muscle disorders[8–12]. By repeatedly selecting slow-adhering cells in long-term cultures of mouse skeletal muscle, we previously isolated muscle-derived stem cells (MDSCs) that better regenerate both skeletal and cardiac muscle compared with myoblasts[9,13]. Mouse MDSCs also differ from myoblasts with regard to marker profile, proliferation and fusion[9,13,14]. Their advantages for muscle regeneration have been attributed to sustained proliferation, self-renewal, multipotency[9,15] and resistance to oxidative/hypoxic stress[13]. Their muscle regeneration capacity is influenced by the gender of both donor cells and host, a previously unsuspected variable[16–19]. MDSCs can also differentiate along diverse cell lineages[9,13,14,20–25].

MDSCs were isolated retrospectively in culture; therefore, their origin, identity and native anatomic location are unknown. This is also the case for other adult multipotent stem cells, such as (i) bone marrow–derived mesenchymal stem cells (MSCs), which can differentiate into mesodermal cells, including myoblasts[26–29] and (ii) multipotent adult progenitor cells (MAPCs), which are endowed with even broader developmental potential[30–34]. MSCs and MAPCs were initially derived from adult bone marrow but are not confined to these tissues. MAPC-like cells are present in mouse brain[34], pancreas[35] and skin dermis[36] as well as in human umbilical cord[37,38], skin[39] and white adipose tissue[40]. Multipotent cells therefore appear to be broadly distributed within developed tissues[41]. However, no markers have yet been validated for the prospective identification and purification of adult multi-lineage stem cells, the isolation of which still relies on selective growth in culture.

Expression of the myogenic cell markers desmin and MyoD distinguishes MDSCs from other known stem cells. A subset of Sca1–expressing cells within the basal lamina of mouse myofibers may include MDSCs and are distinct from satellite cells, as marked by m-cadherin expression[9]. MDSCs can be isolated from Pax7$^{-/-}$ mice (unpublished observations), in which the satellite cell population is very reduced[42]. Here we investigate the relationship between endothelial and myogenic cells in human skeletal muscle. Endothelial cells in the aorta-gonad-mesonephros region of the embryo give rise to hematopoietic stem cells[43–47], suggesting that endothelial cells may have additional differentiation potential. Some MDSCs express endothelial cell markers and differentiate into endothelial cells after implantation into skeletal and cardiac muscle[9,13,14]. MDSCs also promote angiogenesis, probably through vascular endothelial growth factor (VEGF) secretion[9,13,14]. Myogenic and endothelial cells may derive from a common somatic precursor[48], and cells coexpressing myogenic and endothelial cell markers residing in the interstitial spaces of skeletal muscle may contribute to postnatal

[1]Stem Cell Research Center, Children's Hospital of Pittsburgh; Department of Orthopaedic Surgery, [2]Department of Pediatrics, [3]University of Pittsburgh Cancer Institute, [4]Departments of Molecular Genetics & Biochemistry and of Bioengineering, and [5]McGowan Institute for Regenerative Medicine, University of Pittsburgh Children's Hospital and School of Medicine, 4100 Rangos Research Center, 3460 Fifth Avenue, Pittsburgh, Pennsylvania 15213-2583, USA. Correspondence should be addressed to J.H. (jhuard@pitt.edu).

Received 4 April; accepted 12 August; published online 2 September 2007; doi:10.1038/nbt1334

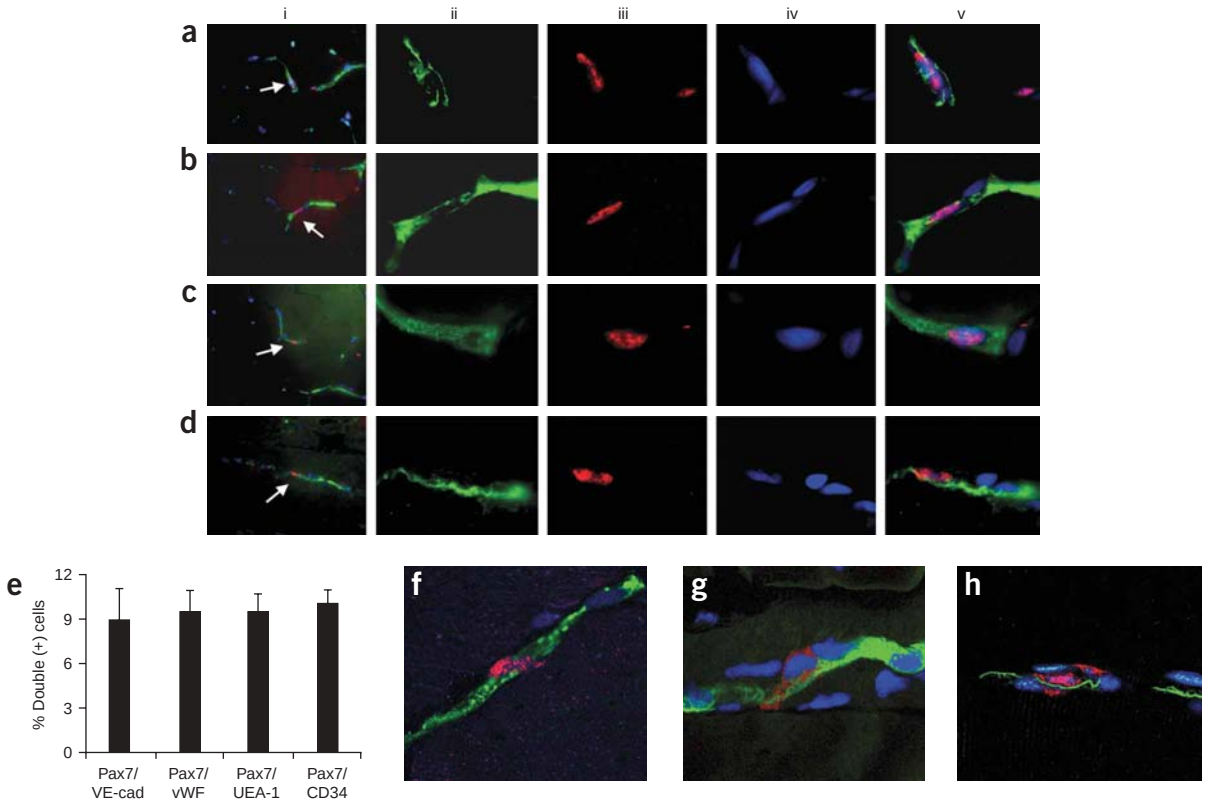


**Figure 1** Colocalization of myogenic and endothelial cell antigens in adult human muscle. (**a**–**d**) Adult human muscle sections were indirectly double-labeled for Pax7 (red) and VE-cadherin (green) (**a**); Pax7 (red) and vWF (green) (**b**); Pax7 (red) and UEA-1 receptor (green) (**c**); Pax7 (red) and CD34 (green) (**d**). In each row, i shows a low-magnification view of merged blue (600×), red and green channels, and a higher-magnification view of the same cells is shown in panels (ii–v) (1,000×). (**e**) The percentages of cells coexpressing myogenic and endothelial cell markers, as counted on at least 100 cells per section. (**f**–**h**) A confocal microscope was used to observe sections double-labeled for Pax7 (red) and vWF (green) (**f**); CD56 (red) and UEA-1 receptor (green) (**g**); CD56 (red) and VE-cadherin (green) (**h**) (**f**–**h** magnification, 1,000×) (**Supplementary Videos 1–3**). Nuclei were stained blue with DAPI. Arrowheads in **a**–**d** show cells coexpressing myogenic and endothelial cell markers.

muscle growth[48,49]. Finally, MDSCs resemble, in terms of antigenic profile and regenerative capacity in dystrophic muscle, mesoangioblasts, blood vessel–associated stem cells initially identified in the embryonic aorta[50,51].

We show that human adult skeletal muscle contains, in addition to satellite cells and endothelial cells, a population of cells that coexpress myogenic and endothelial cell markers. When injected into the injured skeletal muscles of immunodeficient mice, cells expressing exclusively endothelial cell markers ($CD56^-CD34^+CD144^+$) or coexpressing myogenic and endothelial cell markers ($CD56^+CD34^+CD144^+$) regenerated myofibers, with the latter being far more potent. Both populations outperformed conventional myogenic cells ($CD56^+CD34^-CD144^-$). Clonally expanded myoendothelial cells also differentiated into myogenic, chondrogenic and osteogenic cells under appropriate culture conditions.

## RESULTS

### Rare myogenic cells express endothelial cell markers

Human skeletal muscle sections were immunostained with antibodies to myogenic and endothelial cell antigens. Satellite cells ($Pax7^+$ or $CD56^+$) coexpress (or are located close to cells expressing) the following endothelial cell antigens: VE-cadherin (**Fig. 1a**), von Willebrand factor (vWF) (**Fig. 1b**), the UEA-1 receptor (**Fig. 1c**) and CD34 (**Fig. 1d**). Percentages of $Pax7^+$ cells expressing these endothelial cell antigens were, respectively, 8.9%, 9.5%, 9.5% and 9.8%, as determined by counting at least 100 satellite cells in five independent experiments (**Fig. 1e**). We used confocal microscopy to ascertain coexpression of these molecules by individual cells (**Fig. 1f–h** and **Supplementary Videos 1–3** online). vWF is indeed present on cells that express nuclear Pax7 (**Fig. 1f**) and some CD56-positive cells coexpress the UEA-1 receptor (**Fig. 1g**), VE-cadherin (**Fig. 1h**), and von Willebrand factor (not shown). These cells are located between muscle fibers where blood vessels reside.

### Flow cytometry analysis of myoendothelial cells

Eleven dissociated adult skeletal muscles were analyzed by flow cytometry. $CD45^-$ viable cells were gated (**Fig. 2a–c**) and further separated into $CD56^+$ myogenic cells and $CD56^-$ nonmyogenic cells (**Fig. 2d**). Expectedly, the latter subset contained the most endothelial cells ($CD34^+CD144^+$), representing 5.0 ± 1.2% of the total cell population (**Fig. 2e**). However, rare $CD56^+$ cells also expressed CD34 and CD144 (**Fig. 2f**), confirming our immunohistochemical description of cells coexpressing markers of the myogenic and vascular endothelial cell lineages. $CD56^+CD34^+CD144^+CD45^-$ cells accounted for 0.4 ± 0.1% of the starting population (**Fig. 2f**). In parallel, $CD34^-CD144^-$ nonendothelial cells were gated within the starting population (**Fig. 2g**) and $CD56^+$ myogenic cells, representing 3.0 ± 0.7% of the total cell population, were identified therein (**Fig. 2h**). Negative controls for **e** and **h** are shown in **j** and **i**. We then sorted the above cell subsets by fluorescence-activated cell sorting (FACS).

Per experiment, we recovered 4.8 ± 1.3 × $10^4$ $CD56^+CD34^-CD144^-$ myogenic cells, 7.7 ± 2.6 × $10^4$ $CD56^-CD34^+CD144^+$ endothelial cells, and 1.5 ± 0.8 × $10^4$ $CD56^+CD34^+CD144^+$ myoendothelial cells. Purities of these three cell populations were, respectively, 93.8 ± 1.0%, 92.2 ± 1.1%, and 93.5 ± 1.8%, as indicated by FACS re-analysis. All cell populations were also analyzed by RT-PCR after each cell sorting experiment to confirm the absence of contamination (**Fig. 2k**).

## Sorted myogenic cells acquire endothelial markers

Human skeletal muscle whole-cell suspensions were cultured for 2 weeks in endothelial cell growth medium (EGM2). Fusiform m-cadherin$^+$, desmin$^+$, myogenic cells survived in these conditions (**Fig. 3a–d**). As expected, polygonal endothelial cells also developed that expressed the UEA-1 receptor (**Fig. 3a**), VE-cadherin (**Fig. 3b**) and vWF (**Fig. 3c**). Additionally, smaller, rounded cells coexpressed myogenic and endothelial cell markers (**Fig. 3a–d**).

To determine whether committed myogenic cells can express endothelial cell markers, we cultured purified muscle myogenic cells (**Fig. 2h**) in EGM2 medium. Two weeks later, cells expressing VE-cadherin, vWF and the UEA-1 receptor emerged in the culture. In addition, numerous smaller, rounded cells coexpressing myogenic and vascular endothelial cell markers were present (**Fig. 3e–h**). **Figure 3i** shows the percentages (mean values from five distinct experiments) of the latter in 2-week cultures of whole muscle cells (gray bars) and sorted myogenic cells (black bars). On average, 15–35% of cells coexpressing endothelial and myogenic cell markers were detected in whole muscle cell cultures. These percentages were markedly higher in cultures of purified myogenic cells. Importantly, freshly isolated myogenic and endothelial cells did not express endothelial and myogenic cell markers, respectively, before cell culture (**Supplementary Fig. 1** online).

The endothelial identity of the cells differentiated from purified myogenic cells was further assessed by their ability to take up acetylated low-density lipoproteins (Ac-LDL). Myogenic cells cultured in EGM2 medium for 3 weeks expressed endothelial cell markers and incorporated Ac-LDL (**Fig. 3j–m**). Whereas most cells differentiated in these conditions coexpress endothelial cell markers (VE-cadherin, UEA-1 receptor, vWF, LDL uptake) and desmin, a few Ac-LDL$^+$ cells do not express desmin (**Fig. 3j**), suggesting further commitment to the endothelial cell lineage. As a control, myogenic cells cultured for 3 weeks in myogenesis-proliferation medium did not take up Ac-LDL (data not shown).

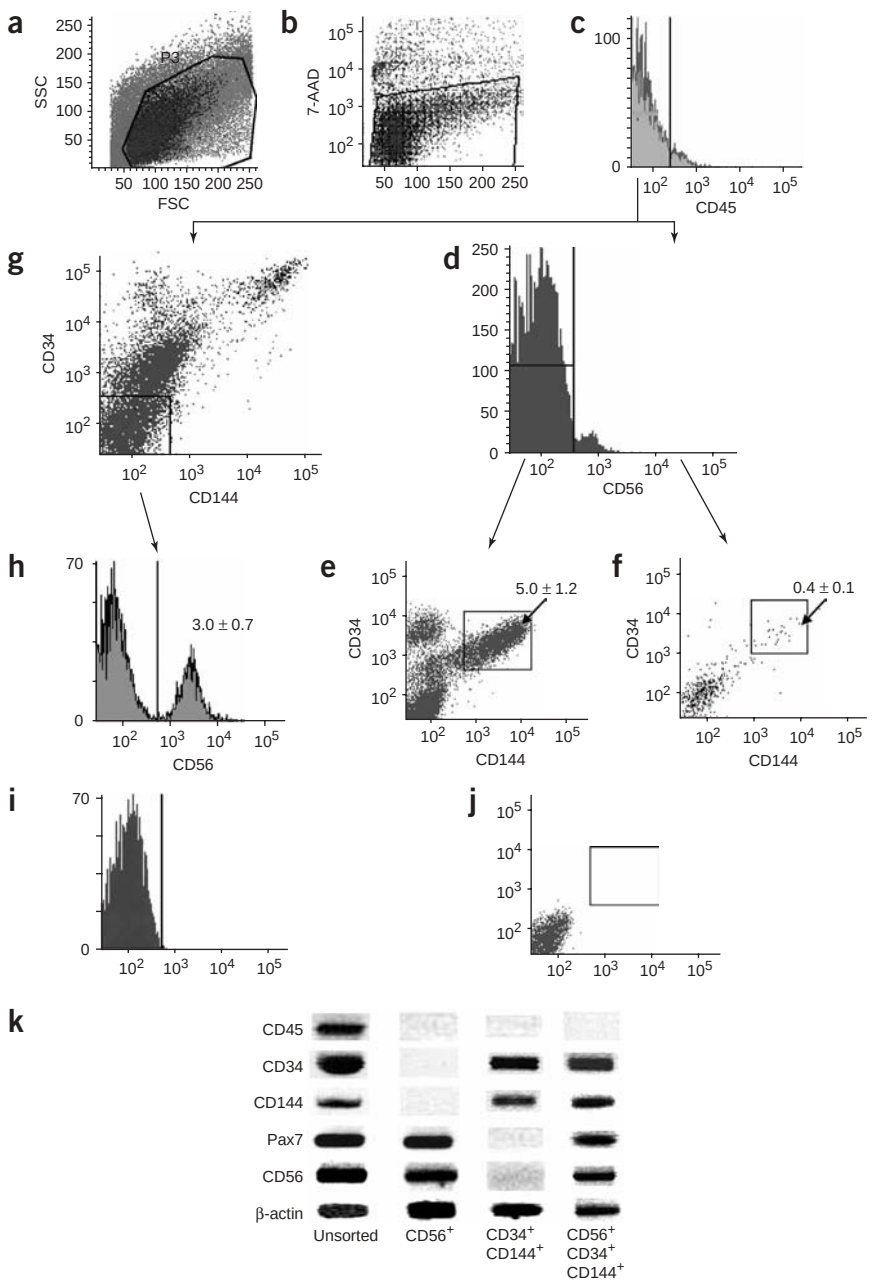


**Figure 2** Flow cytometry analysis and sorting of human muscle cell subsets. (**a**,**b**) Double-scatter (**a**) and cell viability (**b**) gates were set as indicated on the whole muscle cell suspension. (**c**,**d**) Cells negative for CD45 expression were then selected to avoid contamination by hematopoietic cells (**c**) and further separated into $CD56^-$ and $CD56^+$ cells (**d**). (**e**,**f**) The $CD56^-$ cell subset contained $CD34^-CD144^-$ and $CD34^+CD144^+$ cells that were sorted separately (**e**), whereas $CD56^+$ cells also contained a minor subpopulation of cells expressing CD34 and CD144 (**f**). (**g**,**h**) In parallel, nonendothelial $CD34^-CD144^-$ cells were gated from the starting cell population (**g**) and genuine $CD56^+$ myogenic cells were sorted therefrom (**h**). In this representative sample, $CD56^+$ myogenic cells represented 3.0 ± 0.7%, $CD34^+CD144^+$, endothelial cells 5.0 ± 1.2%, and $CD56^+CD34^+CD144^+$ cells, 0.4 ± 0.1% of the starting cell population. Negative (isotype) controls for **h** and **e** are shown in **i** and **j**, respectively. Total RNA was extracted from the unsorted muscle cell population and sorted $CD56^+$, $CD34^+CD144^+$ and $CD56^+CD34^+CD144^+$ cells. (**k**) RT-PCR analysis confirms the purity of the FACS sorted cell populations.

### Muscle regeneration by human muscle cells

Cells dissociated from skeletal muscle were sorted into cell subsets expressing myogenic, myogenic and endothelial (myoendothelial), or only endothelial cell markers. These three cell types were injected intramuscularly, in five distinct experiments, into severe combined immunodeficiency (SCID) mouse skeletal muscles injured by cardiotoxin. After 10 d, recipient muscles were analyzed by immunohistochemistry using an antibody directed against human spectrin. All three cell types regenerated spectrin-expressing muscle fibers (**Fig. 4a–e**). However, the regenerative potential of the cells expressing both myogenic and endothelial cell markers was quantitatively higher than that of endothelial cells, which were more potent than cells expressing CD56 (**Fig. 4e**). A thousand cells coexpressing myogenic and endothelial cell markers generated, on average, 89 spectrin-expressing myofibers, compared with 9 and 5 myofibers produced by the same number of endothelial or myogenic cells, respectively. Similar to mouse MDSCs, human myoendothelial cells regenerate skeletal muscle in a more effective manner than committed myogenic cells[9,12].

We next determined whether human myoendothelial cells fuse with each other and generate purely human myofibers or alternatively fuse with preexisting mouse myofibers. A mouse X chromosome–specific probe was hybridized to sections of SCID mouse muscles regenerated as described above with human myoendothelial cells. None of the nuclei contained within human spectrin-positive myofibers bound the probe, thereby demonstrating their human origin (**Supplementary Table 1** online). In contrast, most nuclei present in human spectrin-negative myofibers and outside myofibers exhibited a prominent hybridization signal. This demonstrated that human myoendothelial cells mediate skeletal muscle regeneration principally, if not exclusively, by fusing with each other in the injured muscle (**Supplementary Table 1**).

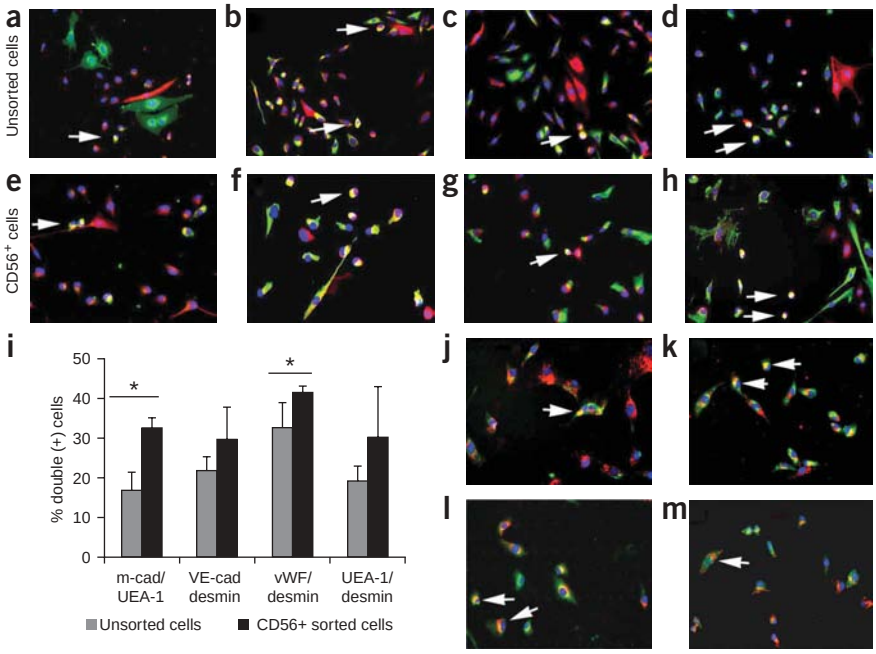


**Figure 3** Culture of whole dissociated human muscle and sorted CD56$^+$ myogenic cells in endothelial cell growth conditions and CD56$^+$ myogenic cells cultured in EGM2 medium for 3 weeks are able to incorporate Ac-LDL. Total unsorted cells dissociated from human skeletal muscle were cultured in EGM2 medium for 2 weeks. CD56$^+$CD45$^-$CD34$^-$CD144$^-$ cells were sorted by FACS from muscle as shown in **Figure 2h**, and then cultured in EGM2 medium for 2 weeks. (**a**–**h**) Cultured cells were then fixed and stained for m-cadherin (red) and UEA-1 receptor (green) (**a**,**e**); VE-cadherin (red) and desmin (green) (**b**,**f**); vWF (red) and desmin (green) (**c**,**g**); and UEA-1 receptor (red) and desmin (green) (**d**,**h**). Double-positive cells are indicated with arrowheads. (**i**) Percentages of cultured cells that coexpress various combinations of myogenic and endothelial cell markers. Nuclei were stained blue with DAPI (200×). In comparison with unsorted cells, CD56$^+$ sorted cells, after culturing, give rise to significantly more cells coexpressing m-cadherin/UEA-1 receptor and vWF/desmin (*, $P < 0.05$). Ac-LDL uptake appears in red. (**j**–**m**) Double stainings in green are for desmin (**j**), VE-cadherin (**k**), vWF (**l**) and UEA-1 receptor (**m**). Double-positive cells are indicated with arrowheads. Nuclei were stained blue with DAPI (200×).

### Long-term cultures of human muscle cells

Myogenic cells, endothelial cells and myoendothelial cells were sorted from human skeletal muscle and cultured independently in MDSC culture medium[9] for 5 to 6 weeks. All three subsets of cells were then switched to low-serum fusion medium in which they all differentiated into myotubes expressing both slow and fast myosin heavy chains. Although the number of myotubes formed varied between the three cell groups tested, this difference was not significant (**Supplementary Fig. 2** online).

Cultured cells were also injected into SCID mouse muscles damaged with cardiotoxin. Myogenic cells (**Fig. 5a**), endothelial cells (**Fig. 5b**), and myoendothelial cells (**Fig. 5c**) all retained their ability to regenerate myofibers upon extended culture. The muscle regeneration capacity of each cell population was lower compared with freshly sorted cells, but myoendothelial cells were still the most efficient (**Fig. 5a–d**). We then retrovirally transduced myoendothelial cells with *LacZ* to track these cells after intramuscular implantation. $1 \times 10^6$ myoendothelial cells, 80% of which expressed *LacZ* (not shown), were injected into the cardiotoxin-injured muscles of SCID mice, which were analyzed after 1 week, 6 weeks and 4 months. Myofibers containing *LacZ*-positive nuclei were detected in the injected muscle for up to 4 months after transplantation (136, 99 and 51 *LacZ*-positive myofibers found, respectively, at the three successive time-points) (**Fig. 5e–h**). *LacZ*-positive nuclei were also located at the periphery of myofibers 4 months after implantation (**Fig. 5h**).

### Proliferation and survival analyses of human muscle cells

The proliferation rates in culture of myogenic cells, endothelial cells and myoendothelial cells were compared (**Fig. 6**). In proliferation medium (DMEM with 10% FBS, 10% horse serum, 1% penicillin/streptomycin and 1% chick embryo extract), myoendothelial cells proliferate significantly faster than the other two cell groups (*, $P < 0.05$; **Fig. 6a**). In low-serum medium (1% FBS), the differences are even more significant (**, $P < 0.001$; **Fig. 6b**), indicating a possible delay in differentiation by myoendothelial cells. There was no significant difference in proliferation rates between myogenic cells and endothelial cells in either proliferation or low-serum medium. All three cell types grew exceptionally well in EGM-2

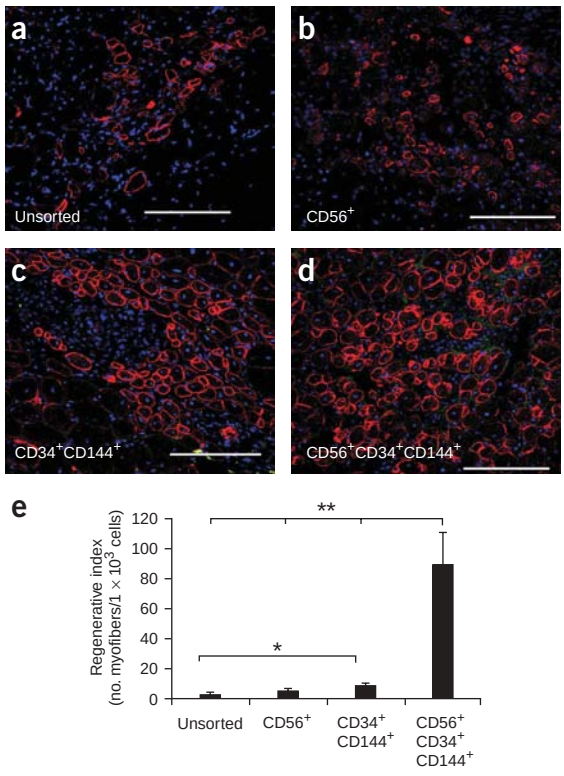


**Figure 4** *In vivo* myogenic potential of endothelium-related cells freshly sorted from human skeletal muscle. (**a**–**d**) Expression of human-specific spectrin (red) in injured skeletal muscle (SCID mice) after injection of sorted cells (total unsorted cells (**a**); $CD56^+$ (**b**); $CD34^+CD144^+$ (**c**); $CD56^+CD34^+CD144^+$ (**d**)) ($n = 5$). Mice were put to death 10 d after injection. (**e**) $CD56^+CD34^+CD144^+$ cells regenerated the highest number of human spectrin-expressing cells among the three cell subsets tested (**, $P < 0.01$, **a**–**e**). $CD34^+CD144^+$ cells generated more spectrin$^+$ myofibers than unsorted cells (*, $P < 0.05$, **a**–**e**). Nuclei were stained blue with DAPI (200×). Scale bars, 100 μm.

medium compared with DMEM supplemented with 20% serum or skeletal muscle cell basal medium (SkBM, Cambrex BioScience) supplemented with recombinant human epidermal growth factor (rhEGF), insulin, fetuin, dexamethasone, GA-1000 and BSA). In DMEM with 20% serum, there was a trend toward faster proliferation of myogenic and myoendothelial cells compared with endothelial cells, but the difference was not significant (**Supplementary Table 2** online). The cultured cells expressed CD56, CD146 and the UEA-1 receptor at different levels, as assessed by FACS analysis (**Supplementary Table 3** online).

The high regenerative capacity of mouse MDSCs in skeletal and cardiac muscles is related in part to their resistance to oxidative stress[13]. We thus treated the three cultured cell populations under study with hydrogen peroxide (400 μM). Cell viability was monitored for 28 h, and cell death was determined by propidium iodide staining. Myoendothelial cells were the most resistant to oxidative stress (**Fig. 6c** and **Supplementary Table 4** online). This resistance was higher than that of $CD56^+$ cells at all time points. Endothelial cells also resisted oxidative stress better than $CD56^+$ cells. However, myoendothelial cells also survived better in these conditions than endothelial cells. This difference was significant at the 20-h time-point (*, $P < 0.05$; **Fig. 6c** and **Supplementary Table 4**).

### Tumorigenic analysis of human muscle cells

Myogenic, endothelial and myoendothelial cells cultured for 5 weeks were analyzed for anchorage-independent growth, a hallmark of transformed cells. Cells were plated in quadruplicate on a layer of 1% agar in proliferation medium at various concentrations, and colony growth was scored 2 and 3 weeks later. Nonadherent cell growth was only observed at densities as high as $1 \times 10^5$ cells/3.8 $cm^2$, whereas cells plated at lower densities (100, 1,000 and 10,000 cells/3.8 $cm^2$) failed to grow and eventually died (data not shown). Furthermore, the three cultured cell populations were implanted independently into muscle pockets in SCID mice. No tumor was seen in any of the mice at 12 weeks after transplantation (not shown).

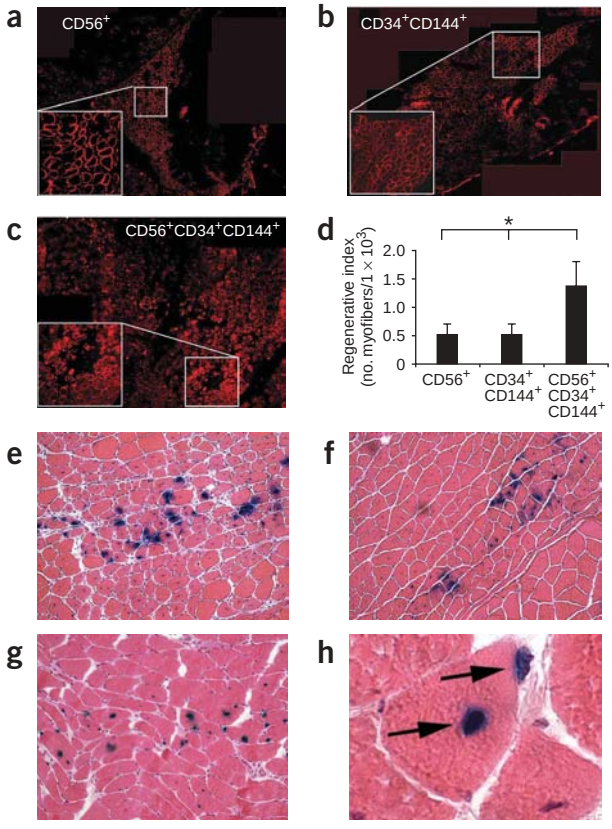


**Figure 5** *In vivo* myogenic potential of long-term cultured human myogenic, endothelial and myoendothelial cells. After 5 weeks of culture, sorted $CD56^+$, $CD34^+CD144^+$ and $CD56^+CD34^+CD144^+$ were injected into SCID mouse muscles injured with cardiotoxin ($n = 5$). (**a**–**c**) Immunostaining of human spectrin revealed that all cultured cell subsets have the capacity to regenerate human spectrin expressing muscle fibers, and that $CD56^+CD34^+CD144^+$ cells still significantly generated the highest number of human spectrin-positive myofibers, as compared with the other cell fractions tested (200×). (**d**) Bars represent the mean number of human spectrin-expressing myofibers generated in these conditions and normalized per 1,000 cells (*, $P < 0.05$). We injected $1 \times 10^5$ cells per injured muscle. A population of myoendothelial cells was genetically engineered to express the *LacZ* reporter gene. (**e**–**h**) X-gal staining with hematoxylin-eosin counterstaining at 1 week (**e**, 200×), 6 weeks (**f**, 200×) and 4 months (**g**, 200× and **h**, 1,000×) after transplantation of *LacZ* expressing myoendothelial cells. Arrows point to muscle fibers containing β-gal–positive nuclei located in the center or at the periphery (**h**).

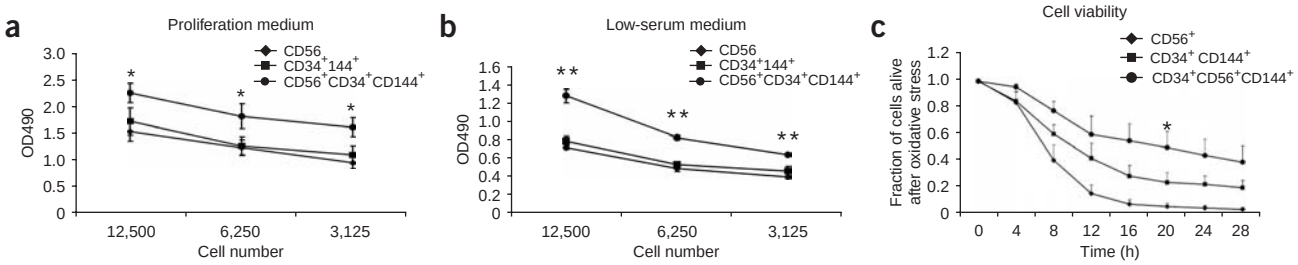


**Figure 6** Proliferation in culture and viability under oxidative conditions of human muscle-derived myogenic, endothelial, and myoendothelial cells. (**a**,**b**) $CD56^+CD34^+CD144^+$ cells proliferate at significantly higher rates than the other two groups of cells ($CD56^+$ and $CD34^+CD144^+$ cells) in both proliferation medium (*, $P < 0.05$, **a**) and low-serum medium (**, $P < 0.001$, **b**) ($n = 3$). (**c**) $CD56^+CD34^+CD144^+$ cells were more resistant to cell death than $CD34^+CD144^+$ cells, and were significantly more resistant to cell death than $CD56^+$ cells when cultivated in 400 μM $H_2O_2$ supplemented proliferation medium ($n = 3$, **Supplementary Table 4**). The cells were treated with $H_2O_2$ at the 0 h time-point after 24 h of proliferation. The percentage of cells alive at each time-point was normalized to the count at 0 h. *, a statistically significant difference between all cell populations at the time-point ($P < 0.05$).

Finally, karyotype analyses revealed no structural or numerical abnormalities in the chromosomal complements of the three long-term cultured cell populations (not shown).

### Clonal culture of myoendothelial cells

Single-sorted myoendothelial cells were cultured in multi-well plates in the absence of feeder cells. Colonies developed in ~2% of the wells, and their developmental potential was tested after 3 to 4 weeks. As detailed in **Figure 7**, clonal myoendothelial cells cultured in fusion medium differentiated into myotubes expressing fast MyHC (**Fig. 7a**). A total of $3 \times 10^5$ cells from clonal colonies injected into *mdx*/SCID mouse skeletal muscle generated dystrophin-positive myofibers containing nuclei expressing human lamin A/C (**Fig. 7b**,**e**–**h**). Clonal myoendothelial cell colonies cultured for 21 d in chondrogenic medium generated chondrocytes as indicated by tissue morphology and confirmed by Alcian blue staining (**Fig. 7c**). Upon culture for 21 d in osteogenic medium, clonal myoendothelial cells produced a calcified extracellular matrix, indicating osteogenic differentiation, which was confirmed by von Kossa staining (**Fig. 7d**).

## DISCUSSION

Here we have provided evidence for the existence of myogenic cells related to the endothelial cell lineage in human skeletal muscle. Blood vessels are localized between myofibers, and our multi-marker analysis confirms that endothelial and satellite cells are closely intermingled, as recently reported[52]. Using confocal microscopy, we documented the existence between muscle fibers of a cell type that coexpresses the Pax7 myogenesis-specific transcription factor and endothelial cell markers. These cells account for about 1% of $Pax7^+$ satellite cells. We then characterized and purified by flow cytometry rare muscle cells that coexpress the myogenic cell antigen CD56 and the endothelial cell markers CD34 and CD144. A relationship between vascular cells and myogenic cells was also suggested by an experiment in which total muscle cells were cultured under conditions that favor endothelial cell growth, yielding 15–35% of cells coexpressing myogenic and endothelial cell markers after 2 weeks. This suggests that the rare myoendothelial cells present in native muscle respond to endothelial cell mitogens. Numerous cells coexpressing myogenic and endothelial cell markers also developed from purified $CD56^+$ myogenic cells

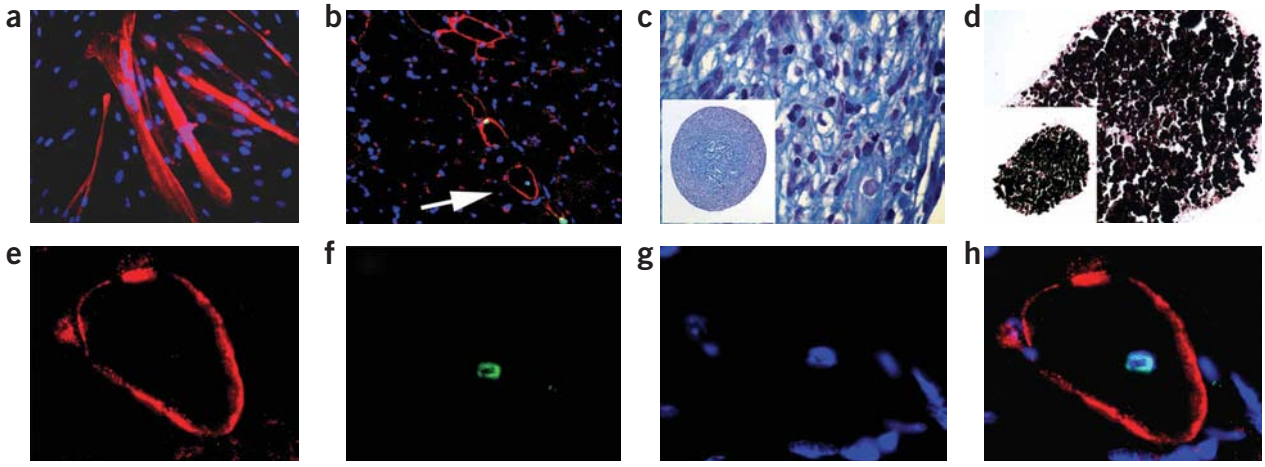


**Figure 7** Multipotency of myoendothelial clonal colonies. (**a**) Clonal myoendothelial cells differentiate into myotubes and express fast MyHC (red) when cultured in fusion medium. Nuclei were stained blue with DAPI (200×). (**b**) Clonal myoendothelial cells participate in muscle regeneration in the injured skeletal muscle of *mdx*/SCID mice, as determined by the presence of dystrophin-positive myofibers (red) containing a nuclei positive for human lamin A/C (green) (400×). (**c**) Chondrocytic differentiation revealed by Alcian blue/nuclear fast red staining of pellets cultured for 21 d in chondrogenic medium supplemented with BMP4 and TGFβ3 (1,000×). (**d**) Osteogenic differentiation revealed by von Kossa staining of pellets cultured for 21 d in osteogenic medium supplemented with BMP4 (1000×) (bottom left corner: insert of whole pellet; 100×). (**e**–**h**) The arrow in **b** shows dystrophin- and lamin A/C-double-positive fibers, as seen at a higher magnification here (1,000×).

cultured in EGM2 medium, indicating that at least some of these cells remain responsive to endothelial cell growth factors, although they do not natively express endothelial cell markers.

The main conclusion of this study is that human muscle–derived endothelial cells ($CD56^-CD34^+CD144^+$) and myoendothelial cells ($CD56^+CD34^+CD144^+$) regenerate skeletal muscle more efficiently compared with myogenic cells ($CD56^+CD34^-CD144^-$). In the cardiotoxin-injured SCID mouse muscle, myoendothelial cells generated about ten times more myofibers compared with endothelial cells, which produced almost twice as many myofibers as myogenic cells from the same donor muscle. The improved myogenic potential of myoendothelial cells may be explained in part by their faster proliferation rate and higher resistance to oxidative stress, as shown *in vitro*. Myofibers regenerated in the injured SCID mouse muscle from injected human myoendothelial cells contained essentially, if not exclusively, human nuclei, indicating that these cells regenerate myofibers primarily by fusing with each other. Myofibers regenerated by *LacZ*-positive myoendothelial cells were still present 4 months after transplantation. Moreover, donor-derived cells were also located at the periphery of myofibers, suggesting that myoendothelial cells may replenish the satellite cell and/or endothelial cell compartments.

Taken together, these data suggest the existence of a hierarchy within human adult skeletal muscle in which vascular endothelial cells give rise to early myogenic stem cells, which in turn replenish the satellite cell population. This would extend the nonvascular developmental potential of endothelial cells, subsets of which are already known to generate hematopoietic stem cells in the incipient blood system[43–47]. Myogenic potential does not appear to be restricted to muscle-derived endothelial cells, as vascular endothelial cells purified from adult human pancreas and adipose tissue also support myofiber regeneration (data not shown). Our results confirm previous reports in which cell clones endowed with high myogenic potential were derived from the avian and mouse embryonic aorta[50]. These clonal myogenic cells coexpressed markers of myogenic and endothelial cell lineages, suggesting their derivation from the aortic wall. In quail-chicken chimeras, the cells produced vascular endothelial cells and other mesodermal derivatives, primarily skeletal muscle, and were therefore named mesoangioblasts, assuming they represent a common progenitor for endothelium and other mesodermal cells[50,51,53–55]. Mesoangioblasts efficiently regenerate muscle in both murine and canine models of muscular dystrophy[54,56].

The existence of mesoangioblasts was demonstrated only retrospectively upon *in vitro* culture of the tissue of origin. Similarly, mouse MDSCs, MSCs and MAPCs have not been identified prospectively, precluding direct identification of these multi-lineage stem cells within native tissues. In contrast, we have prospectively identified in human muscle, by immunohistochemistry and flow cytometry, a population of myoendothelial cells endowed with multilineage potential, including high muscle regenerative potential.

Human myoendothelial cells show several similarities to mouse MDSCs, including multilineage potential as well as the ability to regenerate skeletal and cardiac muscles due to increased resistance to stress compared with myoblasts. Like MDSCs and MSCs, myoendothelial cell clones are osteogenic and chondrogenic when cultured in appropriate conditions, suggesting that the elusive multipotent progenitors found in adult tissues are derived from blood-vessel walls.

Our results indicate that human myoendothelial cells are amenable to biotechnological processing: they can be sorted to homogeneity by flow cytometry and cultured clonally for long periods in basic medium, with sustained developmental potential but no tumorigenicity. These properties, together with their high muscle-regeneration ability, suggest that such autologous progenitors could be envisioned as a therapy for muscle diseases.

## METHODS

**Human muscle samples.** A total of 26 skeletal muscle biopsies (mean age, 27.3 years; range, 12 to 76 years) were obtained during surgery or from the National Disease Research Interchange (NDRI). The described procedure was approved by the Institutional Review Board, and the research protocol was also reviewed and approved by the Animal Research and Care Committee at the Children's Hospital of Pittsburgh and University of Pittsburgh. Samples were placed on ice in Hanks' balanced salt solution (HBSS) (GIBCO-BRL) and transferred to the laboratory.

**Immunohistochemistry.** Samples were frozen in 2-methylbutane pre-cooled in liquid nitrogen, then stored at –80 °C. 10-µm cryosections were fixed in a 1:1 cold (–20 °C) acetone/methanol mixture for 5 min and pre-incubated in 10% horse serum in phosphate-buffered saline (PBS) for 1 h at room temperature (22 °C). Primary antibodies against myogenic cells and their dilutions in PBS were mouse anti-Pax7 (Developmental Studies Hybridoma Bank; 1:100); mouse anti-CD56 (BD Biosciences; 1:100); and rabbit anti-m-cadherin (Santa Cruz Biotechnology, Inc.; 1:200). These were incubated overnight at 4 °C, followed by PBS washes and incubation with secondary antibodies, biotinylated goat anti-mouse IgG or anti-rabbit IgG 1:250 (Vector Laboratories), followed by Cy3-conjugated streptavidin (Sigma; 1:500), both for 1 h at room temperature. Sections were then costained with antibodies to vascular endothelial cell markers: rabbit anti-VE-cadherin (Sigma; 1:200); rabbit anti-human-vWF (DAKO; 1:200) and mouse anti-human CD34 (Novocastra Laboratories; 1:100). These were incubated for 2 h at room temperature, and then followed by donkey anti-rabbit IgG or anti-mouse IgG, both conjugated to AlexaFluor 488 (Molecular Probes; 1:200) for 1 h at room temperature. Biotinylated UEA-1 (*Ulex europaeus* agglutinin-1) (Vector Laboratories; 1:200), followed by AlexaFluor 488-conjugated streptavidin (Molecular Probes; 1:200), was also used. Control stainings without primary antibodies were performed. Nuclei were stained with 4,6-diamidino-2-phenylindole (DAPI, Sigma; 100 ng/ml) and DRAQ5 (Biostatus; 1:1,000). All sections were mounted with Vectashield medium (Vector Laboratories). For quantitative analysis after immunostaining, slides were visualized on a Nikon Eclipse E800 fluorescence microscope. Over 200 cells were counted per section. An Olympus FV 500 confocal scanning microscope was also used for fluorescence colocalization.

**Immunostaining flow cytometry and cell sorting analyses.** Muscle biopsies were finely minced then digested for 60 min at 37 °C with type-I and type-IV collagenases (100 µg/ml) and dispase (1.2 µg/ml; all from GIBCO, Invitrogen Corporation). The digested tissue was pelleted and resuspended in DMEM supplemented with 10% fetal bovine serum (FBS) and 1% penicillin/streptomycin (P/S), triturated and then passed through a 40-µm filter to obtain a single cell suspension. $\sim 7 \times 10^5$ cells were recovered per gram of tissue, of which we usually processed 8 g.

For flow cytometry analysis, dissociated cells were first incubated for 10 min on ice in mouse serum (Sigma) diluted 1:10 in PBS, then for 30 min on ice with appropriately diluted mouse monoclonal antibodies to humanCD45-FITC, CD34-PE, CD56-APC (BD Pharmingen), CD144-PE (Beckman Coulter Company), CD146-FITC (Serotec), or with UEA-1-PE (Biomeda Corporation). Negative control samples received equivalent amounts of FITC-, APC- and PE-conjugated isotype-matched pre-immune antibodies.

For cell sorting, cells were suspended in DMEM supplemented with 2% FBS, and incubated with APC-Cy7-conjugated mouse anti-human CD45, APC-conjugated mouse anti-human CD34, PE-Cy7-conjugated mouse anti-human CD56 (all from BD Biosciences), and PE-conjugated mouse anti-human CD144 (Beckman Coulter). Isotype control antibodies were APC-Cy7-, APC-, PE-Cy7- and PE-conjugated mouse IgG1 (all from BD Biosciences). 7-amino-actinomycin D (7-AAD, ViaProbe; BD Pharmingen) was added to each tube for dead cell exclusion. Background staining was evaluated with isotype-matched control antibodies, and a CompBeads Set (Becton-Dickinson) was used to optimize fluorescence compensation settings for multi-color

analyses and sorts. A minimum of $1 \times 10^5$ live cells were analyzed using a FACSCalibur flow cytometer (Becton-Dickinson) and CellQuest software (Becton-Dickinson). Cell sorting was performed on a FACSAria dual-laser fluorescence cell sorter (Becton-Dickinson). Sorted cells were reanalyzed in all experiments. Cultured cells were first detached from flasks with 0.1% trypsin-EDTA (GIBCO-BRL), washed in cold PBS 2% FBS, then incubated with antibodies, as described above, before FACS analysis.

**RT-PCR analysis.** Total RNA was extracted from $10^4$ freshly sorted cells using the AbsolutelyRNA nanoprep kit (Stratagene). The cDNA was synthesized with SuperScript II reverse transcriptase (Invitrogen) according to manufacturer's instructions. PCR was performed with Taq polymerase (Invitrogen), per manufacturer's instructions, for 35 cycles at 58 °C annealing temperature and PCR products were separated by electrophoresis on 1% agarose gels. The primers used for PCR are listed in **Supplementary Table 5** online. Each set of oligonucleotides was designed to span two different exons so that genomic DNA contamination is of no concern.

**Long-term culture.** FACS-sorted or total unsorted muscle cells were plated ($5.0 \times 10^3$ per well) on 24-well plates coated with collagen-1 (Sigma Aldrich), in endothelial cell growth medium (EGM-2, Cambrex BioScience Inc.). The medium was supplemented with EGM-2 SingleQuots containing 2% FBS, hydrocortisone, hFGF, VEGF, IGF-1, ascorbic acid, hEGF, GA-1000 and heparin. Cultured cells were immunostained for characterization after 5–7 d of culture, using the antibodies and methods mentioned above. To further assess endothelial cell differentiation, 1,1′-dioctadecyl-3,3,3′,3′-tetramethyl-indocarbocyanine (DiI)-labeled acetylated low-density lipoproteins (Ac-LDL; Biomedical Technologies) were added to cultured cells at a final concentration of 10 μg/ml. Cells were then washed with PBS and fixed with 1% paraformaldehyde for 10 min. After washing and, in some instances, immunolabeling as described above, samples were observed through an inverted epifluorescence microscope. $CD56^+CD34^-CD144^-$ myogenic cells cultured for 3 weeks in the proliferation medium used for myogenesis *in vitro* were also exposed to Ac-LDL (see above).

Alternatively, sorted cells were plated in collagen-coated 96-well plates, at a density of 500 cells per well, in proliferation medium (DMEM 10% FBS, 10% horse serum, 1% penicillin/streptomycin, 1% chick embryo extract; GIBCO-BRL) at 37 °C in a 5% $CO_2$ atmosphere. At 70% confluence, cells were detached with trypsin/EDTA, replated after washing at densities between 1.0 and 2.5 $\times$ $10^3/cm^2$ and further cultured for 3–4 weeks for myogenic differentiation and cell transplantation experiments.

**Measure of cell proliferation *in vitro*.** The proliferation kinetics of $CD56^+$ cells, $CD34^+CD144^+$ cells and $CD56^+CD34^+CD144^+$cells were examined. Sorted cells were plated in noncollagenated flasks at an initial density of 600 cells/$cm^2$ (or 15,000 cells per T-25 flask). Proliferation rates were tested in three types of growth medium: 20% serum DMEM (GIBCO), EGM-2 and skeletal muscle cell growth medium (SkGM, Cambrex BioScience) supplemented with rhEGF, insulin, fetuin, dexamethasone, GA-1000 and BSA. After 2 –3 d in culture, the cells were trypsinized and counted using a hemocytometer. Population doubling time was calculated as $PDT = T/(\log_2(N_F/N_0))$, where $T$ = time in culture, $N_0$ = initial number of cells and $N_F$ = final number of cells. For each condition, three independent measurements of PDT were obtained, and statistical comparisons were made using a Student's *t*-test.

In parallel, the same three groups of sorted cells were plated in 96-well plates (12,500, 6,250, 3,125 cells/well) in triplicate and cultured in two different media (proliferation medium (DMEM 10% FBS, 10% horse serum, 1% penicillin/streptomycin, 1% chick embryo extract)and low-serum medium (DMEM with 1% FBS)) for 3 d. Then, 20 μl of CellTiter 96 $AQ_{UEOUS}$ One Reagent (G3582, Promega) was added to each well. The plate was incubated in 5% $CO_2$ at 37 °C for 2 h. A 96-well plate reader was then used to measure absorbance at 490 nm. Cells from three patients were independently evaluated.

**Cell viability assays.** Sorted cells were cultured for 24 h in proliferation medium, then for 24 additional hours in medium containing 400 μM hydrogen peroxide ($H_20_2$) and propidium iodide (PI) (Sigma-Aldrich). PI was added to a final concentration of 1 μl/500 μl medium. Cells were kept in 24-well plates in a previously described time-lapsed microscopic imaging system (Automated Cell) where bright-field and fluorescent pictures were taken every 10 min[16]. These images were analyzed using Image View Software (Automated Cell Technologies) and the number of cells in the bright field and the PI-positive cells were counted at 4-h intervals. We quantified the percentage of viable cells after treatment with $H_20_2$. Statistical significance was determined by one-way analysis of variance (ANOVA) at each time-point. Multiple comparison procedures to determine differences between groups were performed using the Student-Newman-Keuls Method ($P < 0.05$ indicates significance).

**Karyotype analysis.** Sorted myogenic cells, endothelial cells and myoendothelial cells were cultured as described above for 8 weeks, harvested and then the pellets were treated with 0.075 M KCl for 12 to 15 min at 37 °C, spun down and fixed with 3:1 of methanol:glacial acetic acid overnight at 4 °C. The next day, cells were washed and spun down three times with fresh fixative and resuspended in a small volume of fixative. The cell suspension was dropped on slides and dried overnight at 56 °C. The slides were subsequently GTG stained (brief trypsin treatment followed by Giemsa stain). At least ten metaphases were counted for each cell fraction and the chromosomes from three metaphases were paired during the count.

**Tumorigenesis assays.** To monitor growth of cells in soft agar, cells were plated at various densities on a layer of 1% agar in proliferation medium. Cells were plated at 100, 1,000, 10,000 and $1 \times 10^5$ cells/3.8 $cm^2$ in triplicate and colonies were counted at 2 and 3 weeks post seeding. To assay the tumorigenic capacity of the cells *in vivo*, $5 \times 10^5$ cells were seeded on a piece of Gelfoam and implanted into a skeletal muscle pocket in the hind-limb of a SCID mouse. The animals were monitored weekly for tumor formation by physical palpation. At 12 weeks after implantation the animals were killed and the muscles harvested and histologically analyzed for tumor formation.

***In vitro* muscle differentiation.** The ability of sorted cells to differentiate into myotubes *in vitro* was tested by plating them at $1.0 \times 10^5$ cells per well in 6-well plates for 2 d in proliferation medium that was then replaced by fusion medium (DMEM, 2% FBS, 1% penicillin/streptomycin). On day 7, methanol-fixed cultures were blocked with 5% HS then incubated with two monoclonal antibodies directed to slow myosin heavy chain (MyHC) (M8421, Sigma; 1:250), and fast MyHC (M4276, Sigma; 1:250) followed by biotinylated goat anti-mouse IgG (Vector Laboratories; 1:250), and Cy3-conjugated streptavidin (1:500). The fusion index is defined as follows: (number of nuclei within myosin heavy chain–expressing myotubes/total number of nuclei) $\times 100$.

**Cell transplantation in the mouse muscle.** SCID mice (C57BL/6J/SzJ, aged 6–8 weeks) used in this study were purchased from the Jackson Laboratories. All animals were housed in the animal facility of the Rangos Research Center at Children's Hospital of Pittsburgh. Mouse experiments were approved by the Animal Research and Care Committee of the Children's Hospital of Pittsburgh and University of Pittsburgh (protocol 42-04).

Freshly sorted or cultured cells mixed with FluoSpheres (Molecular Probes) were resuspended in 15 μl HBSS and transplanted in a single injection into the SCID mouse gastrocnemius muscle that had been injured 1 d earlier by intramuscular injection of 1 μg cardiotoxin (CTX, Molecular Probes) in 20 μl HBSS. Animals were killed 10 d after injection and treated muscles were fixed and frozen as described above. Human spectrin staining was performed on acetone-fixed, horse serum–blocked sections using a human specific anti-β-spectrin antibody (1:100; Novocastra) to detect human cell–derived myofibers. Sections were then washed in PBS and incubated with a biotinylated anti-mouse IgG antibody following by washing and incubation with Cy3-streptavidin (Sigma). Nuclei were stained with DAPI as described above. Human spectrin-positive myofibers were counted from digital images by using Image View software. Sections containing the highest number of fibers expressing human spectrin were used for each group to determine a regenerative efficiency index, defined as the number of spectrin-positive (human) fibers generated per $1 \times 10^3$ viable cells (that is, no. human spectrin-positive myofibers/thousand viable cells injected).

The long-term regenerative capacity of the cells *in vivo* was evaluated by injecting myoendothelial cells into SCID mice. The animals were killed at different time-points for up to 4 months. To enable tracking of cells after

injection into skeletal muscles, myoendothelial cells were genetically engineered to express the *LacZ* reporter gene. The percentage of *LacZ*-positive cells (myo-endo-*LacZ*) was determined by using β-galactosidase staining. Myo-endo-*LacZ* cells from passages 12–16 were grown to 60% confluence in EGM-2 medium. The cells were harvested and injected ($1 \times 10^6$ cells per injection) into a single site within the gastrocnemius muscles of 6-week-old injured SCID mice, as described above. Injected muscles were harvested at 1 week, 6 weeks and 4 months and frozen sections were stained for *LacZ* and hematoxylin-eosin (HE). For *LacZ* staining, the sections were fixed in 1% glutaraldehyde, incubated overnight with X-gal solution at 37 °C and counterstained with HE.

**Fluorescent *in situ* hybridization.** Slides were first immunostained with a human spectrin-specific antibody (see above) and human spectrin-positive sections were marked with a diamond scriber. Slides were dehydrated in 70, 80, 95 and 100% ethanol for 3 min each and then denatured in 70% formamide-2× saline sodium citrate (SSC) at 75 ± 1 °C. Slides were then dehydrated as above and air dried. A mouse X-chromosome paint probe labeled with FITC (ID Labs) and a hybridization mixture were mixed (ratio 3:10), denatured at 70 °C for 10 min, and allowed to re-anneal for 60–90 min at 37 °C. The mixture was applied to the target area, covered with a plastic coverslip, glued with rubber cement and incubated in a humidity chamber for 18–24 h at 37 °C. On day 2, slides were washed with 2× SSC for 5 min, followed by washes in 50% formamide-2X SSC (12–13 min), 2× SSC (three times for 7 min) and 4× SSC-Tween (2 min). All washes were done at 45 °C. Slides were subsequently counterstained with Vectashield containing DAPI (Vector Laboratories). The hybridized X-chromosome-specific fluorescent probe was detected under a Nikon Eclipse E800 microscope equipped with a Retiga 1300 digital camera and Northern Eclipse software system. Captured images of randomly selected fields were examined for total number of DAPI-positive nuclei, nuclei with a green (X-FITC) signal, and nuclei positive for mouse X- chromosome that were located within human spectrin-positive (red) myofibers.

**Derivation, culture and differentiation of single myoendothelial cells.** Single myoendothelial cells from a 76-year old female donor were sorted directly, using the single-cell deposition unit on the FACS, into individual wells of a flat-bottomed, 96-well plate coated with collagen-1, containing 150 µl proliferation medium. When grown to 40–50% confluence, cells from each well were replated successively into 24-well plates, 6-well plates and eventually 75-$cm^2$ flasks.

**Myogenic differentiation *in vitro* and vivo.** Clonal myoendothelial cells were plated in 6-well plates in fusion medium and stained with antibodies against fast-MHC, as described above. Clonal myoendothelial cells from passage 9 were grown to 60% confluence in proliferation medium, harvested and injected ($3 \times 10^5$ cells per injection) into a single site within the gastrocnemius muscles of 6-week-old *mdx*/SCID mice[14], an animal model previously described. Injected muscles were harvested on day 28 and stained for dystrophin and human lamin A/C. For dystrophin staining, slides were fixed with acetone and blocked with 5% horse serum. The primary rabbit anti-dystrophin antibody (1:400; Abcam) was incubated overnight at 4 °C and subsequently incubated for 1 h with donkey anti-rabbit IgG conjugated to AlexaFluor 594 (1:400; Molecular Probes), and followed by lamin A/C (1:100; Novacastra) for 3 h at room temperature, and then donkey anti-mouse IgG conjugated to AlexaFluor 488 (1:400; Molecular Probes) for 1 h. Nuclei were revealed with DAPI.

**Chondrogenesis assay.** $3.0 \times 10^5$ cells (600*g*, 5 min) were pelleted in 15-ml conical polypropylene tubes and incubated in chondrogenic medium (Cambrex) supplemented with BMP4 (100 ng/ml; R&D Systems) and TGFβ3 (10 ng/ml; R&D Systems). Pellets were harvested on day 21, and then embedded in paraffin as detailed in the standard protocol (available on the Cambrex Company website). Chondrogenesis was determined by Alcian blue staining, as previously described[22,57], which stains the highly sulfated proteoglycans that characterize the cartilaginous matrix. Nuclei were then counterstained with nuclear fast red.

**Osteogenesis assay.** Pellets of $3.0 \times 10^5$ cells (600*g*, 5 min) were cultured for up to 3 weeks in osteogenic medium (DMEM supplemented with dexamethasone [0.1 µM], ascorbate-2-phosphate [50 µM], and β-glycerophosphate [10 mM]; all from Sigma), further supplemented with BMP4 (200 ng/ml). Samples were harvested on day 21 and embedded in paraffin. Pellet sections were stained with the von Kossa method as previously described[21,57].

*Note: Supplementary information is available on the Nature Biotechnology website.*

**ACKNOWLEDGMENTS**

This work was supported in part by grants to J.H. from the Muscular Dystrophy Association (USA), the US National Institutes of Health (R01-AR049684; RO1-DE13420-06; IU54AR050733-01), the William F. and Jean W. Donaldson Chair, the Orris C. Hirtzel and Beatrice Dewey Hirtzel Memorial Foundation at Children's Hospital of Pittsburgh, the Henry J. Mankin Endowed Chair at the University of Pittsburgh and the Lemieux Foundation at the University of Pittsburgh. The authors wish to thank S.C. Watkins for his assistance with confocal microscopy, A. Usas and J.A. Jadlowiec for help with tumorigenesis experiments *in vivo*, J. Tebbets and M. Branca for technical help with cryostat sectioning, and David Humiston for editorial assistance.

**COMPETING INTERESTS STATEMENT**

The authors declare no competing financial interests.

Published online at http://www.nature.com/naturebiotechnology
Reprints and permissions information is available online at http://npg.nature.com/reprintsandpermissions

1. Bischoff, R. Proliferation of muscle satellite cells on intact myofibers in culture. *Dev. Biol.* **115**, 129–139 (1986).
2. Bischoff, R. The satellite cell and muscle regeneration. In *Myology: Basic and Clinical* (Engel, A., Franzini-Armstrong, C. & Fischman D.A., eds.), 97–118, (McGraw-Hill, New York, 1994).
3. Skuk, D. & Tremblay, J.P. Myoblast transplantation: the current status of a potential therapeutic tool for myopathies. *J. Muscle Res. Cell Motil.* **24**, 285–300 (2003).
4. Partridge, T.A. Invited review: myoblast transfer: a possible therapy for inherited myopathies? *Muscle Nerve* **14**, 197–212 (1991).
5. Menasche, P. *et al.* Myoblast transplantation for heart failure. *Lancet* **357**, 279–280 (2001).
6. Cao, B., Deasy, B.M., Pollett, J. & Huard, J. Cell therapy for muscle regeneration and repair. *Phys. Med. Rehabil. Clin. N. Am.* **16**, 889–907, viii (2005).
7. Menasche, P. Cellular transplantation: hurdles remaining before widespread clinical use. *Curr. Opin. Cardiol.* **19**, 154–161 (2004).
8. Miller, J.B., Schaefer, L. & Dominov, J.A. Seeking muscle stem cells. *Curr. Top. Dev. Biol.* **43**, 191–219 (1999).
9. Qu-Petersen, Z. *et al.* Identification of a novel population of muscle stem cells in mice: potential for muscle regeneration. *J. Cell Biol.* **157**, 851–864 (2002).
10. Gussoni, E. *et al.* Dystrophin expression in the mdx mouse restored by stem cell transplantation. *Nature* **401**, 390–394 (1999).
11. Partridge, T.A. Stem cell therapies for neuromuscular diseases. *Acta Neurol. Belg.* **104**, 141–147 (2004).
12. Peault, B. *et al.* Stem and progenitor cells in skeletal muscle development, maintenance, and therapy. *Mol. Ther.* **15**, 867–877 (2007).
13. Oshima, H. *et al.* Differential myocardial infarct repair with muscle stem cells compared to myoblasts. *Mol. Ther.* **12**, 1130–1141 (2005).
14. Payne, T.R. *et al.* Regeneration of dystrophin-expressing myocytes in the mdx heart by skeletal muscle stem cells. *Gene Ther.* **12**, 1264–1274 (2005).
15. Deasy, B.M. *et al.* Long-term self-renewal of postnatal muscle-derived stem cells. *Mol. Biol. Cell* **16**, 3323–3333 (2005).
16. Deasy, B.M. *et al.* A role for cell sex in stem cell-mediated skeletal muscle regeneration: female cells have higher muscle regeneration efficiency. *J. Cell Biol.* **177**, 73–86 (2007).
17. Mueller, G.M., O'Day, T., Watchko, J.F. & Ontell, M. Effect of injecting primary myoblasts versus putative muscle-derived stem cells on mass and force generation in mdx mice. *Hum. Gene Ther.* **13**, 1081–1090 (2002).
18. Jankowski, R.J., Deasy, B.M., Cao, B., Gates, C. & Huard, J. The role of CD34 expression and cellular fusion in the regeneration capacity of myogenic progenitor cells. *J. Cell Sci.* **115**, 4361–4374 (2002).
19. Jankowski, R.J. & Huard, J. Myogenic cellular transplantation and regeneration: sorting through progenitor heterogeneity. *Panminerva Med.* **46**, 81–91 (2004).
20. Cao, B. *et al.* Muscle stem cells differentiate into haematopoietic lineages but retain myogenic potential. *Nat. Cell Biol.* **5**, 640–646 (2003).
21. Wright, V. *et al.* BMP4-expressing muscle-derived stem cells differentiate into osteogenic lineage and improve bone healing in immunocompetent mice. *Mol. Ther.* **6**, 169–178 (2002).
22. Kuroda, R. *et al.* Cartilage repair using bone morphogenetic protein 4 and muscle-derived stem cells. *Arthritis Rheum.* **54**, 433–442 (2006).
23. Winitsky, S.O. *et al.* Adult murine skeletal muscle contains cells that can differentiate into beating cardiomyocytes in vitro. *PLoS Biol.* **3**, e87 (2005).
24. Sarig, R., Baruchi, Z., Fuchs, O., Nudel, U. & Yaffe, D. Regeneration and transdifferentiation potential of muscle-derived stem cells propagated as myospheres. *Stem Cells* **24**, 1769–1778 (2006).

25. Nomura, T. *et al.* Skeletal myosphere-derived progenitor cell transplantation promotes neovascularization in delta-sarcoglycan knockdown cardiomyopathy. *Biochem. Biophys. Res. Commun.* **352**, 668–674 (2007).
26. Beresford, J.N., Bennett, J.H., Devlin, C., Leboy, P.S. & Owen, M.E. Evidence for an inverse relationship between the differentiation of adipocytic and osteogenic cells in rat marrow stromal cell cultures. *J. Cell Sci.* **102**, 341–351 (1992).
27. Pittenger, M.F. *et al.* Multilineage potential of adult human mesenchymal stem cells. *Science* **284**, 143–147 (1999).
28. Toma, C., Pittenger, M.F., Cahill, K.S., Byrne, B.J. & Kessler, P.D. Human mesenchymal stem cells differentiate to a cardiomyocyte phenotype in the adult murine heart. *Circulation* **105**, 93–98 (2002).
29. Prockop, D.J. Marrow stromal cells as stem cells for nonhematopoietic tissues. *Science* **276**, 71–74 (1997).
30. Petersen, B.E. *et al.* Bone marrow as a potential source of hepatic oval cells. *Science* **284**, 1168–1170 (1999).
31. Theise, N.D. *et al.* Derivation of hepatocytes from bone marrow cells in mice after radiation-induced myeloablation. *Hepatology* **31**, 235–240 (2000).
32. Krause, D.S. *et al.* Multi-organ, multi-lineage engraftment by a single bone marrow-derived stem cell. *Cell* **105**, 369–377 (2001).
33. Mezey, E., Chandross, K.J., Harta, G., Maki, R.A. & McKercher, S.R. Turning blood into brain: cells bearing neuronal antigens generated in vivo from bone marrow. *Science* **290**, 1779–1782 (2000).
34. Jiang, Y. *et al.* Multipotent progenitor cells can be isolated from postnatal murine bone marrow, muscle, and brain. *Exp. Hematol.* **30**, 896–904 (2002).
35. Seaberg, R.M. *et al.* Clonal identification of multipotent precursors from adult mouse pancreas that generate neural and pancreatic lineages. *Nat. Biotechnol.* **22**, 1115–1124 (2004).
36. Toma, J.G. *et al.* Isolation of multipotent adult stem cells from the dermis of mammalian skin. *Nat. Cell Biol.* **3**, 778–784 (2001).
37. Wang, H.S. *et al.* Mesenchymal stem cells in the Wharton's jelly of the human umbilical cord. *Stem Cells* **22**, 1330–1337 (2004).
38. Mitchell, K.E. *et al.* Matrix cells from Wharton's jelly form neurons and glia. *Stem Cells* **21**, 50–60 (2003).
39. Shih, D.T. *et al.* Isolation and characterization of neurogenic mesenchymal stem cells in human scalp tissue. *Stem Cells* **23**, 1012–1020 (2005).
40. Zuk, P.A. *et al.* Multilineage cells from human adipose tissue: implications for cell-based therapies. *Tissue Eng.* **7**, 211–228 (2001).
41. Barry, F.P. & Murphy, J.M. Mesenchymal stem cells: clinical applications and biological characterization. *Int. J. Biochem. Cell Biol.* **36**, 568–584 (2004).
42. Seale, P. *et al.* Pax7 is required for the specification of myogenic satellite cells. *Cell* **102**, 777–786 (2000).
43. Kumaravelu, P. *et al.* Quantitative developmental anatomy of definitive haematopoietic stem cells/long-term repopulating units (HSC/RUs): role of the aorta-gonad-mesonephros (AGM) region and the yolk sac in colonisation of the mouse embryonic liver. *Development* **129**, 4891–4899 (2002).
44. Jaffredo, T., Gautier, R., Eichmann, A. & Dieterlen-Lievre, F. Intraaortic hemopoietic cells are derived from endothelial cells during ontogeny. *Development* **125**, 4575–4583 (1998).
45. Nishikawa, S.I. *et al.* In vitro generation of lymphohematopoietic cells from endothelial cells purified from murine embryos. *Immunity* **8**, 761–769 (1998).
46. North, T.E. *et al.* Runx1 expression marks long-term repopulating hematopoietic stem cells in the midgestation mouse embryo. *Immunity* **16**, 661–672 (2002).
47. Oberlin, E., Tavian, M., Blazsek, I. & Peault, B. Blood-forming potential of vascular endothelium in the human embryo. *Development* **129**, 4147–4157 (2002).
48. Kardon, G., Campbell, J.K. & Tabin, C.J. Local extrinsic signals determine muscle and endothelial cell fate and patterning in the vertebrate limb. *Dev. Cell* **3**, 533–545 (2002).
49. Tamaki, T. *et al.* Identification of myogenic-endothelial progenitor cells in the interstitial spaces of skeletal muscle. *J. Cell Biol.* **157**, 571–577 (2002).
50. Minasi, M.G. *et al.* The meso-angioblast: a multipotent, self-renewing cell that originates from the dorsal aorta and differentiates into most mesodermal tissues. *Development* **129**, 2773–2783 (2002).
51. Cossu, G. & Bianco, P. Mesoangioblasts–vascular progenitors for extravascular mesodermal tissues. *Curr. Opin. Genet. Dev.* **13**, 537–542 (2003).
52. Christov, C. *et al.* Muscle satellite cells and endothelial cells: close neighbors and privileged partners. *Mol. Biol. Cell* **18**, 1397–1409 (2007).
53. De Angelis, L. *et al.* Skeletal myogenic progenitors originating from embryonic dorsal aorta coexpress endothelial and myogenic markers and contribute to postnatal muscle growth and regeneration. *J. Cell Biol.* **147**, 869–878 (1999).
54. Sampaolesi, M. *et al.* Cell therapy of alpha-sarcoglycan null dystrophic mice through intra-arterial delivery of mesoangioblasts. *Science* **301**, 487–492 (2003).
55. Galli, D. *et al.* Mesoangioblasts, vessel-associated multipotent stem cells, repair the infarcted heart by multiple cellular mechanisms: a comparison with bone marrow progenitors, fibroblasts, and endothelial cells. *Arterioscler. Thromb. Vasc. Biol.* **25**, 692–697 (2005).
56. Sampaolesi, M. *et al.* Mesoangioblast stem cells ameliorate muscle function in dystrophic dogs. *Nature* **444**, 574–579 (2006).
57. Zheng, B., Cao, B., Li, G. & Huard, J. Mouse adipose-derived stem cells undergo multilineage differentiation in vitro but primarily osteogenic and chondrogenic differentiation in vivo. *Tissue Eng.* **12**, 1891–1901 (2006).

Cell Stem Cell
Article

# A Perivascular Origin for Mesenchymal Stem Cells in Multiple Human Organs

Mihaela Crisan,[1,2] Solomon Yap,[1,2] Louis Casteilla,[1,2,4] Chien-Wen Chen,[1,2,8] Mirko Corselli,[1,2,8] Tea Soon Park,[1,2,8] Gabriella Andriolo,[3,8] Bin Sun,[1,2] Bo Zheng,[1,2] Li Zhang,[5] Cyrille Norotte,[1,2] Pang-Ning Teng,[1,2] Jeremy Traas,[6] Rebecca Schugar,[1,2] Bridget M. Deasy,[1,2] Stephen Badylak,[5] Hans-Jörg Bűhring,[7] Jean-Paul Giacobino,[1,2] Lorenza Lazzari,[3] Johnny Huard,[1,2] and Bruno Péault[1,2,5,*]
[1]Department of Pediatrics
[2]Department of Orthopaedic Surgery
Stem Cell Research Center, Children's Hospital of Pittsburgh, Pittsburgh, PA 15213, USA
[3]Cell Factory, Department of Regenerative Medicine, Fondazione Ospedale Maggiore Policlinico, Milan 20122, Italy
[4]UMR 5018 CNRS-UPS, Toulouse 31059, France
[5]McGowan Institute for Regenerative Medicine, Pittsburgh, PA 15213, USA
[6]Division of Surgery, Children's Hospital of Philadelphia, Philadelphia, PA 19104, USA
[7]Department of Internal Medicine, University Clinic of Tübingen, Tübingen 72076, Germany
[8]These authors contributed equally to this work
*Correspondence: bruno.peault@chp.edu
DOI 10.1016/j.stem.2008.07.003

## SUMMARY

**Mesenchymal stem cells (MSCs), the archetypal multipotent progenitor cells derived in cultures of developed organs, are of unknown identity and native distribution. We have prospectively identified perivascular cells, principally pericytes, in multiple human organs including skeletal muscle, pancreas, adipose tissue, and placenta, on CD146, NG2, and PDGF-Rβ expression and absence of hematopoietic, endothelial, and myogenic cell markers. Perivascular cells purified from skeletal muscle or nonmuscle tissues were myogenic in culture and in vivo. Irrespective of their tissue origin, long-term cultured perivascular cells retained myogenicity; exhibited at the clonal level osteogenic, chondrogenic, and adipogenic potentials; expressed MSC markers; and migrated in a culture model of chemotaxis. Expression of MSC markers was also detected at the surface of native, noncultured perivascular cells. Thus, blood vessel walls harbor a reserve of progenitor cells that may be integral to the origin of the elusive MSCs and other related adult stem cells.**

## INTRODUCTION

Subsets of cells that participate in the architecture of blood vessels exhibit developmental potentials beyond angiogenesis. Vascular endothelium generates hematopoietic cells in the embryo (Jaffredo et al., 1998; Oberlin et al., 2002; Zambidis et al., 2006), and multipotent mesoangioblasts have been derived from the embryonic aorta and other blood vessels (DeAngelis et al., 1999; Cossu and Bianco, 2003; LeGrand et al., 2004). Pericytes, aka Rouget cells or mural cells, also called mesangial cells in the kidney and Ito cells in the liver, closely encircle endothelial cells in capillaries and microvessels (Andreeva et al., 1998). Some contain α-smooth muscle actin (α-SMA) and regulate microvessel contractility (Nehls and Drenckhan, 1991; Boado and Pardridge, 1994). Pericytes can also inhibit, via TGF-β activation, the division of endothelial cells (reviewed in Betsholtz et al., 2005). In addition, pericytes are believed to include progenitors of different cell types, although this assumption relies mostly on indirect evidence. In one study, bovine retinal pericytes implanted in diffusion chambers in nude mice differentiated into chondrocytes and adipocytes (Farrington-Rock et al., 2004). Pericytes are also believed to be osteogenic and, therefore, be responsible for the pathologic calcification of blood vessels, heart valves, and skeletal muscle (reviewed in Collett and Canfield, 2005). The appearance, in pericyte-rich cultures of human dental pulp, of dentin-expressing cells also suggested that odontoblasts can be derived from perivascular cells (Alliot-Licht et al., 2005). However, each of the aforementioned differentiation experiments was performed on pericyte-containing cultures and not on purified pericytes. As a recent exception, Dellavalle et al. (2007) have demonstrated that pericytes sorted from human skeletal muscle by alkaline phosphatase expression can regenerate skeletal myofibers in dystrophic immunodeficient mice. Mesoangioblasts, the blood vessel-associated myogenic stem cells previously identified in vitro (DeAngelis et al., 1999), may therefore be related to perivascular cells. Some of us have previously discovered in "preplate" cultures of skeletal muscle a similar population of muscle-derived stem cells (MDSCs) of unknown identity that regenerate myofibers more efficiently than committed satellite cells (Qu-Petersen et al., 2002; Péault et al., 2007). Mesoangioblasts and MDSCs may be related to other elusive, multilineage progenitor cells encountered in bone marrow and other tissues, such as MSCs (mesenchymal stem cells) (Caplan, 1991; Pittenger et al., 1999) and multipotent adult progenitor cells (MAPCs) (Jiang et al., 2002). White adipose tissue (WAT) also contains progenitors of multiple mesodermal cell lineages and is therefore an attractive source of autologous cells for transplantation. Zuk

et al. (2002) found a putative MSC population in human WAT and drove its differentiation into adipocytes, osteoblasts, chondrocytes, and myoblasts. Gronthos et al. (2001) further showed similarities between human WAT stroma vascular cells and bone marrow stromal cells. Whether these multipotent cells, all of which were isolated retrospectively in culture, share a common ancestor in multiple developed organs is unknown. In order to further explore the presence of multilineage progenitors among human perivascular cells, we first validated a combination of markers to typify these cells, which were then purified from skeletal muscle, pancreas, adipose tissue, and other organs. We demonstrate that human perivascular cells, pericytes in particular, are myogenic in vivo and ex vivo, irrespective of their tissue of origin. Moreover, human perivascular cells sorted from diverse human tissues and cultured over the long term give rise to adherent, multilineage progenitor cells that exhibit the features of MSC.

## RESULTS

### Immunohistochemical Detection of Perivascular Cells in Human Tissues

As a prerequisite to human perivascular cell sorting by flow cytometry, we used immunohistochemistry to establish a relevant combination of markers for this elusive cell population. To this end, we examined each of the following: (1) ten adult (16–78 years of age) and 18 fetal skeletal muscle samples (16–24 weeks of gestation); (2) 5 adult (33–61 years) and 6 fetal pancreases (17–24 weeks); (3) 28 placentas (20 at 17–24 weeks and 8 at term); and (4) 15 adult WAT as well as (5) 3 fetal hearts, 3 fetal skins, 5 lungs, 1 brain, 2 eyes, 1 gut, 1 bone marrow, and 3 term umbilical cords. In all organs, we observed the ubiquitous expression, by perivascular cells surrounding capillaries (diameter <10 μm) and arterioles (diameter from 10 to 100 μm), of NG2, a proteoglycan associated with pericytes during vascular morphogenesis (Ozerdem et al., 2002) and CD146 (aka S-endo1, Mel-CAM, Muc18, or gicerin), an endothelial cell antigen also expressed at the surface of pericytes (Li et al., 2003; Middleton et al., 2005; Sacchetti et al., 2007) (Figures 1A–1C and 1G). CD146 was indeed present on endothelium in capillaries, but not on microvessel endothelial cells (data not shown). CD146 was also detected on perivascular cells around venules. In order to ascertain that CD146+ cells detected around small vessels are indeed pericyte-like cells, tissue sections were double stained with antibodies to CD146 and NG2. As illustrated by Figures 1G–1I, CD146+ perivascular cells are also positive for NG2 expression. Furthermore, all perivascular cells express PDGF-Rβ (Figure 1D), and α-SMA was reproducibly detected in cells surrounding venules and arterioles, but not around most capillaries (Figure 1F and data not shown). In contrast, perivascular cells do not express endothelial cell markers such as CD144 (VE-cadherin) (Figure 1E), von Willebrand factor (vWF) (Figure 1D), CD34 (Figures 1A–1C), the *Ulex europaeus* lectin ligand (Figure 1F), or CD31 (data not shown). The same pericyte/perivascular cell phenotype was found in all other human organs and tissues tested. Most importantly, cells exhibiting this surface phenotype were, in all tissues analyzed, exclusively perivascular.

### Flow Cytometry Sorting of Perivascular Cells

We next proceeded to analyze and sort perivascular cells by using multicolor fluorescence-activated cell sorting (FACS). Twenty-eight fetal (17–23 weeks), 6 adult skeletal muscles (50–78 years), and 8 fetal myocardiums (17–22 weeks) were first processed independently. Twenty fetal (19–22 weeks) and 8 term placentas were also used since microdissected placental blood vessels transplanted intact into SCID/mdx mouse muscles regenerated myofibers (data not shown). Eight fetal (17–23 weeks) and 2 adult human pancreases, 2 fetal skins, 4 fetal brains, 24 fetal bone marrows, and 32 adult WAT samples were used as organs devoid of regular myogenic cells. CD56+ cells were initially gated out of muscle cell suspensions in order to avoid contamination by regular myogenic cells (Péault et al., 2007) and later on eliminated from all tissues used for FACS analysis and sorting (Figure 2B), as were hematopoietic cells (CD45+) (Figure 2C). Perivascular cells were identified and sorted by high CD146 expression and lack of CD34, the latter in order to ascertain the absence of endothelial cells within sorted cells. The same population of CD146+ CD34− CD45− CD56− cells was detected in all tissues analyzed (Figures 2D–2J), amounting to 0.88% ± 0.18% in fetal skeletal muscle, 0.29% ± 0.09% in adult skeletal muscle, 1.4% ± 0.33% in fetal pancreas, 0.65% ± 0.10% in adult pancreas, and 1.79% ± 1.10% in placenta. These cells were more frequent in adipose tissue (14.6% ± 1.02%; Figure 2F), since analysis was performed on the stromal vascular fraction, which is markedly enriched in blood vessels. Perivascular cells from multiple tissues were also observed to express alkaline phosphatase (Figures 2K–2N), a marker used recently to typify pericytes in human skeletal muscle (Dellavalle et al., 2007). Sorted perivascular cells were confirmed by RT-PCR analysis in each experiment, not to include detectable hematopoietic cells (CD34, CD45), endothelial cells (CD34, vWF) or regular myogenic cells (CD56, Pax7) (data not shown).

### Generalized Myogenic Potential of Perivascular Cells

Perivascular cells sorted from four distinct fetal skeletal muscles were first tested for myogenic potential in culture. Sorted cells were cultured for 8–10 days in muscle proliferation medium, then for 5–10 more days in muscle fusion medium. Typical myotubes containing three to five nuclei appeared after 8–10 days and further developed, enclosing up to 15 nuclei 10 days later. All myotubes developed in these conditions expressed human myosin heavy chain (Figure 3A), desmin (Figure 3B), and dystrophin (Figure 3C). Perivascular cells sorted from human muscle were then injected into the skeletal muscles of immunodeficient SCID-NOD mice that had been injured by intramuscular injection of cardiotoxin. Three weeks later, immunohistochemistry on injected muscle sections revealed the presence of myofibers expressing human spectrin (Figure 3D). A fluorescent probe for a human pancentromeric sequence was hybridized on some chimeric muscle sections, confirming the presence of central human nuclei within human spectrin expressing, regenerating myofibers (Figure 3D, insert). These results confirmed that perivascular cells sorted stringently from human skeletal muscle are endowed with myogenic potential. In three independent experiments, the myogenic potentials in vivo of freshly sorted perivascular cells ($CD146^{high}$ CD45− CD34− CD144− CD56−), myoblasts (CD146− CD45− CD34− CD144− CD56+) and total skeletal muscle cells were compared. These three populations generated, respectively, 20.1 ± 11.9, 13.3 ± 5.7, and 3.0 ± 2.5 myofibers expressing human spectrin per $10^3$ cells injected

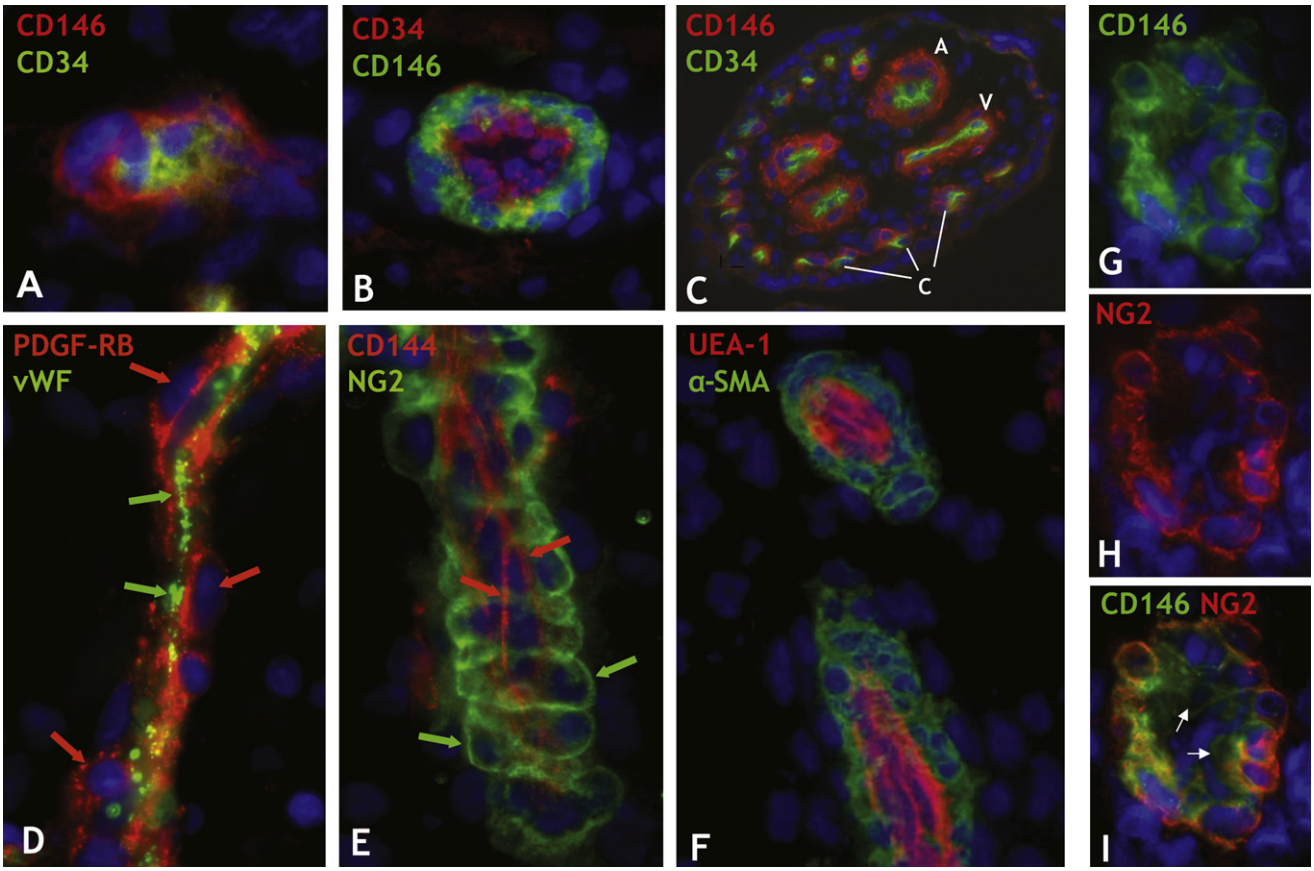


**Figure 1. Immunodetection of Perivascular Cells in Human Organs**

Sections were indirectly immunostained with antibodies to mural and endothelial cell markers. (A) Myocardium: a capillary endothelial cell in transverse section marked by CD34 expression (green) is closely surrounded by a CD146+ pericyte (red) (×900). (B) Skeletal muscle: small vessel transverse section; CD146+ perivascular cells (green) surround CD34+ endothelial cells (red) (×400). (C) Placental villus: arterioles (A), venules (V), and capillaries (C) are all lined with CD34+ endothelial cells (green) surrounded by CD146+ perivascular cells (×100). (D) Skeletal muscle: small vessel longitudinal section; PDGF-Rβ-positive perivascular cells (red; red arrows) surround vWF+ endothelial cells (green; green arrows) (×400). (E) Fetal pancreas: small vessel longitudinal section; NG2-positive perivascular cells (green; green arrows) surround CD144+ endothelial cells (red; red arrows) (×400). (F) Transverse and longitudinal sections of placental small blood vessels. Endothelial cells marked by the *Ulex europaeus* lectin (red) are surrounded by perivascular cells expressing α-SMA (green) (×400). (G–I) Transverse section of a skeletal muscle blood vessel double stained with antibodies to CD146 (G) and NG2 (H). (G) and (H) have been merged to create (I). Perivascular cells marked by CD146 expression also express NG2. Cells in a more central location express exclusively CD146 (arrows) and likely represent endothelial cells (×300). (A) Fetal myocardium; (B, D, G–I) skeletal muscle; (E) fetal pancreas; (C and F) placenta. Nuclei have been labeled blue with DAPI.

into the cardiotoxin conditioned mouse muscle (Figure 3H, red columns). Sorted perivascular cells produced at least as many myofibers as did purified CD56+ myoblasts, which rules out the possibility that the myogenic potential observed in the former is a consequence of their contamination by rare myoblasts.

These results indicate that at least some mural cells associated with muscle blood vessels are endowed with myogenic potential and may play a role in muscle ontogeny and regeneration, and confirm recently published results (Dellavalle et al., 2007). The important question as to whether this myogenic potential can be generalized to perivascular cells residing in nonmuscle tissues was then addressed by examining, in a similar experimental setting, mural cells extracted from pancreas, WAT, and placenta. $CD146^{high}$ CD34− CD45− CD56− cells were sorted from four placentas, 25 WAT samples, and 5 fetal pancreases along an antigen profile very similar to that encountered in the skeletal muscle (Figures 2E, 2F, and 2I). Purity of the sorted cells was confirmed by RT-PCR analysis (data not shown). Strikingly, placenta-, WAT- and pancreas-derived perivascular cells also exhibited potential, as did skeletal muscle perivascular cells, to generate myotubes in culture (data not shown) and to yield human dystrophin- and spectrin-expressing myofibers upon transplantation into SCID-mdx (Figure 3G) or cardiotoxin-treated SCID-NOD mouse muscles (Figures 3E and 3F). The muscle regeneration index of fat-derived perivascular cells was even higher than that of muscle perivascular cells assayed in the same conditions (Figure 3H, yellow bars).

## Cultured Perivascular Cells Retain Myogenic Potential and Exhibit Migratory Ability

Since both mesoangioblasts and MDSC are culture-adapted cell lines (Qu-Petersen et al., 2002; Cossu and Bianco, 2003), we next asked whether purified perivascular cells can be cultured

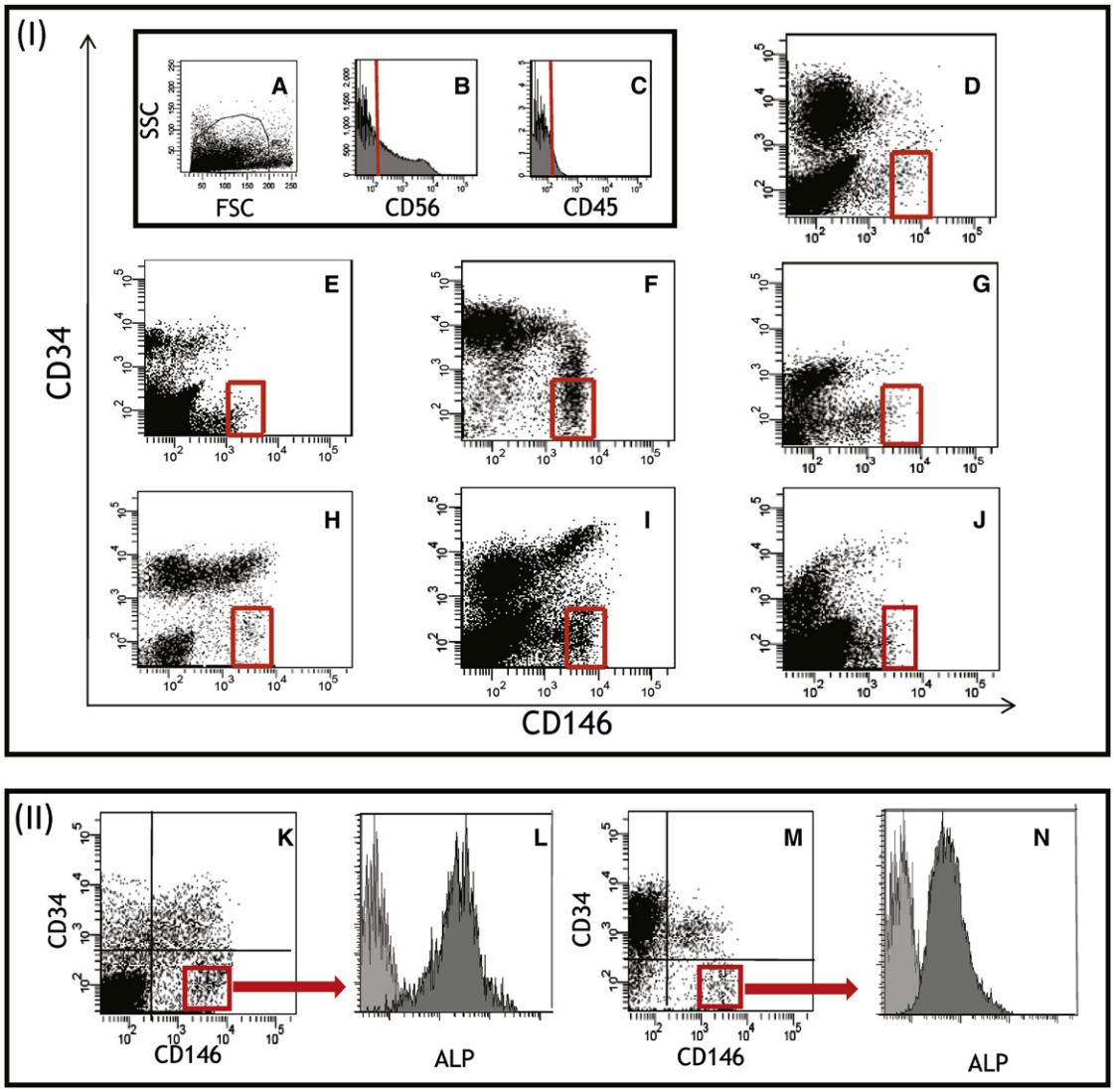


**Figure 2. Flow Cytometry Analysis and Sorting of Perivascular Cells**

Fresh tissues were dissociated enzymatically, and cell suspensions were stained with directly or indirectly labeled antibodies and run on a FACSAria cell sorter. Following double-scatter cell selection (A) and exclusion of CD56+ cells (B) and CD45+ cells (C), $CD146^{high}$ CD34− perivascular cells were sorted inside the gates represented in red. A similar cell subset was detected and sorted in skeletal muscle (D), placenta (E), adipose tissue (F), skin (G), myocardium (H), pancreas (I), and bone marrow (J). (A), (B), and (C) are from skeletal muscle. In box II, perivascular cells were identified (red gates) as described above in adipose tissue (K) and muscle (M). Additional staining of the same cell suspensions with an anti-ALP antibody revealed that virtually all perivascular cells coexpress ALP (L and N).

over the long term and still sustain myogenic potential. Perivascular cells sorted from fetal and adult muscle, midterm placenta, fetal skin, fetal pancreas, bone marrow, and adipose tissue and subsequently seeded into culture adhered and proliferated in a similar manner. Subconfluent perivascular cells generally exhibited an elongated, grossly rectangular shape and displayed short arms at their smaller ends (Figure 4A). At confluence, cells were more polygonal (Figure 4B). Contact inhibition was not obvious, since cells at confluence occasionally grew into spherical structures above the plastic adherent monolayer (data not shown). Figure 4C illustrates the cumulative number of population doublings (PDs) during 20 weeks of continuous perivascular cell culture from a 23-week-old fetal muscle: sorted cells could undergo more than 40 PDs before the onset of senescence. We calculated the perivascular cell population doubling time (PDT) as previously described (Deasy et al., 2005). Growth was slow in the first 6 weeks: approximately one PD per week or PDT = 162 hr. We observed the fastest growth rate during weeks 6–16 (approximately 5–13 passages), during which the PDT was approximately 60 hr. After 17 weeks of culture, perivascular cell growth again slowed down to a PDT of about 106 hr (Figure 4C). The same growth kinetics was observed for perivascular cells sorted from pancreas, skin, adipose tissue, and placenta (data not shown). Gene expression in cultured perivascular cells was analyzed by RT-PCR. After either 4, 8, or 14 passages, muscle-derived perivascular cells stably expressed NG2, CD146, and

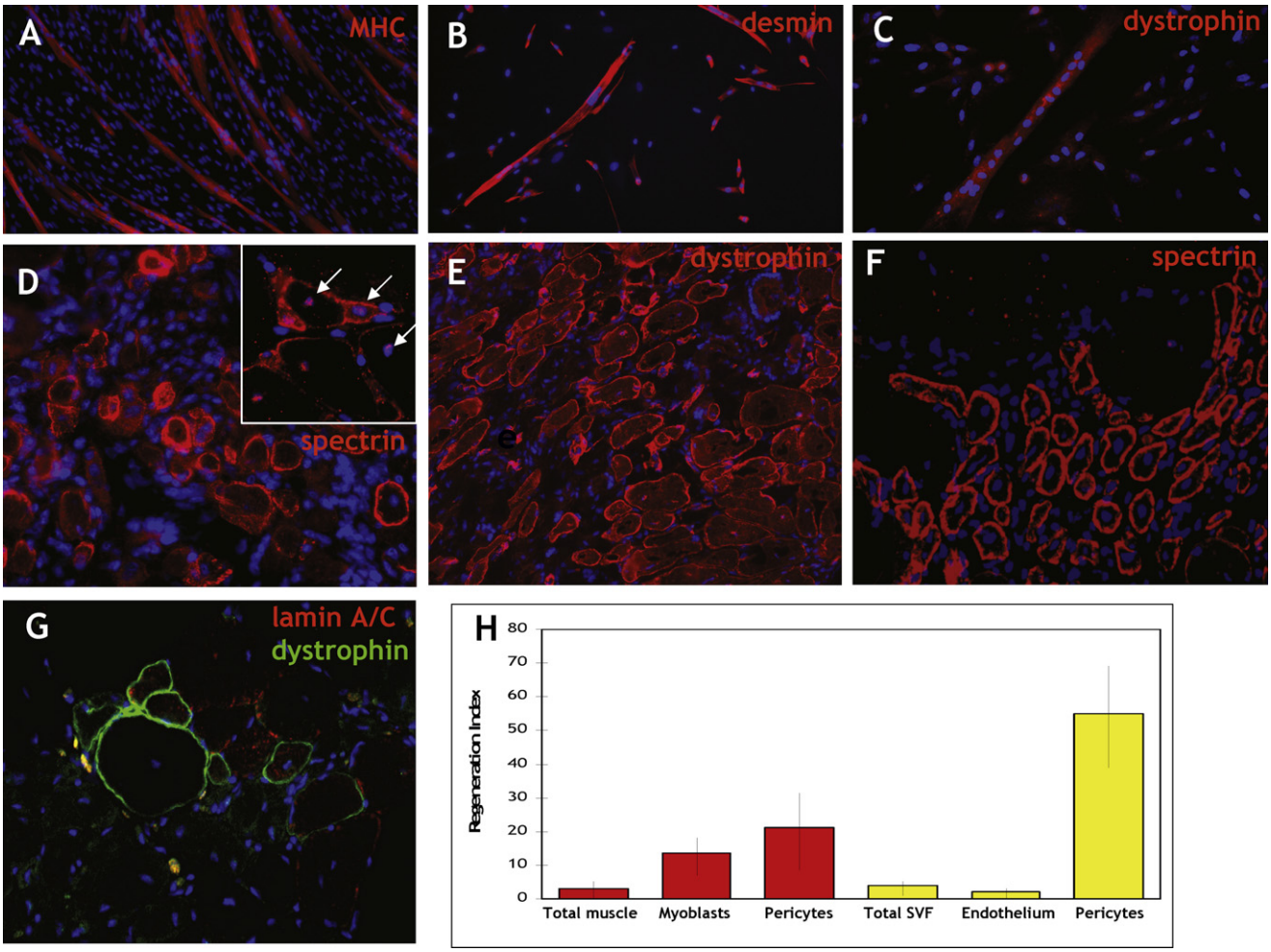


**Figure 3. Myogenic Potential of Perivascular Cells**

Two thousand CD146+ CD56− CD34− CD45− cells sorted from skeletal muscle were seeded per well into a 48-well plate in myogenic culture conditions. Two weeks later, numerous multinucleated muscle fibers expressing slow myosin heavy chain (MHC) (A, ×100), desmin (B, ×100), and dystrophin (C, ×200) had developed. Nuclei have been labeled blue with DAPI. $5 \times 10^3$ perivascular cells sorted from skeletal muscle (D), pancreas (E), or $10^4$ from WAT (F) were injected into cardiotoxin-conditioned SCID-NOD mouse muscles. Three weeks later, recipient muscle frozen sections were stained with antibodies specific to human spectrin (D and F) and human dystrophin (E). Numerous human spectrin- and dystrophin-expressing muscle fibers (red) are present (×200). In one experiment ([D], insert), sections from a recipient mouse muscle were immunostained with an antibody to human spectrin, then exposed to a probe specific for a human pancentromeric sequence. Hybridization products appear conspicuously (pink) in the central nuclei of human spectrin expressing myofibers (arrows). (G) $2.5 \times 10^4$ perivascular cells sorted from the midgestation placenta were injected into dystrophin-deficient SCID-mdx mouse muscles that were harvested 4 weeks later. Frozen sections were stained with antibodies to mouse/human dystrophin (green) and human lamin A/C (red). Clusters of human dystrophin-expressing myofibers are present, and human cells reside near the regenerated myofibers (yellow). Nuclei have been labeled blue with DAPI (×200). (H) Red columns: unfractionated adult skeletal muscle cells, myoblasts (CD146- CD45- CD34- CD56+), and perivascular cells ($CD146^{high}$ CD45− CD34− CD56−) sorted therefrom were injected into the cardiotoxin-treated skeletal muscles of SCID-NOD mice. Yellow columns: the same experiment was performed with the WAT unfractionated stromal vascular fraction (SVF), endothelial cells (CD45− CD34+ CD56−), or perivascular cells ($CD146^{high}$ CD45− CD34− CD56−) purified from the same WAT. Three weeks later, human spectrin-expressing myofibers were counted on sections of recipient mouse muscles, and the regeneration index was calculated as the number of human myofibers produced per $10^3$ donor cells injected (three independent experiments). Error bars represent the standard error of the mean.

α-SMA, but not CD31, CD34, CD45, or CD144, excluding the growth of contaminating endothelial or hematopoietic cells (Figure 4D).

The migration of progenitor cells at the site of injured or missing tissue is logically important for successful organ reconstruction. Degradation products of mammalian extracellular matrix (ECM) are chemotactic for progenitor cells, both in vivo and in culture (Reing et al., 2008). Cultured perivascular cells exhibited strong chemotaxis toward both a papain and a pepsin digest of ECM harvested from porcine urinary bladder (UBM) (Figure 4E).

Importantly, perivascular cells extracted from either muscle, placenta, or pancreas and cultured remained capable, at all passage times tested (5, 9, 11), of differentiating into myotubes in culture (data not shown) and regenerating myofibers in vivo (Figure 5A). Cultured perivascular cells from a 23 week fetal muscle were efficiently infected with recombinant lentiviruses encoding green fluorescent protein (GFP), close to 100%

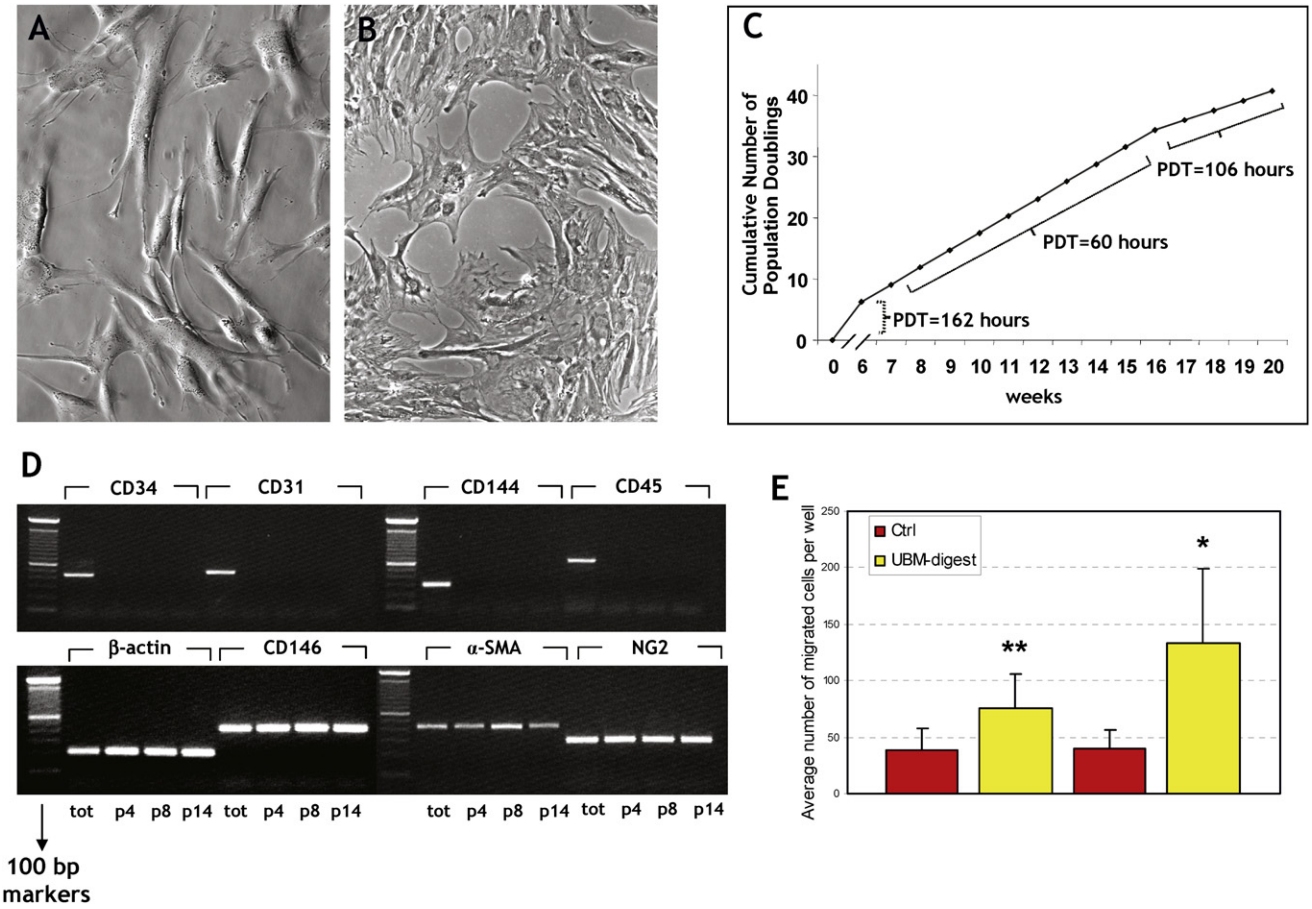


**Figure 4. Long-Term Culture of Purified Perivascular Cells**

Perivascular cells sorted from skeletal muscle and seeded in culture adhere and proliferate ([A], ×400) to confluence ([B], ×100). (C) PDs during 20 weeks of continuous muscle-derived perivascular cell culture. PDTs are indicated on the plot. The fastest growth rate is observed during weeks 6–16, (PDT of about 60 hr). (D) RT-PCR analysis was performed on perivascular cells sorted from the same muscle and cultured for 4, 8, and 14 passages (p4, p8, p14) and total fresh dissociated skeletal muscle cells (tot) to detect expression of markers of endothelial cells (CD31, CD34, CD144), hematopoietic cells (CD45), and perivascular cells (CD146, α-SMA, NG2). Only the latter are detected at all stages of the culture. (E) Perivascular cell migration toward pepsin-digested (left columns) and papain-digested (right columns) ECM was measured in a chemotaxis chamber. Migrations in response to matrix degradation products (yellow columns) and control buffer (red columns) were compared. $^{**}p \leq 0.02$ and $^{*}p \leq 0.05$, respectively. The y axis represents the number of cells per well that have migrated through the filter toward the chemoattractant.

cultured cells expressing GFP upon transduction. When injected into cardiotoxin-injured SCID-NOD mouse skeletal muscles, GFP-transgenic cells gave rise to discrete green fluorescent myofibers, confirming the myogenic potential of cultured perivascular cells (Figure 5B).

## Cultured Perivascular Cells Give Rise to MSCs

We assessed, by flow cytometry and RT-PCR, antigens expressed by long-term cultured human perivascular cells (Figure 6). This confirmed that all perivascular cells still display, over extended culture, the markers their ancestors natively expressed in the tissue of origin (CD146, α-SMA, NG2, PDGF-Rβ, alkaline phosphatase) and that no cells in these cultures express markers of endothelial cells (CD34, CD144, CD31, and vWF), hematopoietic cells (CD45), or myogenic cells (myogenin, m-cadherin, myf-5, and Pax7) (Figures 6A–6C). We also investigated the expression in these cultures of antigens that typify MSCs derived from human bone marrow. Intriguingly, cultured human perivascular cells from either skeletal muscle, pancreas, adipose tissue, placenta, bone marrow, or other organs expressed all recognized markers of MSC, including CD10, CD13, CD44, CD73, CD90, and CD105 (Figure 6A) as well as CD108 (Sema L), CD109 (platelet activation factor), CD140b (PDGF-Rβ), CD164 (MGC 24), CD166 (ALCAM), CD318 (CDCP1), CD340 (HER-2), CD349 (frizzled-9), SSEA-4, and HLA-CL I (data not shown). In contrast, cultured perivascular cells, similar to MSC, do not express CD56, CD106, CD133, CD324 (E-cadherin), CD326 (Ep-CAM), CD344 (frizzled-4), and HLA-DR (Figure 6 and data not shown). These results suggested that the elusive MSCs are derived from perivascular cells. To further document this possible affiliation, we explored whether the developmental potential of cultured perivascular cells reflects that of MSCs. Indeed, when cultured in appropriate inductive conditions, perivascular cells from all tissue sources tested, including bone

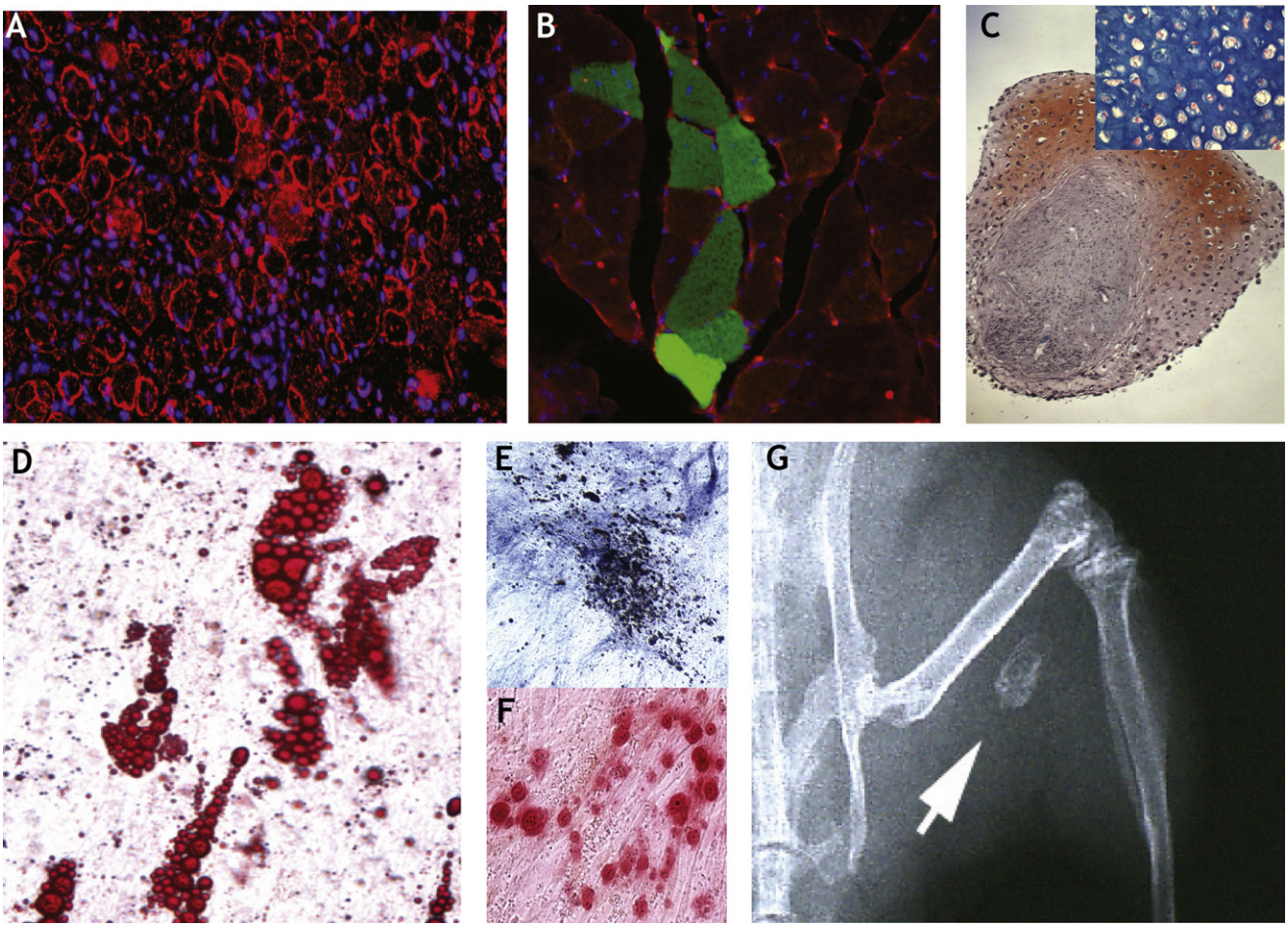


**Figure 5. Multilineage Potential of Long-Term Cultured Perivascular Cells**

(A) Twenty thousand perivascular cells sorted from skeletal muscle and cultured for 9 weeks were injected into the cardiotoxin-treated skeletal muscles of SCID-NOD mice. Three weeks later, human spectrin-expressing myofibers generated by injected perivascular cells are present in the host muscle (red). Nuclei have been labeled blue with DAPI (×200).

(B) $10^6$ GFP-expressing cultured perivascular cells were injected into a cardiotoxin-damaged tibialis anterior skeletal muscle. Fourteen days later, clusters of GFP-expressing myofibers (green) are present throughout the recipient muscle (×30).

(C) Cultured perivascular cells were centrifuged into high-density cell pellets and cultivated in chondrogenic medium in the presence of TGF-β1. Twenty-one days later, fixed pellet sections were stained with safranin O (×20). (Insert) Pellet section stained with Alcian blue and nuclear fast red for the detection of s-GAG and nuclei, respectively (×150).

(D) Cultured perivascular cells were further cultivated in adipogenic medium for 14 days, then fixed and incubated with Oil red O for detection of lipids (×250).

(E) Cells cultivated in osteogenic medium for 21 days were fixed and treated for the detection of alkaline phosphatase, then incubated in a 2.5% silver nitrate solution (von Kossa staining). Alkaline phosphatase-positive cells are blue, and mineral deposits appear in black (×150).

(F) Cells cultivated in osteogenic medium as in (E) were incubated for 10 min in alizarin red at pH 4.2. Calcium deposits are stained in red (×150).

(G) Cultured perivascular cells immobilized in a Gelfoam sponge were implanted in a skeletal muscle pocket cut in the hind limb of a SCID-NOD mouse. X-ray analysis, at day 30 after implantation, reveals a high-density area in the recipient muscle, demonstrating ectopic bone formation by the implanted cells.

marrow, differentiated into chondrocytes (Figure 5C) and multilocular adipocytes (Figure 5D). Cultured perivascular cells also gave rise to osteocytes in vitro (Figures 5E and 5F) and developed into bony nodules when transplanted into a skeletal muscle pocket (Figure 5G) in an immunodeficient mouse. In order to ascertain that individual cultured perivascular cells are multipotent, cells from two independent cultures of muscle pericytes were cloned by limiting dilution. For each starting pericyte population, 480 wells were seeded with single cells, out of which 120 and 48 clones developed, respectively (i.e., 25% and 10% of single seeded perivascular cells grew clonally). Ten randomly chosen clones from each donor tissue were further cultured and split to analyze separately adipogenic, chondrogenic, and osteogenic differentiation potentials. Each one of the 20 perivascular cell clones analyzed differentiated into the three cell lineages, demonstrating that cloned perivascular cells exhibit the typical developmental potential of MSCs (data not shown).

## Perivascular Cells Natively Express MSC Markers

Having shown that perivascular cells sorted to homogeneity from diverse human organs yield in culture a progeny of MSCs, we wished to determine whether this affiliation can be further

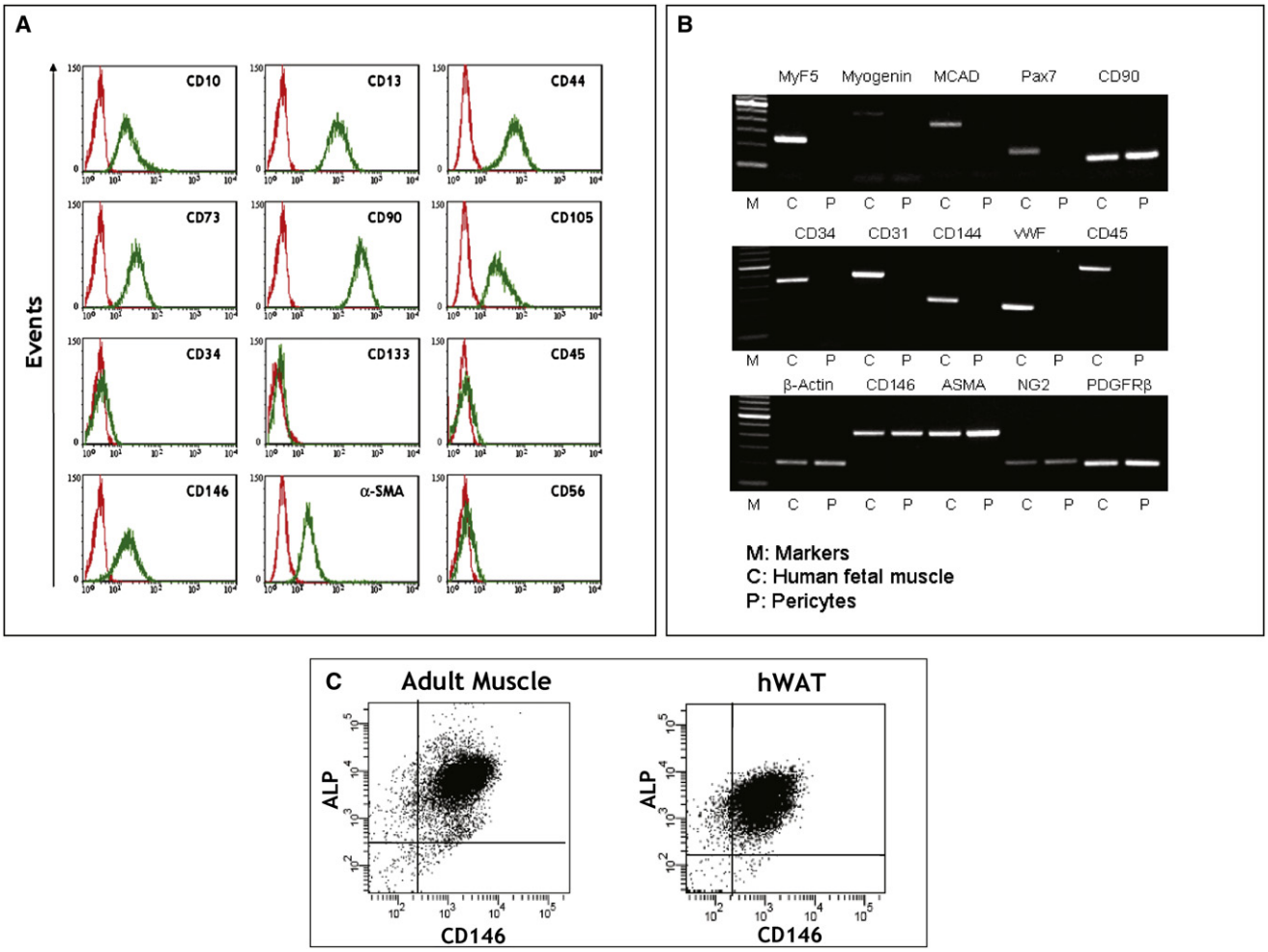


**Figure 6. Long-Term Cultured Perivascular Cells Express Markers of MSCs**

(A) Cells were detached from the culture flask with trypsin, permeabilized with Triton X-100 when required, and stained with directly labeled monoclonal antibodies (green histograms) or exposed to isotype-matched nonimmune directly labeled immunoglobulins (red histograms).

(B) Perivascular cells purified from skeletal muscle and cultured for 7 passages (9 weeks) were analyzed by RT-PCR. Presence of messengers expressed in endothelial cells (CD34, CD144, CD31, and vWF), perivascular cells (CD146, α-SMA, NG2, PDGF-Rβ), hematopoietic cells (CD45), MSC (CD90), and myogenic progenitors (M-cadherin, myogenin, Myf5, and Pax7) was compared between cultured pericytes (P) and total muscle (control, C).

(C) Perivascular cells sorted from adult skeletal muscle and hWAT and cultured for 4 weeks were detached and double stained with antibodies to CD146 and ALP.

supported by showing that mural cells, in their native perivascular arrangement within intact tissues, already express MSC markers. To this end, antibodies to CD44, CD73, CD90, and CD105 were added, in a five-color FACS analysis, to those used to typify perivascular cells as described in Figure 2. One fetal (23 weeks) and four adult skeletal muscles (56–86 years), three midgestation and two term placentas, and two adult WAT samples (27 and 42 years) were analyzed along this strategy. CD146$^{high}$ CD34− CD45− CD56− perivascular cells were found to express CD44, CD73, CD90, and CD105 (Figures 7A–7E), which was confirmed by immunohistochemical staining of tissue sections (Figures 7F–7J). The perivascular location of the cells expressing MSC markers was confirmed in confocal microscopy by triple immunohistostaining with anti-CD146 (Figures 7I and 7J) and anti-α-SMA (data not shown).

## DISCUSSION

We have refined the analysis and purification of cells that constitute the human blood vessel wall. Confirming and extending previous observations (Ozerdem et al., 2002; Middleton et al., 2005; Sacchetti et al., 2007), we have validated the CD146+ NG2+ PDGFRβ+ ALP+ CD34− CD45− vWF− CD144− phenotype as an indicator of pericyte/perivascular cell identity throughout human fetal and adult organs. We demonstrate that perivascular cells isolated prospectively from skeletal muscle and, less expectedly, nonmuscle tissues are myogenic in culture and in vivo. We can rule out that the myogenic potential present in perivascular cells sorted from skeletal muscle is due to contamination by regular myogenic cells since (1) no Pax7 or CD56 expression was ever detected by RT-PCR analysis within

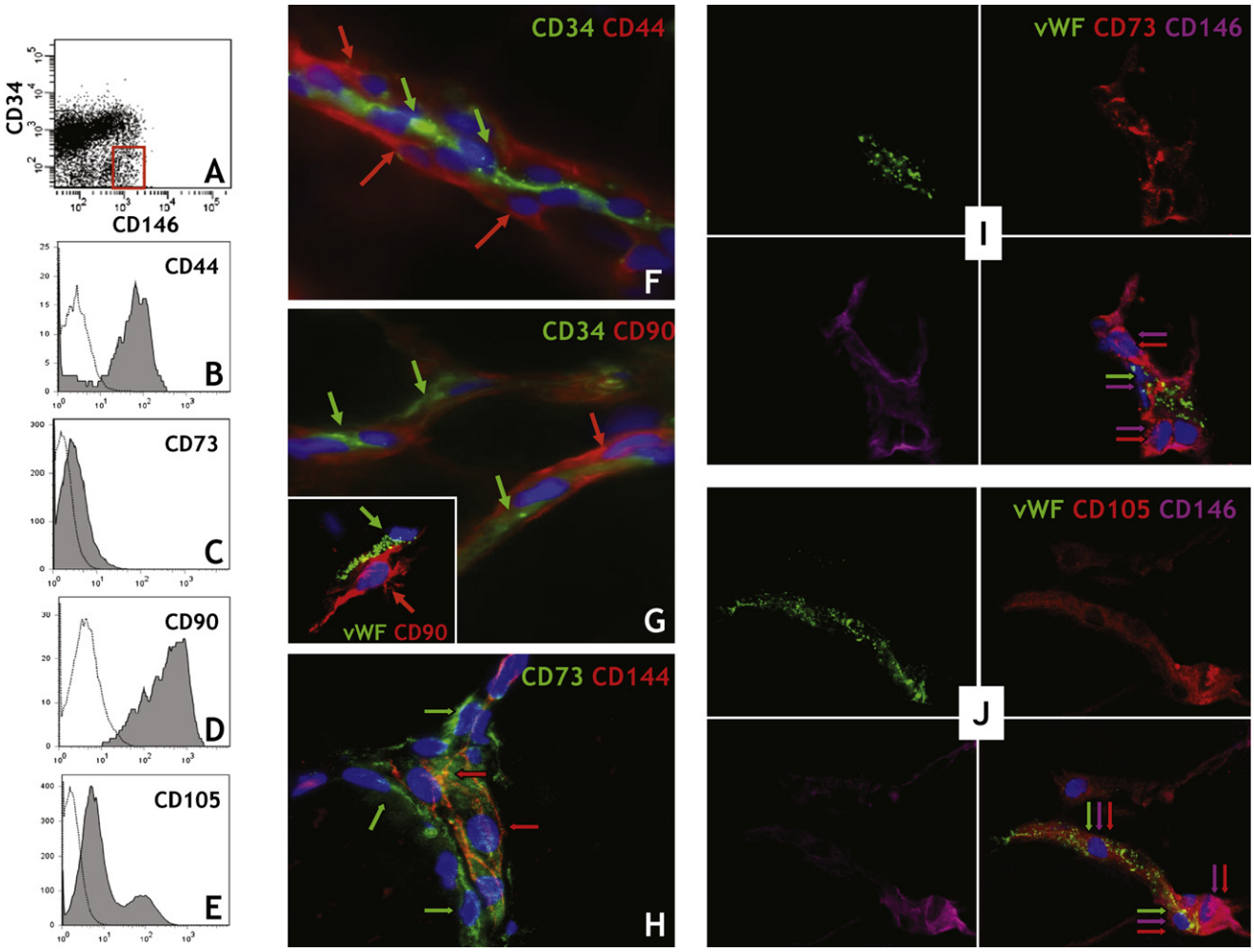


**Figure 7. Perivascular Cells Natively Express MSC Markers**

(Left column) The stromal vascular fraction isolated from human WAT was stained simultaneously with antibodies to perivascular cells and MSCs and analyzed by flow cytometry. CD45− CD56− CD146$^{high}$ CD34− cells were gated (A) and analyzed for coexpression of CD44 (B), CD73 (C), CD90 (D), and CD105 (E). Clear histograms in (B)–(E) represent control cells incubated with unrelated isotype-matched antibodies. (Middle column) Frozen sections of human WAT were costained with antibodies to CD34 (green) or von Willebrand factor (vWF, green) to reveal endothelial cells (green arrows) and either CD44 (red, [F]) or CD90 (red, [G]. Pericytes lining small blood vessels express both CD44 (F) and CD90 ([G], main) (red arrows). Pericytes surrounding capillaries also strongly express CD90 ([G], inlet ×1000) (red arrow). (H) Frozen sections of adult human muscle were costained with antibodies to CD144 (red) to reveal endothelial cells (red arrows) and CD73 (green). Pericytes lining the small blood vessel express CD73 ([H], ×600, green arrows). (Right column) Frozen sections of human WAT were colabeled with antibodies to vWF (green), CD146 (purple), and CD73 ([I], red) or CD105 ([J], red). Confocal microscopy revealed that pericytes lining capillaries express both CD73 ([I], ×1000) and CD105 ([J], ×1000) in addition to CD146 (purple/red arrows). In contrast, endothelial cells express vWF and lower levels of CD146 (I) (green/purple arrows) as well as CD105 (J) (green/purple/red arrows).

extracts of freshly sorted cells or by immunocytochemistry on the long-term cultured progeny thereof and (2) the average muscle regeneration index of perivascular cells was at least as high as that of CD56+ myogenic cells purified from the same muscles. We also confirmed that cultured muscle pericytes, despite their vigorous myogenic potential, do not express any known myogenic cell marker such as MyoD, myogenin, m-cadherin, myf-5, and Pax7. This is an important point inasmuch as some activated myoblasts in fetal muscle express CD146 (Cerletti et al., 2006). These results confirm that pericytes in human skeletal muscle represent a myogenic cell compartment that is distinct from that of satellite cells (Dellavalle et al., 2007) but, importantly, also extend this potential to perivascular cells present in nonmuscle tissues such as pancreas, fat, bone marrow, and placenta, indicating the existence of a ubiquitous myogenic potential throughout the organism. We suppose that this developmental potential is circumscribed to pericytes, i.e., perivascular cells associated with capillaries and microvessels, which build up most of, if not all, the vasculature in some of the tissues analyzed, such as fetal pancreas, muscle, and WAT. However, the presence of myogenic progenitors at the periphery of larger veins and arteries cannot be ruled out, since two of the pericyte markers used in this work, NG2 and CD146, are also expressed around larger blood vessels.

Multilineage progenitor cells have been previously identified in multiple adult human and rodent tissues to include (1) MSCs,

which are derived from bone marrow, placenta, umbilical cord, and cord blood and adipose tissue and can differentiate into mesoderm lineage cells, including myoblasts (Caplan, 1991; Pittenger et al., 1999); (2) muscle-derived MDSCs, which some of us have previously characterized (Qu-Petersen et al., 2002; Péault et al., 2007); and (3) bone marrow-derived MAPCs, which can contribute to mesodermal, endodermal, and ectodermal cell lineages and have equivalents in mouse brain (Jiang et al., 2002), pancreas (Seaberg et al., 2004), and dermis (Toma et al., 2001) as well as in human skin (Shih et al., 2005) and WAT (Zuk et al., 2002). The existence of all these adult multipotent progenitors has been, however, revealed only retrospectively in long-term cultures of the source tissues; therefore, their identity and anatomic distribution in native organs could not be determined. Using a large panel of known and novel cell markers (Battula et al., 2007; Gang et al., 2007), we observed that cultured perivascular cells from a variety of tissues exhibit a phenotype that is strikingly similar to that of MSCs derived from bone marrow. Moreover, we show that long-term cultured perivascular cells sorted from diverse fetal and adult tissues can differentiate into osteocytes, chondrocytes, and adipocytes, which is the cardinal property of MSCs. Most importantly, single cultured perivascular cells seeded in vitro developed at high frequency into clones, which all yielded osteocytes, chondrocytes, and adipocytes when seeded in the appropriate differentiation conditions. This demonstrates that each individual perivascular cell has multilineage mesodermal potential and therefore adheres to the strict definition of a MSC. Conversely, our unpublished observations indicate that the same cultured human perivascular cells can neither differentiate into neural cells nor develop into teratomas when transplanted into mouse brain and testis, respectively (data not shown). These cells therefore appear to be developmentally closer to MSCs than MAPCs or ESCs. In support of a perivascular origin of MSCs, we have also observed that perivascular cells express natively, before culture, CD44, CD73, CD90, and CD105, four surface molecules commonly used as MSC markers. This indicates that perivascular cells—or a subset thereof—have not merely acquired MSC antigens in culture but natively expressed these markers, and therefore further suggests a developmental affiliation between perivascular cells and MSCs. Interestingly, Schwab and Gargett (2007) have also suggested CD146 and PDGFRβ as markers of MSC-like cells in the endometrium, and Traktuev et al. (2008) described multipotent cells in WAT that coexpress some pericyte and MSC markers; that cell subset is, however, marked by CD34 expression and therefore clearly distinct from the cells we describe herein.

Overall, our data support the hypothesis that an ancestor of the MSC is natively associated with the blood vessel wall and, more precisely, belongs to a subset of perivascular cells (da Silva Meirelles et al., 2008), even though it remains possible that some MSCs originate in other cell subsets. The omnipresence of mural cells would explain why such multilineage progenitors have been found in a multitude of organs. In agreement, pericytes surrounding brain blood vessels constitutively express nestin, a marker of neuronal progenitor cells (Alliot et al., 1999), and therefore may play a role in neuronal regeneration. Chemoablated Leydig cells in the rat testis are regenerated by adjacent vascular pericytes which, during this process, transiently express nestin (Davidoff et al., 2004). A study performed in mice also showed that perivascular cells expressing Annexin 5 represent multilineage mesenchymal progenitors (Brachvogel et al., 2005). Interestingly, a population of CD146+ subendothelial cells in human bone marrow contains osteogenic progenitors that are also at the origin of the stromal cells that support hematopoiesis (Sacchetti et al., 2007).

A physiological role of perivascular cells in human skeletal muscle regeneration remains, however, to be formally demonstrated, especially with respect to the observed presence of a similar myogenic potential within pancreas, placenta, or fat. Satellite cells are undifferentiated myoblasts that are integral to myofiber regeneration during postnatal life (Morgan and Partridge, 2003; Péault et al., 2007), and experiments in quail-chicken chimeras have revealed the origin of adult satellite cells in the dermomyotome (Gros et al., 2005). This makes it unlikely that, at least in birds, cells from the vessel wall contribute significantly to the pool of satellite cells.

On the other hand, we have recently identified a population of myoendothelial cells in human skeletal muscle that coexpress markers of both satellite and endothelial cells and exhibit robust myogenic potential (Zheng et al., 2007). While the physiologic role of vascular mesodermal progenitors in tissue development, repair, and homeostasis remains to be elucidated, their practical use to treat medical conditions can be already envisioned, since these cells can be easily purified from convenient tissue sources such as skeletal muscle and adipose tissue and multiplied in culture to therapeutically relevant numbers with no significant loss of developmental potential.

## EXPERIMENTAL PROCEDURES

### Human Tissues

Human fetal tissues were obtained following spontaneous, voluntary, or therapeutic pregnancy interruptions performed at Magee-Womens Hospital (University of Pittsburgh), in compliance with Institutional Review Board protocol number 0506176. Developmental age (16–24 weeks of gestation) was estimated by measuring foot length. Informed consent for the use of fetal tissues was obtained from patients in all instances. Adult human pancreas and muscle were procured by the Center for Organ Recovery and Education (CORE, Pittsburgh) from multiorgan donors. Abdominal subcutaneous fat was obtained anonymously from female patients (mean age of 51 years) undergoing abdominoplasty at the Department of Surgery of the University of Pittsburgh Medical Center.

### Immunohistochemistry and Cytochemistry

Fresh tissues were gradually frozen by immersion in isopentane (Merck) cooled in liquid nitrogen and embedded in tissue freezing medium (Triangle Biomedical Sciences). WAT was impregnated in gelatin/sucrose and frozen in the same conditions. Sections (5–9 μm) were cut on a cryostat (Microm) and fixed for 5 min with 50% acetone (VWR International) and 50% methanol (Fischer Chemical) or for 10 min in 4% paraformaldehyde (PFA, Sigma). Sections were dried for 5 min at room temperature (RT), washed three times for 5 min in PBS, and blocked with 5% goat serum (GIBCO) in PBS for 1 hr at RT. Sections were incubated with uncoupled primary antibodies overnight at 4°C or for 2 hr at RT in the case of directly coupled antibodies. After rinsing, sections were incubated for 1 hr at RT with a biotinylated secondary antibody, then with fluorochrome-coupled streptavidin, both diluted in 5% goat serum in PBS. For intracellular stainings, cells were first permeabilized with PBS 0.1% Triton X-100 (Sigma). Cultured cells were fixed inside wells as described above, then washed three times in PBS 0.1% Triton X-100 and incubated for 1 hr in PBS, 5% goat serum. Cultured cells were then stained as described above, in the presence of 0.1% Triton X-100. The following uncoupled

anti-human primary antibodies were used: anti-CD140b (PDGF-Rβ; clone 28D4; Monoclonal Antibody Facility of the University Clinic of Tübingen, undiluted), anti-CD146 (BD Pharmingen, 1:100), anti-CD31 (DAKO, 1:100), anti-CD34 (Serotec, 1:50), anti-CD44, anti-CD90 (both from Becton Dickinson (BD), 1:20), anti-CD73 and anti-CD105 (both from Invitrogen, 1:50), anti-NG2 (BD Pharmingen, 1:300), and anti-lamin A/C (Novo Castra, 1:100). Coupled antibodies used included the following: anti-CD146-Alexa 488 (Chemicon, 1:200), anti-α-SMA-FITC (Chemicon, 1:100), anti-CD34-FITC (DAKO, 1:50 or Miltenyi, 1:20), anti-vWF-FITC (US Biological, 1:100), biotinylated anti-CD144 (BD, 1:100), and biotinylated anti-CD146 (Miltenyi Biotec, 1:11). Streptavidin-Cy3 (Sigma, 1:500) and Streptavidin-Cy5 (CyDye, 1:500) were used in conjunction with biotinylated antibodies. Skeletal muscle proteins were detected with anti-skeletal myosin heavy chain (fast) (Sigma 1:100), anti-skeletal myosin heavy chain (slow) (Sigma 1:100), anti-spectrin and anti-dystrophin (Novocastra, 1:20) and anti-desmin (1:50, Sigma). Rabbit anti-mouse dystrophin (Abcam, 1:100) was used to detect dystrophin positive myofibers in SCID/mdx mice. Directly biotinylated *Ulex europaeus* lectin (UEA-1) was also used as an endothelial cell marker (Vector, 1:200). Secondary goat anti-mouse antibodies were biotinylated (DAKO and Immunotech, 1:1000) or coupled to Alexa 488 (Molecular Probes, 1:500). Streptavidin-Cy3 (Sigma, 1:1000) was used. Nuclei were stained with DAPI (4′, 6-diamino-2-phenylindole dihydrochloride, Molecular Probes, 1:2000) for 5 min at RT. An isotype-matched negative control was performed with each immunostaining. Slides were mounted in glycerol-PBS (1:1, Sigma) and observed on an epifluorescence microscope (Nikon Eclipse TE 2000-U). Alternatively, sections were analyzed on an Olympus Fluoview 1000 confocal microscope equipped with 100× oil immersion optics.

Fluorescent in situ hybridization, used in one experiment, is described in the Supplemental Data available online.

### Flow Cytometry

Fresh tissues were cut into small pieces in Dulbecco's modified Eagle's medium (DMEM, GIBCO) containing 20% fetal calf serum (FCS, GIBCO), 1% penicillin-streptomycin (PS, GIBCO), and collagenases I, II, and IV (1 mg/mL, Sigma), then incubated at 37°C for 1 hr on a shaker. Final cell dissociation was achieved between ground glass slides. Adipose tissue was minced, then digested in DMEM containing 3.5% bovine serum albumin (Sigma) and collagenase II (1 mg/ml, Sigma) for 70 min under agitation at 37°C. Mature adipocytes were separated from pellets by centrifugation (2000 rpm, 10 min). Pellets were resuspended in erythrocyte lysis buffer (155 mM $NH_4Cl$, 10 mM $KHCO_3$, 0.1 mM EDTA) and incubated for 10 min at RT. Placenta was minced and agitated in DMEM, 1% PS, and 1 mg/ml collagenases I, II, and IV (1 g tissue/1 ml solution) for 30 min at 37°C, 120 rpm; 0.05% trypsin (GIBCO) was added, and the suspension was agitated for 10 min more. Cells were centrifuged and resuspended in DMEM, 1% PS. Cells were passed through a 70 μm cell strainer, centrifuged, and resuspended in erythrocyte lysis buffer and incubated for 15 min at RT.

Cells from all tissues were then processed for immunofluorescence staining as previously described (Zheng et al., 2007). Cells ($10^5$ for analysis and around $30 \times 10^6$ for sorting) were incubated with a combination of the following directly coupled mouse anti-human antibodies: anti-CD34-PE (DAKO, 1:100), anti-CD45-APC-Cy7 (Santa Cruz Biotechnologies, 1:200), or anti-CD45-APC (BD, 1:100), anti-CD56-PE-Cy7 and anti-CD146-FITC (Serotec, 1:100) in 1 ml DMEM, 20% FCS, and 1% PS at 4°C for 15 min in the dark. Cells were then incubated for 15 min with 7-amino-actinomycin D (7-AAD, 1:100, BD) for dead cell exclusion and run on a FACSAria flow cytometer (BD). Five-color analysis of ALP and MSC marker expression by perivascular cells is described in the Supplemental Data.

Cultured cells were labeled at different passages with the following commercial antibodies: anti-CD13-PE, -CD34-PE, -CD44-FITC (BD), anti-CD45-PE-Cy7 (Beckman Coulter), anti-CD56-PE (Chemicon), anti-CD73-PE (BD), anti-CD90-PE (Chemicon), anti-CD105 FITC (ImmunoTools), anti-CD133-2-APC (Miltenyi Biotec), anti-CD146-PE (BioCytex), anti-α-SMA-FITC (Sigma), anti-HLA-ABC-FITC (Immunotech), and anti-HLA-DR-PE, -CXCR4, -NGF-R, and -BB9 (BD), the latter being revealed with anti-mouse IgG1-FITC (Exalpha). The following reagents from the monoclonal antibody facility of the University Clinic of Tübingen were also used for staining of cultured cells: anti-CD10 (CALLA; clone 97C5), anti-CD34 (clone 43A1), anti-CD56 (N-CAM; clone 39D5), anti-CD105 (endoglin; clone 1G2C2), anti-CD109 (clone W7C5), anti-CD133 (clone W6B1C3), anti-CD140b (PDGF-RB; clone 28D4), anti-CD164 (clone 67D2), anti-CD318 (CDCP1; clone CUB1), anti-CD324 (E-cadherin; clone 67A4), anti-CD326 (Ep-CAM; clone 9C4), anti-CD340 (HER-2; clone 24D2), anti-CD344 (frizzled-4; clone CH3A4), and anti-CD349 (frizzled-9; clone W3C4E11). Anti-CD166 was purchased from BD Pharmingen, and the PE conjugates against CD31, CD106, and CD108 were a kind gift from Dr. Gene Lay (BioLegend, San Diego, CA). Full information on the human cell markers used in this study can also be found at: http://www.hcdm.org. Isotype control immunoglobulins used were IgG1-PE, IgG1-FITC (both from Chemicon), IgG1-PE-Cy7 (Beckman Coulter), and IgG1-APC (BD). Resuspended cultured cells were stained as follows. Cells were permeabilized with 0.1% Triton X-100 (Sigma) when necessary. After washing the cells twice with PBS containing 1% FCS and 0.01% $NaN_3$ (FACS buffer), cells were incubated with polyglobin to block nonspecific binding. Cells were then incubated with the indicated primary antibodies for 15 min on ice. After washing in FACS buffer, cells were incubated with a $F(ab)_2$ fragment of goat anti-mouse secondary antibody conjugated with R-PE (Dako Cytomation) for 15 min. Finally, cells were washed twice, and at least 50,000 events were acquired on a FACSCanto II cytometer (BD), using FCS express software for analysis.

### RT-PCR

Total RNA was extracted from $10^4$ cells using the Absolutely RNA Nanoprep Kit (Stratagene). cDNA was synthesized with SuperScript II reverse transcriptase (Invitrogen). PCR was performed for 30 cycles at 58°C annealing temperature with Taq polymerase (Invitrogen), and PCR products were electrophoresed on 1% agarose gels. The primers used for PCR are listed in Table S1. Each set of oligonucleotides was designed to span two different exons so that genomic DNA contamination is of no concern.

### Cell Culture and Gene Transduction

Sorted perivascular cells were seeded at $2 \times 10^4$ cells per $cm^2$ in Endothelial Cell Growth Medium 2 (EGM-2, Cambrex BioScience) and cultured at 37°C for 2 weeks in plates coated with 0.2% gelatin (Calbiochem). Confluent cells were then detached by treatment with trypsin-EDTA (GIBCO) for 10 min at 37°C, then split 1:3 in uncoated plates in DMEM high glucose (GIBCO), 20% FCS, 1% PS (GIBCO). After the fifth passage, cells were then passaged 1:6 in the same conditions, and culture medium was changed every 4 days. We calculated the PDT as previously described (Deasy et al., 2005). Perivascular cells were cloned in 96-well cloning plates (BD) by serial limiting dilution down to a concentration of one cell/well in DMEM, 20% FCS. Medium was changed twice a week. Plates were examined daily under the microscope in order to evaluate cell growth. Each clone was expanded until enough cells were present to test differentiation potentials as described below. For gene transfer, cultured perivascular cells at passage 12 were detached with 0.25% trypsin/EDTA and seeded at a density of 100,000 cells/$cm^2$. After 16 hr, medium was replaced with transduction medium (DMEM high glucose, 20% FCS, 1% PS, 8 μg/mL polybrene), and an EIAV-based CMV-driven eGFP expression vector (Endo et al., 2007) was added at an moi of 100. After 3 days, nearly 100% of cells expressed GFP and were returned to culture medium.

### Myogenesis in Culture

Cells ($2 \times 10^3$ cells per $cm^2$) were cultured for 7 days in proliferation medium (DMEM high glucose, 10% FCS, 10% horse serum [HS, GIBCO], 1% CEE [chicken embryo extract, Accurate], 1% PS) and then for 7–10 days in fusion medium (DMEM high glucose, 1% FCS, 1% HS, 0.5% CEE, 1% PS [GIBCO]). Half of the medium was renewed every 4 days. Myogenesis was induced by lowering serum concentration to 2%, and medium was changed every 4 days until elongated, multinucleated myofibers appeared.

### Muscle Regeneration In Vivo

Eight- to twelve-week old SCID-NOD mice were anaesthetized by inhalation of isofluorane/$O_2$. Cardiotoxin (15 μg; CTX, Molecular Probes) was injected into the gastrocnemius muscle 3 hr prior to cell transplantation. Mice were reanaesthetized, and cells suspended in 35 μl PBS, or the same volume of PBS as a control, were then slowly injected into the injured muscle. Mice were sacrificed 3 weeks later and muscle was harvested. Alternatively, 8- to 12-week old dystrophic SCID-mdx mice were used as recipients. Muscles that had

received GFP+ cultured cells were fixed in 1.5% PFA, mounted in embedding medium (Tissue-Tek, Sakura), and sectioned as 10 μm thick transverse sections. After three 15 min washes in PBS, slides were mounted with 50% glycerol/DAPI solution. GFP was directly visualized by fluorescence microscopy using both standard bandpass as well as ratiometric techniques to eliminate background autofluorescence (Leica DMRBE).

### Adipogenesis, Osteogenesis, and Chondrogenesis in Culture

For adipogenic differentiation, cultured cells at 70% confluence were switched to DMEM, 10% FCS, 1 μM dexamethasone, 0.5 μM isobutylmethylxanthine, 60 μM indomethacine, and 170 μM insulin (all from Sigma-Aldrich). After 14 days, cells were fixed in 2% PFA at RT, washed in 60% isopropanol, and incubated with oil red O for 10 min at RT for the detection of lipids.

For chondrogenesis, pellets were prepared by spinning down $3 \times 10^5$ cultured cells and grown in serum-free DMEM containing an insulin-transferrin-selenious (ITS) acid mix (BD Biosciences), 50 μg/ml L-ascorbic acid 2-phosphate (WAKO), 100 μg/ml sodium pyruvate, 40 μg/ml L-proline (both from Invitrogen), 0.1 μM dexamethasone (Sigma-Aldrich), and 10 ng/ml transforming growth factor β1 (TGF-β1; Peprotech). After 21 days, pellets were fixed in 10% formalin, dehydrated in ethanol, and embedded in paraffin. Sections 5 μm thick were rehydrated and stained with Alcian blue and Nuclear Fast Red for the detection of sulfated glycosaminoglycans and nuclei, respectively.

For in vitro bone formation, cells at 70% confluence were cultivated in DMEM, 10% FCS, 0.1 μM dexamethasone, 50 μg/mL L-ascorbic acid, and 10 mM β-glycerophosphate. After 21 days, cells were fixed in 4% formaldehyde for 2 min and incubated for 10 min with alizarin red (pH 4.2) for the detection of calcium deposits. For detection of alkaline phosphatase activity, fixed cells were incubated for 45 min in a mixture of naphtol AS-BI alkaline solution with Fast Blue BB. Cells were then rinsed with deionized water and incubated in a 2.5% silver nitrate solution for 30 min in order to detect mineral deposition (all reagents from Sigma-Aldrich).

For osteogenesis in vivo, $5 \times 10^5$ cells in 100 μl were seeded on the surface of a 6 × 6 mm piece of sterile gelatin sponge (Gelfoam), which was then placed in a 24-well plate. After the cell suspension was absorbed, 3 ml of DMEM, 10% FCS was added to the well, which was incubated overnight. The Gelfoam scaffold was then implanted into a pocket in the gluteofemoral muscle of a SCID-NOD mouse. X-ray analysis was performed 30 days later to evaluate bone formation.

### Cell Migration Assay

Cultured cells were starved for 15–18 hr in medium containing 0.5% FCS, resuspended in serum-free medium at $6 \times 10^5$ cells/mL, and preincubated for 1 hr at 37°C. Polycarbonate chemotaxis filters (8 μm pore size, Neuro Probe, Gaithersburg, MD) were coated with 0.05 mg/mL collagen I (BD Biosciences, San Jose, CA). Pepsin or papain ECM degradation products (Reing et al., 2008) were added to the bottom wells (100 ug/ml porcine urinary bladder matrix [dry weight] pepsin digest and 100 ug/ml UBM papain digest) of a Neuro Probe 48-well micro chemotaxis chamber (Neuro Probe Inc., Gaithersburg, MD). Thirty thousand cells were then added to each upper well and placed in the incubator for 3 hr. Nonmigrating cells on the top side of the membrane were removed, and migrating cells on the bottom side were stained with Diff Quik (Dade AG Liederbach, Germany). Three fields were counted from each well. Each condition was tested in quadruplicate wells, and the average number of migrating cells was determined. Each experiment was repeated three times. The Student's t test was used to assess differences in cell migration toward ECM degradation products and appropriate control buffer. P values $\leq 0.05$ were considered significant.

## SUPPLEMENTAL DATA

The Supplemental Data include supplemental text and one table and can be found with this article online at http://www.cellstemcell.com/cgi/content/full/3/3/301/DC1/.

## ACKNOWLEDGMENTS

Our thanks are due to Allison Logar for assistance with flow cytometry; Mitra Lavasani for help with in vivo assays; and Dr. Rita Bottino, Dr. Burhan Gharaibeh, Dr. Peter Rubin, and Lindsay Mock for procurement of human tissues. Dr. Simon Watkins assisted with confocal microscopy, Roseanne Perry helped with manuscript preparation, and David Humiston proofread this report. This work was supported in part by grants from the Department of Defense, Commonwealth of Pennsylvania, Children's Hospital of Pittsburgh, University of Pittsburgh Cancer Institute, and National Institutes of Health (RO1 #AR49684-01 and R21 #HL083057-01A2). M.C. was supported by Banca San Paolo of Turin, Italy.

Received: February 18, 2008
Revised: June 4, 2008
Accepted: July 7, 2008
Published: September 10, 2008

## REFERENCES

Alliot, F., Rutin, J., Leenen, P.J., and Pessac, B. (1999). Pericytes and periendothelial cells of brain parenchyma vessels co-express aminopeptidase N, aminopeptidase A, and nestin. J. Neurosci. Res. *58*, 367–378.

Alliot-Licht, B., Bluteau, G., Magne, D., Lopex-Cazaux, S., Lieubeau, B., Daculsi, G., and Guicheux, J. (2005). Dexamethasone stimulates differentiation of odontoblast-like cells in human dental pulp cultures. Cell Tissue Res. *321*, 391–400.

Andreeva, E.R., Pugach, I.M., Gordon, D., and Orekhov, A.N. (1998). Continuous subendothelial network formed by pericyte-like cells in human vascular bed. Tissue Cell *30*, 127–135.

Battula, V.L., Bareiss, P.M., Treml, S., Conrad, S., Albert, I., Hojak, S., Abele, H., Schewe, B., Just, L., Skutella, T., and Bühring, H.J. (2007). Human placenta and bone marrow derived MSC cultured in serum-free, b-FGF-containing medium express cell surface frizzled-9 and SSEA-4 and give rise to multilineage differentiation. Differentiation *75*, 279–291.

Betsholtz, C., Lindblom, P., and Gerhardt, H. (2005). Role of pericytes in vascular morphogenesis. EXS *2005*, 115–125.

Boado, R.J., and Pardridge, W.M. (1994). Differential expression of alpha-actin mRNA and immunoreactive protein in brain microvascular pericytes and smooth muscle cells. J. Neurosci. Res. *39*, 430–435.

Brachvogel, B., Moch, H., Pausch, F., Schlötzer-Schrehardt, U., Hofmann, C., Hallmann, R., von der Mark, K., Winkler, T., and Pöschl, E. (2005). Perivascular cells expressing annexin A5 define a novel mesenchymal stem cell-like population with the capacity to differentiate into multiple mesenchymal lineages. Development *132*, 2657–2668.

Caplan, A.I. (1991). Mesenchymal stem cells. J. Orthop. Res. *9*, 641–650.

Cerletti, M., Molloy, M.J., Tomczak, K.K., Yoon, S., Ramoni, M.F., Kho, A.T., Beggs, A.H., and Gussoni, E. (2006). Melanoma cell adhesion molecule is a novel marker for human fetal myogenic cells and affects myoblast fusion. J. Cell Sci. *119*, 3117–3127.

Collett, G.D., and Canfield, A.E. (2005). Angiogenesis and pericytes in the initiation of ectopic calcification. Circ. Res. *96*, 930–938.

Cossu, G., and Bianco, P. (2003). Mesoangioblasts—vascular progenitors for extravascular mesodermal tissues. Curr. Opin. Genet. Dev. *13*, 537–542.

da Silva Meirelles, L., Caplan, A.I., and Nardi, N.B. (2008). In search of the in vivo identity of mesenchymal stem cells. Stem Cells. Published online June 19, 2008. 10.1634/stemcells.2007-1122.

Davidoff, M.S., Middendorff, R., Enikolopov, G., Riethmacher, D., Holstein, A.F., and Muller, D. (2004). Progenitor cells of the testosterone-producing Leydig cells revealed. J. Cell Biol. *167*, 935–944.

DeAngelis, L., Berghella, L., Coletta, M., Lattanzi, L., Zanchi, M., Cusella-De Angelis, M.G., Ponzetto, C., and Cossu, G. (1999). Skeletal myogenic progenitors originating from embryonic dorsal aorta coexpress endothelial and myogenic markers and contribute to postnatal muscle growth and regeneration. J. Cell Biol. *147*, 869–878.

Deasy, B.M., Gharaibeh, B.M., Pollett, J.B., Jones, M.M., Lucas, M.A., Kanda, Y., and Huard, J. (2005). Long-term self-renewal of postnatal muscle-derived stem cells. Mol. Biol. Cell *16*, 3323–3333.

Dellavalle, A., Sampaolesi, M., Tonlorenzi, R., Tagliafico, E., Sacchetti, B., Perani, L., Innocenzi, A., Galvez, B., Messina, G., Morosetti, R., et al. (2007). Pericytes of human skeletal muscle are myogenic precursors distinct from satellite cells. Nat. Cell Biol. *9*, 255–267.

Endo, M., Zoltick, P.W., Chung, D.C., Bennett, J., Radu, A., Muvarak, N., and Flake, A.W. (2007). Gene transfer to ocular stem cells by early gestational intraamniotic injection of lentiviral vector. Mol. Ther. *15*, 579–587.

Farrington-Rock, C., Crofts, N., Doherty, M.J., Ashton, B.A., Griffin-Jones, C., and Canfield, A.E. (2004). Chondrogenic and adipogenic potential of microvascular pericytes. Circulation *110*, 2226–2232.

Gang, E.J., Bosnakovski, D., Figueiredo, C.A., Visser, J.W., and Perlingeiro, R.C. (2007). SSEA-4 identifies mesenchymal stem cells from bone marrow. Blood *109*, 1743–1751.

Gronthos, S., Franklin, D.M., Leddy, H.A., Robey, P.G., Storms, R.W., and Gimbl, J.M. (2001). Surface protein characterization of human adipose tissue-derived stromal cells. J. Cell. Physiol. *189*, 54–63.

Gros, J., Manceau, M., Thome, V., and Marcelle, C. (2005). A common somitic origin for embryonic muscle progenitors and satellite cells. Nature *435*, 898–899.

Jaffredo, T., Gautier, R., Eichmann, A., and Dieterlen-Lièvre, F. (1998). Intraaortic hemopoietic cells are derived from endothelial cells during ontogeny. Development *125*, 4575–4583.

Jiang, Y., Vaessen, B., Lenvik, T., Blackstad, M., Reyes, M., and Verfaillie, C.M. (2002). Multipotent progenitor cells can be isolated from postnatal murine bone marrow, muscle and brain. Exp. Hematol. *30*, 896–904.

LeGrand, F., Auda-Boucher, G., Levitsky, D., Rouaud, T., Fontaine-Perus, J., and Gardahaut, M.F. (2004). Endothelial cells within embryonic skeletal muscles: a potential source of myogenic progenitors. Exp. Cell Res. *301*, 232–241.

Li, Q., Yu, Y., Bischoff, J., Muliken, J.B., and Olsen, B.R. (2003). Differential expression of CD146 in tissues and endothelial cells derived from infantile haemangioma and normal human skin. J. Pathol. *201*, 296–302.

Middleton, J., Americh, L., Gayon, R., Julien, D., Mansat, M., Mansat, P., Anract, P., Cantagrel, A., Cattan, P., Reimund, J.M., et al. (2005). A comparative study of endothelial cell markers expressed in chronically inflamed human tissues: MECA-79, Duffy antigen receptor for chemokines, von Willebrand factor, CD31, CD34, CD105 and CD146. J. Pathol. *206*, 260–268.

Morgan, J.E., and Partridge, T.A. (2003). Muscle satellite cells. Int. J. Biochem. Cell Biol. *35*, 1151–1156.

Nehls, V., and Drenckhan, D. (1991). Heterogeneity of microvascular pericytes for smooth muscle type alpha-actin. J. Cell Biol. *113*, 147–154.

Oberlin, E., Tavian, M., Blazsek, I., and Péault, B. (2002). Blood-forming potential of vascular endothelium in the human embryo. Development *129*, 4147–4157.

Ozerdem, U., Grako, K.A., Dahlin-Huppe, K., Monosov, E., and Stallcup, W.B. (2002). NG2 proteoglycan is expressed exclusively by mural cells during vascular morphogenesis. Dev. Dyn. *2001*, 218–227.

Péault, B., Rudnicki, M., Torrente, Y., Cossu, G., Tremblay, J., Partridge, T., Gussoni, E., Kunkel, L., and Huard, J. (2007). Stem and progenitor cells in skeletal muscle development, maintenance, and therapy. Mol. Ther. *15*, 867–877.

Pittenger, M.F., MacKay, A.M., Beck, S.C., Jaiswal, R.K., Douglas, R., Mosca, J.D., Moorman, M.A., Simonetti, D.W., Craig, S., and Marshak, D.R. (1999). Multilineage potential of adult human mesenchymal stem cells. Science *284*, 143–147.

Qu-Petersen, Z., Deasy, B.M., Jankowski, R., Ikezawa, M., Cummins, J., Pruchnic, R., Cao, B., Mytinger, J., Gates, C., Wernig, A., and Huard, J. (2002). Identification of a novel population of muscle stem cells in mice: potential for muscle regeneration. J. Cell Biol. *157*, 851–864.

Reing, J.E., Zhang, L., Myers-Irvin, J., Cordero, K.E., Freytes, D.O., Heber-Katz, E., Bedelbaeva, K., McIntosh, D., Dewilde, A., Braunhut, S.J., and Badylak, S.F. (2008). Degradation products of extracellular matrix affect cell migration and proliferation. Tissue Eng. Part A. Published online July 24, 2008. 10.1089/ten.tea.2007.0425.

Sacchetti, B., Funari, A., Michienzi, S., Di Cesare, S., Piersanti, S., Saggio, I., Tagliafico, E., Ferrari, S., Gehron Robey, P., Riminucci, M., and Bianco, P. (2007). Self-renewing osteoprogenitors in bone marrow sinusoids can organize a hematopoietic microenvironment. Cell *131*, 324–336.

Schwab, K.E., and Gargett, C.E. (2007). Co-expression of two perivascular cell markers isolates mesenchymal stem-like cells from human endometrium. Hum. Reprod. *22*, 2903–2911.

Seaberg, R.M., Smukler, S.R., Kieffer, T.J., Enikolopov, G., Asghar, Z., Wheeler, M.B., Korbutt, G., and van der Kooy, D. (2004). Clonal identification of multipotent precursors from adult mouse pancreas that generate neural and pancreatic lineages. Nat. Biotechnol. *22*, 1095–1096.

Shih, D.T., Lee, D.C., Chen, S.C., Tsai, R.Y., Huang, C.T., Tsai, C.C., Shen, E.Y., and Chiu, W.T. (2005). Isolation and characterization of neurogenic mesenchymal stem cells in human scalp tissue. Stem Cells *23*, 1012–1020.

Toma, J.G., Akhavan, M., Fernandes, K.J., Barnabe-Heider, F., Sadikot, A., Kaplan, D.R., and Miller, F.D. (2001). Isolation of multipotent adult stem cells from the dermis of mammalian skin. Nat. Cell Biol. *3*, 778–784.

Traktuev, D.O., Merfeld-Clauss, S., Li, J., Kolonin, M., Arap, W., Pasqualini, R., Johnstone, B.H., and March, K.L. (2008). A population of multipotent CD34-positive adipose stromal cells share pericyte and mesenchymal surface markers, reside in a periendothelial location, and stabilize endothelial networks. Circ. Res. *102*, 77–85.

Zambidis, E.T., Oberlin, E., Tavian, M., and Péault, B. (2006). Blood-forming endothelium in human ontogeny: lessons from in utero development and embryonic stem cell culture. Trends Cardiovasc. Med. *16*, 95–101.

Zheng, B., Cao, B., Crisan, M., Sun, B., Li, G.H., Logar, A., Yap, S., Pollett, J.B., Drowley, L., Cassino, T., et al. (2007). Prospective identification of myogenic endothelial cells in human skeletal muscle. Nat. Biotechnol. *25*, 1025–1034.

Zuk, P.A., Zhu, M., Ashjian, P., De Ugarte, D.A., Huang, J.I., Mizuno, H., Alfonso, Z.C., Fraser, J.K., Benhaim, P., and Hedrick, M.H. (2002). Human adipose tissue is a source of multipotent stem cells. Mol. Biol. Cell *13*, 4279–4295.

HUMAN GENE THERAPY 19:000–000 (March 2008)

DOI: 10.1089/hum.2007.159

# Myostatin Propeptide Gene Delivery by Adeno-Associated Virus Serotype 8 Vectors Enhances Muscle Growth and Ameliorates Dystrophic Phenotypes in *mdx* Mice

CHUNPING QIAO,[1] JIANBIN LI,[1] JIANGANG JIANG,[1] XIAODONG ZHU,[3] BING WANG,[2] JUAN LI,[1] and XIAO XIAO[1]

## ABSTRACT

**Myostatin has been extensively documented as a negative regulator of muscle growth. Myostatin inhibition is therefore considered an attractive strategy for the treatment of muscle-wasting diseases such as muscular dystrophies. To investigate whether systemic gene delivery of myostatin propeptide (MRPO), a natural inhibitor of myostatin, could enhance body-wide skeletal muscle growth, we used adeno-associated virus serotype 8 (AAV8) vectors to deliver the MRPO gene into either normal mice or *mdx* mice, a murine model of Duchenne muscular dystrophy (DMD). In normal mice, a significant increase in skeletal muscle mass was observed after either an intraperitoneal injection of AAV-MPRO into neonates, or an intravenous injection of AAV-MPRO76AFc (a modified MPRO fused with IgG Fc) into adults. Enhanced muscle growth occurred because of myofiber hypertrophy, not hyperplasia. In *mdx* mice, a significant increase in skeletal muscle mass was also observed after AAV-MPRO76AFc injection. The treated *mdx* mice showed larger and more uniform myofibers, fewer infiltrating mononuclear cells, less fibrosis, and lower serum creatine kinase levels. In addition, a grip force test and an *in vitro* tetanic contractile force test showed improved muscle strength. A treadmill test, however, showed reduced endurance of the treated *mdx* mice compared with their untreated counterparts. Importantly, no cardiac hypertrophy was observed in either normal or *mdx* mice after myostatin inhibition by gene delivery. These results clearly demonstrate the efficacy of AAV8-mediated myostatin propeptide gene delivery in a rodent model of DMD, and warrant further investigation in large animal models and eventually in human patients.**

## INTRODUCTION

AMONG THE GENETIC muscle-degenerative diseases, Duchenne muscular dystrophy (DMD) is the most common and lethal, afflicting 1 of every 3500 males. DMD is characterized by progressive muscle weakness and degeneration that often lead to respiratory or cardiac arrest in the patient's late teens and early twenties (Hoffman *et al.*, 1996). DMD is caused by recessive mutations in the dystrophin gene. The dystrophin protein cross-links and stabilizes the muscle cell membrane and cytoskeleton (Hoffman *et al.*, 1987; Koenig and Kunkel, 1990). The absence of a functional dystrophin results in the loss of dystrophin-associated protein complexes and causes instability of myofiber plasma membrane. These deficiencies in turn lead to chronic muscle damage and degenerative pathology. Because of the lack of effective and curative treatment, novel therapeutic approaches are being actively explored (Wang *et al.*, 2000).

Myostatin, also known as growth/differentiation factor-8 (GDF8), is a member of the transforming growth factor (TGF)-$\beta$ super-family (McPherron *et al.*, 1997). Numerous studies have demonstrated that myostatin is a negative regulator of skeletal muscle growth. Like other TGF-$\beta$ family members, myostatin is synthesized as a precursor protein that undergoes proteolytic processing at a dibasic site to generate an N-terminal propeptide, termed myostatin propeptide (MRPO), and disulfide-linked C-terminal dimer, the biologically active part (for a detailed review see Lee, 2004). On cleavage, the mature myostatin C-terminal dimer still remains associated with

[1]Division of Molecular Pharmaceutics, University of North Carolina School of Pharmacy, Chapel Hill, NC 27599.
[2]Department of Orthopedic Surgery, University of Pittsburgh School of Medicine, Pittsburgh, PA 15261.
[3]Cardiovascular Institute, University of Pittsburgh, Pittsburgh, PA 15261.

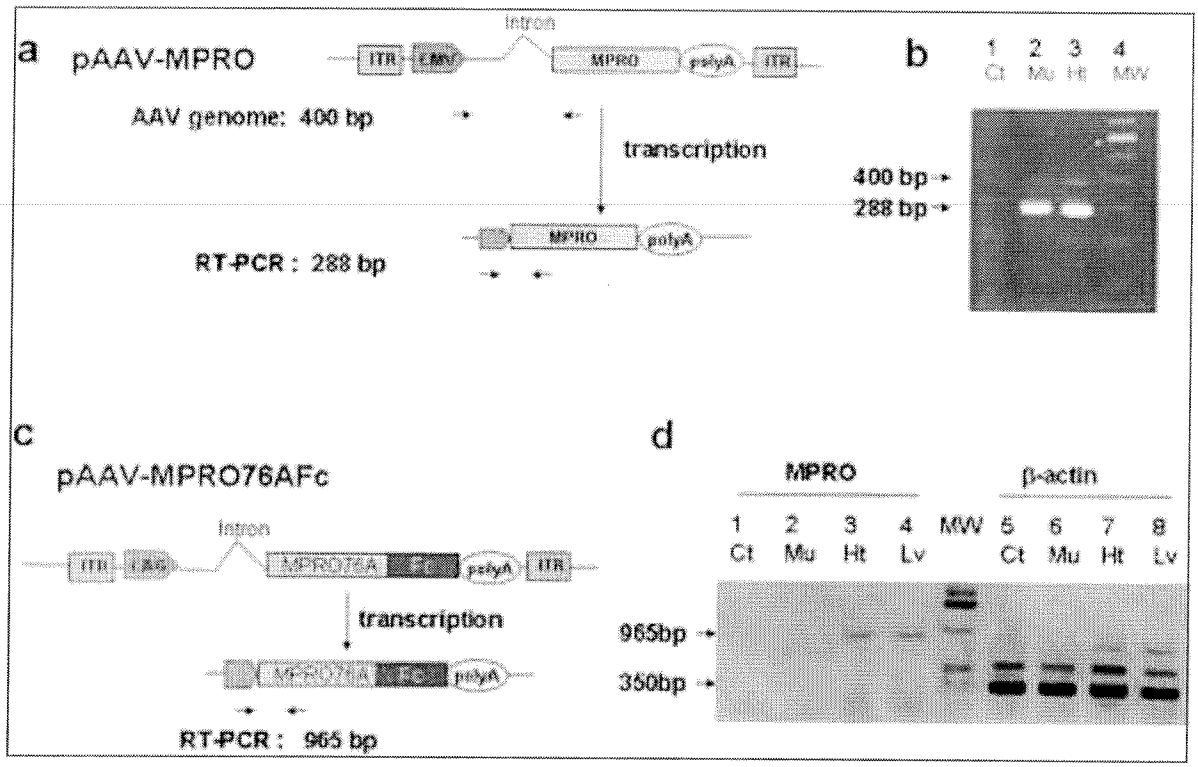


**FIG. 1.** Schematic illustration of AAV plasmids and RT-PCR results. (**a**) Construction of AAV-MPRO plasmid. The myostatin propeptide gene was cloned into the AAV plasmid containing a CMV promoter, chimeric intron, and simian virus 40 (SV40) poly(A) sequence. The 5′ primer (→) precedes the intron and the 3′ primer (←) is in the coding area. A 288-bp band indicated that the PCR product was amplified from mRNA, whereas a 400-bp product appeared if amplified from the AAV genome. ITR, inverted terminal repeat. (**b**) RT-PCR of AAV-MPRO-injected mice. The mice were killed 4 months after treatment. Lane 1, control muscle (Ct); lane 2, treated skeletal muscle (Mu); lane 3, treated heart muscle (Ht); MW, 100-bp DNA ladder. (**c**) Construction of AAV-MPRO76AFc plasmid. A mutated propeptide gene (MPRO76AFc), in which aspartate (amino acid 76) was changed to alanine and the C terminus was fused with a mouse IgG Fc domain, was cloned into AAV plasmid containing a CAG promoter. The predicted size of RT-PCR products originated from mRNA was 965 bp. (**d**) RT-PCR of AAV-MPRO76Afc-injected mice. Lanes 1–4, RT-PCR bands for MPRO76Afc; lanes 5–8, RT-PCR bands (350 bp) for β-actin, which served as an internal control. MW, 1-kb DNA ladder; Ct, control liver; Mu, treated skeletal muscle; Ht, treated heart muscle; Lv, treated liver.

its inhibitor MPRO in a latent complex. Additional inhibitors that can inhibit mature myostatin include follistatin (Hill *et al.*, 2002), the follistatin-related gene (FLRG), growth and differentiation factor-associated serum protein-1 (GASP-1) (Hill *et al.*, 2002), and so on. Myostatin gene knockout mice show significant increases in skeletal muscle mass (McPherron *et al.*, 1997; Tobin and Celeste, 2005), and so do transgenic mice expressing higher levels of myostatin inhibitors (Zhu *et al.*, 2000; Lee and McPherron, 2001). Furthermore, mutations in the myostatin gene in cattle result in double-muscling phenotype (McPherron and Lee, 1997). Downregulation of myostatin gene expression in Texel sheep (Clop *et al.*, 2006) causes muscle hypertrophy as well. In one report, partial loss of myostatin in heterozygous whippet racing dogs resulted in faster running speed, whereas the homozygous whippet dogs are muscular (Mosher *et al.*, 2007). Importantly, a mutation in humans has been identified in a healthy child with muscle hypertrophy and accompanied by unusual strength (Schuelke *et al.*, 2004).

The biological function of myostatin has raised the possibility of using myostatin inhibitors to promote muscle growth and improve the disease phenotypes in a variety of primary and secondary myopathies including muscular dystrophies (Lee, 2004). In the proof-of-principle study, Wagner coworkers (2002) showed improved muscle regeneration in *mdx* mice in the absence of myostatin by crossing myostatin null mutant mice with *mdx* mice. Subsequently, Bogdanovich and coworkers (2002) reported increased muscle strength along with a significant decrease in muscle degeneration in *mdx* mice in the presence of a myostatin inhibitor, the myostatin-blocking antibody. Thereafter, the same group also reported improved dystrophic pathophysiology of *mdx* mice by injection of a purified myostatin propeptide and mouse IgG Fc fusion protein (Bogdanovich *et al.*, 2005). Bartoli and coworkers reported that adeno-associated virus (AAV)-mediated myostatin propeptide was efficacious in ameliorating limb girdle muscular dystrophy in calpain-3-deficient (LGMD2A) mice, but not in α-sarcoglycan-deficient (LGMD2D) mice (Bartoli *et al.*, 2007).

To investigate whether myostatin inhibition by gene delivery can be an effective therapeutic approach in dystrophin-de-

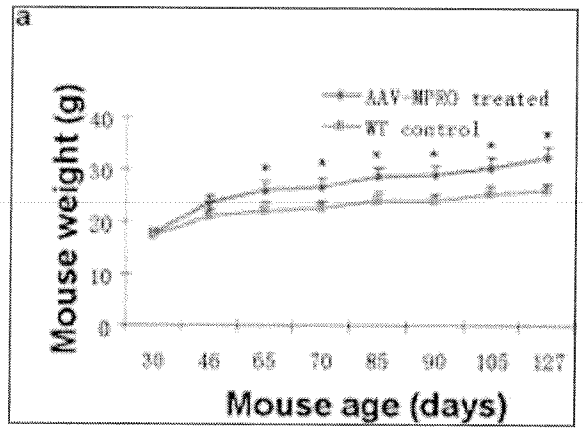


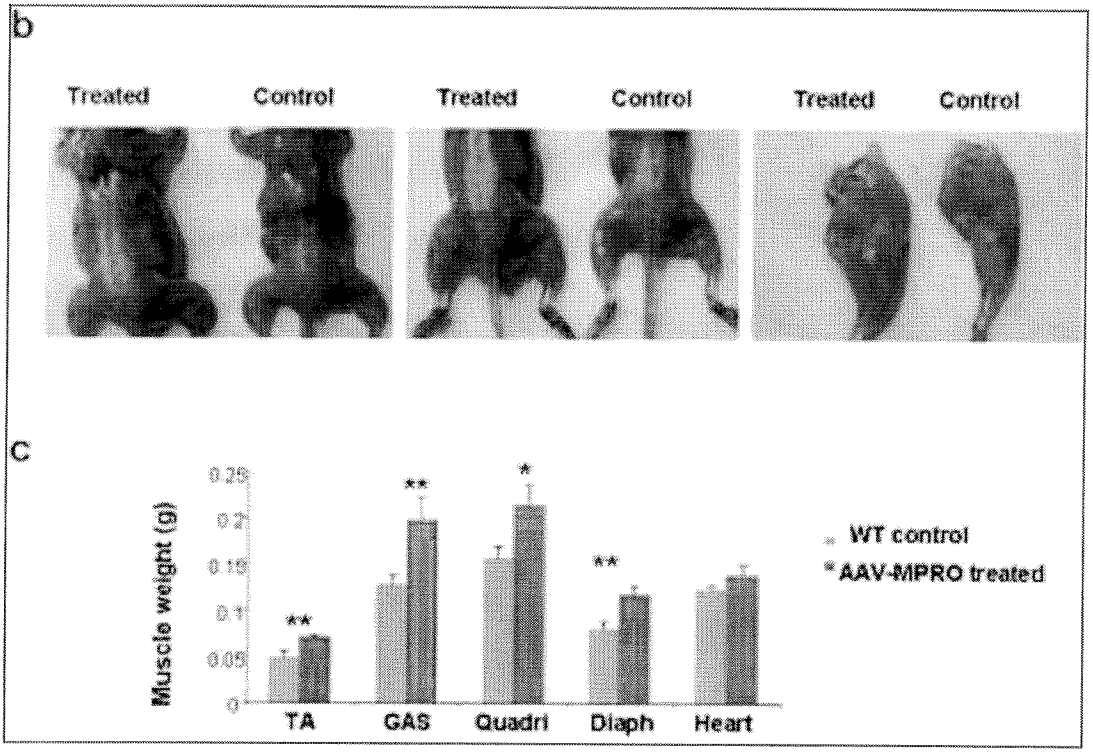


**FIG. 2.** Effects of delivering AAV-MPRO into neonate normal mice. The AAV-MPRO vector was delivered into 3-day-old neonate mice, and the mice were treated for 4 months. (**a**) AAV-MPRO-treated mice gained more weight than did controls ($*p < 0.05$). (**b**) Treated skinned mice appeared more muscular than controls. Three pictures were taken of the same mice from different angles. (**c**) There was an increase in skeletal but not cardiac muscle mass after AAV-MPRO delivery into neonatal mice ($**p < 0.01$; $*p < 0.05$).

ficient (DMD) *mdx* mice, we delivered AAV serotype 8 (AAV8) vector harboring mouse myostatin propeptide (MPRO) gene, or the gene of a fusion protein between MRPO and mouse IgG Fc (MPRO76AFc), into either normal mice or *mdx* mice. For the study in normal mice, we wished to determine whether gene delivery of myostatin propeptide would increase normal muscle mass. For the study in *mdx* mice, we also wished to see whether dystrophic symptoms could be ameliorated.

## MATERIALS AND METHODS

### *Construction of propeptide plasmids, reverse transcription-polymerase chain reaction method, and AAV vector production*

GDF8 cDNA (GenBank CoreNucleotide accession number: NM_010834) was kindly provided by S.-J. Lee (Molecular Bi-

ology and Genetics, Johns Hopkins University School of Medicine, Baltimore, MD). The myostatin propeptide gene was generated by polymerase chain reaction (PCR) methods, and the primers used for amplification of the gene were 5′-gccaccatgatgcaaaaactgcaaatgtatg-3′ and 5′-tcatctccgggacctcttgggtgtg-3′. The propeptide gene was then cloned into an AAV vector plasmid under the transcriptional control of the cytomegalovirus (CMV) promoter, and the final construction was named pAAV-MPRO (Fig. 1a). To construct the mutated propeptide gene, PCR-mediated site-directed mutagenesis at nucleotide position 299 (counting from start codon atg) was performed. The gat (aspartate) codon in the original gene was changed to gct (alanine). The mutated propeptide gene was fused with the IgG Fc domain through a series of processes, and ultimately cloned into the AAV plasmid to form the pAAV-MPRO76AFc construct (Fig. 1c). The MPRO76AFc gene was driven by the CAG promoter including chicken $\beta$-actin promoter, CMV enhancers, and chicken $\beta$-actin and rabbit $\beta$-globin introns (Kootstra *et al.*, 2003). The final constructions were sequenced for verification.

The RT-PCR method was used to detect mRNA expression levels of the propeptide gene after delivery of AAV vectors *in vivo*. The RNA from individual tissues was extracted with TRIzol reagent (Invitrogen, Carlsbad, CA), and cDNA was synthesized with the ThermoScript RT-PCR system (Invitrogen). The primers used for detection of AAV-MPRO were as follows: 5′-AAGCTGCAGAAGTTGGTCG-3′ and 5′-AGTGGAGGCGCTCTTGGC-3′. The primers used for detection of AAV-MPRO76AFc were as follows: 5′-AATAATGACGTATG-3′ and 5′-AGTGGAGGCGCTCTTGGC-3′. The primers for amplification of $\beta$-actin primers were as follows: 5′-ATCACTATTGGCAACGAGCG-3′ and 5′-ACTCATCGTACTCCTGCTTG-3′.

Recombinant viral vector stocks were produced according to the three-plasmid cotransfection method (Xiao *et al.*, 1998). Viral particles were purified twice by CsCl density gradient ultracentrifugation, using a previously published protocol (Qiao *et al.*, 2005). Vector titers of viral particle numbers were determined by the DNA dot-blot method and were in the range of $2 \times 10^{12}$ to $5 \times 10^{12}$ vector genomes/ml.

### *Mice and vector administration*

All experiments involving animals were approved by the University of North Carolina Animal Care and Use Committee. C57/B10 and *mdx* mice were purchased from Jackson Laboratory (Bar Harbor, ME). The AAV-MPRO vector was delivered into the neonates (3–5 days old) of C57/B10 mice by intraperitoneal injection, at 100 $\mu$l/mouse. AAV-MPRO76AFc ($6 \times 10^{11}$ vector genomes/ml) was delivered into 4-month-old female C57/B10 mice by intrasplenic injection. For the *mdx* study, the AAV8-MPRO76AFc vector ($1 \times 10^{12}$ vector genomes/mouse) was administered to 3-month-old male *mdx* mice via tail vein injection.

### *Immunofluorescence staining and morphometric analysis*

Rabbit polyclonal anti-dystrophin antibodies (anti-Rod1 Rod2 regions of human dystrophin, diluted 1:500; produced in the Xiao laboratory, University of North Carolina School of Pharmacy, Chapel Hill, NC) were used to determine the circumferences of myofibers. Thin cryosections of quadriceps muscle from treated and control mice (three mice per group) were produced for dystrophin staining. For morphometric analysis, pictures were taken and the radii of myofibers were analyzed with MetaMorph software (Molecular Devices, Sunnyvale, CA) with a minimum of 600 myofibers from each mouse and three mice for each group.

### *Measurement of muscle force*

The measurement of muscle contractile properties (specific and absolute force of the tibialis anterior [TA] muscles) was done exactly according to Watchko and coworkers (2002). Muscle forearm grip strength was analyzed with an automated strain gauge (Wagner *et al.*, 2002). Five readings were obtained from each mouse, and there were five mice in each group. Data were analyzed by Student *t* test. Treadmill experiments were performed according to Zhu and coworkers (2005).

## RESULTS

### *AAV-MPRO and AAV-MPRO76AFc vector construction*

To construct the AAV-MPRO vector, the mouse myostatin propeptide (MPRO) cDNA was amplified by PCR, cloned into an AAV vector plasmid, and driven by the CMV promoter for robust and long-term gene expression in skeletal muscle (Wang *et al.*, 2000; Qiao *et al.*, 2005). The CMV-MRPO gene cassette (Fig. 1a) was used in all of the neonate treatment groups. Its *in vivo* gene expression was confirmed by RT-PCR (Fig. 1b). To construct the AAV-MPRO76AFc vector, a mutation was introduced (amino acid 76: aspartate to alanine) and a mouse IgG Fc fragment was fused to the C terminus of MRPO, as described by Wolfman and coworkers (2003) (Fig. 1c). The amino acid D $\rightarrow$ A mutation at position 76 renders resistance to proteinase degradation, whereas the IgG Fc fusion prolongs its half-life of circulation *in vivo* (Wolfman *et al.*, 2003). The MPRO76AFc gene cassette was driven by the CAG promoter (Kootstra *et al.*, 2003) (consisting of CMV enhancer, chicken $\beta$-actin promoter, $\beta$-actin and $\beta$-globin introns) for robust and long-term expression *in vivo*, particularly in the liver. This construct was used in adult mice, both normal and *mdx*. Its *in vivo* gene expression was also confirmed by RT-PCR (Fig. 1d).

### *Skeletal muscle hypertrophy after MPRO gene delivery in neonatal mice*

Previously we have shown that widespread and long-term gene expression in both skeletal and cardiac muscle can be readily achieved with AAV8 after neonatal gene delivery into mice (Wang *et al.*, 2005). Here again we used AAV8 and administered the AAV-MPRO vector to 3-day-old neonatal mice by intraperitoneal injection. Body weight gain among the treated mice started to exceed that of untreated control mice. It became statistically significant from 2 months of age (Fig. 2a). The gross appearance of muscles from the AAV-MPRO-treated mice appeared larger than those of the control mice at the age of 4 months (Fig. 2b).

To confirm that the body weight gain was indeed a result of

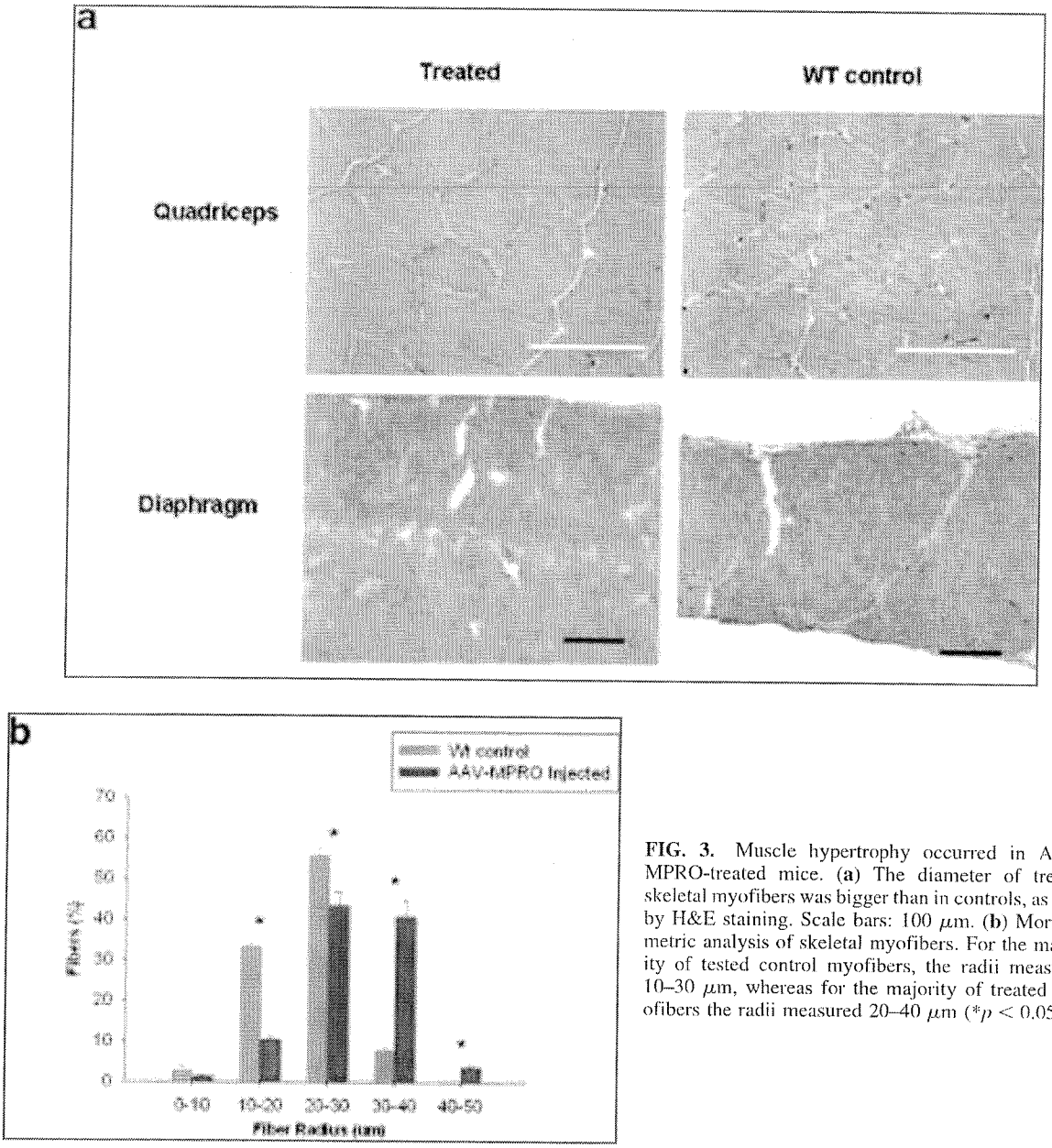


**FIG. 3.** Muscle hypertrophy occurred in AAV-MPRO-treated mice. (**a**) The diameter of treated skeletal myofibers was bigger than in controls, as seen by H&E staining. Scale bars: 100 $\mu$m. (**b**) Morphometric analysis of skeletal myofibers. For the majority of tested control myofibers, the radii measured 10–30 $\mu$m, whereas for the majority of treated myofibers the radii measured 20–40 $\mu$m ($^*p < 0.05$).

increased muscle mass, we weighed individual muscles including the tibialis anterior (TA), gastrocnemius (Gas), quadriceps (Quadri), diaphragm (Diaph), and the heart, after careful dissection from treated and control mice. The weight of the skeletal muscles (TA, Gas, Quadri, and Diaph) of treated mice was significantly greater than that of control mice ($p < 0.05$) (Fig. 2c). Even the quadriceps muscle, which showed the lowest increase among the skeletal muscles examined, displayed a 37% increase in muscle mass over the controls. Importantly, no significant weight increase was observed in the treated cardiac muscle (Fig. 2c), suggesting that cardiac hypertrophy may not be a concern for MRPO gene therapy.

To investigate whether the increase in muscle mass was due to larger myofiber size (hypertrophy), or higher myofiber number (hyperplasia), we examined the histology of quadriceps and diaphragm muscles of AAV-MRPO-treated and untreated control mice. Hematoxylin–eosin (H&E) staining and immunofluorescence staining of dystrophin for quantitative myofiber radius analysis were performed. AAV-MPRO-treated muscles displayed normal histology without centrally localized nuclei. Myofiber sizes were noticeably larger when compared with those of untreated control mice (Fig. 3a). In addition, digital morphometric analyses showed that the radii of a majority of the treated myofibers were measured at 20–40 $\mu$m, whereas

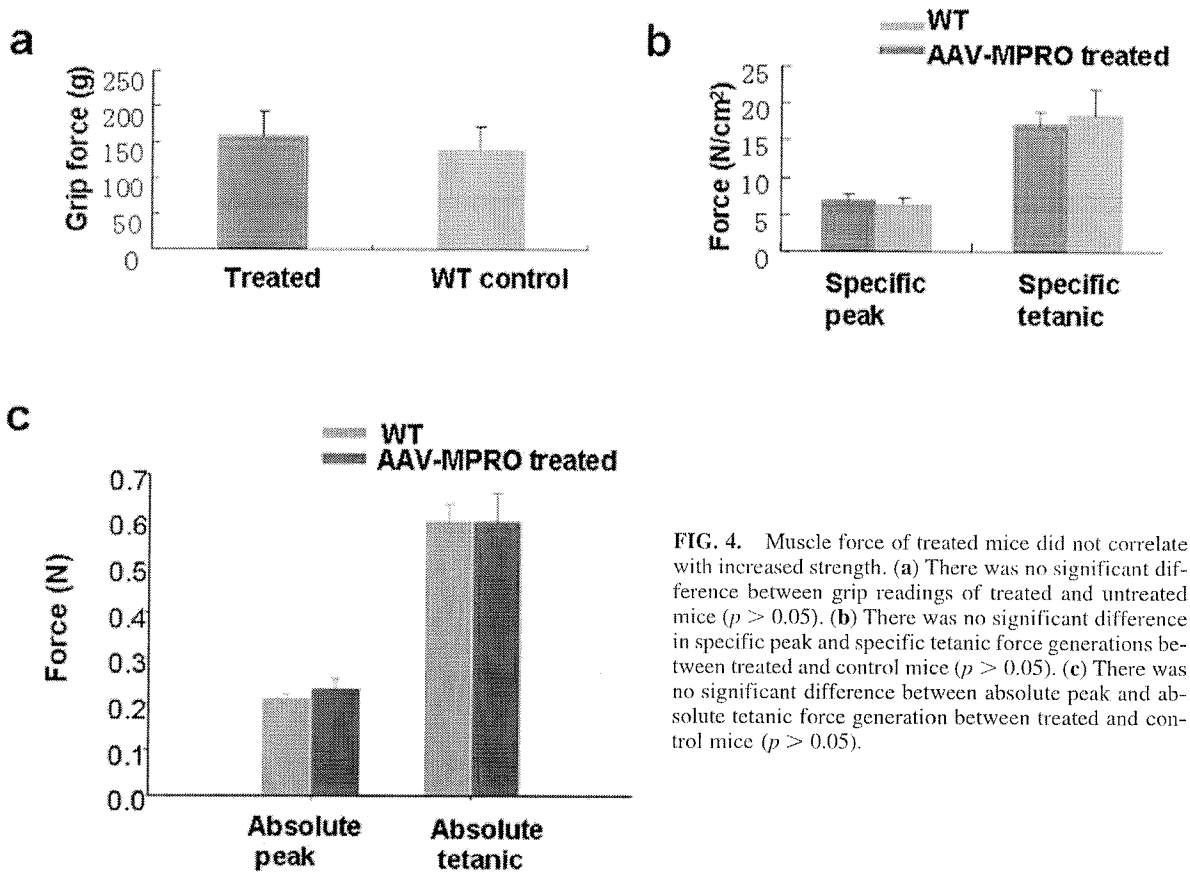


**FIG. 4.** Muscle force of treated mice did not correlate with increased strength. (**a**) There was no significant difference between grip readings of treated and untreated mice ($p > 0.05$). (**b**) There was no significant difference in specific peak and specific tetanic force generations between treated and control mice ($p > 0.05$). (**c**) There was no significant difference between absolute peak and absolute tetanic force generation between treated and control mice ($p > 0.05$).

those of the untreated control myofibers were measured at 10–30 $\mu$m (Fig. 3b). For AAV-MPRO-treated quadriceps muscle, the average myofiber radius was 28.4 ± 6.96 $\mu$m, significantly larger than the average control myofiber radius of 22.29 ± 7.85 $\mu$m ($p < 0.00001$), consistent with the ratio of muscle mass increase. Total muscle myofiber numbers per cross-section showed no significant difference between treated and untreated muscles (data not shown). Taken together, these results strongly suggest that AAV-MPRO vector treatment increases muscle mass by myofiber hypertrophy rather than by hyperplasia.

It is generally believed that the greater the myofiber diameter, the more force it can produce. Therefore, we measured the grip force of the mice, using a digital strain gauge (Wagner *et al.*, 2002), and also the isometric forces of the TA muscle *in vitro* (Wang *et al.*, 2000; Watchko *et al.*, 2002). These experiments were performed in both treated and untreated 4-month-old normal mice. No significant differences were observed between treated and control mice in both the grip force test (Fig. 4a) and the *in vitro* isometric TA muscle force test (Fig. 4b and c). These results clearly show that the observed increases in myofiber diameter did not translate into increased strength in normal mice.

### *Skeletal muscle hypertrophy after MRPO76AFc gene delivery in adult mice*

We next examined whether skeletal muscle mass could be increased by AAV8-mediated propeptide gene delivery in adult mice. Four-month-old C57/BL10 mice (five females) were treated with the AAV8-MPRO76AFc vector by intravenous injection, whereas age-matched control mice were injected with

**FIG. 5.** Effects of myostatin propeptide delivery into adult mice. The AAV-MPRO76AFc vector was delivered into 4-month-old adult mice (five females in each group) by intrasplenic injection. (**a**) There was no significant total weight gain among the treated mice compared with the controls after 4 months of treatment. Mon, month. (**b**) There was an increase in skeletal, but not cardiac, muscle weight in AAV-MPRO76AFc-treated mice (Student *t* test was used: $^{**}p < 0.01$; $^{*}p < 0.05$). (**c**) H&E staining displayed muscle hypertrophy in AAV-MPRO76AFc-treated skeletal muscles. Scale bars: 100 $\mu$m. (**d**) Morphometric analysis indicated that the AAV8-CAG-MPRO myofibers were bigger. Fewer treated myofibers were present in the small myofiber radius range (10–20 $\mu$m), whereas more treated myofibers were present in the larger myofiber radius range (20–40 $\mu$m), as compared with their control counterparts. Error bars represent the standard error. The Student *t* test was used ($^{*}p < 0.05$).

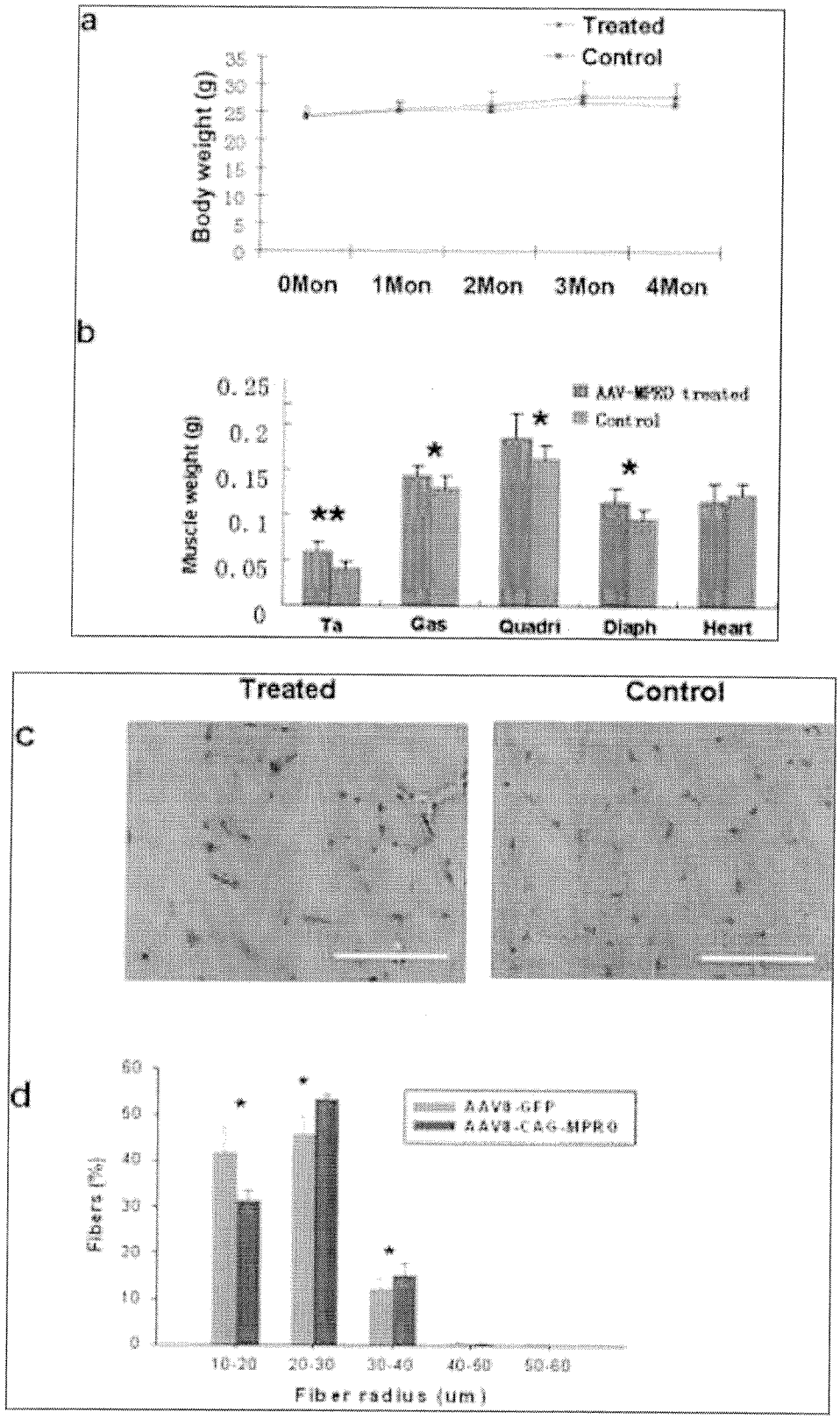
a
Treated
Control
Body weight (g)
35
30
25
20
15
10
5
0
0Mon
1Mon
2Mon
3Mon
4Mon
b
Muscle weight (g)
0.25
0.2
0.15
0.1
0.05
0
AAV-MCK treated
Control
**
*
*
*
Ta
Gas
Quadri
Diaph
Heart
Treated
Control
c
d
Fibers (%)
60
50
40
30
20
10
0
AAV8-GFP
AAV8-CAG-MPRO
*
*
*
10-20
20-30
30-40
40-50
50-60
Fiber radius (um)

FIG. 5.

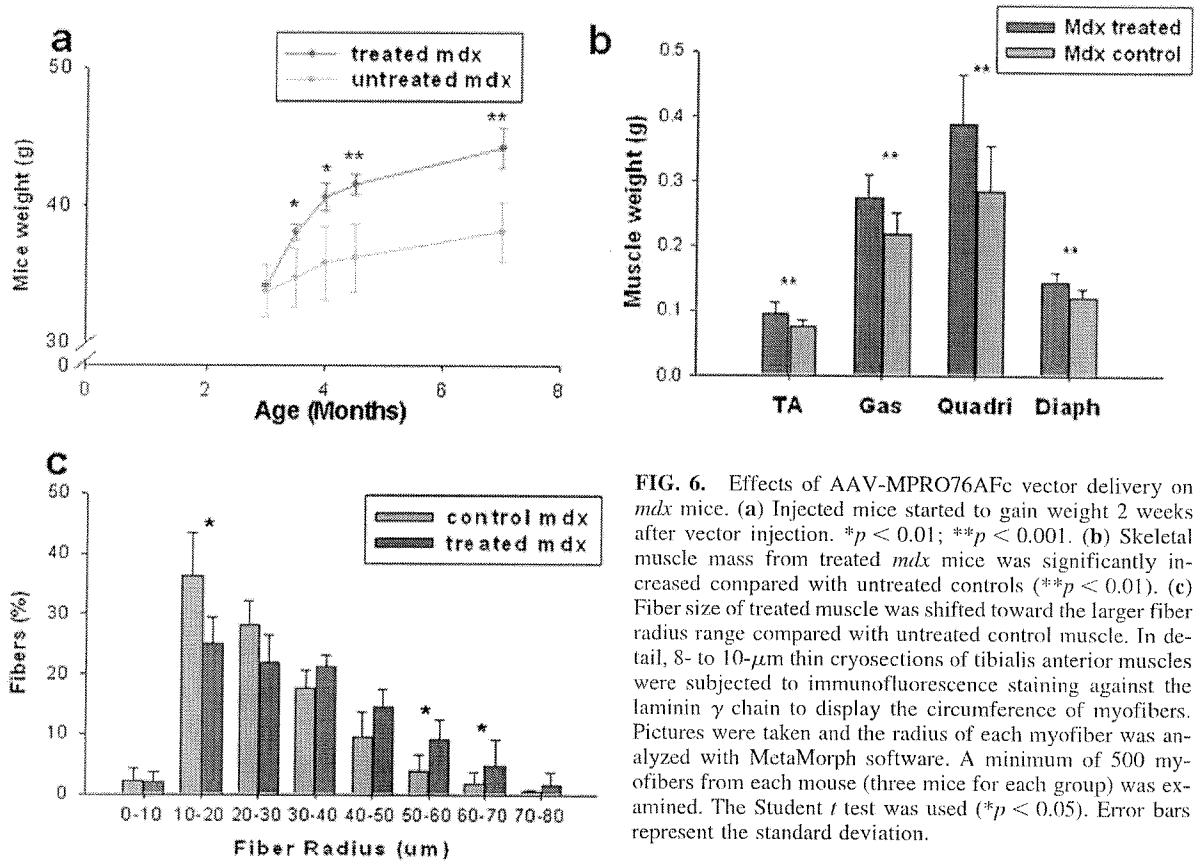


**FIG. 6.** Effects of AAV-MPRO76AFc vector delivery on *mdx* mice. (**a**) Injected mice started to gain weight 2 weeks after vector injection. $*p < 0.01$; $**p < 0.001$. (**b**) Skeletal muscle mass from treated *mdx* mice was significantly increased compared with untreated controls ($**p < 0.01$). (**c**) Fiber size of treated muscle was shifted toward the larger fiber radius range compared with untreated control muscle. In detail, 8- to 10-$\mu$m thin cryosections of tibialis anterior muscles were subjected to immunofluorescence staining against the laminin $\gamma$ chain to display the circumference of myofibers. Pictures were taken and the radius of each myofiber was analyzed with MetaMorph software. A minimum of 500 myofibers from each mouse (three mice for each group) was examined. The Student *t* test was used ($*p < 0.05$). Error bars represent the standard deviation.

an AAV8-CMV-GFP reporter gene vector. RT-PCR confirmed MRPO76AFc expression in the liver as well as in the heart (Fig. 1d). We hypothesized that the propeptide gene produced in the liver would be secreted into the blood circulation and promote skeletal muscle growth throughout the whole body.

The above-treated mice were also weighed at regular time intervals over 4 months. No significant overall body weight gain among AAV-MPRO76AFc-treated normal mice was observed when compared with their AAV-GFP-treated control counterparts in the 4-month period (Fig. 5a). However, when individual muscle tissues were dissected and weighed, a significant increase in skeletal muscle mass was observed, for example, in the tibialis (TA), gastrocnemius (Gas), and quadriceps (Quadri) muscles, as well as in the diaphragm (Diaph) (Fig. 5b). Similar to the observation in the neonatal treatment group, the heart weight was not increased, hence there was no cardiac hypertrophy (Fig. 5b). In addition, the TA muscle, which showed the highest increase in mass, was subjected to histological examination, immunofluorescence staining, as well as morphometric analysis. Similar to the results for the neonate group, H&E staining showed healthy muscle histology and larger myofiber sizes in the MRPO76AFc-treated mice (Fig. 5c). Digital morphometric analysis revealed statistically significant increases in myofiber radius (Fig. 5d). The increase in myofiber sizes was also reflected by a right shift of the myofiber size distribution (Fig. 5d). Thus, fewer myofibers were in the small radius range (10–20 $\mu$m) and more myofibers were in the large myofiber radius range (20–40 $\mu$m), compared with their control counterparts. Taken together, these results strongly indicate that systemic delivery of the modified propeptide gene in adult mice can increase skeletal muscle mass by increasing the size of the myofibers.

### *Amelioration of dystrophic phenotypes after MPRO76AFc gene delivery in mdx mice*

The main purpose of this study was to evaluate the therapeutic effect of myostatin inhibition by gene transfer in the *mdx* mouse model. We therefore delivered AAV8-MPRO76AFc vector into 3-month-old adult *mdx* mice by tail vein injection. As expected, RT-PCR showed transgene expression primarily in the liver and the heart after AAV8 delivery in adults (Fig. 1d). Western blot of the liver and sera from vector-treated *mdx* mice confirmed production of the MRPO76AFc protein and its efficient secretion into the circulation (see Supplementary Fig. 1a at www.liebertonline.com/hum). Two weeks after vector injection, treated *mdx* mouse body weight gain started to exceed that of the untreated controls. The difference became significant 1.5 months after treatment ($p < 0.001$) (Fig. 6a). Four months after treatment, the average body weight of the treated

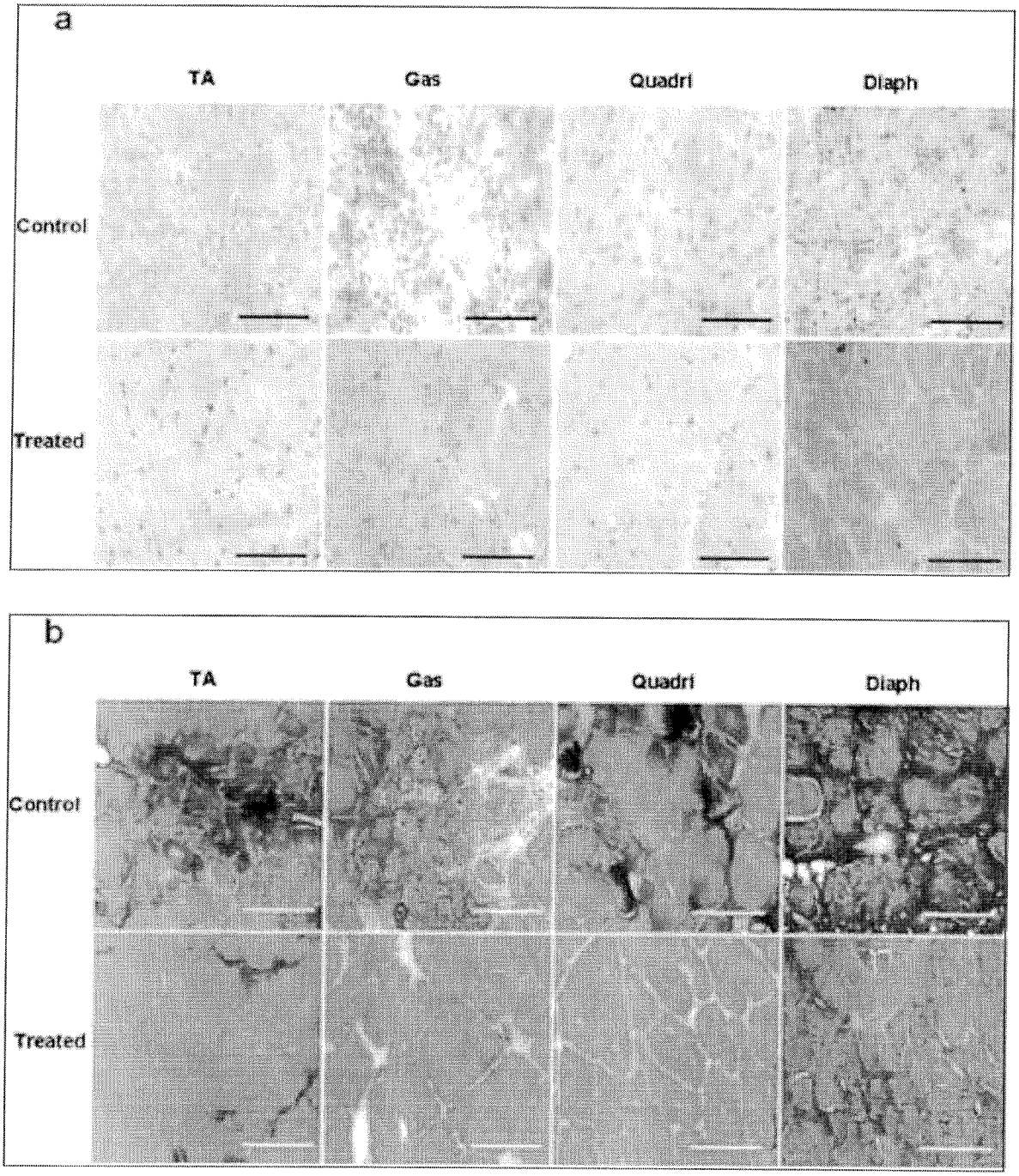


**FIG. 7.** AAV8-MPRO76AFc vector delivery improved muscle pathology in *mdx* mice. (**a**) H&E staining of the treated and control muscle indicated that muscle histology has been improved by the vector delivery. Scale bar: 100 $\mu$m. TA, tibialis anterior muscle; Gas, gastrocnemius muscle; Quadri, quadriceps muscle; Diaph, diaphragm muscle. (**b**) Masson's trichrome staining of treated and control muscle indicated that fibrosis was greatly ameliorated by MPRO76AFc gene transfer. Collagen was stained as blue. Scale bar: 100 $\mu$m.

group was 44 $\pm$ 1.44 g, whereas that of the untreated mice was 38 $\pm$ 2.19 g.

To further study the direct impact of AAV8-MPRO76AFc on individual muscles, we carefully isolated a number of muscles and weighed them. Similar to the normal mouse study, significant muscle mass increase was observed in all the skeletal muscles examined (Fig. 6b). In addition, digital morphometric analysis showed significantly larger myofiber sizes of the

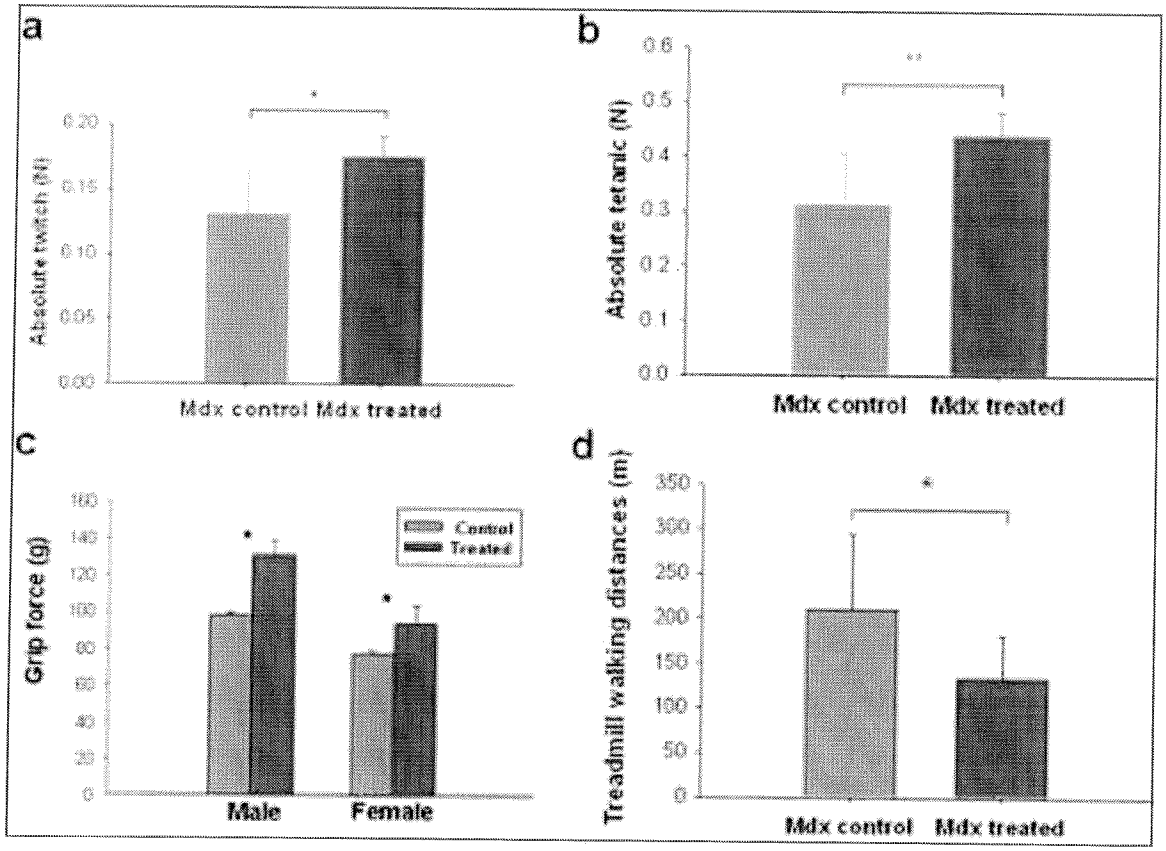


**FIG. 8.** Muscle force outputs from treated and control *mdx* mice. For all the studies, age- and sex-matched controls were used, and five mice were used for each group ($*p < 0.05$; $**p < 0.01$). (**a**) The absolute twitch force of treated tibialis anterior (TA) muscle was stronger than the untreated control. (**b**) The absolute tetanic force of treated TA muscle was stronger than the untreated *mdx* control. (**c**) The grip strength of treated *mdx* mice was significantly greater than that of the controls. (**d**) The treated *mdx* mice ran shorter distance on the treadmills than did their untreated counterparts.

treated *mdx* mice ($p < 0.05$) and the myofiber radius distribution also right shifted when compared with the untreated controls (Fig. 6c).

To evaluate the therapeutic effect of AAV8-MPRO76AFc on the pathological phenotypes, we performed H&E staining (for histology) and Masson's trichrome staining (for fibrosis) on thin cross-sections of muscle from treated and untreated *mdx* mice. Untreated *mdx* muscles were characterized by increased mononuclear cell infiltration, myofiber size variation, as well as centrally localized nuclei (central nucleation). Treated muscles displayed much reduced mononuclear cell infiltration, and larger and more uniform myofibers, although the extent of central nucleation did not change significantly, as expected (Fig. 7a; and see Supplementary Fig. 2 at www.liebertonline.com/hum). Consistent with the H&E staining, Masson's trichrome staining of consecutive sections revealed a significant reduction of fibrosis in treated *mdx* muscle (Fig. 7b; and see Supplementary Fig. 3 at www.liebertonline.com/hum). In addition, the average serum creatine kinase (CK) level of treated *mdx* mice (610 ± 261 IU/liter) was slightly lower than that of the untreated *mdx* mice (906 ± 289 IU/liter) ($n = 5$ for each group; $p = 0.06$), but it was still far above the level of normal C57/B10 control mice (6.7 ± 2.3 IU/liter) (see Supplementary Fig. 1b).

Finally, we examined whether the treated *mdx* mice would exhibit increased muscle strength. *In vitro* muscle contractile function analysis (Watchko *et al.*, 2002), as well as the grip force test (Zhu *et al.*, 2005) and treadmill running (Zhu *et al.*, 2005), were performed. Isolated TA muscle of treated *mdx* mice showed a significant increase in absolute twitch and absolute tetanic forces in the *in vitro* force measurement (Fig. 8a and b). However, no significant increase in specific force (absolute force per muscle size) was observed between the treated and untreated control groups. In addition, treated *mdx* mice also showed stronger grip force (Fig. 8c). Unexpectedly, treated *mdx* mice actually had decreased endurance and ran a shorter distance in the treadmill test compared with their untreated counterparts (Fig. 8d).

## DISCUSSION

Inhibition or blockade of myostatin to promote muscle growth has been explored as a potential treatment for muscle-

wasting diseases, including sarcopenia and muscular dystrophies (Bogdanovich *et al.*, 2002, 2005; Lee *et al.*, 2005; Tobin and Celeste, 2005; Ohsawa *et al.*, 2006; Bartoli *et al.*, 2007). In this study, we investigated the muscle growth effect of myostatin inhibition by gene delivery of a natural inhibitor of myostatin, the myostatin propeptide, in normal as well as *mdx* mice. In the normal mouse study, we observed significant skeletal muscle mass increase after a single-dose intraperitoneal injection into neonates, and after intravenous injection into adults. However, the total body weight of the normal mice treated at the adult age did not increase significantly, most likely because myostatin blockade is well documented to reduce body fat while increasing muscle mass. We further revealed that muscle hypertrophy, but not hyperplasia, contributed to the muscle mass increase. This finding differs from observations of myostatin gene knockout mice, which had both hypertrophy and hyperplasia (McPherron *et al.*, 1997; Nishi *et al.*, 2002). In the *mdx* mouse study, we again observed a significant increase in skeletal muscle mass accompanied by more uniform myofiber sizes, less mononuclear cell infiltration, and decreased fibrosis after a simple tail vein injection. A slight decrease in serum creatine kinase level in the treated *mdx* mice was also noticed. More importantly, the grip force and absolute contractile forces were significantly improved by the vector delivery as well. Our study indicates that myostatin inhibition by systemic delivery of AAV8-MPRO76AFc vector is an efficacious therapeutic approach in *mdx* mice to improve muscle functions and ameliorate dystrophic pathologies.

It is noteworthy that systemic myostatin inhibition did not cause cardiac hypertrophy despite skeletal muscle hypertrophy. This is an important safety factor to be built in for body-wide inhibition of myostatin either by gene therapy or by protein and antibody therapy, because cardiac hypertrophy is a highly unwanted risk factor. Other muscle-enhancing reagents such as insulin-like growth factor I (IGF-I), however, might carry such a potential risk factor (Friberg *et al.*, 1995; Neri Serneri *et al.*, 2001; McMullen and Izumo, 2006). Another interesting observation is the lack of muscle hyperplasia after somatic gene delivery of the myostatin inhibitors. By contrast, myostatin gene knockout (McPherron *et al.*, 1997) or overexpression of other myostatin inhibitors, such as follistatin (Nakatani *et al.*, 2008) and dominant negative type II soluble receptor ActRIIB in transgenic mice (Lee *et al.*, 2005), all resulted in skeletal muscle hypertrophy and hyperplasia. This may be related to the degree and timing of inhibition in the knockout mice and/or nonspecific interactions beyond the myostatin pathways by inhibitors such as follistatin. As a result, hyperplasia may accelerate the exhaustion of muscle satellite and/or stem cells for dystrophic muscle repair and, therefore, raises concern about long-term safety. In our studies, however, hyperplasia is not observed as a result of somatic gene delivery of MRPO in either neonatal mice or adult mice. This could minimize the risk of stem cell exhaustion after somatic gene therapy.

However, we also observed some paradoxical phenomena during the course of our studies. For example, we did not observe stronger muscle force in normal mice despite the larger muscle mass resulting from myostatin blockade by AAV MRPO gene delivery. Similar results were reported in an IGF-I-mediated study (Fourth Round Table conference in Monaco, January 15, 2005; available at http://www.parentprojectmd.org/site/DocServer/2005_monaco_uk.pdf?docID=112 [accessed February 2008]) in which enlarged muscles of mice did not seem to have improved function unless the mice were also exercised. Whether exercise could increase muscle force in our treated neonate group requires further studies. In the *mdx* study, even with the improvement of their grip force and muscle contractile force, we noticed that the treated mice ran shorter distances on treadmills. There are a few possible explanations. First, muscle force output and treadmill running reflect different aspects of the locomotive functions. Stronger force output does not necessarily mean better endurance. Indeed, myostatin-deficient cattle also show reduced endurance, although their muscle sizes are doubled (Holmes *et al.*, 1973). It might be similar for myostatin-inhibited *mdx* mice. In addition, the aberrant vascular structure in *mdx* mice (Loufrani *et al.*, 2004; Ito *et al.*, 2006), as a result of dystrophin deficiency in blood vessel smooth muscle, may also contribute to their poor endurance. The paradoxical phenomenon of myostatin inhibition observed in mice cannot be extrapolated to other species, such as dogs and humans. In fact, heterozygous myostatin gene-mutated whippet dogs are more muscular, and run faster in competitive racing events, than do wild-type dogs (Mosher *et al.*, 2007).

Although muscle histopathology was improved after AAV-MRPO treatment, we must bear in mind that myostatin inhibition does not correct the primary deficiency in *mdx* mice, that is, the loss of dystrophin from the sarcolemma. We believe the improvement in muscle histopathology is due mainly to the improvement of muscle force and mass. In general, a stronger muscle should be less susceptible than a weaker muscle to the same mechanical damage. However, the persistence of myofibers containing centrally localized nuclei in the treated *mdx* mice suggests that chronic muscle damage and regeneration still exist because of dystrophin deficiency. As a result, a combination of dystrophin gene delivery with myostatin inhibition may lead to better therapeutic outcomes. In summary, our studies have demonstrated the effectiveness of myostatin inhibition by somatic delivery of myostatin propeptide gene in both normal and *mdx* mice. This strategy thus warrants further investigation in large animal models of muscular dystrophies and potentially future clinical studies in the DMD patients.

## ACKNOWLEDGMENTS

The authors thank Dr. Se-Jin Lee for providing mouse myostatin cDNA. This work was funded by grants W81XWH-05-0334, AR50595, and AR45967.

## AUTHOR DISCLOSURE STATEMENT

No competing financial interests exist.

## REFERENCES

BARTOLI, M., POUPIOT, J., VULIN, A., FOUGEROUSSE, F., ARANDEL, L., DANIELE, N., ROUDAUT, C., NOULET, F., GARCIA, L., DANOS, O., and RICHARD, I. (2007). AAV-mediated de-

livery of a mutated myostatin propeptide ameliorates calpain 3 but not α-sarcoglycan deficiency. Gene Ther. **14,** 733–740.

BOGDANOVICH, S., KRAG, T.O., BARTON, E.R., MORRIS, L.D., WHITTEMORE, L.A., AHIMA, R.S., and KHURANA, T.S. (2002). Functional improvement of dystrophic muscle by myostatin blockade. Nature **420,** 418–421.

BOGDANOVICH, S., PERKINS, K.J., KRAG, T.O., WHITTEMORE, L.A., and KHURANA, T.S. (2005). Myostatin propeptide-mediated amelioration of dystrophic pathophysiology. FASEB J. **19,** 543–549.

CLOP, A., MARCQ, F., TAKEDA, H., PIROTTIN, D., TORDOIR, X., BIBE, B., BOUIX, J., CAIMENT, F., ELSEN, J.M., EYCHENNE, F., LARZUL, C., LAVILLE, E., MEISH, F., MILENKOVIC, D., TOBIN, J., CHARLIER, C., and GEORGES, M. (2006). A mutation creating a potential illegitimate microRNA target site in the myostatin gene affects muscularity in sheep. Nat. Genet. **38,** 813–818.

FRIBERG, P., ISGAARD, J., WAHLANDER, H., WICKMAN, A., GURON, G., and ADAMS, M.A. (1995). Cardiac hypertrophy and related growth processes: The role of insulin-like growth factor-I. Blood Press. Suppl. **2,** 22–29.

HILL, J.J., DAVIES, M.V., PEARSON, A.A., WANG, J.H., HEWICK, R.M., WOLFMAN, N.M., and QIU, Y. (2002). The myostatin propeptide and the follistatin-related gene are inhibitory binding proteins of myostatin in normal serum. J. Biol. Chem. **277,** 40735–40741.

HOFFMAN, E.P., BROWN, R.H., Jr., and KUNKEL, L.M. (1987). Dystrophin: The protein product of the Duchenne muscular dystrophy locus. Cell **51,** 919–928.

HOFFMAN, E.P., PEGORARO, E., SCACHERI, P., BURNS, R.G., TABER, J.W., WEISS, L., SPIRO, A., and BLATTNER, P. (1996). Genetic counseling of isolated carriers of Duchenne muscular dystrophy. Am. J. Med. Genet. **63,** 573–580.

HOLMES, J.H., ASHMORE, C.R., and ROBINSON, D.W. (1973). Effects of stress on cattle with hereditary muscular hypertrophy. J. Anim. Sci. **36,** 684–694.

ITO, K., KIMURA, S., OZASA, S., MATSUKURA, M., IKEZAWA, M., YOSHIOKA, K., UENO, H., SUZUKI, M., ARAKI, K., YAMAMURA, K., MIWA, T., DICKSON, G., THOMAS, G.D., and MIIKE, T. (2006). Smooth muscle-specific dystrophin expression improves aberrant vasoregulation in *mdx* mice. Hum. Mol. Genet. **15,** 2266–2275.

KOENIG, M., and KUNKEL, L.M. (1990). Detailed analysis of the repeat domain of dystrophin reveals four potential hinge segments that may confer flexibility. J. Biol. Chem. **265,** 4560–4566.

KOOTSTRA, N.A., MATSUMURA, R., and VERMA, I.M. (2003). Efficient production of human FVIII in hemophilic mice using lentiviral vectors. Mol. Ther. **7,** 623–631.

LEE, S.J. (2004). Regulation of muscle mass by myostatin. Annu. Rev. Cell Dev. Biol. **20,** 61–86.

LEE, S.J., and McPHERRON, A.C. (2001). Regulation of myostatin activity and muscle growth. Proc. Natl. Acad. Sci. U.S.A. **98,** 9306–9311.

LEE, S.J., REED, L.A., DAVIES, M.V., GIRGENRATH, S., GOAD, M.E., TOMKINSON, K.N., WRIGHT, J.F., BARKER, C., EHRMANTRAUT, G., HOLMSTROM, J., TROWELL, B., GERTZ, B., JIANG, M.S., SEBALD, S.M., MATZUK, M., LI, E., LIANG, L.F., QUATTLEBAUM, E., STOTISH, R.L., and WOLFMAN, N.M. (2005). Regulation of muscle growth by multiple ligands signaling through activin type II receptors. Proc. Natl. Acad. Sci. U.S.A. **102,** 18117–18122.

LOUFRANI, L., DUBROCA, C., YOU, D., LI, Z., LEVY, B., PAULIN, D., and HENRION, D. (2004). Absence of dystrophin in mice reduces NO-dependent vascular function and vascular density: Total recovery after a treatment with the aminoglycoside gentamicin. Arterioscler. Thromb. Vasc. Biol. **24,** 671–676.

McMULLEN, J.R., and IZUMO, S. (2006). Role of the insulin-like growth factor 1 (IGF1)/phosphoinositide-3-kinase (PI3K) pathway mediating physiological cardiac hypertrophy. Novartis Found. Symp. **274,** 90–111; discussion 111–117, 152–115, 272–116.

McPHERRON, A.C., and LEE, S.J. (1997). Double muscling in cattle due to mutations in the myostatin gene. Proc. Natl. Acad. Sci. U.S.A. **94,** 12457–12461.

McPHERRON, A.C., LAWLER, A.M., and LEE, S.J. (1997). Regulation of skeletal muscle mass in mice by a new TGF-β superfamily member. Nature **387,** 83–90.

MOSHER, D.S., QUIGNON, P., BUSTAMANTE, C.D., SUTTER, N.B., MELLERSH, C.S., PARKER, H.G., and OSTRANDER, E.A. (2007). A mutation in the myostatin gene increases muscle mass and enhances racing performance in heterozygote dogs. PLoS Genet. **3,** e79.

NAKATANI, M., TAKEHARA, Y., SUGINO, H., MATSUMOTO, M., HASHIMOTO, O., HASEGAWA, Y., MURAKAMI, T., UEZUMI, A., TAKEDA, S., NOJI, S., SUNADA, Y., and TSUCHIDA, K. (2008). Transgenic expression of a myostatin inhibitor derived from follistatin increases skeletal muscle mass and ameliorates dystrophic pathology in *mdx* mice. FASEB J. **22,** 477–487.

NERI SERNERI, G.G., BODDI, M., MODESTI, P.A., CECIONI, I., COPPO, M., PADELETTI, L., MICHELUCCI, A., COLELLA, A., and GALANTI, G. (2001). Increased cardiac sympathetic activity and insulin-like growth factor-I formation are associated with physiological hypertrophy in athletes. Circ. Res. **89,** 977–982.

NISHI, M., YASUE, A., NISHIMATU, S., NOHNO, T., YAMAOKA, T., ITAKURA, M., MORIYAMA, K., OHUCHI, H., and NOJI, S. (2002). A missense mutant myostatin causes hyperplasia without hypertrophy in the mouse muscle. Biochem. Biophys. Res. Commun. **293,** 247–251.

OHSAWA, Y., HAGIWARA, H., NAKATANI, M., YASUE, A., MORIYAMA, K., MURAKAMI, T., TSUCHIDA, K., NOJI, S., and SUNADA, Y. (2006). Muscular atrophy of caveolin-3-deficient mice is rescued by myostatin inhibition. J. Clin. Invest. **116,** 2924–2934.

QIAO, C., LI, J., ZHU, T., DRAVIAM, R., WATKINS, S., YE, X., CHEN, C., and XIAO, X. (2005). Amelioration of laminin-$\alpha_2$-deficient congenital muscular dystrophy by somatic gene transfer of miniagrin. Proc. Natl. Acad. Sci. U.S.A. **102,** 11999–12004.

SCHUELKE, M., WAGNER, K.R., STOLZ, L.E., HUBNER, C., RIEBEL, T., KOMEN, W., BRAUN, T., TOBIN, J.F., and LEE, S.J. (2004). Myostatin mutation associated with gross muscle hypertrophy in a child. N. Engl. J. Med. **350,** 2682–2688.

TOBIN, J.F., and CELESTE, A.J. (2005). Myostatin, a negative regulator of muscle mass: Implications for muscle degenerative diseases. Curr. Opin. Pharmacol. **5,** 328–332.

WAGNER, K.R., McPHERRON, A.C., WINIK, N., and LEE, S.J. (2002). Loss of myostatin attenuates severity of muscular dystrophy in *mdx* mice. Ann. Neurol. **52,** 832–836.

WANG, B., LI, J., and XIAO, X. (2000). Adeno-associated virus vector carrying human minidystrophin genes effectively ameliorates muscular dystrophy in *mdx* mouse model. Proc. Natl. Acad. Sci. U.S.A. **97,** 13714–13719.

WANG, Z., ZHU, T., QIAO, C., ZHOU, L., WANG, B., ZHANG, J., CHEN, C., LI, J., and XIAO, X. (2005). Adeno-associated virus serotype 8 efficiently delivers genes to muscle and heart. Nat. Biotechnol. **23,** 321–328.

WATCHKO, J., O'DAY, T., WANG, B., ZHOU, L., TANG, Y., LI, J., and XIAO, X. (2002). Adeno-associated virus vector-mediated minidystrophin gene therapy improves dystrophic muscle contractile function in *mdx* mice. Hum. Gene Ther. **13,** 1451–1460.

WOLFMAN, N.M., McPHERRON, A.C., PAPPANO, W.N., DAVIES, M.V., SONG, K., TOMKINSON, K.N., WRIGHT, J.F., ZHAO, L., SEBALD, S.M., GREENSPAN, D.S., and LEE, S.J. (2003). Acti-

vation of latent myostatin by the BMP-1/tolloid family of metalloproteinases. Proc. Natl. Acad. Sci. U.S.A. **100,** 15842–15846.

XIAO, X., LI, J., and SAMULSKI, R.J. (1998). Production of high-titer recombinant adeno-associated virus vectors in the absence of helper adenovirus. J. Virol. **72,** 2224–2232.

ZHU, T., ZHOU, L., MORI, S., WANG, Z., McTIERNAN, C.F., QIAO, C., CHEN, C., WANG, D.W., LI, J., and XIAO, X. (2005). Sustained whole-body functional rescue in congestive heart failure and muscular dystrophy hamsters by systemic gene transfer. Circulation **112,** 2650–2659.

ZHU, X., HADHAZY, M., WEHLING, M., TIDBALL, J.G., and McNALLY, E.M. (2000). Dominant negative myostatin produces hypertrophy without hyperplasia in muscle. FEBS Lett. **474,** 71–75.

Address reprint requests to:
*Dr. Xiao Xiao*
*Division of Molecular Pharmaceutics*
*UNC School of Pharmacy*
*303B Beard Hall CB#7360*
*Chapel Hill, NC 27599*

*E-mail:* xxiao@email.unc.edu

Received for publication November 20, 2007; accepted after revision January 3, 2008.

Published online: February 14, 2008.

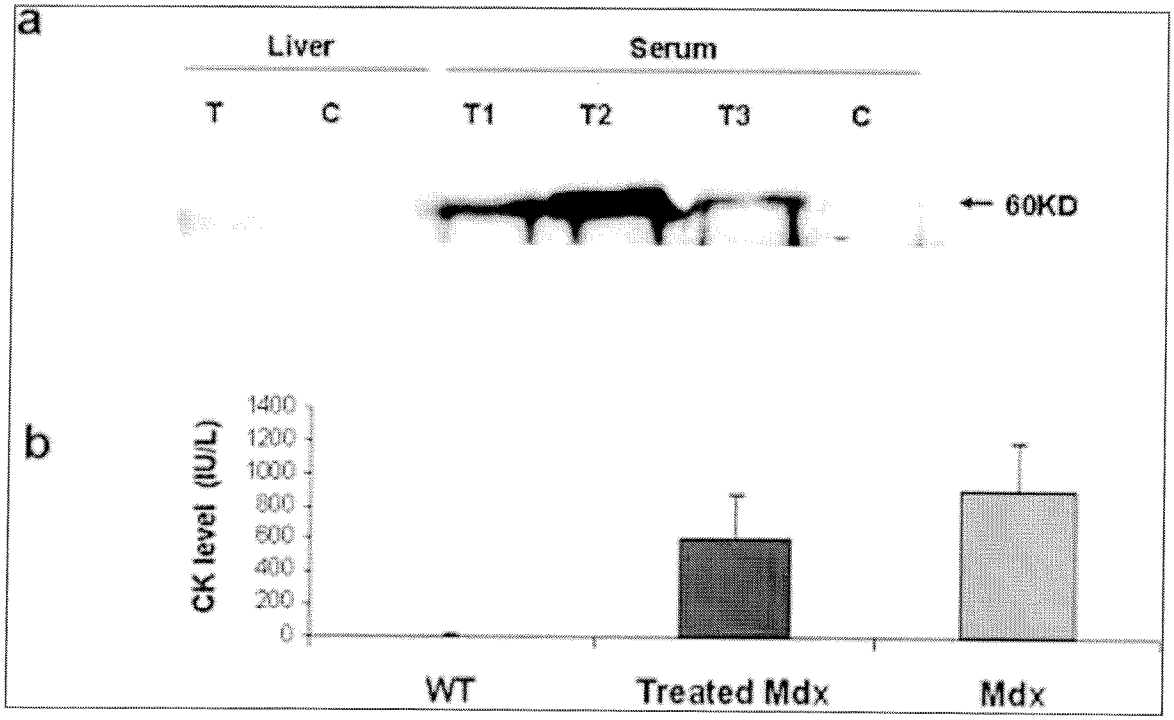


**SUPPL. FIG. 1.** Myostatin propeptide expression and serum creatine kinase level. (**a**) Western analysis against myostatin propeptide from treated and control *mdx* samples. T, treated *mdx*; C, control *mdx*; T1, T2, and T3 were from three different treated *mdx* mice, respectively. (**b**) Serum creatine kinase level was slightly decreased after delivery of AAV8-MPRO76AFc vector into *mdx* mice ($n = 5$ for each group; $p = 0.06$). WT, C57BL/6 mouse.

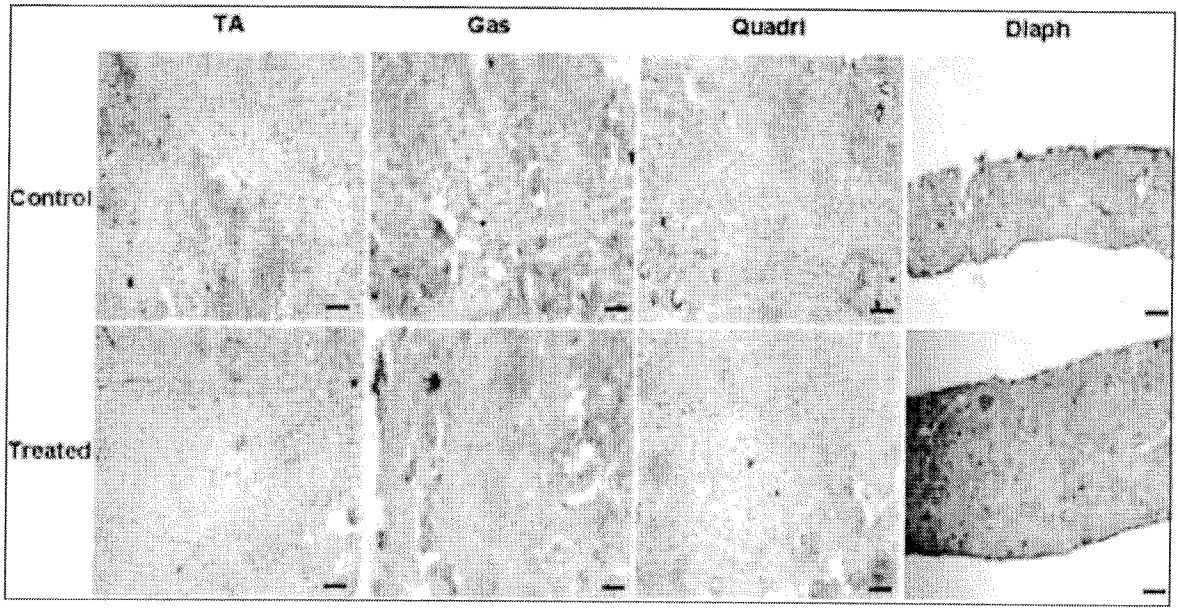


**SUPPL. FIG. 2.** Histological examination by H&E staining. Scale bars: 100 $\mu$m. TA, tibialis anterior muscle; Gas, gastrocnemius muscle; Quadri, quadriceps muscle; Diaph, diaphragm muscle.

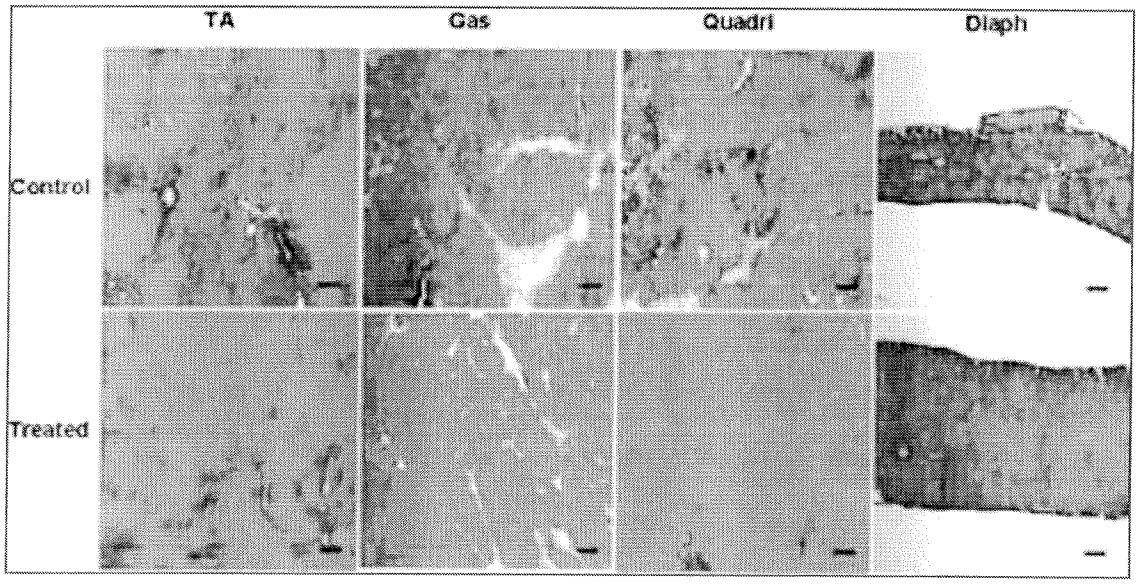


**SUPPL. FIG. 3.** Masson's trichrome staining. Collagen, which is an indication of fibrosis, is stained blue. Scale bars: 100 $\mu$m.